New insights into BRCA1 function and its role in cancer development

New insights into BRCA1 function and its role in cancer development

A dissertation presented

by

Sarah James Hill

to

The Division of Medical Sciences

in partial fulfillment of the requirements

for the degree of

Doctor of Philosophy

in the subject of

Genetics

Harvard University

Cambridge, Massachusetts

May 2014

Dissertation Advisor: Professor David M. Livingston Sarah James Hill

New insights into BRCA1 function and its role in cancer development

Abstract

BRCA1 is a breast and ovarian tumor suppressor. The role of BRCA1 in the repair of double strand DNA breaks by homologous recombination [HR] is its best understood function and the function most often implicated in BRCA1 breast cancer suppression. However, BRCA1 has less well defined roles in multiple other molecular processes.

Given its numerous, incompletely understood functions and the possibility that more exist, we performed complementary systematic screens in search of new BRCA1 protein interacting partners and functions. We detected a new function for BRCA1 in the response to transcription-associated DNA damage, based on the screening results. Genetic interactions were detected between BRCA1 and four of the newly identified interacting proteins [interactors] involved in transcription, TONSL, SETX, TCEANC, and TCEA2, and with specific interactors of one of these proteins. This new function may be important in BRCA1 tumor suppression, since the expression of several interactors, including some of the above-noted transcription proteins, is aberrant in both breast and ovarian cancers.

These findings may be particularly meaningful with respect to the sporadic basal-like breast cancer [BLC] subtype. This common subtype shares multiple biological properties with BRCA1 mutated breast tumors. Despite being BRCA1+/+, sporadic BLCs are widely viewed as phenocopies of BRCA1-mutated breast cancers and are hypothesized to manifest a BRCA1 functional defect or breakdown of a pathway[s] in which BRCA1 plays a major role. Given that

the BRCA1 role in HR is its best understood function, it is suspected that sporadic BLC exhibit an HR defect.

To test this hypothesis and to search for other BRCA1 pathway defects, multiple HR assays were performed on a group of cell lines classified as sporadic BLC and on controls. The sporadic BLC lines failed to exhibit an overt HR defect. Rather, they exhibited defects in the repair of stalled replication forks and potentially damage associated with stalled transcription, a new BRCA1 function.

These results provide insight into why clinical trials of PARP inhibitors, which require HR defects for efficacy, have been unsuccessful in sporadic BLC, unlike cisplatin which elicits stalled replication and transcription fork repair and has shown efficacy in sporadic BLC.

Table of Contents

Figures and Tables

Acknowledgements

SJH wishes to thank David Livingston and members of the Livingston lab for helpful discussion and technical advice, Jarrod Marto and members of the Marto lab for their collaboration, Marc Vidal and members of the Vidal lab for their collaboration, Keith Joung and members of the Joung lab for their collaboration, and Myles Brown and Min Ni for helpful discussion regarding Oncomine Concepts Map analysis. SJH wishes to thank in particular David Livingston, Kristine McKinney, Daniel P. Silver, and David E. Hill for constant experimental and scientific advice throughout the dissertation process. SJH also wishes to thank the Harvard MD/PhD program, in particular Loren Walensky and Amy Cohen, the HST program, in particular Rick Mitchell and Patty Cunningham, and the BBS program, in particular Kate Hodgins, for their support throughout this process. Finally, SJH wishes to thank her DAC committee, Joan Brugge, Myles Brown, and Bob Weinberg for their careful thought and advice throughout her dissertation. SJH was supported initially by DOD BCRP Fellowship W81XWH-08-1-0748 and subsequently by NCI Fellowship 1F30CA167895-01.

Dedication

This thesis is dedicated to my parents, James and Charlotte Hill, for the never-ending guidance and support.

Chapter 1: Introduction (All writing in this chapter was performed by SJH.)

Breast Cancer Genetics

5-10% of all breast cancer cases are familial (Melchor and Benitez, 2013; Venkitaraman, 2002). Of these cases, up to 25% are caused by mutations in the BRCA1 and BRCA2 gene products, both high penetrance breast and ovarian tumor suppressors (Melchor and Benitez, 2013; Miki et al., 1994; Venkitaraman, 2002; Wooster et al., 1994). Women with mutations in the BRCA1 gene have a 46-68% cumulative risk of breast cancer and a 39-60% cumulative risk of ovarian cancer by 70 years of age (Antoniou et al., 2003; Chen et al., 2006; Evans et al., 2008; Ford et al., 1998). However, carrying a mutation in the BRCA1 locus may not be the only way to develop BRCA1 mutant breast cancer. Multiple studies have now shown that it is common for the BRCA1 promoter to be methylated in sporadic breast and ovarian tumors (Dworkin et al., 2009; Press et al., 2008).

Mutations in other high penetrance cancer genes such as p53 or PTEN and mutations in a variety of lower penetrance cancer genes whose gene products are BRCA1 protein binding or physiological partners, such as PALB2, Rad50, NBS1, and BACH1, amongst others, account for another 5-10% of familial cases of breast cancer (Melchor and Benitez, 2013; Silver and Livingston, 2012). However, the majority of familial cases, along with most sporadic cases, are likely caused by both environmental factors and combinations of mutations in low penetrance genes, some discovered but many likely as yet undiscovered. Thus, it is important to gain a mechanistic understanding of known breast cancer gene product action. By doing so, the first goal is to identify pathways that may be defective and can thus be targeted in both familial and sporadic breast cancer. The second goal is to use such an understanding to help to define protein

binding partners of these cancer gene products that function in those same pathways. Some of these binding partners may be low penetrance cancer gene products themselves. Given the high penetrance and organ specificity of BRCA1 mutations in breast cancer, a great deal of focus has been placed on understanding the molecular functions of BRCA1, with the hope of gaining insights into which of its functional pathways is/are defective in either familial or sporadic breast cancer and which of those defective pathways can be therapeutically targeted.

Molecular functions of full length BRCA1 [p220]

Functional Domains of p220

The 23-exon *BRCA1* gene encodes at least three known proteins: full length p220, Δ11b, and IRIS (Figure 1); although it is likely that more isoforms are yet to be discovered (Tammaro et al., 2012). The most studied isoform is the 1,863 amino acid full length protein referred to as p220. Full length p220 [referred to as BRCA1 from now on] contains multiple functional domains including an N-terminal RING domain, a central protein scaffold encoded by exon 11, a coiled-coil domain that facilitates protein interactions, and two tandem BRCT motifs that both act to mediate various DNA damage protein interactions and help localize BRCA1 to sites of DNA damage through their phospho-peptide binding ability (Manke et al., 2003; Yu et al., 2003). All four of these domains are sites of well characterized clinical mutations as well as many sequence changes of unknown clinical significance (http://research.nhgri.nih.gov/bic/, Breast Cancer Information Core (BIC) Database; Szabo et al., 2000).

The BRCA1-BARD1 heterodimer

BRCA1 stably interacts through its RING domain with another RING domain containing protein, BARD1 (Wu et al., 1996). BARD1 is a major heterodimeric binding partner of BRCA1

Figure 1. Map of BRCA1 isoforms: The three known isoforms encoded by the human BRCA1 locus, p220, IRIS, and Δ11b, are shown here with all functional domains indicated. In addition, the structure of mouse Δ11 is also shown to demonstrate the small difference between it and human Δ11b.

Figure 1 (Continued)

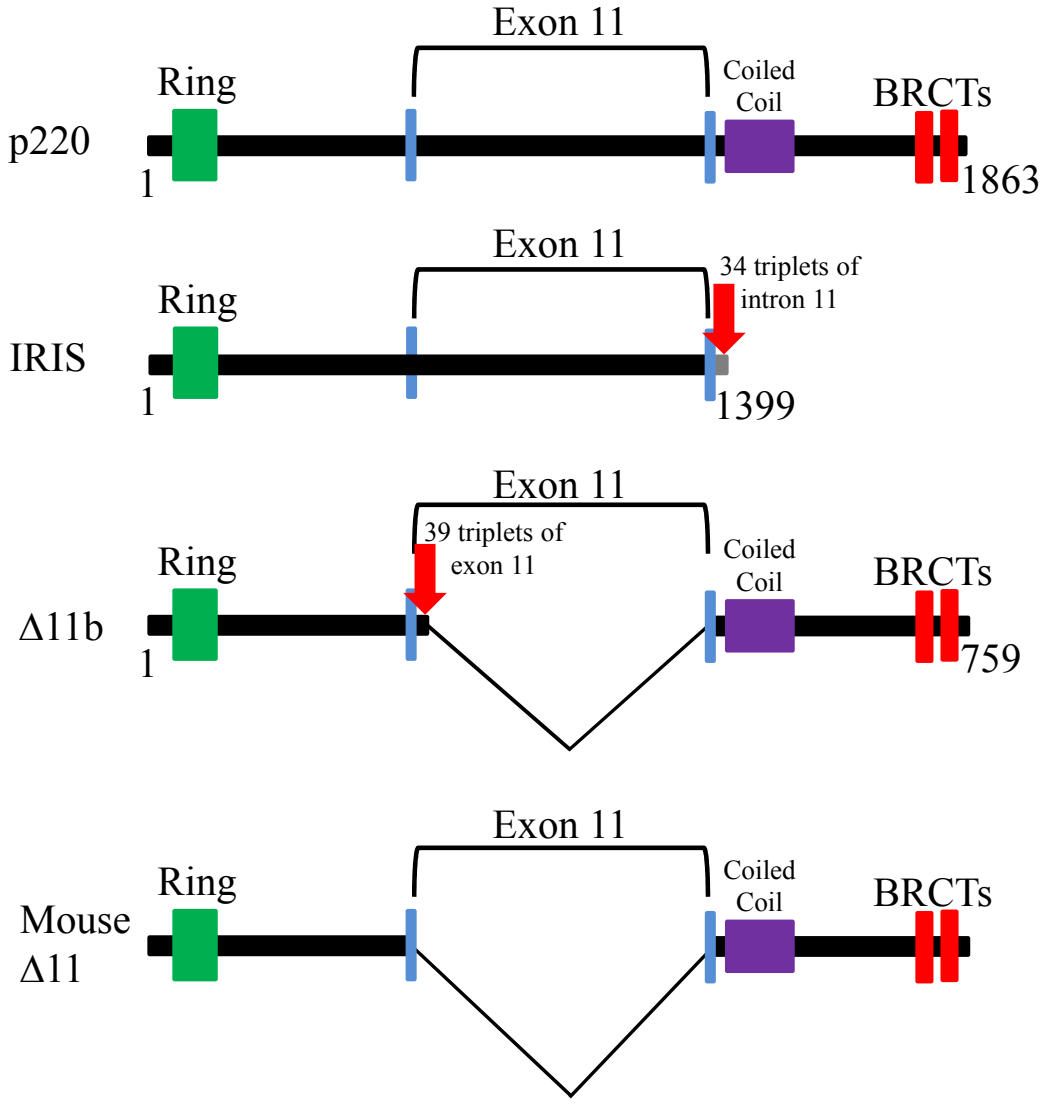

given that a majority of BRCA1 in cells interacts with BARD1(Yu and Baer, 2000) and nearly all detectable BRCA1 exists in complex with BARD1 in *Xenopus* extracts (Joukov et al., 2001). The RING domains of both BRCA1 and BARD1 exhibit E3 ligase activity on their own (Hashizume et al., 2001; Lorick et al., 1999; Ruffner et al., 2001), and this activity is enhanced when BRCA1 and BARD1 interact (Hashizume et al., 2001). Although the substrates of the BRCA1-BARD1 E3 ligase are not yet well-defined, the E3 ligase function is required for BRCA1-BARD1-dependent repair of double strand breaks [DSB] by homologous recombination [HR] (Ruffner et al., 2001; Silver and Livingston, 2012). This is demonstrated by the fact that when the E3 ligase function is disturbed by mutations in the BRCA1 RING domain, like C61G, cells exhibit increased sensitivity to gamma irradiation (Ruffner et al., 2001).

Role in repair of double strand DNA breaks

The best studied BRCA1 function is its role in the maintenance of genome integrity. Major elements of this function are exhibited in cellular DNA damage responses. The HR process and the repair of other forms of DNA damage, such as stalled and collapsed replication forks, are all BRCA1-affected processes. Upon induction of DNA damage by various agents including UV light, hydroxyurea, mitomycin C, and gamma irradiation, BRCA1 is phosphorylated and moves from its normal S-phase foci to areas of DNA damage along with BARD1 (Scully et al., 1997b). At genomic DSBs, e.g. sites of gamma irradiation-induced damage, BRCA1 concentrates and directs error-free repair by HR. For example, in a BRCA1 mutant cell line known to be supersensitive to gamma irradiation [HCC1937], reconstitution with wildtype BRCA1 rescues this supersensitivity (Scully et al., 1999). In addition, using an

integrated HR reporter, others have shown that reconstitution of p220 null mouse cells with p220 significantly alleviates the HR defect (Moynahan et al., 2001).

BRCA1 does not carry out its role in HR-DSB repair alone. Rather, the BRCA1-BARD1 heterodimer does so as a member of multiple protein complexes. Each complex is dedicated to executing a specific biochemical task and is composed of some common and other unique protein binding partners such as BRCA2, Rad51, NBS1, MRE11, BACH1, CtIP, RAP80, and PALB2 (Greenberg, 2008; Huen et al., 2010). Some of these binding partners interact with well-defined regions of the previously mentioned BRCA1 domains. PALB2 binds to the coiled-coil (Xia et al., 2006) and phosphorylated BACH1 binds to the phospho-peptide binding BRCTs (Cantor et al., 2001; Yu et al., 2003).

Normally, the repair of DSBs is performed in either an error prone manner by NHEJ or what is considered to be an error free manner by HR. Both processes are complex and involve multiple steps performed by dedicated sets of proteins and protein complexes. Multiple factors govern the choice of which pathway is selected to conduct repair of a DSB. The most dominant factor is likely the stage in the cell cycle in which the break occurs; however, recent evidence suggests that there is an antagonistic relationship between BRCA1 and 53BP1, in which 53BP1 prevents DSB end resection by BRCA1-MRN-CtIP (MRN corresponds to MRE11, RAD50, NBS1) in G1 cells thereby preventing HR and promoting NHEJ (Chapman et al., 2012; Panier and Boulton, 2014). NHEJ is the repair mechanism that is preferred in G0, G1, or very early S phase cells, and it involves the simple joining of the two ends of the broken DNA (Delacote and Lopez, 2008; Takata et al., 1998).

In brief, the Ku70/Ku-80-DNA-PK_{CS} complex binds to both sides of the DSB and recruits Artemis to process the ends of the break (Cary et al., 1997; Gottlieb and Jackson, 1993; Ma et al., 2002; Moshous et al., 2001; Walker et al., 2001; Yaneva et al., 1997; Yoo and Dynan, 1999). XRCC4 then recruits DNA Ligase IV to the processed ends to join them together (Grawunder et al., 1997; Gu et al., 2007). This process can be error-prone, based largely on the sequence at the break and whether or not it requires extensive processing to be re-joined. There is conflicting evidence from multiple studies about whether or not BRCA1 plays a role in NHEJ, so if BRCA1 does have a function in NHEJ, the mechanism is not currently well defined (Zhang and Powell, 2005). However, recent studies suggesting that 53BP1 and BRCA1 play antagonistic roles in promoting NHEJ, in the case of 53BP1, and HR, in the case of BRCA1, imply that BRCA1 may not function in NHEJ (Panier and Boulton, 2014).

The error-free mechanism of DSB repair, HR, takes place in either S or G2 because it requires a specific template/substrate, usually the homologous sister chromatid or a sequence very similar to it, to execute repair. If both ends of a break are present and share significant homology with an available donor template, HR occurs as follows (Anand et al., 2013; O'Donovan and Livingston, 2010; Svendsen and Harper, 2010). The MRN complex is critical in the initial steps of HR. It is responsible for recognizing both ends of a break and keeping them near each other, as well as recruiting and activating the ATM kinase which is important in modifying other DNA damage response proteins (Hopfner et al., 2002; Lee and Paull, 2004). In addition, the MRN complex is important in initiating the resection at the ends of a break to create single stranded DNA (ssDNA) ends that are initially coated by RPA and later by Rad51 (O'Donovan and Livingston, 2010; Paull and Gellert, 1998; Yu et al., 2001). Rad51 is

responsible for invasion of a ssDNA end into the sister chromatid in search of a homologous sequence (O'Donovan and Livingston, 2010; Svendsen and Harper, 2010). Once the homologous region is found, the invading strand synapses with the homologous strand leaving the non-bound strand to bubble out forming a structure called a D loop (Adelman and Boulton, 2010; O'Donovan and Livingston, 2010; Panier and Boulton, 2014; Svendsen and Harper, 2010). This ssDNA functions as a primer for DNA synthesis to replace the DNA at the break site (Adelman and Boulton, 2010; O'Donovan and Livingston, 2010; Panier and Boulton, 2014; Svendsen and Harper, 2010). The D-loop must be resolved, and this can occur in multiple ways (Adelman and Boulton, 2010; O'Donovan and Livingston, 2010; Panier and Boulton, 2014; Svendsen and Harper, 2010). In one method, called synthesis-dependent strand annealing, one of the invading strands dissociates from the sister chromatid with the help of RTEL-1, thereby resolving the D-loop (Adelman and Boulton, 2010). In another, the displaced D-loop interacts with the second 3’ overhang of the break which synapses with the homologous region of the D-loop and also acts as a primer for DNA synthesis to repair the break, thereby linking the two sister chromatids in a complex structure termed a double Holliday junction (Adelman and Boulton, 2010; O'Donovan and Livingston, 2010; Panier and Boulton, 2014; Svendsen and Harper, 2010). This structure can be resolved either by one of multiple resolvases or the BLM-RecQ-RMI-TOP3α complex in methods that can result in a gene conversion or non-conversion event depending on which complex resolves the Holliday junction (Adelman and Boulton, 2010; O'Donovan and Livingston, 2010; Panier and Boulton, 2014; Svendsen and Harper, 2010).

When only one end of the DSB is available or only one is homologous to an available donor, a process called break-induced replication (BIR) may occur instead (Anand et al., 2013;

Malkova and Ira, 2013). There is limited understanding of if or how this process occurs in mammalian cells (Anand et al., 2013; Malkova and Ira, 2013). Recent data, however, has indicated that BIR is likely responsible for repair of replication stalling in mammalian cells and that POLD3 is the DNA polymerase responsible for the repair (Costantino et al., 2014). In this process, the broken DSB end invades the homologous sequence and acts as a primer for DNA synthesis off the sister strand potentially to the end of the chromosome (Anand et al., 2013; Malkova and Ira, 2013). It is not clear yet whether or not BRCA1 is involved in BIR.

Currently, BRCA1 is believed to participate in three separate steps of the HR process. It does so as a member of three separate protein complexes. In one complex, after a DSB is generated, BRCA1 is recruited to the site of the DSB through an interaction between the BRCA1 BRCT motifs, Abraxas, and RAP80, which complex also plays a part in activating the G2-M checkpoint response (Kim et al., 2007a; Kim et al., 2007b; Liu et al., 2007; Sobhian et al., 2007; Wang et al., 2007; Yan et al., 2007). The BRCA1-RAP80 complex has also been shown to control the amount of BRCA1 driven HR by controlling the rate at which other HR related proteins localize to DSBs with BRCA1 (Hu et al., 2011). Once recruited to these sites, BRCA1 functions in multiple aspects of the repair of these DSBs by HR as a member of different protein complexes. In one complex, BRCA1-BARD1 interacts with CtIP and the MRN complex to aid in resection of the ends of the DSB to ssDNA to allow for the eventual loading of Rad51 onto the ssDNA (Chen et al., 2008; Yu et al., 1998; Yun and Hiom, 2009). Not only does BRCA1 aid in this end resection, it also indirectly participates in the recruitment of Rad51 to the ssDNA ends. BRCA1 does not directly bind Rad51 to recruit it, rather it interacts with PALB2 which, in turn, binds to BRCA2 which directly interacts with and recruits Rad51 to DSB sites (Sy et al., 2009;

Xia et al., 2006; Zhang et al., 2009). Rad51 then directs strand invasion of the resected end of the DSB to initiate the process of annealing with the intact sister strand.

p220 participates in the repair of stalled replication forks

In addition to its role in the repair of DSBs by HR, BRCA1 also interacts with multiple protein partners to participate in the repair of stalled and collapsed replication forks. Replication stalling can be caused by many different agents, but the forms of replication stalling that BRCA1 has been linked to so far are those caused by UV damage, hydroxyurea [HU], and inter-strand crosslinking agents like cisplatin. It occurs spontaneously in the setting of unresolved DNA lesions caused by various endogenous and exogenous agents, misincorporated nucleotides, challenging DNA templates, stalled transcription machinery, and problems with RNA processing (Zeman and Cimprich, 2014).

In the setting of UV damage, once a replication fork stalls, large areas of ssDNA coated with phosphorylated RPA are generated (Jones and Petermann, 2012; Parrilla-Castellar et al., 2004; Walter and Newport, 2000; Zeman and Cimprich, 2014). This coated ssDNA recruits ATRIP and ATR as well as other repair and checkpoint proteins like RAD17 and the 9-1-1 complex (RAD1, RAD9, and HUS1) (Jones and Petermann, 2012; Parrilla-Castellar et al., 2004; Zou and Elledge, 2003).

The 9-1-1 complex is responsible for initiation of a replication-DNA damage checkpoint after activation (Jones and Petermann, 2012; Parrilla-Castellar et al., 2004). Once recruited to the stalled fork, the 9-1-1 complex is loaded on to DNA by RAD17, and this promotes activation of CHK1 by ATR (Jones and Petermann, 2012; Parrilla-Castellar et al., 2004). Once activated,

CHK1 can slow S phase and allow time to repair or proceed through damage at stalled forks (Jones and Petermann, 2012; Parrilla-Castellar et al., 2004).

Once the cell cycle has slowed, a stalled replicase may succeed in replicating through the lesion in a process called translesion synthesis (TLS). Here a special polymerase capable of replicating through such abnormal structures is temporarily substituted for the existing replicase to allow replication through the lesion (Branzei and Foiani, 2010; Jones and Petermann, 2012). This method can be error prone and thus lead to mutations. These lesions may also be overcome by HR mediated template switching in which Rad51 coats the nascent DNA and causes it to invade the sister strand and to use it as a replication template (Branzei and Foiani, 2010; Jones and Petermann, 2012). If the fork collapses into a DSB, then HR repair of the break must occur before any replication can continue. BRCA1 participates at UV stalled replication forks in multiple ways.

BRCA1 is required for elimination of UV photoproducts at UV stalled forks (Pathania et al., 2011). It also licenses efficient generation of the RPA-coated ssDNA at sites of UV damage induced replication stress, one of the first steps in repair of these lesions (Pathania et al., 2011). In addition, BRCA1 has been shown to recruit the RFC-RAD17/9-1-1 complex to these sites (Pathania et al., 2011). Finally, BRCA1 inhibits TLS after UV damage, and in the absence of BRCA1, the recruitment of the major polymerase required for TLS [PolH] is greatly increased and the number of DNA mutations occurring after UV greatly increases (Pathania et al., 2011). There is potential for stalled fork-associated hypermutagenesis to be relevant to BRCA1 breast/ovarian cancer development, since gross genome instability, a likely by-product of failed stalled fork repair, appears to be a hallmark of loss of function BRCA1 and other inherited breast

cancer genes. This raises the possibility that the BRCA1 function in stalled fork repair participates in BRCA1 tumor suppression.

In addition to its role at UV stalled forks, BRCA1 also plays a role at both HU and interstrand crosslinking agent-induced stalled forks, the latter in connection with members of the Fanconi Anemia pathway. In the event of fork stalling due to an interstrand crosslink [ICL], the ICL is recognized by the FANCM-FAAP24 complex (Ciccia et al., 2007; Meetei et al., 2005). Once at the ICL site, FANCM-FAAP24 plays multiple roles. It helps activate ATR checkpoint signaling and slows the cell cycle to allow repair by interacting with HCLK2 which aids in mediating ATR dependent checkpoint signaling, likely mediated by RPA coated ssDNA at these sites (Collis et al., 2008). FANCM-FAAP24 also recruits the Fanconi anemia core complex which includes FANC- A, B, C, E, F, G, and L, which in turn leads to the monubiquitination of FANCD2 and the recruitment of the FANCD2-FANCI complex to the chromatin at the ICL site (Alpi et al., 2008; Garcia-Higuera et al., 2001; Smogorzewska et al., 2007; Taniguchi et al., 2002; Wang et al., 2004). This leads to the recruitment of various DNA repair nucleases (FAN1, EME1, MUS81, SLX4), TLS polymerases, and HR factors (Deans and West, 2011). Either the stalled fork is stabilized or a DSB may form at this site when the fork collapses, at which point HR and FA proteins stabilize the break (Deans and West, 2011). Various nucleases, chosen likely based on the structure of the DNA at the ICL, then excise the ICL (Deans and West, 2011). The excised area is filled in via TLS, HR is completed, and replication can continue (Deans and West, 2011). The nucleases may also be necessary for resolution of HR repair structures (Al-Minawi et al., 2009; Wechsler et al., 2011).

BRCA1 is involved in this process in multiple ways. Through its role in directing key elements of HR, it participates in either the stabilization of stalled forks or the repair of collapsed forks. In addition, multiple groups have shown that BRCA1 co-localizes with FANCD2 at damage sites and that BRCA1 is required for FANCD2 localization to ICL sites in a manner that is independent of its HR function (Bunting et al., 2012; Garcia-Higuera et al., 2001; Vandenberg et al., 2003). Finally, BRCA1 is known to form a complex with BACH1 (FANCJ) and TopBP1 (Cantor et al., 2001; Greenberg et al., 2006; Kim et al., 2005; Kumaraswamy and Shiekhattar, 2007; Makiniemi et al., 2001; Xu et al., 2001a; Xu et al., 2002; Yu et al., 2003). This complex helps mediate cell cycle arrest through checkpoint activation during replication stress and also functions to unwind DNA structures inhibiting replication progression (Cantor et al., 2001; Kim et al., 2005; Kumaraswamy and Shiekhattar, 2007; Makiniemi et al., 2001; Xu et al., 2001a; Xu et al., 2002; Yu et al., 2003)

Independent of its HR and ICL functions, BRCA1 also participates in confronting replication stress at HU stalled forks. HU stalls replication by depleting the pool of nucleotides available, not by generating a DNA lesion that must be overcome, unlike UV and interstrand crosslinks. Rad51 and BRCA2 have already been shown to protect stalled replication forks from degradation, independent of any HR function (Hashimoto et al., 2010; Schlacher et al., 2011). By measuring replication tract length in various settings, another study showed that BRCA1 and FANCD2 protect HU stalled replication forks from being degraded by the MRN complex (Schlacher et al., 2012). Without this protection, chromosomal instability appeared (Schlacher et al., 2012), further supporting the idea that replication-associated DNA damage may foster the appearance of genomic instability thereby accelerating the development of breast tumorigenesis.

Other functions for BRCA1

BRCA1 has been linked to multiple other molecular processes, but these functions are either not as well defined as HR or stalled fork repair, or are linked to BRCA1 indirectly.

BRCA1 functions in mitosis

BRCA1 is active in mitosis. One study showed that BRCA1 participates in mitotic spindle pole formation (Joukov et al., 2006). BRCA1 interacts with the spindle pole assembly proteins TPX2, XRHAMM, and NuMA (Joukov et al., 2006). Through these interactions, BRCA1 is responsible for localizing the spindle pole assembly protein TPX2 to spindle poles and for attenuating levels of XRHAMM function in microtubule nucleation and spindle pole assembly (Joukov et al., 2006). Loss of this BRCA1-BARD1 function led to spindle pole breakdown, improper chromosome segregation, and improper nuclear assembly in both *Xenopus* extracts and HeLa cells (Joukov et al., 2006). These findings fit well with an early network analysis study of BRCA1 function (Pujana et al., 2007).

In addition to its role in mitotic spindle pole assembly, BRCA1 plays an important role in the maintenance of normal centrosome number (Hsu et al., 2001; Xu et al., 1999b). Mouse embryonic fibroblasts that synthesized only the Δ11 isoform and not p220 exhibited an abnormal number of centrosomes which led to improper chromosome segregation and aneuploidy (Xu et al., 1999b). In support of this finding, BRCA1 has been shown to interact with gamma tubulin, and when this interaction was disrupted, cells exhibited an abnormal number of centrosomes and abnormal mitotic spindle poles (Hsu et al., 2001).

This control of centrosome number is carried out, in part, by the BRCA1-BARD1 complex along with the interacting protein OLA1, which, like BRCA1, binds γ-tubulin (Hsu et

al., 2001; Matsuzawa et al., 2014). BRCA1 is responsible for localizing OLA1 at centrosomes, and the OLA1-BRCA1 complex likely plays a role in controlling centrosome number as depletion of either protein leads to the presence of extra centrosomes (Matsuzawa et al., 2014). An OLA1 mutant protein in breast cancer cells failed to bind to BRCA1, and this disruption of the BRCA1-OLA1 complex led to increased centrosome number when the mutant was expressed in the setting of endogenous OLA1 depletion, further suggesting that this complex is important in controlling centrosome number (Matsuzawa et al., 2014). Thus in addition to its S-phase roles, BRCA1 is also important in regulating centrosome number and in supporting mitotic spindle pole formation in M phase. Disruption in either of these processes can lead to both DNA damage and aneuploidy, both hallmarks of BRCA1 mutant cancers.

Potential roles for BRCA1 in transcription-associated processes

BRCA1 has also been indirectly linked to transcription and various forms of transcription-associated damage. Two independent studies have shown by immunofluorescence staining that BRCA1 co-localizes with the RNA helicase SETX at sites of DNA damage (Becherel et al., 2013; Yuce and West, 2013). In one of those studies, BRCA1 was shown to be necessary for the recruitment of SETX to these damage sites on meiotic chromosomes which also contain transcription-associated R-loops (Becherel et al., 2013). This is interesting because SETX is among a group of RNA binding proteins, including ASF, the loss of function of which can lead to stabilization of physiological structures called R loops and subsequent DNA damage (Li and Manley, 2005a, b, 2006; Mischo et al., 2011; Skourti-Stathaki et al., 2011).

R loops occur normally during transcription when the nascent RNA transcript binds to the transcribed strand of DNA and leaves the non-transcribed strand to bubble out. Normally,

these structures are resolved quickly by unwinding helicases or potentially prevented from stabilizing by hnRNPs binding to the nascent transcript. However, if proteins responsible for preventing R loop stabilization are lost, then the non-transcribed strand becomes susceptible to exogenous forms of damage which can lead to single strand breaks that evolve into double strand breaks. Thus, loss of function of certain hnRNPs could lead to DNA damage in this way. Indeed, genomic instability has already been demonstrated upon loss of function of ASF and R loop induction (Li and Manley, 2005a), and thus repair of DNA damage at R loops or prevention of R loop stabilization may be yet another method for BRCA1 to prevent genomic instability. BRCA1 co-localization with SETX and recruitment of SETX to R loop associated DNA damage strongly suggests this possibility. Our data will further support this.

In addition to a potential role in suppression of R loop associated DNA damage, BRCA1 has also been implicated in transcription-coupled repair. BRCA1 and BRCA2 were shown to be necessary for the removal of 8-oxoguanine (8-oxoG) lesions typically caused by oxidative stress in a plasmid recovery assay conducted in BRCA1 and BRCA2 deficient cell lines and controls, and the BRCA1 repair defect was rescued by expression of wildtype BRCA1 from an adenovirus (Le Page et al., 2000). The inability to repair these lesions was the result of stalled transcription complexes at the 8-oxoG site, which suggests some role for BRCA1 in transcription coupled repair (Le Page et al., 2000). The exact function BRCA1 plays in transcription coupled repair and the protein binding partners it executes this function with are not known.

Finally, BRCA1 has been indirectly linked to mRNA processing through its interactions with BARD1 and RNA Polymerase II (Scully et al., 1997a). The functional relevance of the interaction with RNA Polymerase II is still unclear, but BARD1 has been linked to mRNA

processing and transcription associated damage, thereby suggesting a role for BRCA1 in these processes as well.

BARD1 interacts with the polyadenylation factor CstF50 to form a complex that inhibits polyadenylation of mRNA transcripts (Kleiman and Manley, 1999). UV- and HU- induced DNA damage led to an increase in the inhibition of 3' mRNA processing by this complex (Kleiman and Manley, 2001). Although the protein levels do not change after UV exposure, the amount of BRCA1, BARD1, and CstF50 that interact, as shown by co-immunoprecipitation, increases after UV treatment. Moreover, at least the BARD1-CstF50 complex is necessary for the inhibition of 3' processing observed after UV damage (Kleiman and Manley, 2001). This inhibition of processing likely results from the ubiquitination of active RNA Polymerase II, as triggered directly or indirectly, by the BRCA1-BARD1 complex and its subsequent degradation (Kleiman et al., 2005). The inhibition of mRNA processing in each of these studies was BARD1-dependent. Nevertheless, the close association between BRCA1 and BARD1 suggests that there may be a role for BRCA1 in this process as well, even if it is simply to enhance the E3 activity of BARD1.

Given the above-noted evidence, there are likely multiple possible roles for BRCA1 in transcription or transcription-associated DNA damage, and our work supports this possibility and suggests new roles for BRCA1 in these processes.

In this regard, multiple studies have already shown that loss of function of certain RNA binding proteins can lead to DNA damage (Li and Manley, 2005a; Mischo et al., 2011; Paulsen et al., 2009), making transcription another source of genomic instability. Dysfunction in any of

the above BRCA1-linked processes can lead to DNA damage and genomic instability, suggesting a possible role for RNA-based DNA damage control in BRCA1 tumor suppression.

BRCA1 suppresses satellite RNA expression

Unexpectedly, BRCA1 maintains heterochromatic silencing of satellite DNA repeats through its monubiquitination of histone H2A (Zhu et al., 2011). Loss of BRCA1 results in expression of other silenced genes as well, and this can be rescued by either expressing wildtype BRCA1 or an H2A-Ubiquitin (Ub) fusion protein, H2A-Ub (Zhu et al., 2011). Expression of the H2A-Ub fusion protein in BRCA1 deficient cells also rescued multiple phenotypic traits associated with BRCA1 deficiency including cell cycle arrest and an HR defect, suggesting that BRCA1 control of heterochromatin silencing is actually its major function and that all of the other phenotypes observed with BRCA1 loss of function may just be byproducts of loss of this singular BRCA1 function (Zhu et al., 2011). Readily detectable satellite RNA expression was observed in both BRCA1-deficient mouse mammary tumors and human tumors; and, following forced satellite RNA expression in a human mammary epithelial cell line, that line exhibited multiple characteristics of BRCA1-deficient cells, including a defect in HR, increased γ-H2AX foci, and impaired cell cycle checkpoints, all of which indicates that increased satellite RNA expression could lead to many of the BRCA1 functional defects associated with tumorigenesis (Zhu et al., 2011). Thus, it is possible that the individual BRCA1 functions that are alleged to be important in tumor suppression may, at least in part, be dependent upon BRCA1 maintaining the integrity of heterochromatin through the monubiquitination of H2A, making this another potential tumor suppressor function.

BRCA1 repairs DNA damage induced by estrogen metabolites

BRCA1 has recently been shown to be important in repairing DSBs generated by certain estrogen metabolites and also regulating the level of certain estrogen metabolizing enzymes at the transcriptional level in estrogen-receptor-α negative cells (Savage et al., 2014). DNA damage caused by estrogen metabolites was increased in both BRCA1 depleted cells and cells heterozygous for a BRCA1 mutation compared to controls (Savage et al., 2014). This function is intriguing, since it may offer insight into why BRCA1 mutations cause female-specific disease.

BRCA1 and tumor suppression

Given the collective evidence, it is clear that p220 performs a variety of molecular functions. The molecular steps in the execution of most of the above functions are not well understood, and it is likely new functions and new BRCA1-containing protein complexes remain to be discovered. Therefore, one aspect of my work was to generate a larger BRCA1 interactome with the goal of elucidating new functions for BRCA1 based on known functions of its interactors and/or to better understand known functions of BRCA1.

Of equal importance, which, if any, of the above-noted functions is important in BRCA1 tumor suppression has not been determined. There is in vitro and in some cases limited mouse model or human tumor evidence suggesting that some of these functions are perturbed in tumor cell lines or tumors, but there is only indirect but no direct evidence demonstrating which, if any, of these processes is important in BRCA1 tumor suppression, despite the fact that loss of a number of them is associated with sporadic breast and other cancer development. Therefore, an additional goal of the BRCA1 interactome work performed and reported in this thesis was to better understand which pathways are deficient in BRCA1 mutant and sporadic breast cancers so that the therapeutic value of targeting those pathways could be assessed and the pathways could

be mined for potential biomarkers. In addition, by better defining the BRCA1 interactome, we may detect clues to the existence and identities of new low penetrance breast cancer susceptibility genes among those encoding newly identified BRCA1 interacting proteins.

There are at least two other BRCA1 isoforms with incompletely defined functions

In discussing BRCA1 function, it is important to remember that BRCA1 encodes at least two other known isoforms (Figure 1). In addition, it is also not clear whether p220 is the only isoform important in tumor suppression, since little is known of the function of the other two isoforms, IRIS and Δ11b.

The *IRIS* coding sequence is composed of an uninterrupted open reading frame extending from exon 2 to the end of exon 11 and ending 34 triplets into intron 11, which are in frame with the exon 11 open reading frame (Figure 1) (ElShamy and Livingston, 2004). Little is known of IRIS function other than that the endogenous protein normally stimulates DNA replication, can modulate certain transcriptional events, and, when endogenously overexpressed, exhibits certain properties of an oncoprotein (ElShamy and Livingston, 2004; Nakuci et al., 2006). Unlike full length p220 and Δ11b, IRIS does not bind BARD1 (ElShamy and Livingston, 2004). There are no mouse models lacking or expressing only IRIS, so its role in disease has not been explored beyond cell culture and tissue studies.

The knowledge of Δ11b function is also limited, despite the fact that it is the most conserved of all the known isoforms (Boulton et al., 2004). When discussing Δ11b, a distinction must be made between Δ11 and Δ11b (Figure 1). In mice, in contrast to humans, only a Δ11 transcript (lacking all of exon 11) has been found, and no Δ11b transcript has been found (Figure 1). In humans, only the Δ11b transcript which contains a small portion of the exon 11 sequence

has been found, and no true Δ11 mRNA (lacking all of exon 11) has been found (Figure 1). The sequences of mouse Δ11 and human Δ11b are similar enough that the information gathered on Δ11 function in mice can likely be taken as relevant to Δ11b in humans. Therefore, much information regarding Δ11b has been inferred from mice either lacking Δ11 expression or only expressing Δ11 and not full length BRCA1.

Two conditional BRCA1 mutant mouse models that only express Δ11 have been generated. One strain is homozygous for an exon 11 deleted allele (*BRCA1* $^{\Delta 11/\Delta 11}$) (Xu et al., 2001b), and the other contains one *BRCA1*-null allele and one allele with exon 11 flanked by *loxP* sites that can be excised by Cre under the control of a breast-specific promoter (*BRCA1*$^{-/\Delta 11}$) (Xu et al., 1999a). The *BRCA1*$^{-/\Delta 11}$ mice exhibited abnormal mammary gland development due to extensive apoptosis, increased mammary tumor development after long latency, and accelerated mammary tumor development in a *Trp53*$^{+/-}$ background similar to human BRCA1 related tumors (Xu et al., 1999a). This data was then extended in *BRCA1* $^{\Delta 11/\Delta 11}$ mice. *BRCA1* $^{\Delta 11/\Delta 11}$ embryos survived longer than *BRCA1*$^{-/-}$ embryos, but still died late in gestation due to increased apoptosis (Xu et al., 2001b). However, this gestational death could be reversed by crossing the *BRCA1* $^{\Delta 11/\Delta 11}$ mice with *Trp53*$^{+/-}$ mice to give rise to *BRCA1* $^{\Delta 11/\Delta 11}$ *Trp53*$^{+/-}$ mice (Xu et al., 2001b). The rescue resulted from reversal of cell cycle arrest and apoptosis caused by the complete loss of p220, suggesting the importance of p220 in cell cycle checkpoint control. The loss of one *p53* allele rescued the gestational lethality, but most of these mice developed mammary tumors within 6-10 months at which point the mice had almost all lost the remaining *p53* allele (Xu et al., 2001b). In addition, the male mice were shown to be sterile and to have problems with meiosis (Xu et al., 2003).

Taken together, these two mouse models indicate that Δ11 provides enough function to allow normal development, at least in a p53+/- setting, but it does not provide enough BRCA1 function to prevent cancer as both mouse models developed breast tumors. Thus Δ11, and likely Δ11b in humans, is not sufficient for tumor suppression. These data are supported by the fact that two published BRCA1 mutant breast cancer cell lines were derived from patients with mutations in exon 11 of the BRCA1 gene which cause them to express Δ11b only (Elstrodt et al., 2006; Johannsson et al., 2003). In addition, a patient carrying bi-allelic BRCA1 mutations which only allowed her to express Δ11b exhibited early onset ovarian cancer and developmental abnormalities (Domchek et al., 2013). Despite these results, further transgenic mouse experiments have shown that Δ11, and likely Δ11b in humans, is not inert.

Mice lacking Δ11 expression and only expressing p220 ($BRCA1^{FL/FL}$) have been generated via a knock-in approach that abrogated the ability to generate the Δ11 splice variant (Kim et al., 2006). These mice lack gestational development issues, but they do show breast and uterine hyperplasia after one year of age and also spontaneously develop breast tumors (Kim et al., 2006). In addition, $BRCA1^{FL/FL}$ mice are not hypersensitive to gamma irradiation and the MEFs from these mice lack defects in cell cycle checkpoints induced by gamma irradiation (Kim et al., 2006). In cultured $BRCA1^{FL/FL}$ MEFs, there are increases in centrosome amplification and a decreased number of G1 cells with most cells containing increased levels of cyclin E and A which accelerate the transition from G1 to S (Kim et al., 2006). Taken together, this data shows that Δ11, and probably Δ11b in humans, plays a role in preventing tumor formation (along with p220), controlling centrosome amplification, and directing the G1/S transition, possibly as a manifestation of a breakdown in checkpoint control. It is not clear from these mouse models

whether or not Δ11b has a role in HR, but work shown here and also from others, suggests that this may be the case.

Like p220, Δ11b binds BARD1; and like p220, Δ11b has been shown to localize to post-IR damage foci, which would concentrate it in the right place to perform HR (Huber et al., 2001). It is not clear whether Δ11b is active in HR, however. When an HR reporter was integrated into the genome of mouse ES cells that only express Δ11, the level of HR in those cells was not zero, indicating that Δ11 could perform some level of HR (Moynahan et al., 2001). The level of HR increased when a p220 cDNA was expressed in that line (Moynahan et al., 2001). Our results will support the possibility that Δ11b manifests HR capacity in the absence of p220 but is not the dominant isoform in performing this function and does not have enough HR capacity to prevent tumor formation. Taken together, none of the existing data defines which BRCA1 function is most important in tumor suppression nor which isoform is solely responsible for this function.

Sporadic BRCA1-like basal-like breast cancer

HR is widely believed to participate in BRCA1-driven breast cancer suppression (Li and Greenberg, 2012; Silver and Livingston, 2012; Walsh and King, 2007). In keeping with this view, BRCA1 mutant cell lines and tumors are generally defective in HR (Moynahan et al., 1999; Scully et al., 1999), but they are also sensitive to other drugs that require other forms of DNA damage repair such as UV, mitomycin C, cisplatin, and hydrogen peroxide (Alli et al., 2009; Bhattacharyya et al., 2000; Pathania et al., 2011). In addition, some BRCA1 HR binding partners are known breast cancer susceptibility gene products, further implicating loss of HR function, or at least genomic instability, as playing a major role in breast tumorigenesis. For this

reason, a major hypothesis in the field is that BRCA1 mutant, BRCA1 promoter methylated, or BRCA1-like sporadic tumors (especially sporadic basal-like breast tumors) harbor a defect in HR. This has been a topic of debate.

Gene expression profiling of breast cancers has led to the identification of five subtypes: luminal A, luminal B, Her2 amplified, basal like, and normal breast like (Perou et al., 2000; Sorlie et al., 2001). The basal-like subtype is of particular interest due to the lack of relevant targeted therapies as well as its similarity to BRCA1-/- tumors. BRCA1-/- tumors segregate with the basal-like cancer [BLC] subtype by gene expression profiling (Sorlie et al., 2003; van 't Veer et al., 2002). These tumor species exhibit multiple biological similarities. For example, both commonly fail to express ER, PR, and Her2 and are mutant for p53 (1997; Crook et al., 1998; Lakhani et al., 2005; Lakhani et al., 2002; Manie et al., 2009). Moreover, both are associated with early relapse following clinically active breast cancer chemotherapy and experience similar patterns of metastasis (Valentin et al., 2012). Not all BRCA1 mutant tumors are categorized as basal-like, since 20% are ER positive (Tung et al., 2010). However, given the above similarities and the fact that the majority of BRCA1 mutant tumors segregate with the basal-like subtype, it is widely speculated that sporadic BLCs manifest a defect in a pathway(s) that is/are dependent upon BRCA1 function.

The prevailing hypothesis in the BLC field was that the defect was in HR for the reasons noted above, and this thinking has spurred clinical trials with drugs that target HR deficiencies, like PARP inhibitors. The prevailing hypothesis for PARP efficacy in cells with an HR defect is that its primary target, PARP1, binds to DNA damage sites where it parsylates and recruits members of the BER repair pathway (Telli and Ford, 2010). Upon PARP1 inhibition, BER

repair is not executed at these sites, and DSBs result (Telli and Ford, 2010). If a cell is defective in DSB repair, like a BRCA1 deficient cell would be, the cells will eventually be killed by the generation of such breaks in a synthetic lethal manner (Telli and Ford, 2010). The first PARP inhibitor studies in BRCA1 and BRCA2 mutant cell lines strongly suggested this hypothesis (Bryant et al., 2005; Farmer et al., 2005), and this spurred clinical trials in BRCA1 mutant cancers and BRCA1-like cancers. While PARP inhibitors have been successful in treating BRCA1 mutant breast tumors and sporadic ovarian tumors, there has been no success in treating sporadic BLC with PARP inhibitors (Fong et al., 2009; Gelmon et al., 2011; Liu et al., 2013) indicating that the BRCA1 HR function may be intact in these tumors and that there is another defective BRCA1 pathway that should be specifically targeted in this subtype. Determining whether sporadic BLC do harbor an HR defect or perhaps a defect in a different BRCA1 pathway was one goal of this work.

Conclusion

In summary, BRCA1 is a multi-functional breast and ovarian tumor suppressor gene. There are three BRCA1 isoforms, but the best studied isoform is full length p220. Despite great effort since its discovery, there is limited in depth understanding of BRCA1-p220 molecular and tumor suppression function, and this has resulted in a lack of effective targeted therapies for BRCA1 mutant and BRCA1-like breast cancers. These issues spurred both of the projects in this thesis work.

The first project, covered in chapters two through four, involved a complementary set of protein interactor screens, performed in search of new BRCA1 binding partners. The question in this screen was whether or not there are any as yet undetected BRCA1 functions, and with what

protein binding partners BRCA1 carries out these new functions or any known ones. By gaining a better understanding of the pathways in which BRCA1 functions and with what interacting partners it does so, one should gain better insight into what pathways to target in certain cancers and become aware of new lower penetrance cancer genes.

To address these questions, I carried out both a yeast two hybrid screen and mass spectrometry (MS) analysis of BRCA1-BARD1 protein complexes. The reason for the dual screen was that both methodologies detect different types of interactions and are therefore capable of generating complementary results. In the yeast two hybrid screen, one can detect direct interactions between BRCA1 and binding partners that do not require post-translational modifications. In the MS analysis, one can detect both direct and indirect interactions with all post-translational modifications intact.

However, there is a caveat with the latter method. Specifically, one cannot know whether a putative interaction is direct or indirect and mediated by many other proteins. The pitfalls of each methodology were ameliorated by the results of the other methodology, and the screening effort led to an expansion of the BRCA1 interactome, the discovery of a new BRCA1 function, and the identification of several interacting proteins with which BRCA1 might carry out this function. Conceivably, the products of new breast cancer genes exist among the BRCA1-interacting proteins.

The second project, covered in chapters five and six, focused on the question of what BRCA1 functional pathway(s) is/are defective in the sporadic BLC subtype. A major goal was to determine whether or not these tumors exhibit a defect in HR or perhaps in a different BRCA1

functional pathway, either one that is already known or potentially one that emerged from the results of our screening effort.

Chapter 2: Complementary screening effort identifies new BRCA1 protein binding partners and a new role for BRCA1 in the repair of transcription-associated DNA damage

-Chapters 2-4 adapted from the following manuscript:

Title: Systematic screening reveals a role for BRCA1 in the response to transcription-associated DNA damage

Authors: Sarah J. Hill[1,2], Thomas Rolland[1,2,3], Guillaume Adelmant[1,4,5], Amélie Dricot[1,2,3], Travis I. Zack[1,6], Nidhi Sahni[1,2,3], Yves Jacob[1,2,3,10,11,12], Tong Hao[1,2,3], Kristine M. McKinney[1,2], Allison P. Clark[1,2,], Deepak Reyon[8,9], Shengdar Q. Tsai[8,9], J. Keith Joung[8,9], Rameen Beroukhim[1,6,7], Jarrod A. Marto[1,4,5], Marc Vidal[1,2,3], David E. Hill[1,2,3†], and David M. Livingston[1,2†*]

Affiliations:
[1]Department of Cancer Biology, Dana-Farber Cancer Institute, Boston, MA 02215, USA.
[2]Department of Genetics, Harvard Medical School, Boston, MA 02115, USA.
[3]Center for Cancer Systems Biology (CCSB), Dana-Farber Cancer Institute, Boston, MA 02215, USA
[4]Department of Biological Chemistry and Molecular Pharmacology, Harvard Medical School, Boston, MA 02115, USA
[5]Blais Proteomics Center, Dana-Farber Cancer Institute, Boston, MA 02215, USA
[6]The Broad Institute, Cambridge, MA 02142, USA
[7]Department of Medical Oncology, Dana-Farber Cancer Institute, Boston, MA 02215, USA
[8]Molecular Pathology Unit, Center for Computational and Integrative Biology, and Center for Cancer Research, Massachusetts General Hospital, Charlestown, MA 02129, USA
[9]Department of Pathology, Harvard Medical School, Boston, MA 02115, USA
[10]Institut Pasteur, Unité de Génétique Moléculaire des Virus à ARN, Département de Virologie, F-75015 Paris, France
[11]CNRS, UMR3569, F-75015 Paris, France
[12]Université Paris Diderot, Sorbonne Paris Cité, Unité de Génétique Moléculaire des Virus à ARN, EA302, F-75015 Paris, France
[†]These authors share equal seniority

* To whom correspondence should be addressed: David M. Livingston, M.D.
Professor of Genetics and Medicine
Harvard Medical School and
Dana-Farber Cancer Institute
450 Brookline Avenue,
Boston, MA 02215, USA
david_livingston@dfci.harvard.edu

-All writing for this chapter was performed by SJH. All experiments in this chapter were performed by SJH with help in the mass spectrometry and its analysis form Guillaume Adelmant and Jarrod Marto. All yeast two hybrid screening was performed by SJH with initial guidance from Amélie Dricot, Nidhi Sahni, David E. Hill, and Marc Vidal. All figures in this chapter were generated by SJH, with help generating Figure 2B from Thomas Rolland. Thomas Rolland aided in bioinformatics analysis of the combined screen hits and statistical analysis of the data, and Tong Hao aided in the sequencing verification of the Y2H hits.

Rationale

BRCA1 is a breast and ovarian tumor suppressor gene (Miki et al., 1994), and its full length protein product, p220, is a genome integrity maintenance protein (Silver and Livingston, 2012). Its validated functions include but are not limited to its role in the repair of double strand DNA breaks by homologous recombination (Silver and Livingston, 2012). However, how and with what protein-binding partners BRCA1 executes its molecular and tumor suppression functions are not well understood. Gaining a better understanding of these processes will be beneficial in conceiving new therapies for BRCA1 and BRCA1-like cancers.

Success in gaining a better understanding of the functions of certain proteins has been achieved through systematic mapping of their protein interaction networks (Rual et al., 2005; Stelzl et al., 2005) like that performed for a group of tumor viral oncoproteins (Rozenblatt-Rosen et al., 2012). Focused work has identified such BRCA1 and BRCA2 interactors as BARD1 and PALB2 (Wu et al., 1996; Xia et al., 2006), while network analysis (Pujana et al., 2007), an immunoprecipitation-based study (Wang et al., 2000), and a yeast two hybrid and mass spectrometry-based analysis of a BRCA1 functional motif have identified yet other BRCA1-

interacting proteins (Woods et al., 2012). However, gaps in the BRCA1 network likely remain, given the limited understanding of BRCA1 function.

Therefore, we have carried out protein-protein interaction screens using two complementary methodologies to search for new BRCA1 interacting partners (Figure 2A). A primary goal was to gain evidence of new functions for BRCA1 based on known functions of newly detected interacting proteins (aka interactors). Another was to identify new cancer genes or therapeutically targetable signal transduction pathways served by newly identified interacting proteins.

Results

Bipartite screening effort identifies new BRCA1 interacting partners

The bipartite screening effort involved two, complementary approaches. The first consisted of a systematic, binary screen, using both full length BRCA1 protein (aka p220) and strategically designed fragments thereof (Table 1) tested against the gene products present in the human ORFeome v5.1 collection in a high throughput yeast two-hybrid (Y2H) format (Dreze et al., 2010). We screened BRCA1 only as prey since the BRCT domain of this protein acted as an autoactivator. The complementary screen was a tandem affinity purification followed by mass-spectrometry (TAP-MS) analysis of BARD1-BRCA1 complexes isolated from the nuclei of HeLa S3 cells (Figure 2A). BARD1 is the heterodimeric binding partner of BRCA1 (Silver and Livingston, 2012), and it was used as bait because expression of BRCA1 at levels high enough for TAP-MS is toxic to cells.

In the TAP-MS screen, we identified 96 individual interactors (Table 2). From the Y2H screen, we identified 54 individual interactors (Table 3). Since some of the Y2H interactors

Figure 2. Bipartite screening effort to identify new protein interacting partners for BRCA1: A) The Y2H and TAP-MS screening methods used are outlined here. In the Y2H screen, depicted on the left, full length BRCA1 (p220) and fragments strategically designed to contain specific BRCA1 functional domains (shown in the map) were screened against the human ORFeome version 5.1. The two example plates shown represent full length BRCA1 and fragment 33 screened against the same 94 members of the ORFeome. The TAP-MS sequence is depicted on the right. Nuclei were harvested from HeLa S3 cells stably expressing FLAG-Streptactin [SII] tagged BARD1 or empty vector as a control. The nuclei were fractionated into soluble nuclear and chromatin fractions from which the complexes were tandemly immunoprecipitated. A silver-stained gel depicting a small fraction of one of the three purifications is shown at the bottom of the panel. **B)** This network represents BARD1 and BRCA1 as the central nodes for TAP-MS associations and direct biophysical Y2H interactions respectively with all interactors from the screen emanating from them. The code for edge color and style as well as node color is defined in the key below the network.

Figure 2 (Continued)

A

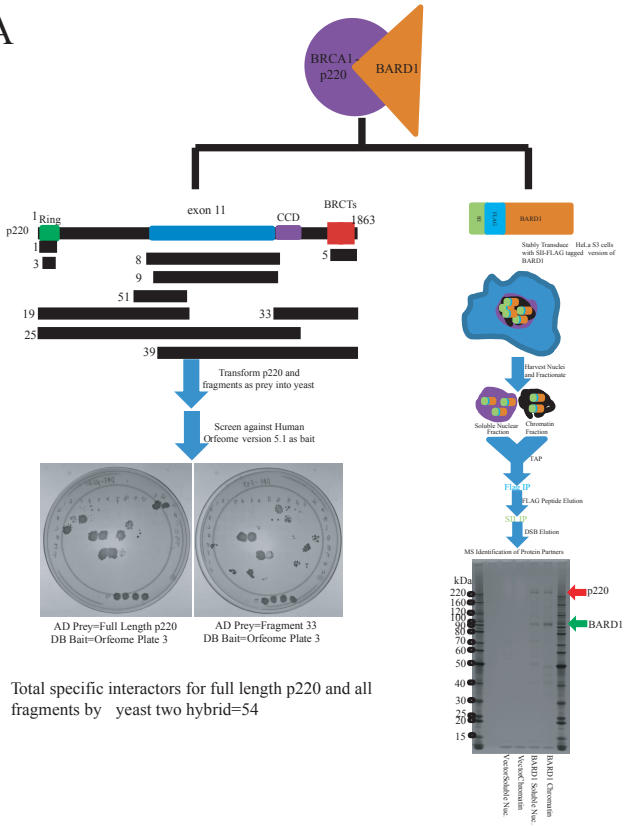

Total specific interactors for full length p220 and all fragments by yeast two hybrid=54

Total unique BARD1/p220 interactors in all fractions via TAP/MS=96

B

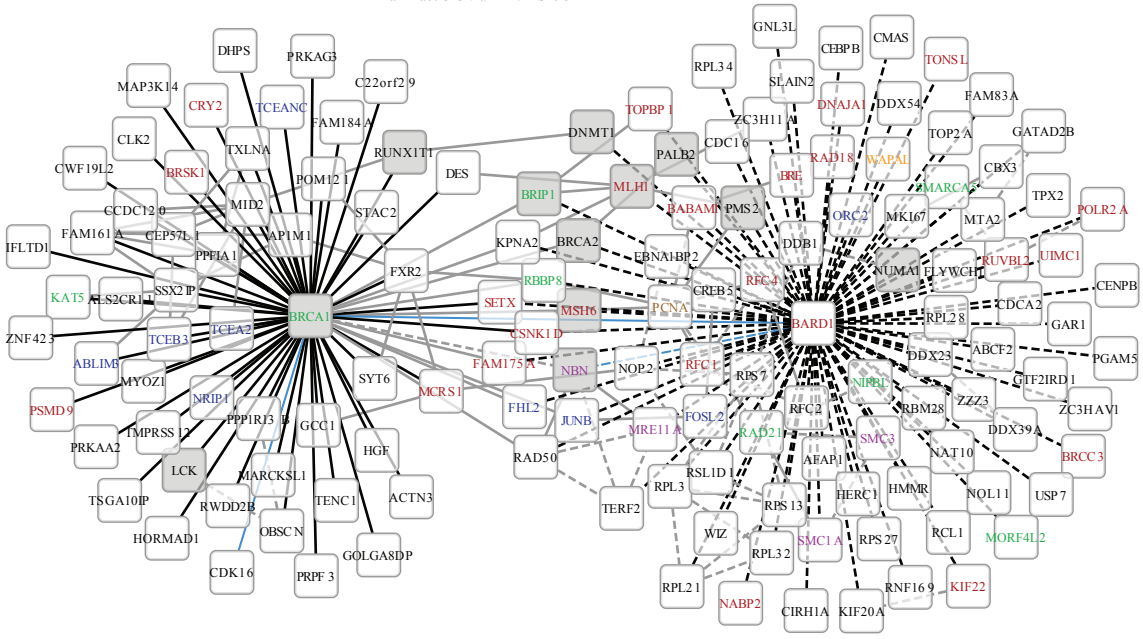

Y2H interactions found in this work
Y2H interactions found in this work and in the binary literature
Y2H interactions found in the binary literature
TAP-MS interactions found in this work
TAP-MS interactions found in this work and in the non-binary literature
TAP-MS interactions found in the non-binary literature

Proteins found in this work
Damage
Transcription
Replication
Damage, Transcription
Transcription, Replication
Damage, Replication, Transcription
Known cancer genes

Table 1. Sequence information for full length BRCA1 and fragments used in Y2H screen, Related to Figure 2: The base pair and amino acid coordinates in the BRCA1 coding sequence are given for each fragment used in the Y2H screen.

Table 1 (Continued). Sequence information for full length BRCA1 and fragments used in Y2H screen, Related to Figure 2

Fragment #	Amino Acid Coordinates	Base Pair Coordinates
Full Length BRCA1 (p220)	1-1863	1-5592
Fragment 1	1-110	1-330
Fragment 3	24-78	70-234
Fragment 5	1649-1863	4945-5592
Fragment 8	224-1366	670-4098
Fragment 9	250-1366	748-4098
Fragment 19	1-550	1-1650
Fragment 25	1-1485	1-4455
Fragment 33	1366-1863	4096-5592
Fragment 39	250-1863	748-5592
Fragment 51	200-550	598-1650

Table 2. Full list of TAP-MS interactors sorted by soluble nuclear fraction, chromatin fraction, and combined list, Related to Figure 2: The interactors detected by TAP-MS are listed here in full. The first two columns show the gene symbol and gene ID for interactors detected in the soluble nuclear fraction. The gene symbol and gene ID for interactors detected in the chromatin fraction are shown in the middle two columns. The final four columns show the gene symbol and gene ID for all interactors with interactors found in the soluble nuclear fraction highlighted in blue and interactors found in the chromatin fraction highlighted in purple.

Table 2 (Continued). Full list of TAP-MS interactors sorted by soluble nuclear fraction, chromatin fraction, and combined list, Related to Figure 2

Soluble Nuclear Interactors

Gene Symbols	Gene IDs
BARD1	580
BRCA1	672
BRCC3	79184
BRE	9577
BRIP1	83990
C19orf62 (aka BABAM1)	29086
CENPB	1059
DDB1	1642
DDX54	79039
DNAJA1	3301
EBNA1BP2	10969
FAM175A	84142
FAM83A	84985
GAR1	54433
GNL3L	54552
HERC1	8925
KPNA2	3838
MLH1	4292
MSH6	2956
NAT10	55226
NOP2	4839
NUMA1	4926
PGAM5	192111
PMS2	5395
RBBP8	5932
RBM28	55131
RCL1	10171
RPL21	6144
RPL28	6158
RPL3	6122
RPL32	6161
RPL34	6164
RPS27	6232
RPS7	6201
RSL1D1	26156
RUVBL2	10856
SETX	23064
UIMC1	51720
ZC3HAV1	56829

Chromatin Interactors

Gene Symbols	Gene IDs
ABCF2	10061
AFAP1	60312
BARD1	580
BRCA1	672
BRCA2	675
BRCC3	79184
BRE	9577
BRIP1	83990
C19orf62 (aka BABAM1)	29086
CBX3	11335
CDC16	8881
CDCA2	157313
CEBPB	1051
CIRH1A	84916
CMAS	55907
CREB5	9586
CSNK1D	1453
DDB1	1642
DDX23	9416
DDX39 (aka DDX39A)	10212
DNMT1	1786
FAM175A	84142
FAM83A	84985
FHL2	2274
FLYWCH1	84256
FOSL2	2355
GATAD2B	57459
GTF2IRD1	9569
HMMR	3161
JUNB	3726
KIF20A	10112
KIF22	3835
KPNA2	3838
MKI67	4288
MLH1	4292
MORF4L2	9643
MRE11A	4361
MTA2	9219
NBN	4683
NIPBL	25836
NOL11	25926
NOP2	4839
NUMA1	4926
OBFC2B	79035
ORC2	4999
PALB2	79728
PCNA	5111
POLR2A	5430
RAD18	56852
RAD21	5885
RAD50	10111
RBBP8	5932
RFC1	5981
RFC2	5982
RFC4	5984
RNF169	254225
RPS13	6207
RPS27	6232
RUVBL2	10856
SLAIN2	57606
SMARCA5	8467
SMC1A	8243
SMC3	9126
TERF2	7014
TONSL (aka NFKBIL2)	4796
TOP2A	7153
TOPBP1	11073
TPX2	22974
UIMC1	51720
USP7	7874
WAPAL	23063
WIZ	58525
ZC3H11A	9877
ZZZ3	26009

Soluble Nuclear Fraction		Chromatin Fraction	
Combined TAP-MS Interactors			
Gene Symbols	**Gene IDs**	**Gene Symbols**	**Gene IDs**
ABCF2	10061	RAD50	10111
AFAP1	60312	RBBP8	5932
BARD1	580	RBBP8	5932
BARD1	580	RBM28	55131
BRCA1	672	RCL1	10171
BRCA1	672	RFC1	5981
BRCA2	675	RFC2	5982
BRCC3	79184	RFC4	5984
BRCC3	79184	RNF169	254225
BRE	9577	RPL21	6144
BRE	9577	RPL28	6158
BRIP1	83990	RPL3	6122
BRIP1	83990	RPL32	6161
C19orf62 (aka BABAM1)	29086	RPL34	6164
C19orf62 (aka BABAM1)	29086	RPS13	6207
CBX3	11335	RPS27	6232
CDC16	8881	RPS27	6232
CDCA2	157313	RPS7	6201
CEBPB	1051	RSL1D1	26156
CENPB	1059	RUVBL2	10856
CIRH1A	84916	RUVBL2	10856
CMAS	55907	SETX	23064
CREB5	9586	SLAIN2	57606
CSNK1D	1453	SMARCA5	8467
DDB1	1642	SMC1A	8243
DDB1	1642	SMC3	9126
DDX23	9416	TERF2	7014
DDX39 (aka DDX39A)	10212	TONSL (aka NFKBIL2)	4796
DDX54	79039	TOP2A	7153
DNAJA1	3301	TOPBP1	11073
DNMT1	1786	TPX2	22974
EBNA1BP2	10969	UIMC1	51720
FAM175A	84142	UIMC1	51720
FAM175A	84142	USP7	7874
FAM83A	84985	WAPAL	23063
FAM83A	84985	WIZ	58525
FHL2	2274	ZC3H11A	9877
FLYWCH1	84256	ZC3HAV1	56829
FOSL2	2355	ZZZ3	26009
GAR1	54433		
GATAD2B	57459		
GNL3L	54552		
GTF2IRD1	9569		
HERC1	8925		
HMMR	3161		
JUNB	3726		
KIF20A	10112		
KIF22	3835		
KPNA2	3838		
KPNA2	3838		
MKI67	4288		
MLH1	4292		
MLH1	4292		
MORF4L2	9643		
MRE11A	4361		
MSH6	2956		
MTA2	9219		
NAT10	55226		
NBN	4683		
NIPBL	25836		
NOL11	25926		
NOP2	4839		
NOP2	4839		
NUMA1	4926		
NUMA1	4926		
OBFC2B	79035		
ORC2	4999		
PALB2	79728		
PCNA	5111		
PGAM5	192111		
PMS2	5395		
POLR2A	5430		
RAD18	56852		
RAD21	5885		

Table 3. Full list of Y2H interactors and the BRCA1 fragments with which they interact, Related to Figure 2: All Y2H BRCA1 interacting proteins are listed. The gene symbol, Entrez gene ID, and all BRCA1 fragments with which the interactor was detected are given. In some cases the fragments were used to map the domain of BRCA1 with which the interactor bound.

Table 3 (Continued). Full list of Y2H interactors and the BRCA1 fragments with which they interact, Related to Figure 2

Gene Symbols	Gene IDs	Fragments Interacted With
ABLIM3	22885	Full Length, 5, 33, 39
ACTN3	89	Full Length
ALS2CR11	151254	33
AP1M1	8907	Full Length
BARD1	580	Full Length, 1, 19, 25
BRSK1	84446	Full Length, 33, 39
C22orf29	79680	33
C6orf182 (aka CEP57L1)	285753	Full Length
CCDC120	90060	Full Length, 33, 39
CDK16 (aka PCTK1)	5127	Full Length, 5, 33, 39
CLK2	1196	33
CRY2	1408	33
CSNK1D	1453	Full Length, 19, 25, 39
CWF19L2	143884	Full Length, 39
DES	1674	Full Length, 5, 33, 39
DHPS	1725	3
FAM161A	84140	Full Length
FAM184A	79632	Full Length, 25, 39
FXR2	9513	Full Length, 25
GCC1	79571	Full Length, 25, 39
GOLGA8DP	100132979	25, 39
HGF	3082	33
HORMAD1	84072	Full Length, 19, 25
IFLTD1	160492	Full Length, 33, 39
KAT5	10524	Full Length
LCK	3932	39
MAP3K14	9020	33
MARCKSL1	65108	5
MCRS1	10445	Full Length, 33, 39
MID2	11043	Full Length, 1
MYOZ1	58529	39
NRIP1	8204	Full Length, 5, 33, 39
OBSCN	84033	33
POM121	9883	5, 33, 39
PPFIA1	8500	Full Length
PPP1R13B	23368	Full Length, 33
PRKAA2	5563	Full Length, 39
PRKAG3	53632	5
PRPF3	9129	Full Length
PSMD9	5715	Full Length, 19, 25, 39
RUNX1T1	862	Full Length, 25
RWDD2B	10069	Full Length
SETX	23064	Full Length, 33
SSX2IP	117178	Full Length
STAC2	342667	33
SYT6	148281	Full Lenth, 33, 39
TCEA2	6919	Full Length, 39
TCEANC	170082	39
TCEB3	6924	39
TENC1	23371	33
TMPRSS12	283471	33
TSGA10IP	254187	33
TXLNA	200081	Full Length, 25
ZNF423	23090	Full Length

bound to multiple, overlapping BRCA1 fragments, we were able to map these interactions to specific domains of BRCA1 (Figure 3A, Table 3). For example, based on the BRCA1 fragments with which it interacted, we were able to predict that a newly detected BRCA1 interactor, SETX, binds to the coiled coil domain of BRCA1 (Figure 2, Figure 3A, Table 3). We also predict that the N-terminus of SETX interacts with this domain, since only full length SETX and not a shorter C-terminal fragment interacted with BRCA1 (Figure 3A). Knowing the BRCA1 domain with which proteins interact may be important in predicting the subtype of disease or treatment strategies that can be deployed in association with a BRCA1 mutation that alters a highly specific BRCA1-protein X interaction.

Co-immunoprecipitation (IP) was performed on a select subset of exogenously overexpressed interactors from both modalities as a quality assessment of the dataset, and we observed frequent co-precipitation with either exogenously overexpressed or endogenous BRCA1 (Figure 4A-H).

In total, 147 interactors were identified in the combined screening effort (Table 4). The overlap between the methodologies was small, but it was significant (3 common network edges BARD1, CSNK1D, and SETX, P =0.002) and within the range expected based on the results of previous dual screens (Rozenblatt-Rosen et al., 2012). The 147 interactors were grouped into a network in which the central nodes are BRCA1 and BARD1 (Figure 2B). Twenty-five of these interactions had been previously detected in other screening efforts as physical interactors (Pujana et al., 2007; Wang et al., 2000; Woods et al., 2012). The other 122 were novel. In addition, 47 of the hits were identified as potential cancer genes in systematic cancer gene screening efforts (Beroukhim et al., 2010; Rozenblatt-Rosen et al., 2012; Tasan et al., 2014),

Figure 3. Analysis of Y2H screen hits, Related to Figure 2: A) Based on the smallest fragment interaction detected for each bait, some of the interactions detected in the yeast two hybrid (Y2H) screen were mapped to specific functional domains of BRCA1. The interactors from our screen mapping to each domain are listed below the domains in black (RING, Exon 11, Coiled Coil Domain (CCD), and BRCTs). In the bottom left part of this panel is a map of full length SETX, with which BRCA1 did interact by Y2H, and a C-terminal SETX fragment with which BRCA1 did not interact by Y2H. **B)** A graph demonstrating the results of an analysis performed on each BRCA1 interacting partner to determine whether it was associated with a specific "GO annotation" of interest (transcription, replication, DNA damage), whether it had been identified in any completed "systematic screens" searching for cancer genes (Sleeping Beauty, GWAS, SCNA, Somatic Mutations, tumor virus protein interactors), whether it had been identified in any previous "BRCA1 protein-protein interaction (PPI)" screens, or whether it is a "known cancer gene" in the Sanger Census or other relevant lists. Hits that fit any of these criteria align with one or more black boxes, each representing one of the above-noted criteria. The hits that were validated through genetic analysis are represented in red.

Figure 3 (Continued)

A

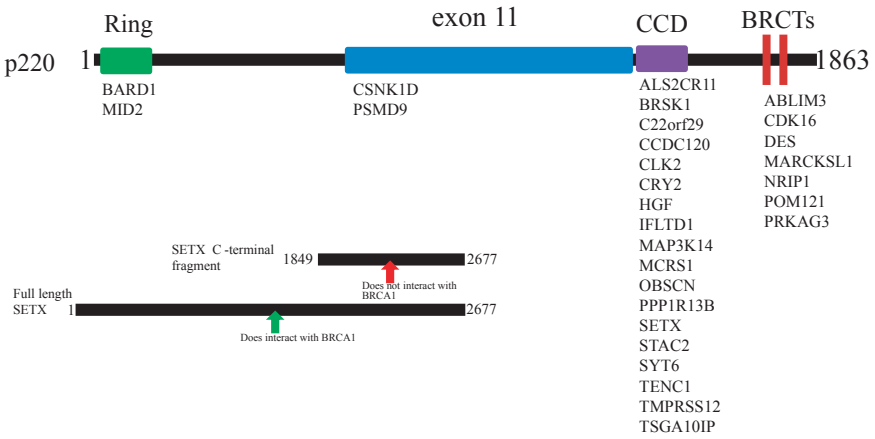

B

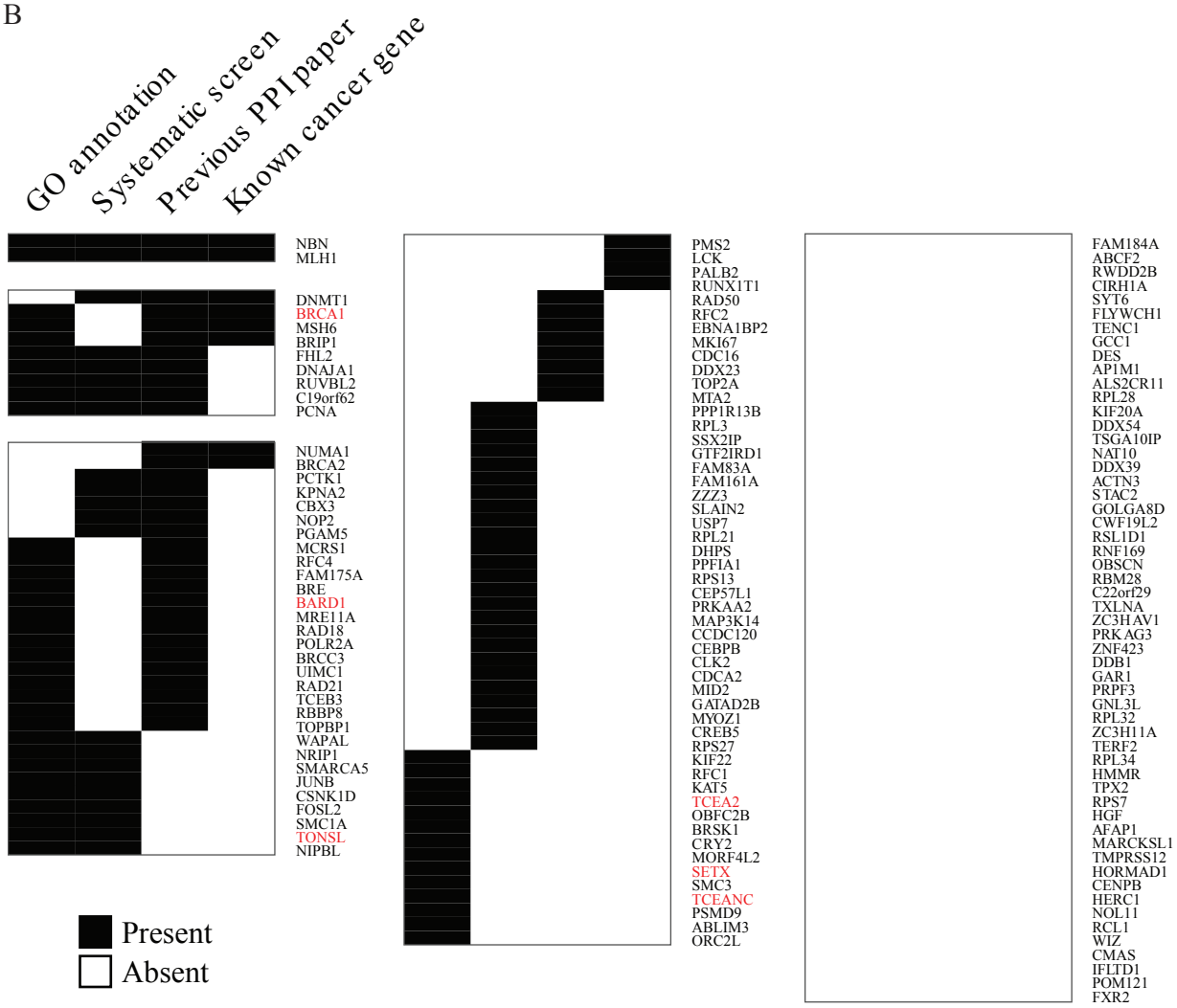

Figure 4. Overexpression co-IPs of select screen hits with BRCA1 isoforms, related to Figure 2: A) Cells were transiently transfected with an HA-FLAG tagged gene of interest (TONSL, a TAP-MS identified interactor, in this case) and a myc-tagged BRCA1 isoform (Full Length BRCA1 p220 which we have referred to as BRCA1 throughout the text or the exon 11 missing isoform Δ11b). Lysates from these cells were immunoprecipitated (IP'd) with FLAG, electrophoresed, blotted with a myc antibody, and in some cases the blots stripped and then reacted with FLAG antibody. Arrows denote the migration of proteins of interest. **B)** HA-FLAG tagged TONSL was tandem affinity purified from the soluble nuclear and chromatin fractions of 293FT cells stably overexpressing this protein. A silver stain showing the results of these purifications along with those performed on extracts of cells transduced by empty vector can be seen in the left panel. A western blot of 10% of the purified fraction stained for BRCA1 is shown in the right panel. Endogenous p220/BRCA1 and Δ11b are marked by arrows. **C)** Co-transfections, IPs, and blots were performed as noted for panel A, but here with HA-FLAG tagged MAP3K14 (from the Y2H screen) or BARD1 as a control. Arrows indicate the location of p220/BRCA1 and Δ11b in this myc blot. **D)** HA-FLAG-tagged MAP3K14 was IP'd from lysates of cells stably expressing it, and these IPs were blotted with a BRCA1 antibody (left panel) and a FLAG antibody (right panel). Arrows demonstrate the proteins of interest. **E)** Co-transfections, IPs, and blots were performed as in panel A, but here with HA-FLAG tagged PPFIA1 (from the Y2H screen) or BARD1 as a control. Arrows indicate the location of p220/BRCA1 and Δ11b on this myc blot. **F)** Co-transfections, IPs, and blots were performed as in panel A but with HA-FLAG tagged CLK2 or CWF19L2 (both interactors from the Y2H screen). Arrows indicate the location of p220/BRCA1 and Δ11b on the myc blot shown in the

Figure 4 (Continued). Overexpression co-IPs of select screen hits with BRCA1 isoforms, related to Figure 2: left panel. This blot was stripped and re-probed with FLAG antibody, as shown in the right panel where arrows indicate the migration of CLK2 and CWF19L2. **G)** Co-transfections, IPs, and blots were performed as in panel A but with HA-FLAG tagged PRKAA2 (from the Y2H screen) or HA-FLAG-MLLT6 (a false positive from the Y2H screen). Arrows indicate the migration of p220/BRCA1 and Δ11b on this myc blot. **H)** Co-transfections, IPs, and blots were performed as in panel A this time with HA-FLAG tagged MCRS1 (from the Y2H screen) or BARD1 as a control. Arrows indicate the migration of p220/BRCA1 and Δ11b on this myc blot.

Figure 4 (Continued)

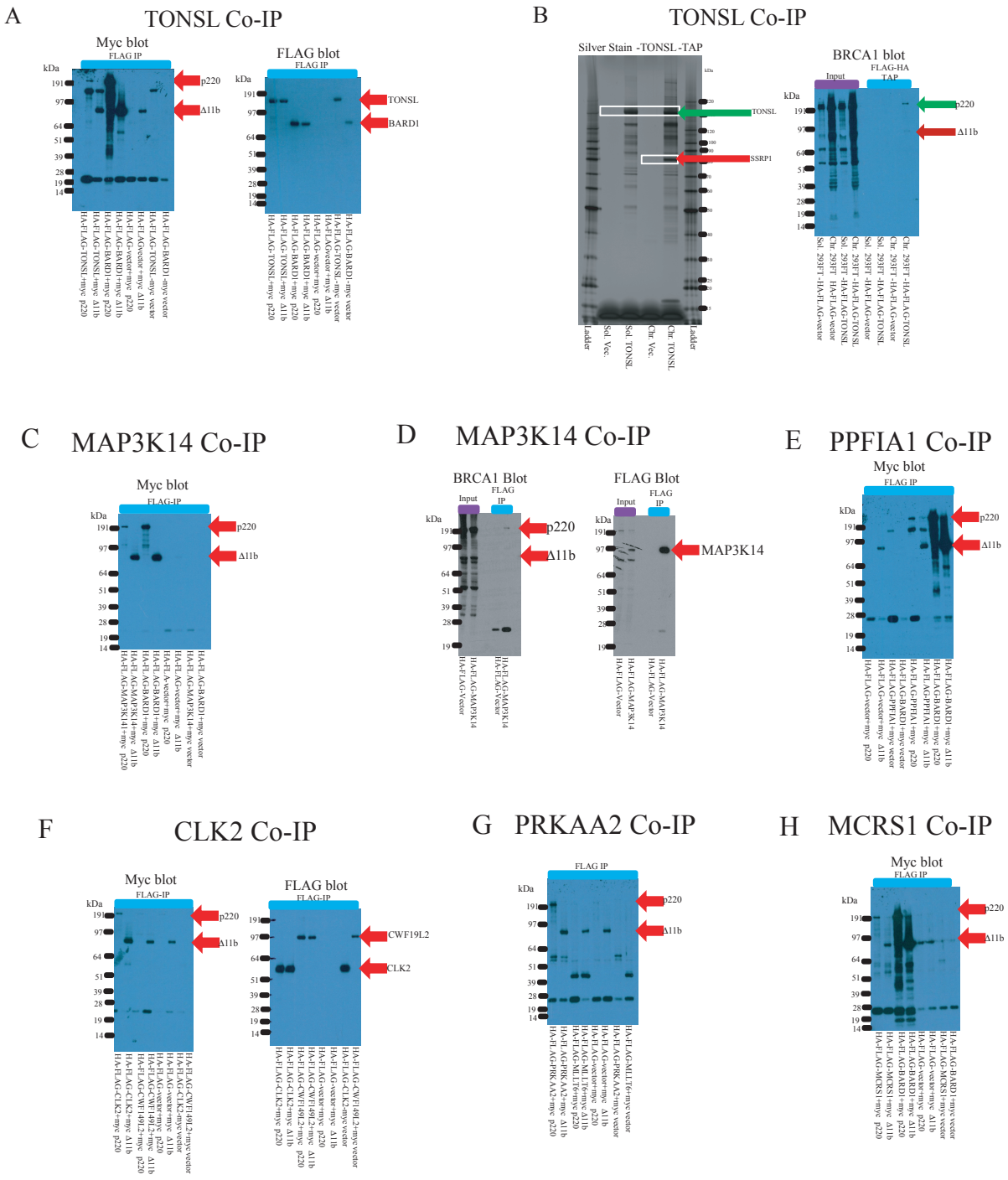

Table 4. Combined list of Y2H and MS interactors, Related to Figure 2: Complete list of all interactors detected in the bipartite screening effort. Interactors detected by both modalities are highlighted in pink.

Table 4 (Continued). Combined list of Y2H and MS interactors, Related to Figure 2

Indicates Interactor found in both modalities

Technology	Gene Symbols	Gene IDs
TAP	ABCF2	10061
TAP	AFAP1	60312
TAP	BARD1	580
TAP	BRCA1	672
TAP	BRCA2	675
TAP	BRCC3	79184
TAP	BRE	9577
TAP	BRIP1	83990
TAP	C19orf62 (aka BABAM1)	29086
TAP	CBX3	11335
TAP	CDC16	8881
TAP	CDCA2	157313
TAP	CEBPB	1051
TAP	CENPB	1059
TAP	CIRH1A	84916
TAP	CMAS	55907
TAP	CREB5	9586
TAP	CSNK1D	1453
TAP	DDB1	1642
TAP	DDX23	9416
TAP	DDX39 (aka DDX39A)	10212
TAP	DDX54	79039
TAP	DNAJA1	3301
TAP	DNMT1	1786
TAP	EBNA1BP2	10969
TAP	FAM175A	84142
TAP	FAM83A	84985
TAP	FHL2	2274
TAP	FLYWCH1	84256
TAP	FOSL2	2355
TAP	GAR1	54433
TAP	GATAD2B	57459
TAP	GNL3L	54552
TAP	GTF2IRD1	9569
TAP	HERC1	8925
TAP	HMMR	3161
TAP	JUNB	3726
TAP	KIF20A	10112
TAP	KIF22	3835
TAP	KPNA2	3838
TAP	MKI67	4288
TAP	MLH1	4292
TAP	MORF4L2	9643
TAP	MRE11A	4361
TAP	MSH6	2956
TAP	MTA2	9219
TAP	NAT10	55226
TAP	NBN	4683
TAP	NIPBL	25836
TAP	NOL11	25926
TAP	NOP2	4839
TAP	NUMA1	4926
TAP	OBFC2B	79035
TAP	ORC2	4999
TAP	PALB2	79728
TAP	PCNA	5111
TAP	PGAM5	192111
TAP	PMS2	5395
TAP	POLR2A	5430
TAP	RAD18	56852
TAP	RAD21	5885
TAP	RAD50	10111
TAP	RBBP8	5932
TAP	RBM28	55131
TAP	RCL1	10171
TAP	RFC1	5981
TAP	RFC2	5982
TAP	RFC4	5984
TAP	RNF169	254225
TAP	RPL21	6144
TAP	RPL28	6158
TAP	RPL3	6122
TAP	RPL32	6161
TAP	RPL34	6164
TAP	RPS13	6207
TAP	RPS27	6232
TAP	RPS7	6201
TAP	RSL1D1	26156
TAP	RUVBL2	10856
TAP	SETX	23064
TAP	SLAIN2	57606
TAP	SMARCA5	8467
TAP	SMC1A	8243
TAP	SMC3	9126
TAP	TERF2	7014
TAP	TONSL (aka NFKBIL2)	4796
TAP	TOP2A	7153
TAP	TOPBP1	11073
TAP	TPX2	22974
TAP	UIMC1	51720
TAP	USP7	7874
TAP	WAPAL	23063
TAP	WIZ	58525
TAP	ZC3H11A	9877
TAP	ZC3HAV1	56829
TAP	ZZZ3	26009
Y2H	ABLIM3	22885
Y2H	ACTN3	89
Y2H	ALS2CR11	151254
Y2H	AP1M1	8907
Y2H	BARD1	580
Y2H	BRSK1	84446
Y2H	C22orf29	79680
Y2H	C6orf182 (aka CEP57L1)	285753
Y2H	CCDC120	90060
Y2H	CDK16 (aka PCTK1)	5127
Y2H	CLK2	1196
Y2H	CRY2	1408
Y2H	CSNK1D	1453
Y2H	CWF19L2	143884
Y2H	DES	1674
Y2H	DHPS	1725
Y2H	FAM161A	84140
Y2H	FAM184A	79632
Y2H	FXR2	9513
Y2H	GCC1	79571
Y2H	GOLGA8DP	100132979
Y2H	HGF	3082
Y2H	HORMAD1	84072
Y2H	IFLTD1	160492
Y2H	KAT5	10524
Y2H	LCK	3932
Y2H	MAP3K14	9020
Y2H	MARCKSL1	65108
Y2H	MCRS1	10445
Y2H	MID2	11043
Y2H	MYOZ1	58529
Y2H	NRIP1	8204
Y2H	OBSCN	84033
Y2H	POM121	9883
Y2H	PPFIA1	8500
Y2H	PPP1R13B	23368
Y2H	PRKAA2	5563
Y2H	PRKAG3	53632
Y2H	PRPF3	9129
Y2H	PSMD9	5715
Y2H	RUNX1T1	862
Y2H	RWDD2B	10069
Y2H	SETX	23064
Y2H	SSX2IP	117178
Y2H	STAC2	342667
Y2H	SYT6	148281
Y2H	TCEA2	6919
Y2H	TCEANC	170082
Y2H	TCEB3	6924
Y2H	TENC1	23371
Y2H	TMPRSS12	283471
Y2H	TSGA10IP	254187
Y2H	TXLNA	200081
Y2H	ZNF423	23090

and 12 are present in two large cancer gene lists (the overlap between our 147 hits and those two cancer gene lists was significant, P=0.001) (Futreal et al., 2004; Vogelstein et al., 2013) (Figure 2B, Figure 3B, Table 5).

We queried the GO term (Ashburner et al., 2000) association of the interactors and found an enrichment (47 of the 147 hits) for proteins involved in DNA damage repair, replication, and transcription (all highlighted in the network with the gene symbol being selectively colored to reflect various GO term associations as indicated in the key), among other functions (Figure 2B, Figure 3B, Table 5). BRCA1 is already known to participate in the first two functions, but the mechanisms by which it operates in these settings are not completely understood. There is strong evidence that BARD1 plays a role in transcription/RNA processing-associated DNA damage (Kleiman and Manley, 1999, 2001; Kleiman et al., 2005), and BRCA1 is known to interact with RNA Polymerase II and has been suggested to have some role in transcription and transcription coupled repair (Le Page et al., 2000; Scully et al., 1997a). However, the relevance of this interaction and the link between BRCA1 and transcription is mechanistically undefined. Therefore, insights into such a BRCA1 function would be valuable.

Defective RNA processing or halting of transcription may arise from loss of function of relevant RNA binding proteins or physiological transcription modulating sites or from exogenous lesions in the DNA. All can lead to DNA damage. This can occur through the stabilization of physiologic R loops (structures that consist of the DNA loop formed when a nascent RNA transcript anneals to the transcribed DNA strand leaving the non-transcribed single strand to bubble out and become susceptible to damage if unresolved for prolonged periods), the

Table 5. Association of interactors with various datasets, Related to Figure 2 and Figure 3B: We analyzed our interactors for specific GO term association and also searched various datasets to see if our interactors were included in them. We searched various large cancer screens (Grouped as "Systematic Screens") including the Sleeping Beauty dataset, a list of genes with somatic mutations, a list of genes with significant somatic copy number alterations, a GWAS cancer study, and the interactors identified in a screen of tumor virus proteins. For the "Previous BRCA1 Paper" analysis, we searched for overlap with three other studies that searched for BRCA1 interactors. For the "Known Cancer Gene Analysis" we searched the Sanger Census and results from a group that generated a similar list. The results of these analyses are shown here. A '1' in the column next to the interactor for the various analyses indicates that the interactor was in the dataset or had that GO term associated with it. A 0 indicates that was not the case. These analyses are mapped on the heat map in Figure 3B.

Table 5 (Continued). Association of interactors with various datasets page 1, Related to Figure 2 and Figure 3

Gene annotation		Systematic screen					Previous BRCA1 paper			Known cancer gene		GO annotation			Any list	Categories				
EntrezGeneID	Gene Symbol	Sleeping Beauty	Somatic mutations	Virhost	GWAS	SCNA	Woods et al.	Pujana et al.	Wang et al.	Sanger Census	Vogelstein et al.	Damage	Replication	Transcription	Sum	Systematic screen	Previous BRCA1 paper	Known cancer gene	GO annotation	Sum2
4683	NBN	0	1	0	0	0	1	0	1	1	0	1	1	0	6	1	1	1	1	4
4292	MLH1	0	1	0	0	0	0	0	1	1	1	1	0	0	5	1	1	1	1	4
672	BRCA1	0	0	0	0	0	1	1	0	1	1	1	0	1	6	0	1	1	1	3
5111	PCNA	0	0	1	0	0	0	1	0	0	0	1	1	1	5	1	1	0	1	3
2956	MSH6	0	0	0	0	0	0	0	1	1	1	1	0	0	4	0	1	1	1	3
29086	BABAM1	0	1	0	1	0	1	0	0	0	0	1	0	0	4	1	1	0	1	3
83990	BRIP1	0	0	0	0	0	1	0	0	1	0	1	0	1	4	0	1	1	1	3
1786	DNMT1	0	0	0	0	1	0	1	0	0	1	0	0	0	3	1	1	1	0	3
3301	DNAJA1	0	0	1	0	0	1	0	0	0	0	1	0	0	3	1	1	0	1	3
2274	FHL2	0	0	1	0	0	1	0	0	0	0	0	0	1	3	1	1	0	1	3
10856	RUVBL2	0	0	1	0	0	1	0	0	0	0	1	0	0	3	1	1	0	1	3
4361	MRE11A	0	0	0	0	0	1	1	0	0	0	1	1	0	4	0	1	0	1	2
5932	RBBP8	0	0	0	0	0	1	1	0	0	0	1	0	1	4	0	1	0	1	2
5984	RFC4	0	0	0	0	0	1	1	0	0	0	1	0	0	3	0	1	0	1	2
675	BRCA2	0	0	0	0	0	0	1	0	1	1	0	0	0	3	0	1	1	0	2
8467	SMARCA5	1	0	0	0	0	0	0	0	0	0	1	0	1	3	1	0	0	1	2
5885	RAD21	0	0	0	0	0	0	1	0	0	0	1	0	1	3	0	1	0	1	2
8243	SMC1A	0	1	0	0	0	0	0	0	0	0	1	1	0	3	1	0	0	1	2
25836	NIPBL	1	0	0	0	0	0	0	0	0	0	1	0	1	3	1	0	0	1	2
3838	KPNA2	0	0	1	0	0	1	0	0	0	0	0	0	0	2	1	1	0	0	2
10445	MCRS1	0	0	0	0	0	1	0	0	0	0	1	0	0	2	0	1	0	1	2
84142	FAM175A	0	0	0	0	0	1	0	0	0	0	1	0	0	2	0	1	0	1	2
9577	BRE	0	0	0	0	0	1	0	0	0	0	1	0	0	2	0	1	0	1	2
580	BARD1	0	0	0	0	0	1	0	0	0	0	1	0	0	2	0	1	0	1	2
8204	NRIP1	1	0	0	0	0	0	0	0	0	0	0	0	1	2	1	0	0	1	2
5127	CDK16	1	0	0	0	0	1	0	0	0	0	0	0	0	2	1	1	0	0	2
23063	WAPAL	1	0	0	0	0	0	0	0	0	0	0	1	0	2	1	0	0	1	2
56852	RAD18	0	0	0	0	0	1	0	0	0	0	1	0	0	2	0	1	0	1	2
5430	POLR2A	0	0	0	0	0	1	0	0	0	0	1	0	0	2	0	1	0	1	2
79184	BRCC3	0	0	0	0	0	1	0	0	0	0	1	0	0	2	0	1	0	1	2
11335	CBX3	1	0	0	0	0	1	0	0	0	0	0	0	0	2	1	1	0	0	2
3726	JUNB	0	0	1	0	0	0	0	0	0	0	0	0	1	2	1	0	0	1	2
4839	NOP2	1	0	0	0	0	1	0	0	0	0	0	0	0	2	1	1	0	0	2
1453	CSNK1D	1	0	0	0	0	0	0	0	0	0	1	0	0	2	1	0	0	1	2
51720	UIMC1	0	0	0	0	0	1	0	0	0	0	1	0	0	2	0	1	0	1	2
2355	FOSL2	0	0	1	0	0	0	0	0	0	0	0	0	1	2	1	0	0	1	2
4926	NUMA1	0	0	0	0	0	1	0	0	1	0	0	0	0	2	0	1	1	0	2
6924	TCEB3	0	0	0	0	0	1	0	0	0	0	0	0	1	2	0	1	0	1	2
4796	NFKBIL2	1	0	0	0	0	0	0	0	0	0	1	0	0	2	1	0	0	1	2
192111	PGAM5	0	0	1	0	0	1	0	0	0	0	0	0	0	2	1	1	0	0	2
11073	TOPBP1	0	0	0	0	0	0	1	0	0	0	1	0	0	2	0	1	0	1	2
23368	PPP1R13B	1	0	1	0	0	0	0	0	0	0	0	0	0	2	1	0	0	0	1
10524	KAT5	0	0	0	0	0	0	0	0	0	0	1	0	1	2	0	0	0	1	1
10111	RAD50	0	0	0	0	0	1	0	1	0	0	0	0	0	2	0	1	0	0	1
7874	USP7	1	0	1	0	0	0	0	0	0	0	0	0	0	2	1	0	0	0	1
9643	MORF4L2	0	0	0	0	0	0	0	0	0	0	1	0	1	2	0	0	0	1	1
9126	SMC3	0	0	0	0	0	0	0	0	0	0	1	1	0	2	0	0	0	1	1
285753	CEP57L1	0	0	1	1	0	0	0	0	0	0	0	0	0	2	1	0	0	0	1
57459	GATAD2B	1	0	1	0	0	0	0	0	0	0	0	0	0	2	1	0	0	0	1
6122	RPL3	0	0	1	0	0	0	0	0	0	0	0	0	0	1	1	0	0	0	1
5982	RFC2	0	0	0	0	0	1	0	0	0	0	0	0	0	1	0	1	0	0	1
5981	RFC1	0	0	0	0	0	0	0	0	0	0	1	0	0	1	0	0	0	1	1
117178	SSX2IP	0	0	1	0	0	0	0	0	0	0	0	0	0	1	1	0	0	0	1
9569	GTF2IRD1	1	0	0	0	0	0	0	0	0	0	0	0	0	1	1	0	0	0	1
3835	KIF22	0	0	0	0	0	0	0	0	0	0	1	0	0	1	0	0	0	1	1
84985	FAM83A	0	1	0	0	0	0	0	0	0	0	0	0	0	1	1	0	0	0	1
3932	LCK	0	0	0	0	0	0	0	0	1	0	0	0	0	1	0	0	1	0	1
6919	TCEA2	0	0	0	0	0	0	0	0	0	0	0	0	1	1	0	0	0	1	1
84140	FAM161A	0	0	1	0	0	0	0	0	0	0	0	0	0	1	1	0	0	0	1
79035	OBFC2B	0	0	0	0	0	0	0	0	0	0	1	0	0	1	0	0	0	1	1
10969	EBNA1BP2	0	0	0	0	0	1	0	0	0	0	0	0	0	1	0	1	0	0	1
26009	ZZZ3	1	0	0	0	0	0	0	0	0	0	0	0	0	1	1	0	0	0	1
57606	SLAIN2	0	0	1	0	0	0	0	0	0	0	0	0	0	1	1	0	0	0	1
5395	PMS2	0	0	0	0	0	0	0	0	1	0	0	0	0	1	0	0	1	0	1
84446	BRSK1	0	0	0	0	0	0	0	0	0	0	1	0	0	1	0	0	0	1	1
6144	RPL21	0	0	1	0	0	0	0	0	0	0	0	0	0	1	1	0	0	0	1
4288	MKI67	0	0	0	0	0	1	0	0	0	0	0	0	0	1	0	1	0	0	1
79728	PALB2	0	0	0	0	0	0	0	0	1	0	0	0	0	1	0	0	1	0	1
8881	CDC16	0	0	0	0	0	1	0	0	0	0	0	0	0	1	0	1	0	0	1
1408	CRY2	0	0	0	0	0	0	0	0	0	0	1	0	0	1	0	0	0	1	1
1725	DHPS	0	0	0	0	1	0	0	0	0	0	0	0	0	1	1	0	0	0	1
23064	SETX	0	0	0	0	0	0	0	0	0	0	1	0	0	1	0	0	0	1	1
9416	DDX23	0	0	0	0	0	1	0	0	0	0	0	0	0	1	0	1	0	0	1
8500	PPFIA1	0	0	1	0	0	0	0	0	0	0	0	0	0	1	1	0	0	0	1
170082	TCEANC	0	0	0	0	0	0	0	0	0	0	0	0	1	1	0	0	0	1	1
7153	TOP2A	0	0	0	0	0	0	1	0	0	0	0	0	0	1	0	1	0	0	1
6207	RPS13	0	0	1	0	0	0	0	0	0	0	0	0	0	1	1	0	0	0	1
5563	PRKAA2	0	0	1	0	0	0	0	0	0	0	0	0	0	1	1	0	0	0	1
9020	MAP3K14	1	0	0	0	0	0	0	0	0	0	0	0	0	1	1	0	0	0	1
5715	PSMD9	0	0	0	0	0	0	0	0	0	0	1	0	0	1	0	0	0	1	1
862	RUNX1T1	0	0	0	0	0	0	0	0	1	0	0	0	0	1	0	0	1	0	1
22885	ABLIM3	0	0	0	0	0	0	0	0	0	0	0	0	1	1	0	0	0	1	1
90060	CCDC120	0	0	1	0	0	0	0	0	0	0	0	0	0	1	1	0	0	0	1
1051	CEBPB	0	0	1	0	0	0	0	0	0	0	0	0	0	1	1	0	0	0	1
1196	CLK2	0	0	1	0	0	0	0	0	0	0	0	0	0	1	1	0	0	0	1
157313	CDCA2	0	0	0	1	0	0	0	0	0	0	0	0	0	1	1	0	0	0	1
9219	MTA2	0	0	0	0	0	1	0	0	0	0	0	0	0	1	0	1	0	0	1
11043	MID2	0	0	1	0	0	0	0	0	0	0	0	0	0	1	1	0	0	0	1
58529	MYOZ1	0	0	1	0	0	0	0	0	0	0	0	0	0	1	1	0	0	0	1

Table 5 (Continued). Association of interactors with various datasets page 2, Related to Figure 2 and Figure 3

Gene annotation		Systematic screen					Previous BRCA1 paper			Known cancer gene		GO annotation			Any list						Categories
EntrezGeneID	Gene Symbol	Sleeping Beauty	Somatic mutations	Virhost	GWAS	SCNA	Woods et al.	Pujana et al.	Wang et al.	Sanger Census	Vogelstein et al.	Damage	Replication	Transcription	Sum	Systematic screen	Previous BRCA1 paper	Known cancer gene	GO annotation		Sum2
9586	CREB5	0	0	1	0	0	0	0	0	0	0	0	0	0	1	1	0	0	0		1
6232	RPS27	1	0	0	0	0	0	0	0	0	0	0	0	0	1	1	0	0	0		1
4999	ORC2L	0	0	0	0	0	0	0	0	0	0	0	0	1	1	0	0	0	1		1
10061	ABCF2	0	0	0	0	0	0	0	0	0	0	0	0	0	0	0	0	0	0		0
79632	FAM184A	0	0	0	0	0	0	0	0	0	0	0	0	0	0	0	0	0	0		0
10069	RWDD2B	0	0	0	0	0	0	0	0	0	0	0	0	0	0	0	0	0	0		0
84916	CIRH1A	0	0	0	0	0	0	0	0	0	0	0	0	0	0	0	0	0	0		0
148281	SYT6	0	0	0	0	0	0	0	0	0	0	0	0	0	0	0	0	0	0		0
84256	FLYWCH1	0	0	0	0	0	0	0	0	0	0	0	0	0	0	0	0	0	0		0
23371	TENC1	0	0	0	0	0	0	0	0	0	0	0	0	0	0	0	0	0	0		0
79571	GCC1	0	0	0	0	0	0	0	0	0	0	0	0	0	0	0	0	0	0		0
1674	DES	0	0	0	0	0	0	0	0	0	0	0	0	0	0	0	0	0	0		0
8907	AP1M1	0	0	0	0	0	0	0	0	0	0	0	0	0	0	0	0	0	0		0
151254	ALS2CR11	0	0	0	0	0	0	0	0	0	0	0	0	0	0	0	0	0	0		0
6158	RPL28	0	0	0	0	0	0	0	0	0	0	0	0	0	0	0	0	0	0		0
10112	KIF20A	0	0	0	0	0	0	0	0	0	0	0	0	0	0	0	0	0	0		0
79039	DDX54	0	0	0	0	0	0	0	0	0	0	0	0	0	0	0	0	0	0		0
254187	TSGA10IP	0	0	0	0	0	0	0	0	0	0	0	0	0	0	0	0	0	0		0
55226	NAT10	0	0	0	0	0	0	0	0	0	0	0	0	0	0	0	0	0	0		0
10212	DDX39	0	0	0	0	0	0	0	0	0	0	0	0	0	0	0	0	0	0		0
89	ACTN3	0	0	0	0	0	0	0	0	0	0	0	0	0	0	0	0	0	0		0
342667	STAC2	0	0	0	0	0	0	0	0	0	0	0	0	0	0	0	0	0	0		0
100132979	GOLGA8D	0	0	0	0	0	0	0	0	0	0	0	0	0	0	0	0	0	0		0
143884	CWF19L2	0	0	0	0	0	0	0	0	0	0	0	0	0	0	0	0	0	0		0
26156	RSL1D1	0	0	0	0	0	0	0	0	0	0	0	0	0	0	0	0	0	0		0
254225	RNF169	0	0	0	0	0	0	0	0	0	0	0	0	0	0	0	0	0	0		0
84033	OBSCN	0	0	0	0	0	0	0	0	0	0	0	0	0	0	0	0	0	0		0
55131	RBM28	0	0	0	0	0	0	0	0	0	0	0	0	0	0	0	0	0	0		0
79680	C22orf29	0	0	0	0	0	0	0	0	0	0	0	0	0	0	0	0	0	0		0
200081	TXLNA	0	0	0	0	0	0	0	0	0	0	0	0	0	0	0	0	0	0		0
56829	ZC3HAV1	0	0	0	0	0	0	0	0	0	0	0	0	0	0	0	0	0	0		0
53632	PRKAG3	0	0	0	0	0	0	0	0	0	0	0	0	0	0	0	0	0	0		0
23090	ZNF423	0	0	0	0	0	0	0	0	0	0	0	0	0	0	0	0	0	0		0
1642	DDB1	0	0	0	0	0	0	0	0	0	0	0	0	0	0	0	0	0	0		0
54433	GAR1	0	0	0	0	0	0	0	0	0	0	0	0	0	0	0	0	0	0		0
9129	PRPF3	0	0	0	0	0	0	0	0	0	0	0	0	0	0	0	0	0	0		0
54552	GNL3L	0	0	0	0	0	0	0	0	0	0	0	0	0	0	0	0	0	0		0
6161	RPL32	0	0	0	0	0	0	0	0	0	0	0	0	0	0	0	0	0	0		0
9877	ZC3H11A	0	0	0	0	0	0	0	0	0	0	0	0	0	0	0	0	0	0		0
7014	TERF2	0	0	0	0	0	0	0	0	0	0	0	0	0	0	0	0	0	0		0
6164	RPL34	0	0	0	0	0	0	0	0	0	0	0	0	0	0	0	0	0	0		0
3161	HMMR	0	0	0	0	0	0	0	0	0	0	0	0	0	0	0	0	0	0		0
22974	TPX2	0	0	0	0	0	0	0	0	0	0	0	0	0	0	0	0	0	0		0
6201	RPS7	0	0	0	0	0	0	0	0	0	0	0	0	0	0	0	0	0	0		0
3082	HGF	0	0	0	0	0	0	0	0	0	0	0	0	0	0	0	0	0	0		0
60312	AFAP1	0	0	0	0	0	0	0	0	0	0	0	0	0	0	0	0	0	0		0
65108	MARCKSL1	0	0	0	0	0	0	0	0	0	0	0	0	0	0	0	0	0	0		0
283471	TMPRSS12	0	0	0	0	0	0	0	0	0	0	0	0	0	0	0	0	0	0		0
84072	HORMAD1	0	0	0	0	0	0	0	0	0	0	0	0	0	0	0	0	0	0		0
1059	CENPB	0	0	0	0	0	0	0	0	0	0	0	0	0	0	0	0	0	0		0
8925	HERC1	0	0	0	0	0	0	0	0	0	0	0	0	0	0	0	0	0	0		0
25926	NOL11	0	0	0	0	0	0	0	0	0	0	0	0	0	0	0	0	0	0		0
10171	RCL1	0	0	0	0	0	0	0	0	0	0	0	0	0	0	0	0	0	0		0
58525	WIZ	0	0	0	0	0	0	0	0	0	0	0	0	0	0	0	0	0	0		0
55907	CMAS	0	0	0	0	0	0	0	0	0	0	0	0	0	0	0	0	0	0		0
160492	IFLTD1	0	0	0	0	0	0	0	0	0	0	0	0	0	0	0	0	0	0		0
9883	POM121	0	0	0	0	0	0	0	0	0	0	0	0	0	0	0	0	0	0		0
9513	FXR2	0	0	0	0	0	0	0	0	0	0	0	0	0	0	0	0	0	0		0

References	
Sleeping Beauty	Rozenblatt-Rosen et al. Nature 2012
Somatic mutations	Rozenblatt-Rosen et al. Nature 2012
Virhost	Rozenblatt-Rosen et al. Nature 2012
GWAS	Tasan et al. in preparation
SCNA	Beroukhim et al. Nature 2010
Woods et al.	Woods et al. Science Signaling 2012
Pujana et al.	Pujana et al. Nature Genetics 2007
Wang et al.	Wang et al. Genes & Development 2000
Sanger Cancer Gene Census	Futreal et al. Nature Rev. Cancer 2004
Vogelstein et al.	Vogelstein et al. Science 2013
GO Damage, Replication, Transcription	The Gene Ontology Consortium. Nature Genetics 2000

damaging of DNA opened up for transcription by exogenous agents, the collision of active transcription complexes and replication forks, and/or through the collapse of stalled transcription complexes (Aguilera and Garcia-Muse, 2012; Helmrich et al., 2013; Li and Manley, 2006; Mischo et al., 2011; Paulsen et al., 2009; Skourti-Stathaki et al., 2011).

BRCA1 is already linked to transcription through its interaction with RNA Polymerase II (Scully et al., 1997a) and to mRNA processing in its binding to BARD1 (Kleiman and Manley, 1999, 2001; Kleiman et al., 2005). Therefore, we hypothesized that BRCA1 plays a significant role in the prevention or repair of DNA damage associated with transcription arrest and/or RNA processing, perhaps along with some of the proteins in our BRCA1 interactor dataset.

BRCA1 depletion leads to increased sensitivity of cells to transcription arrest

To test the validity of this hypothesis, we asked whether BRCA1 depletion leads to increased cell sensitivity to the development of DNA damage that arises in the setting of transcription arrest induced by certain compounds. We found that depletion of BRCA1 led to increased sensitivity to two compounds, each known to halt transcription and to induce DNA damage, DRB (Chodosh et al., 1989) (Figures 5A and 5B, Figure 6A) and alpha-Amanitin (Lindell et al., 1970) (Figures 5C and 5D, Figure 6A). We also demonstrated that the DNA damage caused by alpha-Amanitin is exacerbated in the setting of BRCA1 depletion (Figure 5E, Figure 6A).

To ascertain whether this was a BRCA1 depletion-specific effect, we attempted to rescue the alpha-Amanitin sensitivity of cells depleted of BRCA1 by stably expressing an siRNA-resistant BRCA1 cDNA in these cells (Figures 5F and 5G). Rescue was achieved in repeated

Figure 5. BRCA1 is required to prevent or repair DNA damage associated with transcription arrest: *See also Figure 6A for siRNA validation. **A)** Dose curves and IC50s from the average of a minimum of three experiments in which U2OS cells were transfected with either siGL2, siBRCA1 exon 13, or siBRCA1 3'UTR and tested for sensitivity to varying doses of DRB by colony formation assay. The error bars at each data point of the curves represent the standard deviation between the values from three or more experiments for each siRNA for that data point. The bar graphs represent the IC50 estimated by GraphPad Prism by fitting a non-linear regression to the curves from a minimum of three experiments. In the bar graph, the error bars represent the 95% confidence interval for the estimation of the IC50 from all replicates of the experiment. **B)** Representative photos of U2OS cells incubated in media containing either 40uM DRB or an equivalent volume of ethanol and then stained for the DNA damage marker, γH2AX. **C)** Dose curves and IC50s from the average of three or more experiments for each siRNA in which U2OS cells were transfected with either siGL2, siBRCA1 exon 13, or siBRCA1 3'UTR and tested for sensitivity to varying doses of alpha-Amanitin by colony formation assay. The data were plotted as described in 5A. **D)** Representative photos of U2OS cells incubated in media containing either 0.35uM alpha-Amanitin (AA) or an equivalent volume of ddH2O and stained for the DNA damage marker, γH2AX. **E)** Bar graphs from one of three experiments representing the percentage of cells with two different tail length ranges from alkaline comet assays performed on U2OS cells transfected with siGL2 or siBRCA1 exon 13 in the bar graph on the left or with siGL2 or siBRCA1 3'UTR in the bar graph on the right and then cultured in media containing either 0.35uM alpha-Amanitin (AA) or the equivalent amount of water (H2O) for 24 hours. The differences observed for tail lengths greater than 60 between the different

Figure 5 (Continued). BRCA1 is required to prevent or repair DNA damage associated with transcription arrest: siRNAs and different treatments were all statistically significant (comparisons indicated by brackets connecting pairs of bars being compared) as determined by calculations discussed in Materials and Methods. The results of one of three replicates of these experiments are shown here. All three replicates showed an identical pattern of DNA damage, and all were statistically significant (data not shown). **F)** IP-Western blot of WT HCC38 and HCC38+BRCA1 cDNA lines transfected with siRNAs used in panel G. Arrows indicate various BRCA1 isoforms (p220 is full length BRCA1 and is what we refer to as BRCA1 throughout the text, Δ11b is a shorter isoform lacking exon 11 and with no known functions). **G)** Dose curves and IC50s from the average of three separate experiments in which either WT HCC38 cells or HCC38 cells stably expressing HA-tagged BRCA1 (HCC38 +BRCA1) were transfected with either siGL2 or a BRCA1 siRNA targeting its 3'UTR and tested for sensitivity to varying doses of alpha-Amanitin by colony formation assay plotted as described in 5A

Figure 5 (Continued)

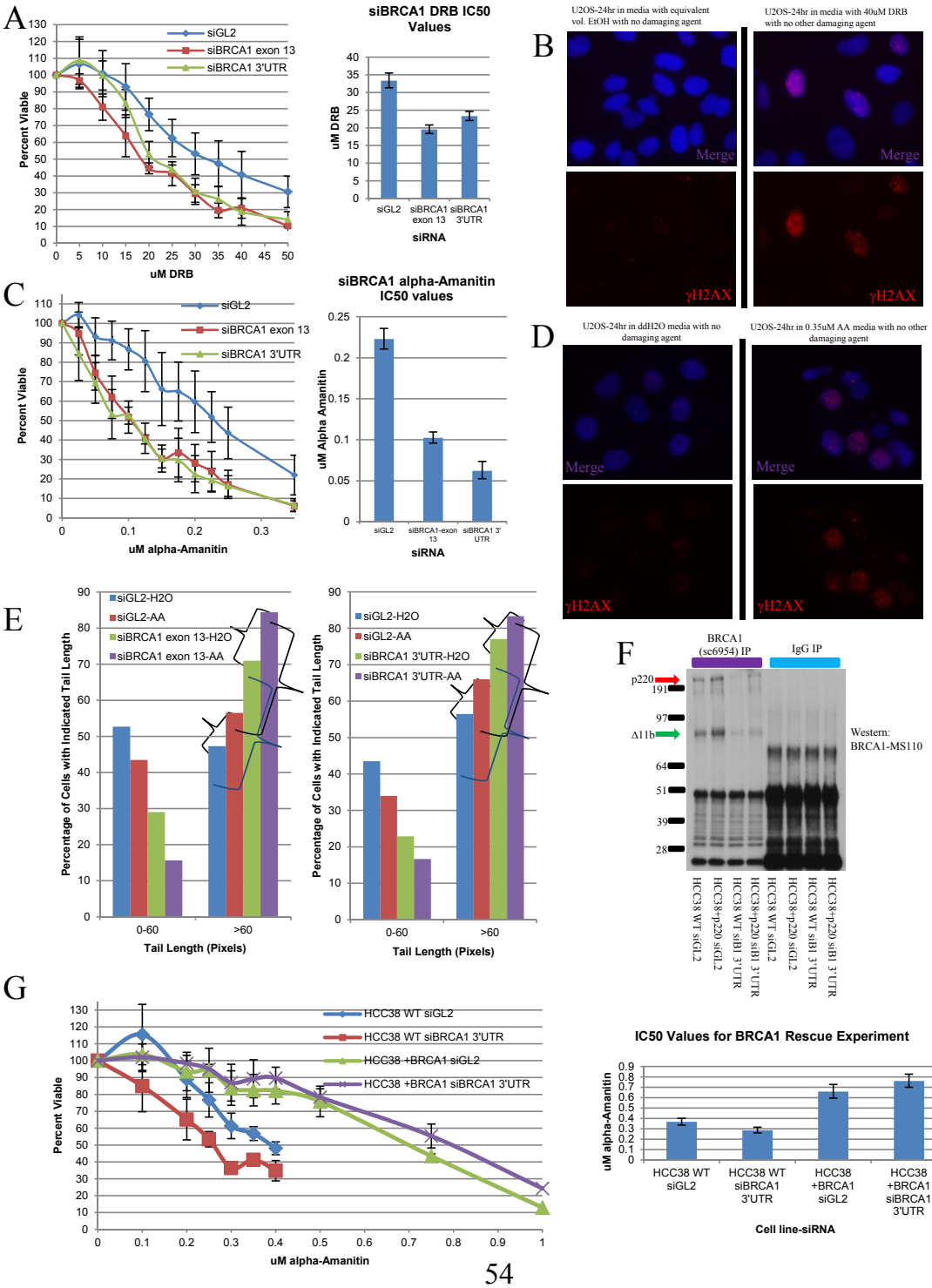

Figure 6. Assessment of siRNAs used in various experiments: A) IP-Western for BRCA1 in the WT/WT, BRCA1+/- and TONSL+/- lines transfected with each BRCA1 siRNA. B1 stands for BRCA1 in all of the cell line and siRNA names below the blots. The exon 13 and 3'UTR targeting siRNAs were used in multiple experiments in WT/WT cells throughout the thesis. **B)** IP-Western for TONSL in the WT/WT, BRCA1+/-, and TONSL+/- lines with each TONSL siRNA. These two TONSL siRNAs were used in multiple experiments in WT/WT cells throughout the thesis. **C)** Western blot of extracts of cells that were transfected with each SSRP1 siRNA. The left panel is blotted with SSRP1, and the right panel is the same blot stripped and re-probed with a tubulin antibody to demonstrate equal loading. These two SSRP1 siRNAs were used in multiple experiments in WT/WT cells throughout the thesis. **D)** IP-Western of WT/WT and BRCA1+/- cells transfected with SUPT16H siRNAs. These two SUPT16H siRNAs were used in multiple experiments in WT/WT cells throughout the thesis. **E)** IP-Western of WT/WT and BRCA1+/- lines transfected with SETX siRNAs. The IP was carried out with an antibody targeting the C-terminus of SETX and the blot with an antibody targeting the N-terminus. **F)** qRT-PCR on cDNAs generated from whole cell RNA harvested from cells transfected with TCEANC siRNAs. The bars represent the average of 5 replicates for the oligo pair/cell line, and the error bars represent the deviation between the replicates. **G)** qRT-PCR on cDNAs generated from whole cell RNA harvested from cells transfected with TCEA2 siRNAs. The bars represent the average of 5 replicates for the oligo pair/cell line, and the error bars represent the deviation between the replicates.

Figure 6 (Continued)

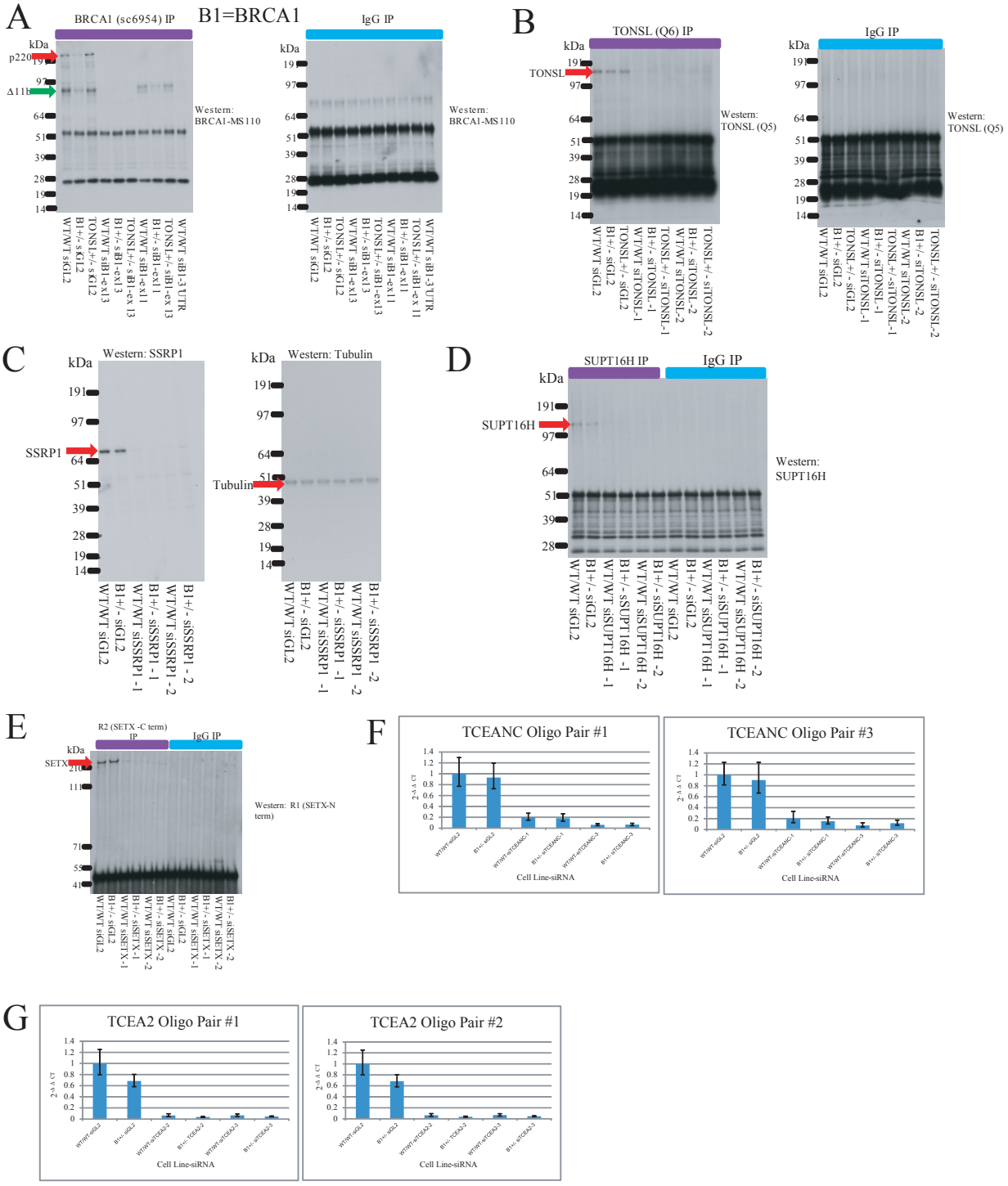

assays.

Taken together, these data support the hypothesis that BRCA1 plays a role in the response to transcription arrest-associated DNA damage. Moreover, BRCA1 may well play a major role in this process, since, when the BRCA1 concentration was increased over the baseline level, alpha-Amanitin sensitivity decreased significantly (Figure 5G-right panel, compare lanes 1 and 3).

Chapter 3-Physiologic and clinical validation of hits from bipartite screening effort

-All writing for this chapter was performed by SJH. All experiments in this chapter were performed by SJH. J. Keith Joung, Deepak Reyon, and Shengdar Q. Tsai generated the TALEN plasmids. Ronny Drapkin aided in the IHC in Figure 10. Thomas Rolland aided in the statistical analysis of the data and Travis I. Zack and Rameen Beroukhim aided in the TCGA analysis of the screen hits. All figures in this chapter were generated by SJH.

BRCA1 interacts genetically with transcription-associated proteins

The results in Chapter 2 prompted a search for links between BRCA1 and transcription-related proteins identified in our screens. To assess the physiological relevance between BRCA1 and previously unknown interactors from our screens, we searched for genetic interactions in cell lines bearing heterozygous mutations (generated by TALENs (Joung and Sander, 2013)) in *BRCA1* or a given interactor. Verification of mutations, and, where relevant, of the decreased expression of a protein of interest is shown in Figure 7A-F. We confirmed that all cells that were studied proliferated and cycled at the same rate as wild-type (WT) controls, so that no abnormal phenotypes could be attributed to a cell cycle proliferation defect (Figure 7G). Searching for genetic interactions in such heterozygous mutant lines as a means of validating novel interactions is a reasonable approach, given that a recent study in cells heterozygous for mutations in the BRCA1 binding partner, PALB2, demonstrated that PALB2 heterozygosity can be associated with phenotypes that have mechanistic and biological implications (Nikkila et al., 2013).

Thus, we posed the question of whether a BRCA1 heterozygous cell line reveals synthetic lethality upon depletion of a BRCA1 interacting protein of interest. Positive results would reflect a breakdown in the physiological interaction between these proteins.

Figure 7. Generation of U2OS cells heterozygous for mutations in either BRCA1 or TONSL: A) Chromatogram depicting the TALEN cut site in a wildtype BRCA1 cDNA clone (left panel) and in a clone heterozygous for a BRCA1 mutation (right panel). The red arrow indicates the start of the mutation in one copy. **B)** On the top, the sequences of the wildtype BRCA1 copy and mutant BRCA1 copy in the heterozygous clone are overlaid to depict the four base pair deletion in the mutant copy. Below this is depicted the mRNA coding sequence for p220, and the start site of the four base pair deletion early in the coding sequence is indicated by a red arrow. **C)** BRCA1 IP-Western in the WT/WT line and BRCA1 +/- clone. **D)** Chromatogram depicting the TALEN cut site in a wildtype TONSL line (left panel) and a clone heterozygous for a TONSL mutation (right panel). The red arrow indicates the start of the mutation in one copy. **E)** On the top, the sequences of the wildtype TONSL copy and mutant TONSL copy in the heterozygous clone are overlaid to depict the two base pair deletion in the mutant copy. Below this is the mRNA coding sequence for TONSL, and the start site of the two base pair deletion in the coding sequence is indicated by a red arrow. **F)** TONSL IP-Western in the WT/WT line and TONSL +/- clone. **G)** BrdU FACS profiles of the WT/WT control line, the BRCA1+/- clone (B1=BRCA1), and the TONSL+/- clone. On three separate days, each cell line was plated individually and incubated with BrdU for 30 minutes prior to harvesting for FACS. The bar graphs represent the percentage of cells for each clone in each phase of the cell cycle as an average of the results of three experiments with the error bars representing the standard deviations between the three experiments.

Figure 7 (Continued)

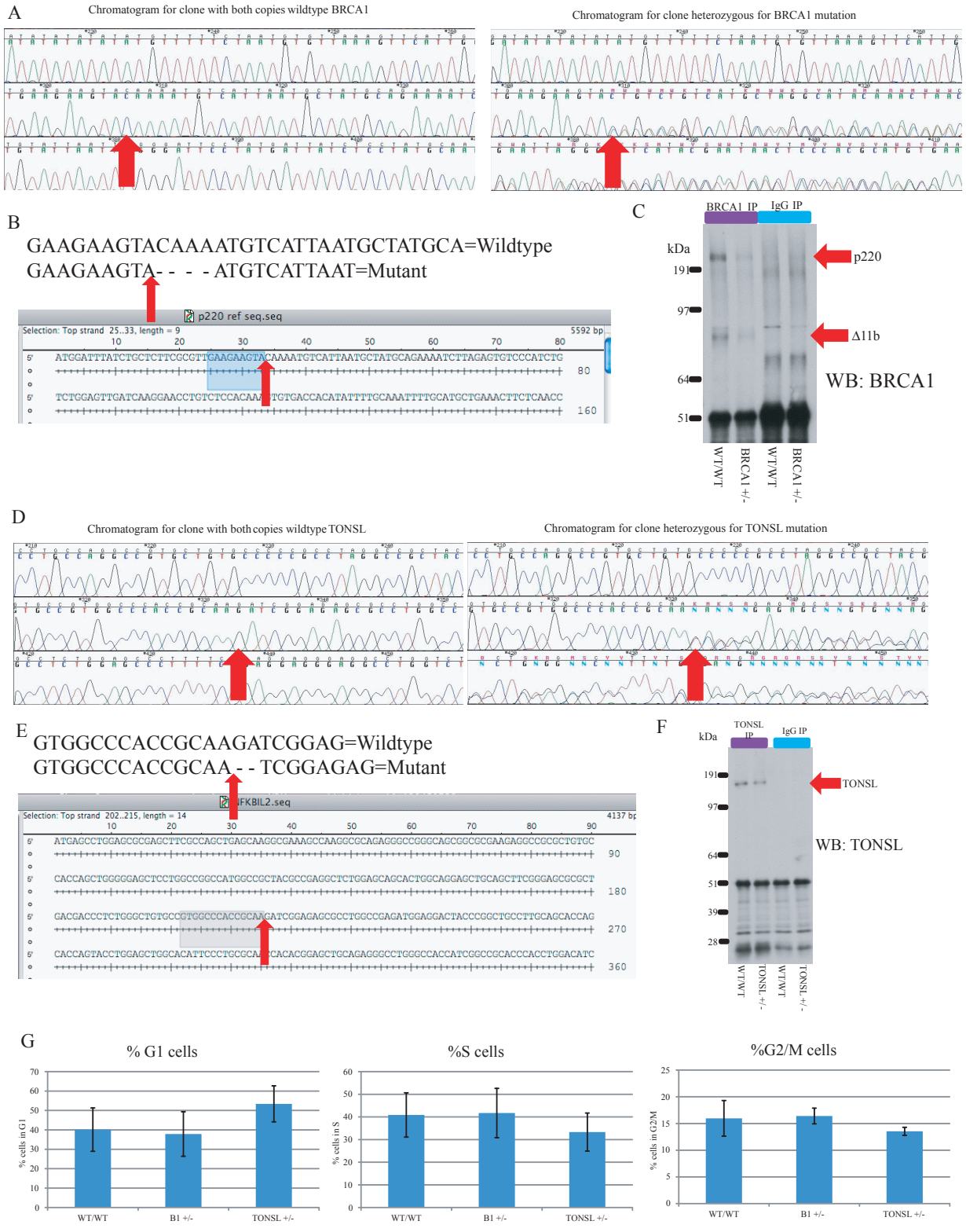

Genetic interaction between BRCA1 and an interactor from the screen was demonstrated by colony formation assays performed on WT/WT and BRCA1+/- cell lines transfected with a control siRNA (siGL2) or with two siRNAs targeting the interactor of interest. If gene-specific depletion led to fewer colonies in the BRCA1+/- line than the WT/WT control, that would reflect a genetic interaction between BRCA1 and the interactor gene of interest.

By colony formation assay, we detected a genetic interaction between BRCA1 and SETX, an RNA helicase that prevents R loop associated damage (Mischo et al., 2011; Skourti-Stathaki et al., 2011) (Figure 8A, Figure 6E). BRCA1 and SETX co-occupy sites on selected meiotic chromosomes (XY body), where the possibility of R loop involvement for both proteins in this setting exists (Becherel et al., 2013). We also detected genetic interactions between BRCA1 and both TCEANC, a transcription elongation factor (Figure 8B and Figure 6F), and TCEA2, yet another transcription elongation factor (Figure 8C and Figure 6G). TCEA2 is a member of a family of proteins that assists RNA polymerase II in traversing pause sites and certain transcription arresting sites (Wind and Reines, 2000). It also engages in responses to DNA damage/errors that arise during transcription (Wind and Reines, 2000). By contrast, the BRCA1-interacting and transcription elongating protein, TCEB3, failed this test, indicating that not all core transcription factors that directly interact with BRCA1 do so in a genetically definable manner.

These results reinforce the view that BRCA1 responds to transcription-based DNA damage, since it influences or is influenced by these transcription-engaging proteins.

Since some of the BRCA1 interactors with which genetic interactions were detected perform different biochemical activities related to this function, one can speculate that BRCA1

Figure 8. BRCA1 genetically interacts with various transcription-associated proteins, one of which has not been previously linked with transcription or transcription-associated DNA damage: A-C) WT/WT and BRCA1+/- cell lines were treated with a control and multiple gene specific siRNAs to look for synthetic lethality upon co-depletion of specific genes with BRCA1. The average number of colonies from one representative experiment is shown for the WT/WT and BRCA1+/- cell lines transfected with either siGL2 or two different siRNAs targeting either SETX **(A)**, TCEANC **(B)**, or TCEA2 **(C)**. The error bars represent the standard deviation between replicates, and the p-values indicate the significance of the difference in colony number between heterozygous mutants and the WT/WT line for the gene-specific siRNA transfections. Due to differences in colony forming efficiency with each siRNA, the siGL2 results can only be compared to siGL2 and so forth. **D)** The average number of colonies from one representative experiment is shown for WT/WT, BRCA1+/-, and TONLS+/- cell lines transfected with either siGL2, siBRCA1 exon 13, or siBRCA1 exon 11. The plots are designed as described above. **E)** The average number of colonies from one representative experiment is shown for WT/WT, BRCA1+/-, and TONLS+/- cell lines transfected with siGL2, siTONSL #1, or siTONSL #2, plotted as described above. The results of only one representative experiment are shown for panels A-E, but these results were replicated in multiple repeats of the same experiments (data not shown). **F)** UV dose curves (left panel) and IC50s (right panel) for cells depleted of TONSL or BRCA1 compared to controls. Cells were transfected with siRNAs, plated at a suitable density for colony formation, treated with varying doses of UV, and later stained and counted. The curves represent the average of four experiments, and the error bars at each data point represent the standard deviation between those four experiments for that point. The bar graphs

Figure 8 (Continued). BRCA1 genetically interacts with various transcription-associated proteins, one of which has not been previously linked with transcription or transcription-associated DNA damage: represent the IC50s estimated by GraphPad Prism from these experiments, and the error bars represent the 95% confidence interval for those estimates. **G)** Representative IF photo of U2OS cells treated with 30J UV-C through micropores and stained for TONSL and BRCA1 four hours after treatment. **H and I)** U2OS cells stably expressing either G1-specific Cdt1-RFP (H) or S phase specific Geminin-GFP (I) degrons were irradiated with 30J through micropores and, 4 hours later, they were stained for BRCA1 and TONSL. Yellow arrows indicate phase-specific cells in which TONSL localized in UV micropores. ** Please note that these images are best viewed in the electronic version of the figure and not on a printed page.

Figure 8 (Continued)

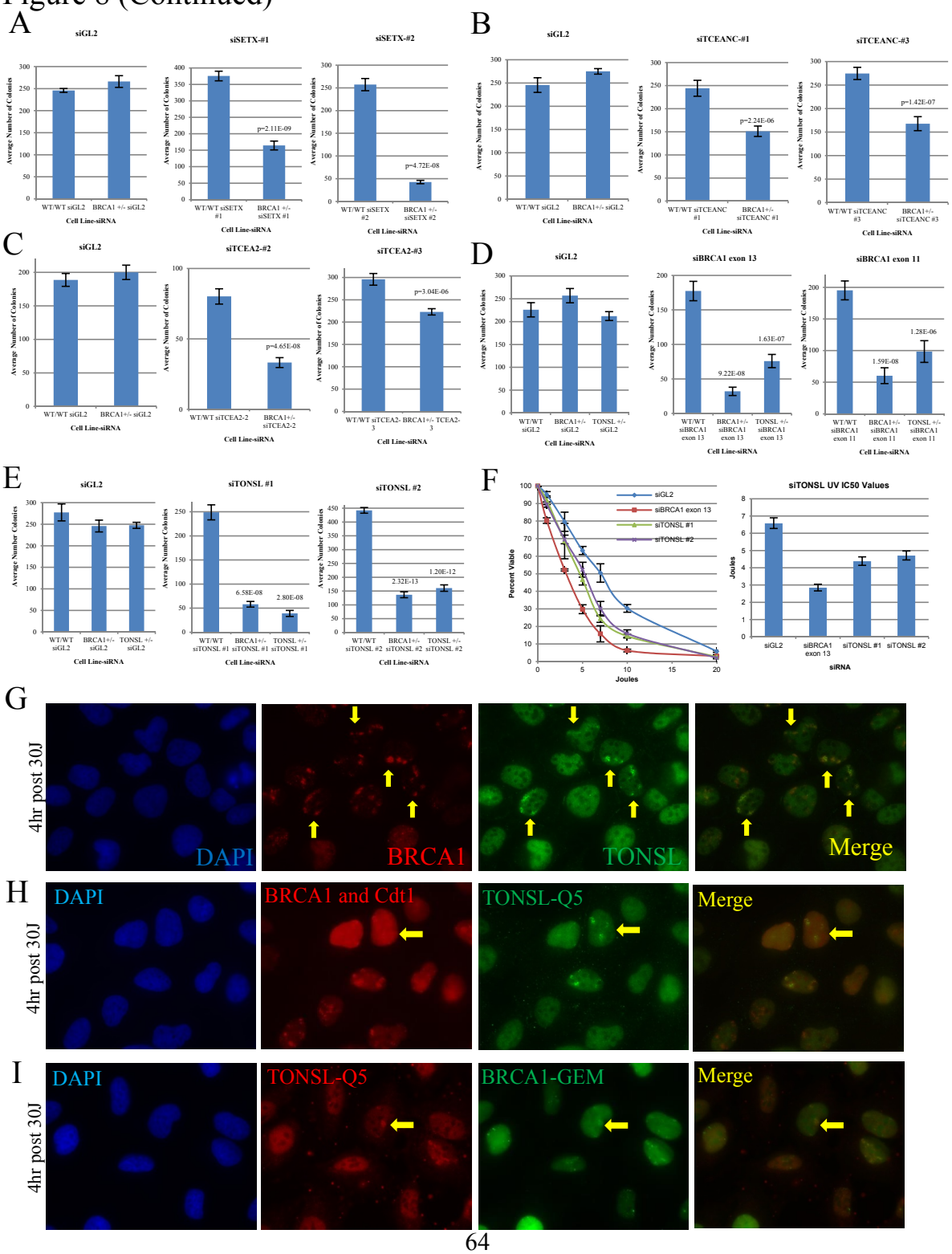

performs its role(s) in this process through a number of biochemical routes, depending upon the specific functionality of its interacting partner protein(s).

Genetic interaction between TONSL and BRCA1

In addition to testing the above-noted transcription related proteins, we also tested another interactor and potential transcription protein, TONSL, which was identified as an interactor in the BARD1 TAP-MS analysis. We focused on TONSL for multiple reasons. First, it was identified in Sleeping Beauty transposon tumorigenesis screens in mice (Figure 3B, Table 5), signifying it as a candidate cancer gene (Starr et al., 2009). In addition, complexes of overexpressed, tagged TONSL and endogenous BRCA1 concentrated in chromatin, consistent with them exerting a genome-associated function(s) (Figure 4B). In this regard, TONSL is already known to participate in the repair of collapsed or stalled replication forks (Duro et al., 2010; O'Connell et al., 2010; O'Donnell et al., 2010; Piwko et al., 2010), which is also a known BRCA1 function (Pathania et al., 2011; Schlacher et al., 2012). However, we have found that TONSL may also participate in the response to transcription-associated damage.

Genetic interaction between BRCA1 and TONSL was demonstrated by colony formation assays performed on WT/WT, BRCA1+/-, and TONSL+/- cells lines (Figure 7A-G) transfected with a control siRNA (siGL2), with two siRNAs targeting BRCA1 (Figure 8D and Figure 6A), or two siRNAs targeting TONSL (Figure 8E and Figure 6B). Compared to WT/WT controls, the BRCA1+/- and TONSL+/- lines were more sensitive to depletion of their respective WT residual proteins, showing that adequate function of each protein was essential for colony formation.

TONSL and BRCA1 localize to UV-induced DNA damage sites

Since TONSL and BRCA1 are both known to participate in the repair of stalled replication forks (Duro et al., 2010; O'Connell et al., 2010; O'Donnell et al., 2010; Pathania et al., 2011; Piwko et al., 2010; Schlacher et al., 2012), we asked whether a BRCA1-TONSL complex is engaged in this repair. To test this possibility, we searched for TONSL localization in UV irradiation-associated nuclear territories (micropores) (Polo et al., 2006) where BRCA1 localizes and where its only known function in such territories, thus far, is in the repair of stalled replication forks (Pathania et al., 2011). Thus, cells were exposed to UV micropore irradiation and then immunostained for TONSL and BRCA1 up to 24 hours thereafter. Like BRCA1, TONSL also localized in micropores (Figure 8G and Figure 9). However, TONSL first appeared there 4-8 hours after irradiation, which is long after BRCA1 had concentrated at these sites (Figure 8G and Figure 9) (Pathania et al., 2011).

Therefore, one manifestation of the BRCA1-TONSL genetic interaction may well operate at sites of UV-induced damage, where both proteins are normally engaged in a complex DNA damage response(s) (Duro et al., 2010; O'Connell et al., 2010; O'Donnell et al., 2010; Pathania et al., 2011; Piwko et al., 2010). Indeed, as one might expect for a protein involved in a UV damage response, cells depleted of TONSL become more sensitive to UV treatment than controls, but not as sensitive as when BRCA1 is depleted (Figure 8F, Figure 6A and 6B). Since TONSL did not localize at micropores in every cell in which BRCA1 was so localized, it is possible that co-localization only occurs during a limited cell cycle interval which may offer a clue as to the function of the BRCA1-TONSL complex.

Figure 9. TONSL localizes to sites of UV damage between four and eight hours after irradiation, Related to Figure 8G: A-G) U2OS cells were exposed to 0 or 30J UV irradiation through micropores and fixed at various timepoints for up to 24 hours thereafter. Cells at the indicated timepoints were stained by immunofluorescence for BRCA1 (red) and TONSL (green). A representative photo for each timepoint is shown here. Yellow arrows indicate cells that reveal TONSL co-localized at UV micropores with BRCA1 (D-F) or in which TONSL co-localized with BRCA1 in nuclear foci in undamaged cells (A). ** Please note that these images are best viewed in the electronic version of the figure and not on a printed page.

Figure 9 (Continued)

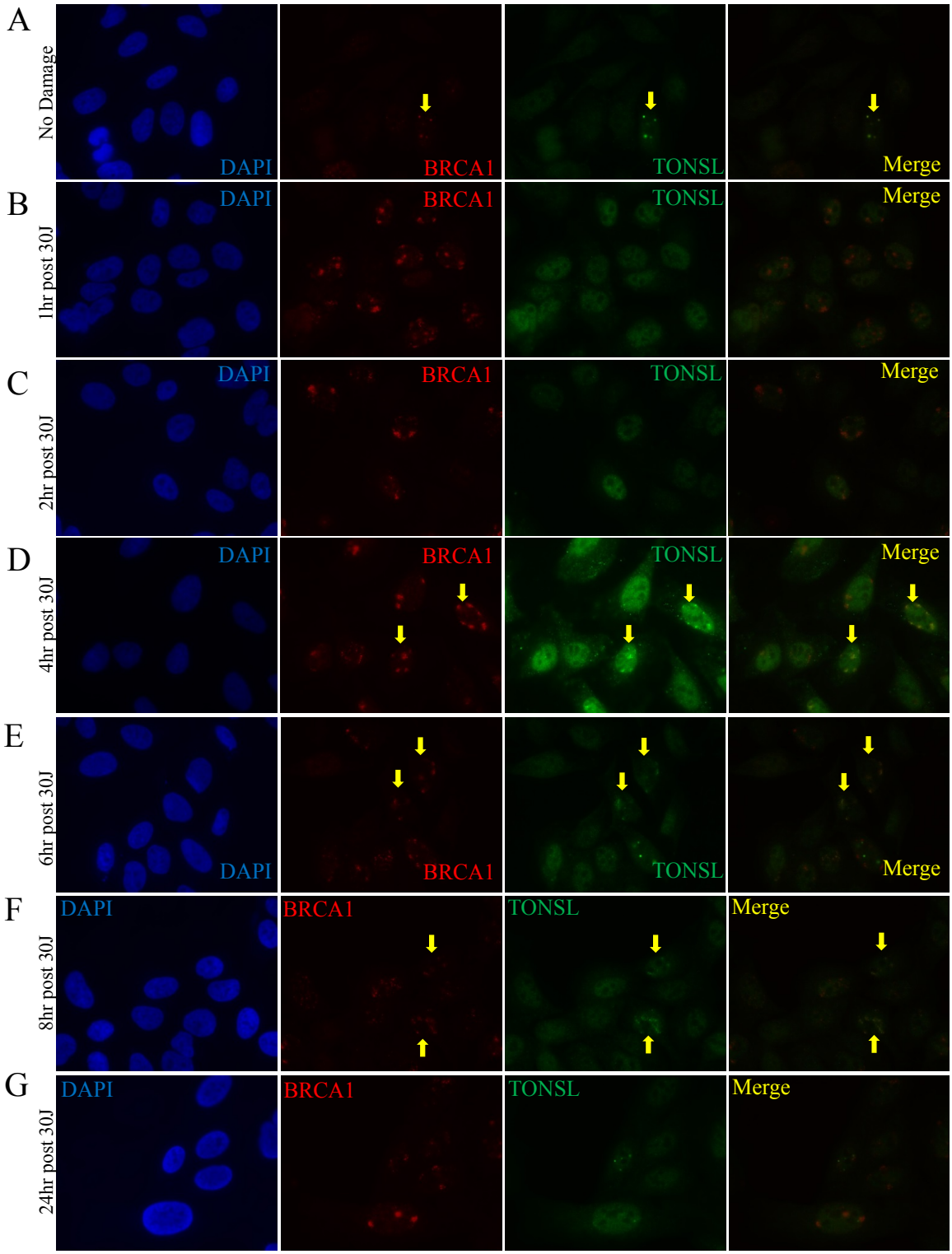

To test this possibility, detection of TONSL and BRCA1 in micropores was assessed in cells expressing cell cycle-dependent reporters (Mechali and Lutzmann, 2008; Sakaue-Sawano et al., 2008). The results showed that TONSL concentrates in these damage sites during both S and G1 phases (Figure 8H and I). The S-phase localization supports the suggested role for TONSL in repair of stalled and collapsed replication forks, but the G1-phase localization does not. The G1 localization result is supported by IHC staining that we had independently performed on normal human fallopian tube for TONSL. We found that TONSL stained the nuclei in both cycling and terminally differentiated cells in this tissue (Figure 10) suggesting that its function may not solely be directed at replication-associated repair. A putative role in the response to transcription-associated DNA damage was also possible.

Indeed, the list of known TONSL interactors includes proteins that function in transcription and that likely operate both in S and G1, in particular both members of the FACT complex, SSRP1 and SUPT16H (Duro et al., 2010; O'Connell et al., 2010; O'Donnell et al., 2010; Piwko et al., 2010). The FACT complex supports transcription elongation through regions of chromatin by facilitating alteration of and accurate replacement of nucleosome structure (Reinberg and Sims, 2006). This allows transcription progression through chromatin regions without permanently disrupting epigenetic markers (Reinberg and Sims, 2006). Such a function could occur in either G1 or S.

TONSL and BRCA1 function at sites of transcription-associated damage together with the FACT complex

Thus, we searched for evidence linking FACT, TONSL, and BRCA1 at UV damage sites. We first asked whether TONSL localization at micropores is dependent upon BRCA1 or FACT.

Figure 10. TONSL is expressed in both cycling and terminally differentiated cells:

A and B) Sections of normal human fallopian tube were stained with both polyclonal antibodies generated against human TONSL for this work (Antibodies Q5 shown in 10A and Q6 shown in 10B). Staining with both antibodies indicated that TONSL was expressed in the nuclei of both cycling fimbriated cells (red arrows) and terminally differentiated secretory cells (green arrows) in this tissue.

Figure 10 (Continued)

Normal Fallopian Tube- TONSL Q5

A

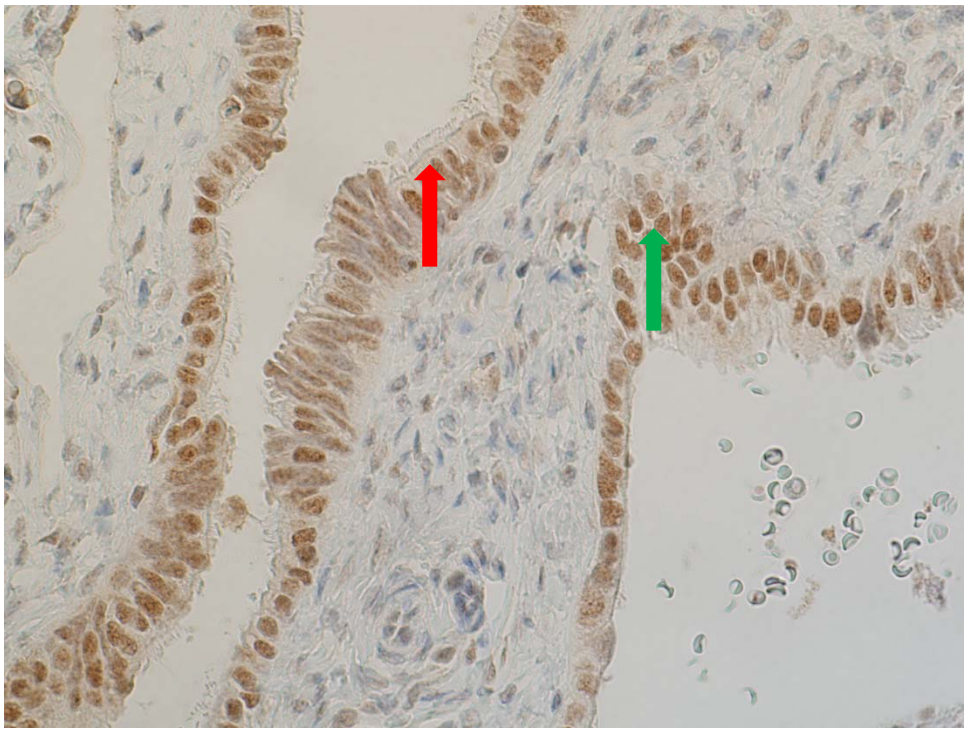

B

Normal Fallopian Tube-TONSL Q6

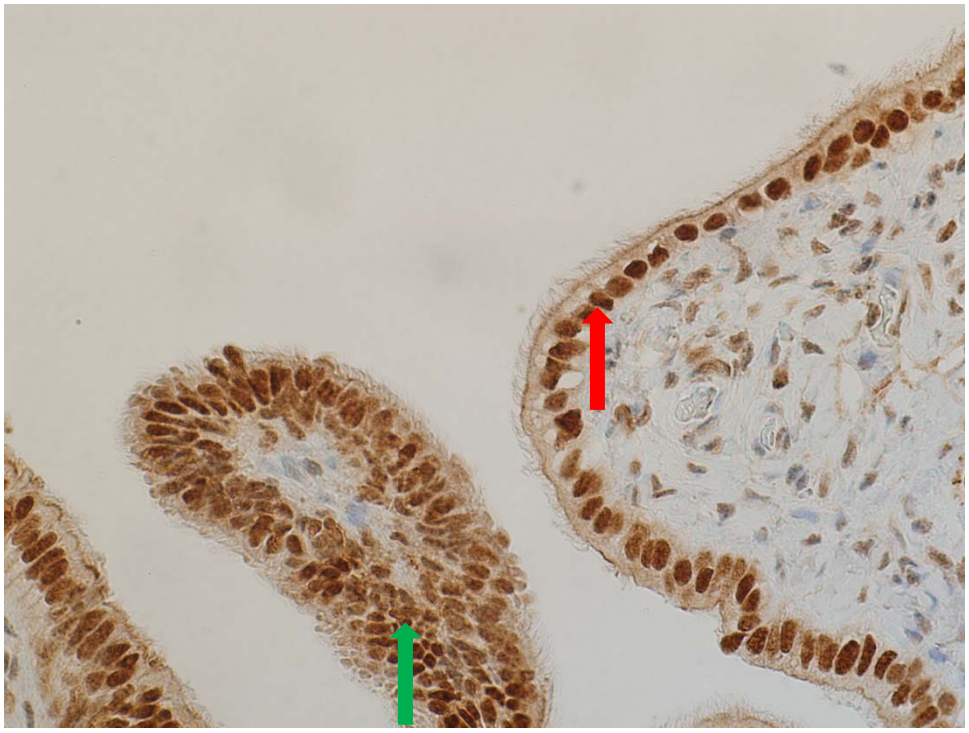

We performed UV micropore assays with and without BRCA1, SSRP1, SUPT16H, and TONSL depletion (Figure 11A, Figure 6A, 6B, 6C, and 6D, and Figure 12A and 12B). While SSRP1, SUPT16H, and TONSL depletion had no effect on BRCA1 micropore localization (Figure 12A), BRCA1, SSRP1, and SUPT16H depletion led to fewer cells exhibiting TONSL in micropores (Figure 11A). Under the conditions employed, none of these depletions caused significant cell cycle arrest (Figure 12B). Thus, BRCA1, SSRP1, and SUPT16H expression is necessary for TONSL localization at these damage sites in asynchronous cells.

Given the influence of FACT on TONSL and the link between TONSL and BRCA1, it was possible that there was also a link between FACT and BRCA1. Thus, we tested for a genetic interaction between BRCA1 and either SSRP1 (Figure 11B and Figure 6C) or SUPT16H (Figure 11C and Figure 6D), again using the colony-formation assay. The BRCA1+/- line produced significantly fewer colonies than the WT/WT line when transfected with siRNAs specific for either SSRP1 or SUPT16H. We concluded that BRCA1 interacts genetically with TONSL and with the TONSL partners SSRP1 and SUPT16H.

Given this association, we wondered if either member of the FACT complex also localizes to UV induced damage sites with BRCA1, and if so, in which phase of the cell cycle this occurs. Therefore, we searched for SSRP1 and SUPT16H in micropores with either TONSL or BRCA1 in both asynchronous cells and cells arrested in G1 by mimosine (Figure 11D-F and Figure 12C). We failed to detect SUPT16H in micropores, but we did find that SSRP1 co-localized with both BRCA1 (Figure 11D) and TONSL (Figure 11E) in micropores in both asynchronous and G1-arrested cells. We also observed that TONSL co-localizes with BRCA1 in both asynchronous and G1-arrested cells (Figure 11F).

Figure 11. BRCA1, TONSL, and FACT functionally interact at sites of UV damage: *See also Figure 6A, 6B, 6C and 6D, Figure 7, and Figure 12. **A)** This bar graph represents the average number of cells containing TONSL in CPD (cyclobutane pyrimidine dimer)-positive micropores from four, separate experiments in which cells were transfected with a control siRNA (siGL2) or one of two different BRCA1, SSRP1, or SUPT16H specific siRNAs. After transfection, the cells were irradiated with 30J UV and stained for BRCA1, CPDs, and TONSL four hours later. The error bars represent the standard deviation between the counts from the four experiments. **B and C)** The average number of colonies from one of three, separate experiments is shown for the WT/WT and BRCA1+/- cell lines transfected with either siGL2 or two different siRNAs targeting either SSRP1 (B) or SUPT16H (C). The plots are designed as described in Figure 8. The results of only one experiment are shown here, but at least two other replicates of these experiments yielded similar data (data not shown). **D-F)** U2OS cells were incubated in media containing 0.5mM mimosine or an equivalent volume of vehicle for 24 hours, then irradiated with 30J through micropores, allowed to recover for 4 hours, and co-stained for SSRP1 and BRCA1 (D), SSRP1 and TONSL (E), and TONSL and BRCA1 (F). Arrows mark some of the cells where co-localization is observed. ** Please note that these images are best viewed in the electronic version of the figure and not on a printed page.

Figure 11 (Continued)

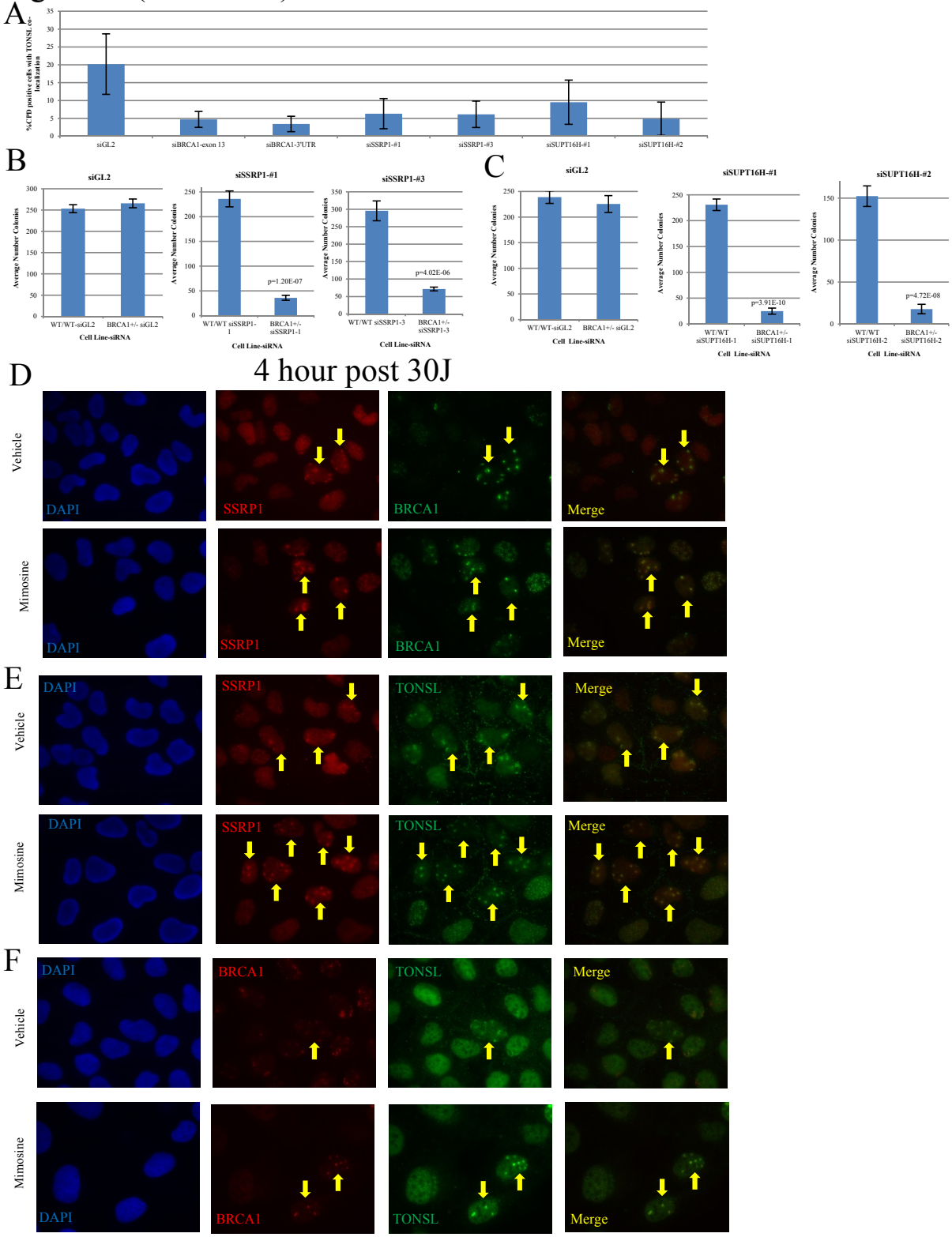

Figure 12. TONSL localizes to sites of UV damage in a BRCA1- and FACT- dependent manner, Related to Figure 11A, 11D, 11E, and 11F: A) Representative photos are shown here for each siRNA treatment demonstrating that BRCA1 localization to micropores was not altered by any of the siRNA treatments from the experiments quantified in figure 11A. U2OS cells were transfected with siRNAs directed at firefly luciferase (siGL2), BRCA1 exon 13, SSRP1, SUPT16H, or TONSL. These cells were irradiated with 30J UV, and 4 hours later were stained for BRCA1, CPDs, and TONSL. ** Please note that these images are best viewed in the electronic version of the figure and not on a printed page. **B)** Representative BrdU FACS analyses on one set of cells studied in figure 11A. The various phases of the cell cycle for each siRNA treatment are depicted here. Below the plots of cells are the percentages of cells in each phase (S, G1, G2/M) for each siRNA treatment. **C)** Representative BrdU FACS analyses on one set of cells studied in the UV micropore mimosine experiments in Figures 11D-F. Plots are as described above in Figure 12B.

Figure 12 (Continued)

A

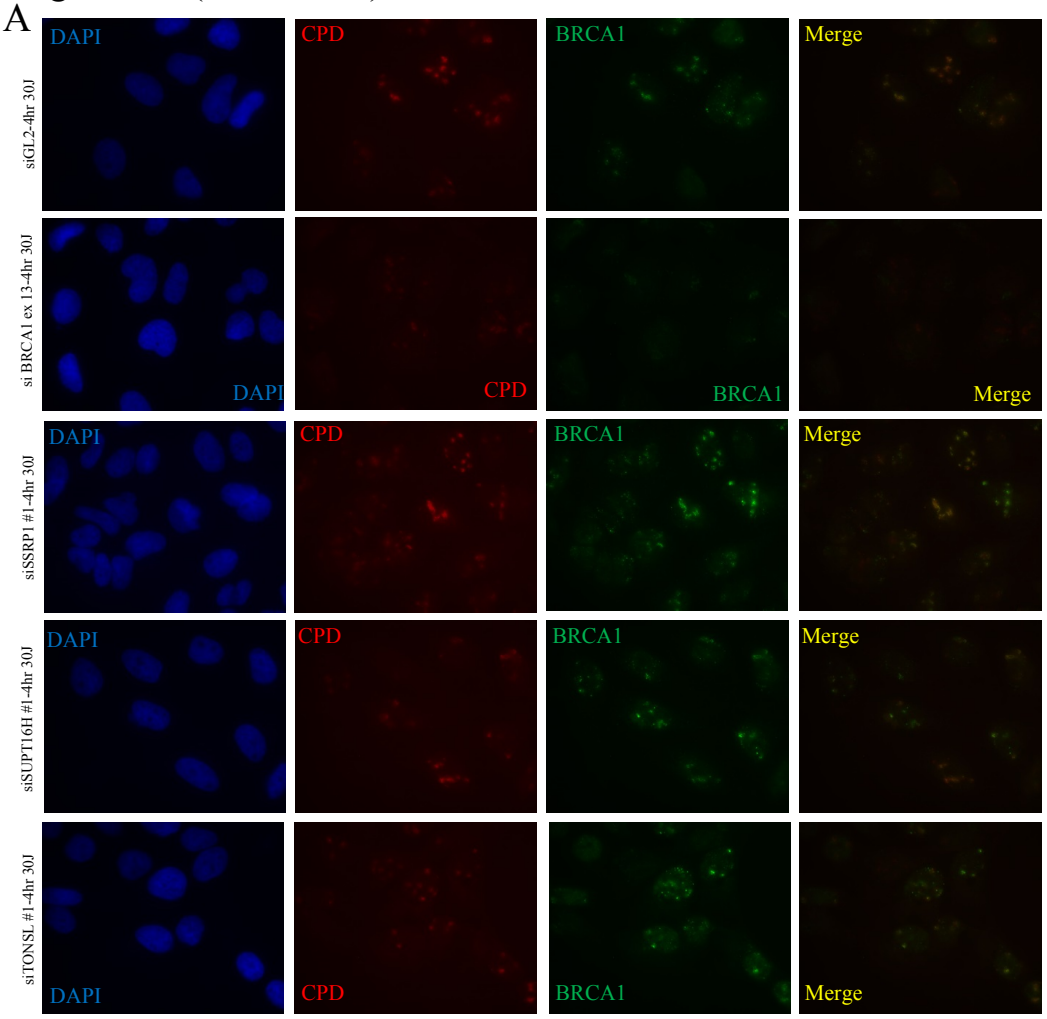

B

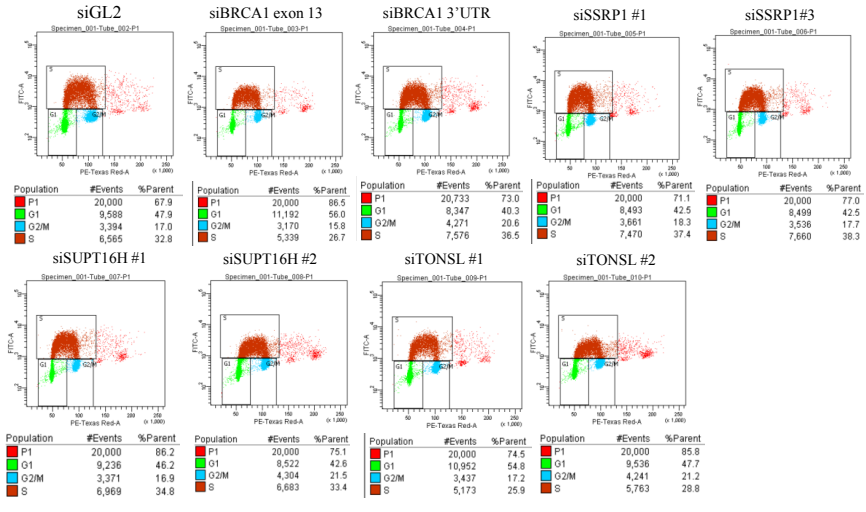

C

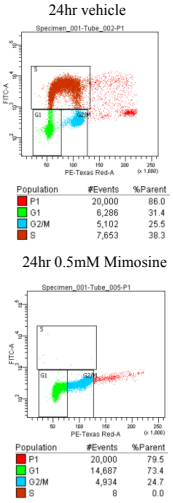

Given the influence of FACT and BRCA1 on TONSL localization, the genetic interactions between FACT and BRCA1 and between TONSL and BRCA1, and the co-localization of FACT, BRCA1, and TONSL at UV damage sites in G1 arrested cells, we speculated that, in addition to aiding in the repair of stalled replication forks, TONSL and BRCA1 co-function with FACT at sites of UV damage to prevent transcription through such sites or contribute to its restart or repair. This hypothesis is supported by the fact that, after UV damage, the FACT complex interacts with RNA PolII pS5 and certain transcription-coupled NER proteins and participates in transcription restart (Dinant et al., 2013).

BRCA1 localizes to sites of post-UV transcription associated DNA damage

To test this hypothesis and determine whether the UV sites at which BRCA1, TONSL, and FACT co-localize do contain transcription associated DNA damage, we asked whether actively transcribing RNA Polymerase II (RNA PolII pS5) co-localizes with the DNA damage marker γH2AX and BRCA1 after UV treatment. We were not able to perform micropore assays because RNA PolII pS5 does not concentrate in these large territories at levels greater than those detected in an unirradiated nucleus. Thus, we performed whole cell UV irradiation since RNA PolII pS5 has been shown to form distinct foci in this setting when cells are appropriately fixed (Espinosa et al., 2003). In preparation for these assays, we validated the specificity of our BRCA1 and RNA PolII pS5 antibodies by various means, since RNA Pol II detection requires harsher fixation conditions than micropore immunofluorescence (IF) staining (Figure 13A-E).

The results showed that active RNA Pol II forms an increased number of distinct foci after UV treatment (Figure 14 and Figure 15B). These foci co-stained with the DNA damage marker, γH2AX, as well as BRCA1 in increased quantities after UV treatment (Figure 14A and

Figure 13. Specificity of RNA Polymerase phospho-S5 antibody, SD123 BRCA1 antibody, and TFIIS antibody all used for immunofluorescence, Related to Figures 14 and 15: A and B) Antibody mixtures to be used for RNA PolII pS5 immunofluorescence staining were prepared as described in Materials and Methods, except 2ug of either an un-phosphorylated peptide encoding the C-terminal domain (CTD) of RNA polymerase II or a peptide encoding the C-terminal domain of RNA polymerase II phosphorylated on serine 5 were added to the mix. These mixtures were incubated at 4° with end over end rotation and were later used to stain U2OS cells that had been treated with 0J or 25J and fixed with methanol-acetic acid four hours later. RNA PolII pS5 staining was unaffected by the un-phosphorylated peptide (A) but was eliminated by the peptide phosphorylated on serine 5 (B). **C-E)** U2OS cells were transfected with either a control siRNA (siGL2) or two different siRNAs targeting BRCA1, treated with 0J or 25J, fixed with methanol-acetic acid 4 hours later, and stained for BRCA1 foci. The BRCA1 foci are greatly reduced in the BRCA1 siRNA treated cells (D and E) compared to the control (C). **F-H)** U2OS cells were transfected with either siGL2 as a control or two different TCEA1 (aka TFIIS) siRNAs, treated with 0J or 25J, fixed with methanol-acetic acid 4 hours later, and stained for TFIIS (aka TCEA1) foci. The TFIIS foci are greatly reduced by the TCEA1 siRNAs (G and H) compared to the control (F). ***The brightness for every photo in the figure has been increased by 40% using Powerpoint to overcome the difficulty of converting to PDF. Please note that these images are best viewed in the electronic version of the figure and not on a printed page.

Figure 13 (Continued)

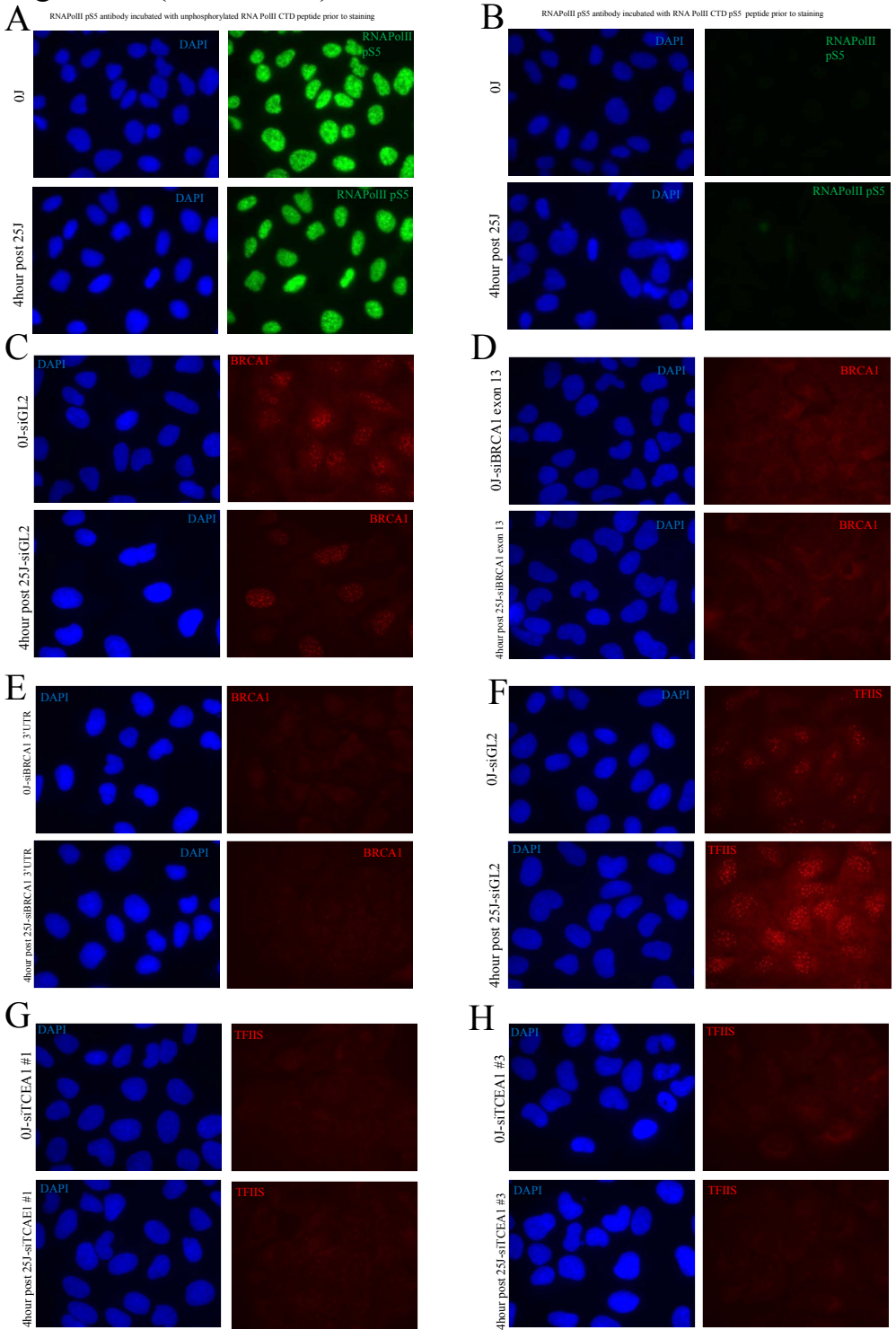

Figure 14. Active RNA Polymerase and BRCA1 co-localize in distinct foci after UV damage: A and B) U2OS cells were treated with 0J or 25J (whole cell irradiation, without micropore filters), fixed with methanol-acetic acid four hours later, and co-stained for either (A) active RNA Polymerase (RNA PolII pS5) and γH2AX or (B) RNA PolII pS5 and BRCA1. One representative photo of a field of cells is shown for each staining after 0J and 25J of UV, and one representative cell from the 25J photo in which there is significant co-localization between the co-stained proteins has been cut out and magnified using Powerpoint below the two fields. Yellow arrows point to the magnified cell in the 25J field of cells photos. In addition, below the photos for each co-staining are counts of the indicated foci present in equivalent numbers of cells after exposure to 0J and 25J. For these counts the same number of nuclei in the 0J and 25J slides were counted, and then the number of individual foci for each antibody and also the number of co-localizing foci from the co-stain were counted within those nuclei. These numbers are represented in the charts below the photos. ***The brightness for every photo in the figure has been increased by 40% using Powerpoint to overcome the difficulty of converting to PDF. Please note that these images are best viewed in the electronic version of the figure and not on a printed page.

Figure 14 (Continued)

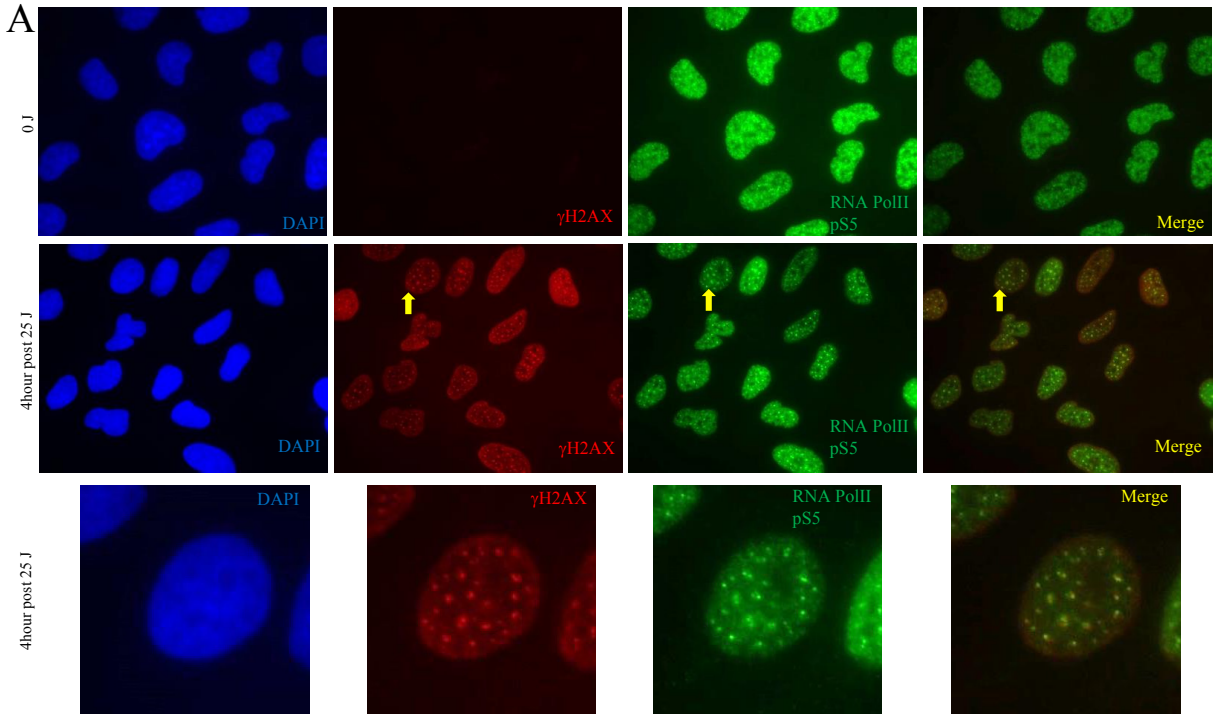

UV Dose	# RNA PolII pS5 foci	# γH2AX foci	#RNA PolII pS5-γH2AX co-localizing foci
0 J	46	10	1
4 hours post 25J	382	498	367

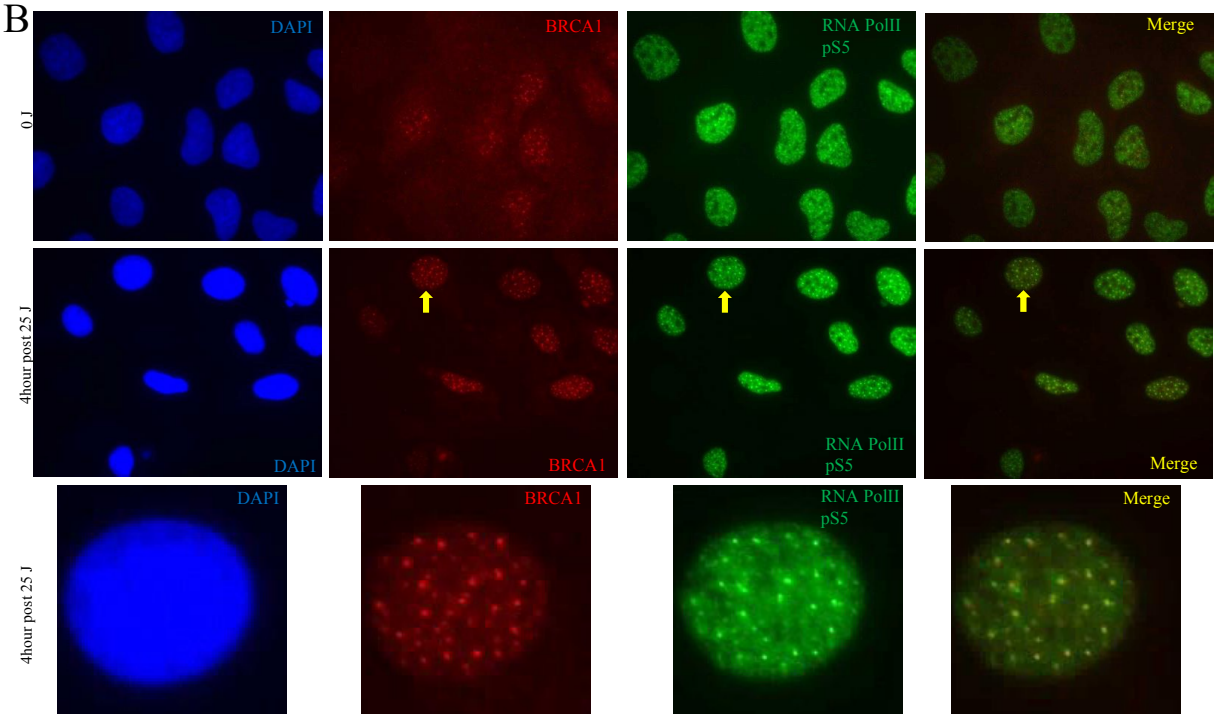

UV Dose	#RNAPolII pS5 foci	#BRCA1 foci	#RNA PolII pS5-BRCA1 co-localizing foci
0 J	93	364	32
4 hours post 25 J	307	213	117

Figure 15. BRCA1 and TFIIS localize to sites of UV induced transcription-associated DNA damage: A and B) U2OS cells were treated with 0J or 25J (whole cell irradiation, without micropore filters), fixed with methanol-acetic acid four hours later, and co-stained for either (A) γH2AX and BRCA1 or (B) RNA PolII pS5 and TFIIS. One representative photo of a field of cells is shown for each staining for 0J and 25J, and one representative cell from the 25J photo in which there is significant co-localization between the co-stained proteins has been cut out and magnified using Powerpoint below the two fields. Yellow arrows point to the magnified cell in the 25J photos. In addition, below the photos for each co-staining are counts of the indicated foci present in equivalent numbers of cells after exposure to 0J and 25J. For these counts the same number of nuclei in the 0J and 25J slides were counted, and then the number of individual foci for each antibody and also the number of co-localizing foci from the co-stain were counted within those nuclei. These numbers are represented in the charts below the photos. ***The brightness for every photo in the figure has been increased by 40% using Powerpoint to overcome the difficulty of converting to PDF. Please note that these images are best viewed in the electronic version of the figure and not on a printed page.

Figure 15 (Continued)

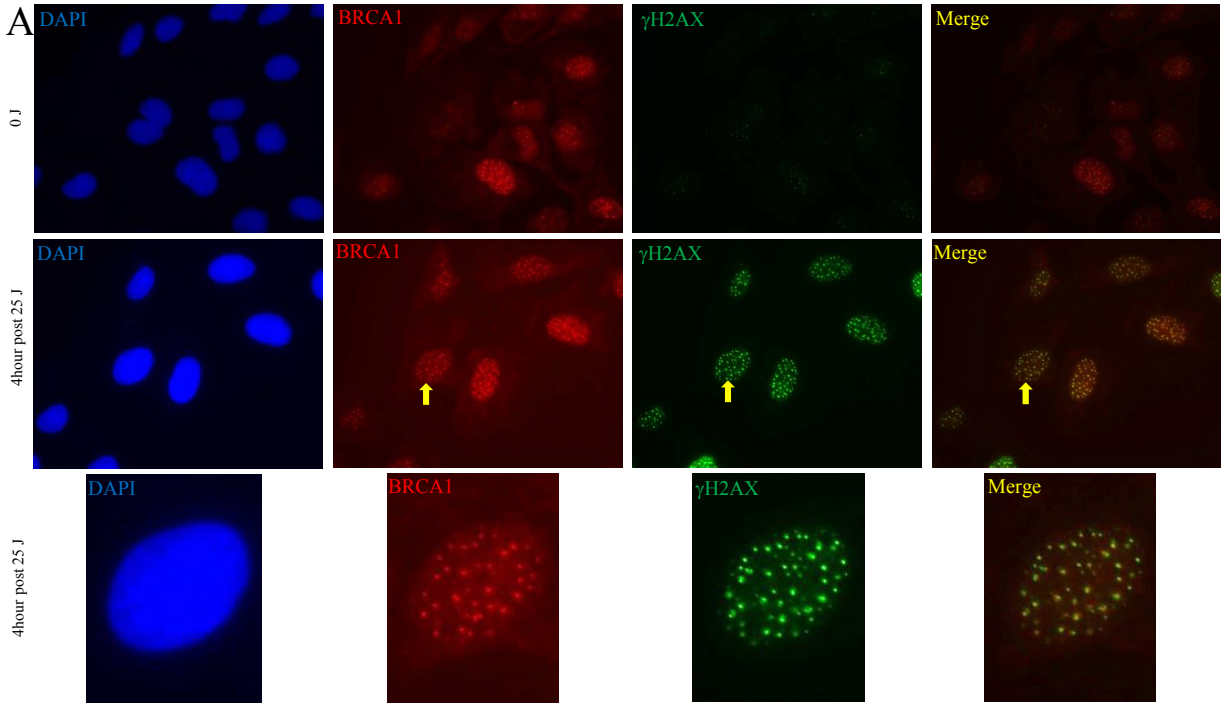

UV Dose	#γH2AX foci	#BRCA1 foci	#γH2AX-BRCA1 co-localizing foci
0 J	83	127	43
4hr post 25 J	410	258	177

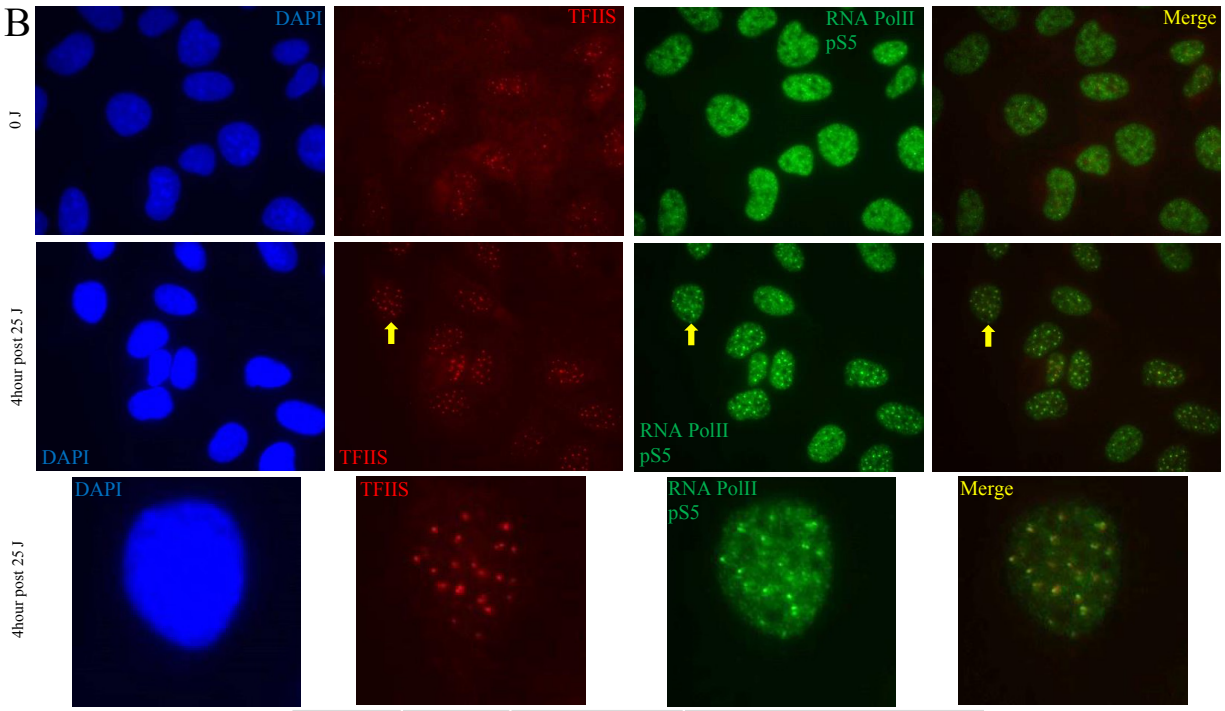

UV Dose	#TFIIS Foci	#RNAPolII pS5 foci	#TFIIS-RNAPolII pS5 co-localizing foci
0J	120	40	1
4hr post 25 J	784	276	174

14B). BRCA1 also co-localized with γH2AX foci after UV treatment (Figure 15A), and since almost all RNA Pol II pS5 foci co-localized with γH2AX after UV and approximately two thirds of all BRCA1 foci co-localize with γH2AX foci after treatment, it appeared that BRCA1 and active RNA Pol II co-localized at most γH2AX-marked damage sites after UV exposure.

To test whether there is single-stranded DNA and, thus, R-loops, collapsed transcription complexes, or perhaps collapsed replication forks that had collided with a transcription fork at these damage sites, we stained for co-localization between BRCA1 and phosphorylated RPA which is known to coat single stranded DNA at such sites (Figure 16B). We found that only one third of BRCA1 foci co-localize with pRPA after UV. Thus R-loops, collapse, and collisions are unlikely to be the only types of transcription associated DNA damage being confronted by BRCA1 at these sites.

One possibility is that BRCA1 has recognized a stalled transcription fork and recruits other proteins to assist its restart. One of the interactors detected in our screen, TCEA2, is a member of the TFIIS family of transcription factors which is responsible for assisting RNA polymerase in overcoming various obstacles encountered while transcribing DNA (Wind and Reines, 2000). Although no available TCEA2 antibodies worked with the relevant fixation protocol, an antibody directed at a closely related isoform, TCEA1 (commonly referred to as TFIIS and referred to as TFIIS in figures and other parts of the thesis), did operate in this staining protocol (Figure 13F-H). Moreover, after UV irradiation almost two thirds of RNA Pol II pS5 foci co-localized with TFIIS (Figure 15B); and almost two thirds of TFIIS foci co-localized with γH2AX (Figure 16A). Thus, TFIIS also localized at post-UV transcription

Figure 16. TFIIS and BRCA1 co-localize with DNA damage markers after UV treatment, Related to Figures 14 and 15: A and B) U2OS cells were treated with 0J or 25J (whole cell irradiation, without micropore filters), fixed with methanol-acetic acid four hours later, and co-stained for either (A) TFIIS and γH2AX or (B) BRCA1 and phosphorylated-RPA (pRPA). One representative photo of a field of cells is shown for each staining for 0J and 25J, and one representative cell from the 25J photo in which there is significant co-localization between the co-stained proteins has been cut out and magnified using Powerpoint below the two fields. Yellow arrows point to the magnified cell in the 25J photos. In addition, below the photos for each co-staining are counts of the indicated foci present in equivalent numbers of cells after exposure to 0J and 25J. For these counts the same number of nuclei in the 0J and 25J slides were counted, and then the number of individual foci for each antibody and also the number of co-localizing foci from the co-stain were counted within those nuclei. These numbers are represented in the charts below the photos. ***The brightness for every photo in the figure has been increased by 40% using Powerpoint to overcome the difficulty of converting to PDF. Please note, that these images are best viewed in the electronic version of the figure and not on a printed page.

Figure 16 (Continued)

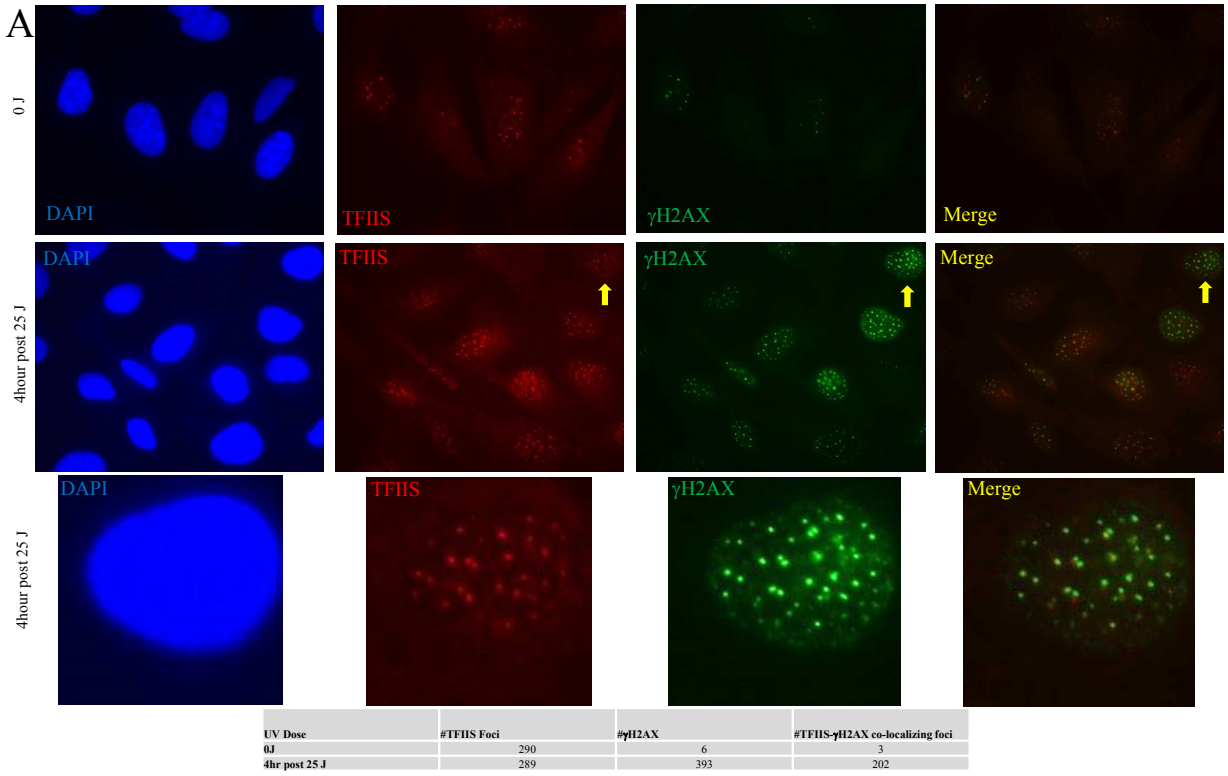

UV Dose	#TFIIS Foci	#γH2AX	#TFIIS-γH2AX co-localizing foci
0J	290	6	3
4hr post 25 J	289	393	202

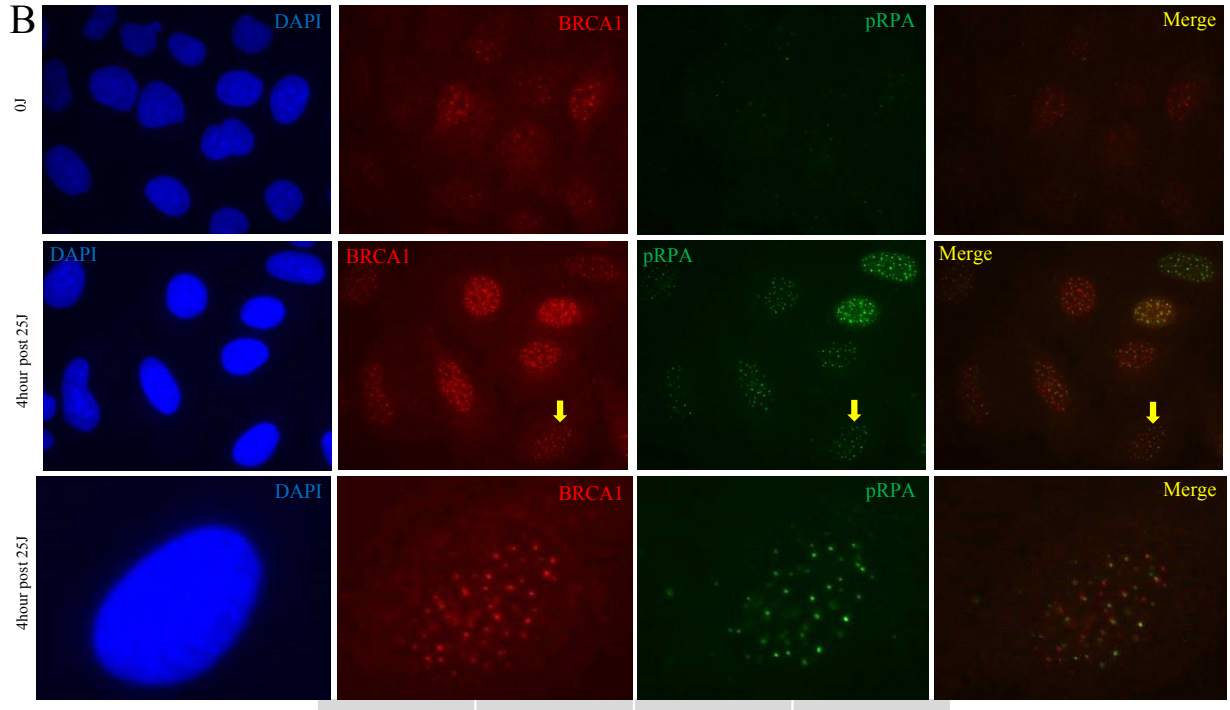

UV Dose	#BRCA1 foci	#pRPA foci	#BRCA1-pRPA foci co-localizing
0 J	125	108	22
4hr post 25 J	468	661	150

associated damage foci, and, given the frequency of TFIIS and BRCA1 foci co-localizing with γH2AX, it is likely that BRCA1 and TFIIS co-localize in some of these foci, as well.

We were unable to test TCEANC, SETX, TONSL, SSRP1, or SUPT16H for RNAPolII pS5 co-localization, since we lacked antibodies that function in this fixation protocol. Nevertheless, this evidence further supports the hypothesis that BRCA1 functions at sites of transcription associated damage and the notion that a BRCA1-TONSL-FACT complex functions at these sites. Given the co-localization of BRCA1 with active RNA Polymerase II at post-UV damage structures, it is likely that a BRCA1-TONSL-FACT complex participates in some part of the recognition or repair of these structures, since these proteins do localize to sites of UV damage in G1-arrested cells where transcription and not DNA replication is in progress and since FACT has already been implicated in such a function (Dinant et al., 2013).

Furthermore, this evidence, along with the above-noted TFIIS staining, implies that BRCA1 can participate in the response to various forms of transcription-associated DNA damage or stalling and that it does so in different ways by interacting with different protein binding partners, such as TFIIS or TONSL-FACT.

Novel BRCA1 interactors identified in our screen exhibit cancer links with therapeutic implications

The question of whether any of our interactors or the new role(s) for BRCA1 in dealing with transcription-associated DNA damage is clinically relevant was also addressed. Oncomine Concepts Map was used (Rhodes et al., 2007) to search for associations between our results and those of prior gene expression profiling studies performed on breast and ovarian cancers. BRCA1 tumor suppression largely extends to these two organs.

The results show that our 147 screening hits are enriched for proteins that are significantly over- or under- expressed in tumors associated with negative clinical outcomes (Figure 17A), high grade pathology (Figure 17B), and advanced clinical stage (Figure 17C). This suggests that a number of interactors experience altered expression in clinically aggressive tumors and may, therefore, contribute to disease progression and lack of therapeutic benefit.

In keeping with these observations, we also asked whether any of our interactors are encoded by genes that map to amplified or deleted regions in breast tumors, ovarian tumors, or across a set of 11 cancer types that have been systematically analyzed (Zack et al., 2013). Indeed, 90 out of 147 of our hits were located within these genomic regions (Figure 17D, Table 6). Sixty-three hits were localized to amplified regions, of which 15 are involved in transcription, replication, and/or DNA damage. Thirty-nine additional hits mapped to deleted regions, of which 12 are known to engage in one or more of these same functions. Moreover, some of the genes we demonstrated as being genetically associated with BRCA1 are located in these regions, including TONSL, TCEA2, and SETX. These data are particularly interesting with respect to TONSL since it was found in a Sleeping Beauty tumor enhancement screen, thereby implying that it affects tumorigenesis, at least in animal models (Figure 3B and Table 5).

One caveat associated with this data is that the regions identified here are large and contain multiple genes. Hence, there is no guarantee that a BRCA1 interactor gene of interest operates as a tumor suppressor or an oncogene in these regions. However, this concern is ameliorated by the fact that 12 of our hits are already known to be cancer-associated (Figure 2B, Figure 3B, Table 5) (Futreal et al., 2004; Vogelstein et al., 2013). Therefore, these data suggest

Figure 17. Clinical outcome relationships of BRCA1 interactome members: A, B, and C) Networks representing statistically significant ($p<0.05$ and $q<0.25$) associations of the 147 hits (central white node) in the BRCA1 interactome with various expression profiling datasets for negative clinical outcomes (Figure 17A), high tumor grade (Figure 17B), and advanced clinical stage (Figure 17C) in Oncomine Concept Map. The key for node color and statistical ranges is defined beneath each network. The edge widths correspond to the p-value for the particular association. **D)** Networks representing the genes from our datasets that were found to be in either amplification (top panel) or deletion (bottom panel) regions in a statistically significant way ($p<0.05$ and $q<0.25$) in a TCGA dataset for breast cancers, ovarian cancers, or across 11 different cancers. The nodes are grouped according to association with select GO terms, and the key to node color is noted below the networks. *See also Table 6.

Figure 17 (Continued)

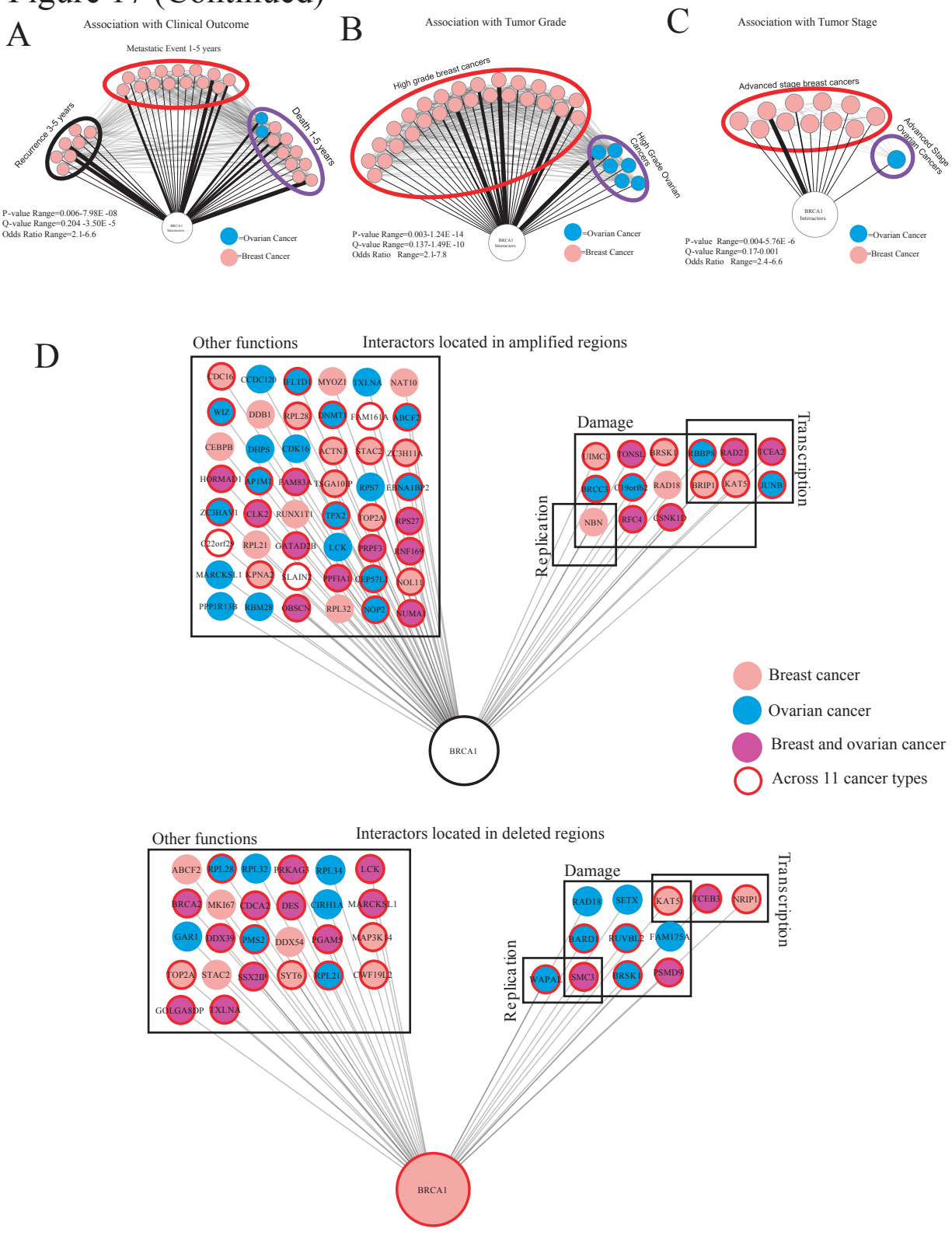

Table 6. Search for location of genes identified in screens in either amplification or deletion regions in breast tumors, ovarian tumors, or across 11 different tumor types, Related to figure 17D: We queried the gene loci of the genes detected as BRCA1 interactors in our screens in TCGA amplification and deletion region datasets for breast cancer, ovarian cancer, and across 11 different cancer types to see if our interactors were in any of these regions. The p-value and q-value for each gene from our dataset being present in each type of region in each type of cancer is shown here. We only plotted genes in the networks in 17D that had a p-value<0.05 and q-value <0.25.

Table 6 (Continued). Search for location of genes identified in screens in either amplification or deletion regions in breast tumors, ovarian tumors, or across 11 different tumor types, Related to figure 17D, page 1

**Only graphed genes with p<0.05 and q<0.25 in the networks

		Across all cancers				Breast Cancer				Ovarian Cancer			
Gene Symbol	Gene ID	Amplification region p-value	Amplification region q-value	Deletion Region p-value	Deletion Region q-value	Amplification region p-value	Amplification region q-value	Deletion Region p-value	Deletion Region q-value	Amplification region p-value	Amplification region q-value	Deletion Region p-value	Deletion Region q-value
ABCF2	10061	0.0012045	0.0084028	0.054063	0.24244	0.94633	1	0.018521	0.12265	4.80E-12	1.06E-10	0.94708	1
AFAP1	60312	1	1	1	1	1	1	0.96952	1	0.58955	1	1	1
BARD1	580	1	1	1.83E-16	2.53E-15	0.99481	1	0.06519	0.33665	0.99134	1	0.020708	0.11162
BRCA1	672	1	1	3.27E-05	0.00020142	0.99493	1	8.74E-10	3.23E-08	1	1	0.055355	0.26118
BRCA2	675	0.99998	1	1.31E-14	1.66E-13	0.79552	1	1.12E-05	0.0001539	0.99999	1	0.0018446	0.012981
BRCC3	79184	2.35E-17	3.79E-16	0.99994	1	0.17132	0.85779	0.97771	1	1.65E-10	3.17E-09	0.97778	1
BRE	9577	0.99338	1	1	1	0.99982	1	0.98595	1	0.18278	0.92775	0.99999	1
BRIP1	83990	7.96E-11	9.78E-10	1	1	1.71E-32	2.83E-30	0.99998	1	0.99936	1	1	1
BABAM1	29086	0.0020904	0.014154	1	1	0.76098	1	0.99966	1	3.88E-13	9.16E-12	1	1
CBX3	11335	1.00E+00	1	1	1	0.94785	1	0.99983	1	0.97911	1	0.93677	1
CDC16	8881	8.76E-05	0.00070575	0.85639	1	0.0074902	0.056489	0.75998	1	0.45917	1	0.11573	0.48507
CDCA2	157313	1	1	0.024477	0.11665	1.00E+00	1.00E+00	0.014146	0.09754	1	1	0.0010028	0.0075064
CEBPB	1051	0.079969	0.41148	1	1	5.64E-07	7.44E-06	1	1	0.61676	1	1	1
CENPB	1059	0.99351	1	1	1	0.99292	1	0.88573	1	0.56957	1	0.99985	1
CIRH1A	84916	1	1	0.99527	1	0.99999	1	0.99563	1	1	1	0.015524	0.08677
CMAS	55907	0.86051	1	1	1	0.99526	1	0.78925	1	0.092626	0.51636	1	1
CREB5	9586	1.00E+00	1.00E+00	1	1	9.46E-01	1.00E+00	0.99981	1	0.99986	1	0.99855	1
CSNK1D	1453	8.56E-16	1.30E-14	0.90241	1	1.97E-11	4.06E-10	0.12375	0.58024	0.00050354	0.0050126	0.99944	1
DDB1	1642	0.7559	1	1	1	0.03889	0.23843	0.19406	0.84057	0.99971	1	0.99998	1
DDX23	9416	1	1	0.99998	1	0.9999	1	0.38568	1	1	1	0.99986	1
CEP57L1	285753	1	1	0.00035964	0.0020665	0.17558	0.87602	2.59E-05	0.00033108	0.99998	1	0.0076158	0.046148
DDX54	79039	1.00E+00	1.00E+00	0.8077	1	1	1	0.025523	0.16082	1.00E+00	1.00E+00	0.11414	0.47933
DNAJA1	3301	2.11E-01	9.63E-01	1	1	0.98058	1	0.96781	1	1.00E+00	1.00E+00	1	1
DNMT1	1786	1.01E-05	8.81E-05	0.94226	1	0.24997	1	0.98405	1	9.52E-08	1.43E-06	0.10792	0.45729
EBNA1BP2	10969	9.45E-12	1.22E-10	1	1	4.41E-01	1.00E+00	0.96952	1	4.50E-18	1.29E-16	1	1
FAM175A	84142	1	1	0.41534	1	0.99919	1	0.96415	1	1	1	0.038954	0.1925
FAM83A	84985	2.46E-108	1.35E-106	1	1	1.41E-19	7.76E-18	1	1	5.58E-79	5.78E-77	1	1
FHL2	2274	1	1	1	1	0.99985	1	0.98502	1	0.99999	1	0.81145	1
FLYWCH1	84256	1	1	0.91383	1	0.77666	1	0.99997	1	1	1	0.42926	1
FOSL2	2355	9.58E-01	1.00E+00	1	1	1.00E+00	1.00E+00	0.99695	1	5.75E-02	3.41E-01	1	1
GAR1	54433	1	1	0.72402	1	0.99936	1	0.74638	1	1	1	0.022744	0.12154
GATAD2B	57459	2.64E-57	9.27E-56	1	1	3.41E-19	1.79E-17	1	1	1.84E-12	4.18E-11	1	1
GNL3L	54552	0.99576	1	1	1	0.91413	1	1	1	0.58457	1	1	1
GTF2IRD1	9569	0.65236	1	1	1	0.29732	1	0.99057	1	0.57207	1	0.9998	1
HERC1	8925	1	1	1	1	0.99049	1	0.99824	1	1.00E+00	1.00E+00	0.998	1
HMMR	3161	0.95437	1	0.16659	0.67451	0.99799	1	0.63524	1	0.94765	1	0.27648	0.97725
JUNB	3726	0.0074187	0.046098	1	1	0.66209	1	0.99719	1	3.23E-09	5.43E-08	0.98556	1
KIF20A	10112	1.00E+00	1.00E+00	1	1	1.00E+00	1.00E+00	0.99986	1	0.99999	1	0.99939	1
KIF22	3835	0.96969	1	1	1	0.92925	1	1	1	0.99982	1	1	1
KPNA2	3838	1.14E-19	2.02E-18	1	1	1.75E-33	3.08E-31	1	1	0.98805	1	1	1
MKI67	4288	0.99993	1	0.078588	0.34003	0.99143	1	0.029823	0.181	0.3493	1	0.18691	0.71768
MLH1	4292	1	1	0.99997	1	0.99886	1	0.81658	1	0.99986	1	0.86253	1
MORF4L2	9643	1	1	1	1	1	1	0.99772	1	1	1	1	1
MRE11A	4361	0.97561	1	0.99998	1	0.60854	1	0.7955	1	0.19725	0.98849	0.99992	1
MSH6	2956	0.90061	1	1	1	0.98161	1	1	1	0.1989	0.9954	1	1
MTA2	9219	0.87351	1	0.99993	1	0.20743	1	0.068603	0.35123	0.99827	1	1	1
NAT10	55226	0.12245	0.60024	1	1	0.0012066	0.010733	1	1	0.32695	1	1	1
NBN	4683	6.03E-02	3.19E-01	1	1	1.41E-04	1.44E-03	1	1	0.80934	1	0.99321	1
NIPBL	25836	2.92E-01	1.00E+00	1	1	0.88025	1	0.99883	1	0.57708	1	1	1
NOL11	25926	9.91E-21	1.85E-19	1	1	6.55E-35	1.35E-32	1	1	9.97E-01	1	1	1
NOP2	4839	1.52E-06	1.41E-05	1	1	0.17273	0.86401	0.97568	1	0.0043685	0.03556	1	1
NUMA1	4926	2.65E-35	6.94E-34	1	1	3.04E-13	8.34E-12	0.24369	1	1.80E-05	0.0002221	1	1
OBFC2B	79035	0.31559	1	1	1	0.99783	1	0.77647	1	0.209	1	1	1
ORC2	4999	0.32231	1	0.94942	1	0.91836	1	0.97637	1	0.34704	1	0.99167	1
PALB2	79728	1	1	1.00E+00	1.00E+00	0.9999	1	1	1	1	1	1.00E+00	1.00E+00
PCNA	5111	1	1	1	1	0.99872	1	0.99871	1	0.69303	1	1.00E+00	1.00E+00
PGAM5	192111	1	1	1.02E-06	7.06E-06	0.99883	1	0.0025126	0.021154	0.99151	1	8.41E-08	1.08E-06
PMS2	5395	0.97109	1	0.001002	0.0055727	0.94318	1	0.32423	1	1	1	3.03E-20	9.60E-19
POLR2A	5430	1.00E+00	1.00E+00	1	1	1.00E+00	1.00E+00	0.81068	1	1.00E+00	1.00E+00	1	1
RAD18	56852	0.80568	1	0.73981	1	0.017541	0.11977	0.9994	1	0.91111	1	0.00095397	0.0071832
RAD21	5885	9.80E-76	3.86E-74	1	1	1.37E-22	9.79E-21	1	1	9.55E-53	5.69E-51	1	1
RAD50	10111	1	1	0.95726	1	1	1	0.97196	1	1	1	0.6562	1
RBBP8	5932	6.21E-05	0.00050746	1	1	0.99992	1	1	1	0.013051	0.0943	1	1
RBM28	55131	0.7004	1	1	1	0.89691	1	0.99871	1	0.032503	0.20781	1	1
RCL1	10171	0.23955	1	0.27781	1	0.85141	1	0.26493	1	0.99729	1	0.30883	1
RFC1	5981	1.00E+00	1.00E+00	1	1	1.00E+00	1.00E+00	0.99999	1	1.00E+00	1.00E+00	0.99956	1
RFC2	5982	9.74E-01	1.00E+00	1	1	6.25E-01	1.00E+00	0.9918	1	9.37E-01	1.00E+00	0.99929	1
RFC4	5984	1.67E-125	1.52E-123	1.00E+00	1.00E+00	3.15E-06	3.85E-05	0.9994	1	7.35E-46	3.78E-44	1	1
RNF169	254225	2.15E-30	5.05E-29	1	1	1.28E-22	9.18E-21	0.3139	1	1.69E-08	2.70E-07	1	1
RPL21	6144	0.22908	1	2.65E-08	2.08E-07	0.023842	0.15667	0.19663	0.84884	1	1	0.026361	0.13797
RPL28	6158	0.0016969	0.011622	0.0059534	0.030961	4.76E-05	0.00051606	0.99772	1	0.88929	1	0.00054519	0.0043454
RPL3	6122	1	1	1	1	0.99999	1	1	1	1	1	0.94152	1
RPL32	6161	0.71615	1	0.99085	1	0.0050735	0.039773	1	1	0.99079	1	0.02939	0.15145
RPL34	6164	1.00E+00	1.00E+00	0.60522	1	9.98E-01	1.00E+00	0.84975	1	1.00E+00	1.00E+00	0.0050569	0.03174
RPS13	6207	1	1	0.99757	1	0.99261	1	0.98302	1	1	1	0.16529	0.64848
RPS27	6232	2.05E-53	6.84E-52	1	1	1.37E-19	7.53E-18	1	1	5.93E-11	1.19E-09	1	1
RPS7	6201	0.40123	1	5.56E-01	1.00E+00	0.86341	1	0.59165	1	0.031309	0.20103	8.31E-02	3.68E-01
RSL1D1	26156	1	1	1	1	0.99987	1	1	1	0.99895	1	1.00E+00	1.00E+00
RUVBL2	10856	1	1	4.21E-09	3.52E-08	0.91732	1	0.45119	1	1	1	8.21E-09	1.15E-07
SETX	23064	1	1	0.25838	0.98991	0.99578	1	0.89635	1	1	1	6.41E-06	6.71E-05
SLAIN2	57606	0.0065212	0.040905	1	1	0.96484	1	0.99999	1	0.99848	1	1	1
SMARCA5	8467	0.99928	1	0.99995	1	0.7862	1	0.9999	1	0.99901	1	0.95418	1
SMC1A	8243	0.99994	1	1	1	0.99883	1	1	1	0.75656	1	1	1
SMC3	9126	1.00E+00	1.00E+00	0.0033566	0.017849	1.00E+00	1.00E+00	0.0077094	0.057606	9.99E-01	1.00E+00	0.010404	0.060873
TERF2	7014	1.00E+00	1.00E+00	0.99983	1	1.00E+00	1.00E+00	1.00E+00	1	1	1	0.064956	0.29907

Table 6 (Continued). Search for location of genes identified in screens in either amplification or deletion regions in breast tumors, ovarian tumors, or across 11 different tumor types, Related to figure 17D, page 2

**Only graphed genes with p<0.05 and q<0.25 in the networks

		Across all cancers				Breast Cancer				Ovarian Cancer			
Gene Symbol	Gene ID	Amplification region p-value	Amplification region q-value	Deletion Region p-value	Deletion Region q-value	Amplification region p-value	Amplification region q-value	Deletion Region p-value	Deletion Region q-value	Amplification region p-value	Amplification region q-value	Deletion Region p-value	Deletion Region q-value
TONSL	4796	1.91E-109	1.09E-107	1	1	1.72E-15	6.11E-14	0.71821	1	3.49E-88	4.16E-86	0.99998	1
TOP2A	7153	5.42E-07	5.22E-06	0.029257	0.1379	4.73E-17	1.92E-15	5.03E-05	0.00060338	1	1	0.42582	1
TOPBP1	11073	9.98E-01	1.00E+00	1	1	0.99069	1	0.99912	1	0.20729	1	1	1
TPX2	22974	9.50E-14	1.35E-12	1	1	0.69356	1	1	1	0.0018586	0.016541	1	1
UIMC1	51720	2.29E-06	2.10E-05	0.89983	1	0.029524	0.18894	0.97568	1	0.071843	0.41322	9.79E-01	1
USP7	7874	1.00E+00	1.00E+00	1	1	0.99879	1	1	1	1.00E+00	1.00E+00	0.99961	1
WAPAL	23063	1.00E+00	1.00E+00	0.002413	0.01298	9.97E-01	1.00E+00	0.6776	1	1	1	6.06E-05	0.00055438
WIZ	58525	1.48E-08	1.60E-07	1	1	0.16031	0.81048	1	1	1.24E-18	3.62E-17	1	1
ZC3H11A	9877	1.34E-15	2.02E-14	1	1	6.99E-07	9.13E-06	1	1	0.18122	0.92084	0.99995	1
ZC3HAV1	56829	0.007127	0.044384	0.99929	1	0.7386	1	0.92082	1	4.56E-09	7.58E-08	1	1
ZZZ3	26009	1.00E+00	1.00E+00	0.074188	0.32262	9.50E-01	1.00E+00	0.49901	1	0.99996	1	0.51335	1
ABLIM3	22885	0.99947	1	0.99999	1	0.99999	1	0.99546	1	0.97758	1	0.99737	1
ACTN3	89	2.16E-21	4.11E-20	1	1	3.69E-22	2.56E-20	0.97116	1	8.79E-01	1.00E+00	1	1
ALS2CR11	151254	0.71504	1	6.73E-01	1.00E+00	0.99261	1	0.65081	1	0.51171	1	0.99191	1
AP1M1	8907	0.00011767	0.00093477	1	1	7.24E-01	1	0.99998	1	9.16E-15	2.34E-13	1	1
BRSK1	84446	0.0046499	0.029862	0.0089421	0.045368	6.05E-05	0.00064867	0.99386	1	8.60E-01	1.00E+00	0.0026875	0.018071
C22orf29	79680	0.030443	0.16997	0.99999	1	0.84359	1	0.92419	1	1.96E-01	0.98128	1	1
DDX39	10212	6.11E-07	5.86E-06	1	1	4.86E-01	1.00E+00	0.99995	1	2.29E-19	6.82E-18	1	1
CCDC120	90060	0.40982	1	1	1	0.99985	1	1	1	3.15E-10	5.84E-09	1	1
CDK16	5127	2.63E-01	1.00E+00	1	1	7.84E-01	1.00E+00	1	1	1.96E-05	0.0002405	1	1
CLK2	1196	2.20E-63	8.07E-62	1.00E+00	1.00E+00	1.06E-20	6.49E-19	1.00E+00	1.00E+00	1.49E-15	3.92E-14	1	1
CRY2	1408	0.9969	1	1.00E+00	1.00E+00	0.89321	1	0.96602	1	0.99993	1	0.99999	1
CWF19L2	143884	1	1	8.32E-06	5.38E-05	1	1	7.49E-10	2.79E-08	0.99623	1	0.58752	1
DES	1674	1	1	4.03E-19	6.46E-18	0.99991	1	0.011436	0.081114	0.98939	1	0.049352	0.23636
DHPS	1725	0.061704	0.32534	1	1	0.75497	1	0.99752	1	2.25E-07	3.27E-06	0.93554	1
FAM161A	84140	0.0073595	0.045753	1	1	0.73235	1	1	1	0.28234	1	1	1
FAM184A	79632	1	1	4.66E-01	1.00E+00	0.48634	1	2.65E-01	1.00E+00	1	1	0.23032	0.84816
FXR2	9513	1	1	0.99986	1	1	1	0.57963	1	0.99999	1	1	1
GCC1	79571	1.00E+00	1.00E+00	0.99999	1	9.98E-01	1.00E+00	0.99781	1	4.52E-01	1.00E+00	1	1
GOLGA8DP	100132979	1.00E+00	1.00E+00	6.00E-15	7.73E-14	0.99261	1	3.73E-09	1.26E-07	1.00E+00	1.00E+00	0.00095397	0.0071832
HGF	3082	0.99943	1	1	1	0.976	1	0.99893	1	0.99656	1	0.99984	1
HORMAD1	84072	2.33E-106	1.23E-104	1.00E+00	1.00E+00	1.25E-33	2.24E-31	1	1	3.96E-28	1.44E-26	1.00E+00	1.00E+00
IFLTD1	160492	1.50E-09	1.71E-08	1	1	0.30531	1	9.99E-01	1.00E+00	2.80E-11	5.85E-10	1	1
KAT5	10524	0.0004255	0.0031504	9.99E-01	1.00E+00	0.0031047	0.025651	0.0036914	0.029673	0.73322	1	1.00E+00	1.00E+00
LCK	3932	0.91831	1	2.90E-14	3.63E-13	0.99588	1	0.0010175	0.0095333	0.004577	0.037131	1.76E-06	1.99E-05
MAP3K14	9020	1	1	0.016366	0.079907	1	1	1.18E-10	5.04E-09	1	1	0.88624	1
MARCKSL1	65108	0.92999	1	5.05E-14	6.21E-13	0.9974	1	0.00072492	0.0070127	0.0050216	0.04037	3.60E-06	3.93E-05
MCRS1	10445	1	1	0.99999	1	0.99998	1	0.32771	1	1	1	0.99984	1
MID2	11043	1.00E+00	1.00E+00	1	1	1.00E+00	1.00E+00	0.99998	1	1.00E+00	1.00E+00	1	1
MYOZ1	58529	0.13461	0.65262	1	1	0.019376	0.13064	0.99991	1	0.22297	1	0.92911	1
NRIP1	8204	7.51E-01	1.00E+00	0.00024433	0.00142	9.18E-01	1.00E+00	0.00035112	0.003595	9.82E-01	1.00E+00	0.82634	1
OBSCN	84033	7.24E-09	7.96E-08	1	1	2.21E-08	3.38E-07	0.99987	1	1.37E-06	1.87E-05	1	1
POM121	9883	0.99643	1	1	1	0.5007	1	0.99363	1	0.98606	1	1	1
PPFIA1	8500	3.24E-306	1.61E-302	1.00E+00	1.00E+00	1.18E-155	3.84E-152	0.99923	1	5.64E-09	9.30E-08	1	1
PPP1R13B	23368	1.41E-01	6.80E-01	0.058496	0.2603	9.60E-01	1.00E+00	0.20979	0.89578	1.65E-02	1.16E-01	0.24874	0.90354
PRKAA2	5563	0.91984	1	0.99944	1	0.40671	1	0.94091	1	0.086131	0.48592	0.92777	1
PRKAG3	53632	1	1	1.52E-18	2.38E-17	0.99996	1	0.019687	0.12946	0.98782	1	0.038287	0.18989
PRPF3	9129	2.37E-93	1.08E-91	1	1	2.33E-29	3.00E-27	1	1	3.44E-22	1.11E-20	1	1
PSMD9	5715	1	1	0.01654	0.080692	0.99909	1	0.00063518	0.0062417	0.99382	1	3.16E-03	2.09E-02
RUNX1T1	862	0.11939	0.58674	1.00E+00	1	0.00012492	0.0012828	1	1	0.72669	1	0.9977	1
RWDD2B	10069	1.00E+00	1.00E+00	1	1	9.99E-01	1.00E+00	0.99741	1	1	1	0.99994	1
SSX2IP	117178	1.00E+00	1.00E+00	2.46E-05	0.00015322	9.82E-01	1.00E+00	0.00060231	0.0059504	1.00E+00	1.00E+00	0.031012	0.15866
STAC2	342667	2.50E-30	5.86E-29	0.17337	0.69833	5.45E-54	3.00E-51	0.025026	0.15812	1	1	0.40199	1
SYT6	148281	1	1	2.74E-15	3.58E-14	0.99999	1	2.26E-04	2.37E-03	0.99134	1	5.73E-01	1.00E+00
TCEA2	6919	9.55E-25	1.95E-23	1	1	9.63E-13	2.45E-11	0.99956	1	1.11E-10	2.18E-09	1	1
TCEANC	170082	1	1	1	1	0.99975	1	0.97116	1	0.99515	1	0.98438	1
TCEB3	6924	1	1	2.59E-87	4.17E-85	1	1	1.93E-20	2.86E-18	0.99998	1	2.50E-30	1.33E-28
TENC1	23371	0.99999	1	1.00E+00	1.00E+00	0.99995	1	0.11476	0.54294	0.99979	1	1.00E+00	1.00E+00
TMPRSS12	283471	1	1	1	1	0.99968	1	0.2557	1	1	1	0.99999	1
TSGA10IP	254187	0.00010556	0.00084307	1	1	0.0013894	0.012223	0.81658	1	0.58207	1	1	1
TXLNA	200081	0.92672	1	1.63E-15	2.16E-14	0.98227	1	0.0014188	0.012785	0.023337	0.15642	3.45E-07	4.21E-06
ZNF423	23090	1	1	0.98992	1	0.78808	1	0.15173	0.68452	1	1	0.9986	1

that a number of the hits from our BRCA1 interactome screens and the new functional role proposed for BRCA1 do participate in human tumorigenesis.

Chapter 4-Discussion of bipartite screening results

-All writing in this chapter was performed by SJH.

The complementary protein interaction screening approaches used here have led to the generation of a more complete BRCA1 protein interaction network. Knowledge of the anatomy of this network has made possible genetic tests of the physiological relevance of certain interactions. From the results of these analyses, the relevance of the function of certain BRCA1-interacting proteins to BRCA1 function was demonstrated, and a combined role for BRCA1 and these interacting proteins in the response to transcription-associated DNA damage was detected.

Assessing the significance of protein interactions in this manner may be useful in the future, since detection of binary interactions and, more importantly, detection of the physiological relevance of such interactions can be challenging. This is especially true for BRCA1, since its complete depletion can lead to cell cycle arrest (Xu et al., 2001b), complicating mechanistic studies on several of its functions. The BRCA1+/- lines used in our experiments cycled normally, and thus, it may be easier to study certain functions through genetic manipulations in such lines, allowing physiologically relevant insights to be made.

Our approach has led to observations that may also be meaningful in the context of cancer development and treatment. Determining the overlap between a physical and genetic interaction map may contribute to increased appreciation of important steps in disease development and towards the discovery of relevant, mechanism-driven treatment strategies.

The results of our screening and of the validation of multiple interactors identified in it have uncovered a new role for BRCA1 in the prevention and/or repair of DNA damage associated with transcription arrest. Imputed functions of TONSL and known functions of the

TONSL-binding FACT complex and of SETX, TCEANC, and TCEA2, all proteins engaged in transcription and/or RNA processing and all proteins that genetically interact with BRCA1, represent new processes through which BRCA1 participates in the prevention and/or repair of DNA damage. That BRCA1 is engaged in transcription-associated damage control is supported as a concept by these results and phenomena observed by others for both BRCA1 and BARD1 (Becherel et al., 2013; Kleiman and Manley, 1999, 2001; Kleiman et al., 2005; Le Page et al., 2000; Yuce and West, 2013). However, the current link between BRCA1 and transcription-associated damage is poorly defined, and data reported here now strongly suggest that BRCA1 responds to DNA damage at sites of stalled or defective transcription. These findings are also consistent with the hypothesis that BRCA1 can perform different functions at these sites depending on the type of damage and on the particular interacting proteins (TONSL-FACT, TCEA2, etc.) that are co-recruited with it.

For example, SETX is involved in preventing R loop stabilization (Mischo et al., 2011; Skourti-Stathaki et al., 2011). Thus, it is conceivable that BRCA1 accompanies RNAPII, with which it is known to interact (Scully et al., 1997a), to prevent stalling and damage at R loops. Alternatively, BRCA1 might be recruited to RNAPII that collects at pause sites or sites of DNA damage and recruits SETX to these sites to prevent R loop stabilization or repair of R loop associated damage.

The FACT complex functions in rearranging chromatin to allow transcription elongation to proceed through chromatin without disturbing its epigenetic architecture (Reinberg and Sims, 2006); and it has been implicated both in transcription restart after and potentially repair of UV-induced transcription-associated damage (Dinant et al., 2013), as well as, R-loop-associated

damage (Herrera-Moyano et al., 2014). Conceivably, a BRCA1-TONSL-FACT complex is recruited to active RNA Pol II, particularly after the kind of damage induced by UV irradiation or stabilized R-loops, to respond to damage at that site.

In keeping with this theme, the interactor TCEA2 is a member of the TFIIS family of transcription elongation factors. TCEA1 (aka TFIIS or S-II) is the most studied member of this family. TCEA1 promotes transcription elongation-associated RNA transcript cleavage when RNA Pol II encounters various endogenous and exogenously induced DNA obstacles as well as the elimination of transcript errors (Wind and Reines, 2000). While TCEA2 was originally identified as a testes- and ovary- specific version of TFIIS (Wind and Reines, 2000), it is also expressed in certain somatic cells (Figure 6G). TCEA2 and TCEA1 are homologous for a functional domain that is critical for TFIIS transcription elongation function (Wind and Reines, 2000), and both stimulate RNA Pol II in the same way (Wind and Reines, 2000). Since BRCA1 and the closely related TCEA1 (labelled TFIIS in the figures) co-localized at UV induced sites of transcription-associated damage, it is likely that TCEA2 operates similarly. These hypotheses fit with our observation that BRCA1 depletion leads to increased sensitivity to the halting of transcription.

The possibility that BRCA1 responds to transcription-associated damage by all of the mechanisms described above may mean that there are multiple steps in these repair/response pathway(s) that could be targets for mutation and, possibly, even therapy. The TCGA data cited earlier indicate that multiple transcription-associated proteins are altered across different types of cancers. For example, TCEA2 is amplified across 11 different tumor types, including breast and ovarian cancers (Figure 17D). One wonders whether this is a manifestation of compensation for

ongoing, broadly based threats to transcription procession, given the known functional interaction of TCEA2 with BRCA1. If demonstrated, increasing transcription-associated damage or blocking TCEA2 involvement in such tumors may both be relevant therapeutic strategies for these cancers.

In considering the therapeutic relevance of the new BRCA1 interaction network, the cell line used in the alpha-Amanitin rescue experiments, HCC38, is a cancer cell line in which the BRCA1 promoter is methylated, causing it to express less BRCA1 than normal cells (Xu et al., 2010). This makes HCC38 suspect for harboring a defect(s) in BRCA1 function (Xu et al., 2010). Not only did we observe rescue of alpha-Amanitin sensitivity induced by BRCA1 depletion in this line by overexpression of the BRCA1 cDNA, there was also decreased sensitivity to alpha-Amanitin in the BRCA1 cDNA-expressing line compared to naïve WT cells (Figure 5G, compare lanes 1 and 3 in right panel). This suggests that promoter methylation-associated depletion of BRCA1 can give rise to increased sensitivity of cells to alpha-Amanitin or other transcription inhibitors. If proven, residual BRCA1-driven transcription-associated DNA damage control might become a therapeutic target in tumors with decreased WT BRCA1 levels.

There may be an example of clinical success in targeting this BRCA1-driven transcription-associated damage control in BRCA1 mutant and sporadic basal-like breast tumors. These tumors are, in part, BRCA1 mutant breast cancer phenocopies. Multiple clinical trials and retrospective studies in BRCA1 mutant (Silver et al., 2010) and sporadic basal-like breast tumors (Chew et al., 2009; Hurley et al., 2013; Silver et al., 2010; Sirohi et al., 2008; Staudacher et al., 2011) reveal signs of efficacy following administration of the crosslinking agent, cisplatin.

Cisplatin crosslinks cause DNA damage by blocking the procession of transcription or DNA replication (Todd and Lippard, 2009). BRCA1 is known to participate in the repair of stalled replication forks, and loss of this function could explain the therapeutic efficacy of cisplatin in these tumors (Pathania et al., 2011; Schlacher et al., 2012). However, data shown here suggest that a block of BRCA1 participation in transcription-associated damage control could also contribute to cisplatin efficacy in these tumors. Indeed, cisplatin is also known to cause damage and cell death through transcription arrest (Todd and Lippard, 2009). Thus, it is reasonable to speculate that cisplatin efficacy in these tumors is enhanced by simultaneously eliciting a defect in BRCA1-driven, transcription-associated DNA damage control.

In conclusion, gaining a better understanding of how BRCA1 functions at sites of transcription-associated DNA damage with the interactors we have identified and likely other proteins yet to be detected may prove to be of therapeutic interest. It could also provide opportunities to generate biomarkers useful in identifying subsets of breast and ovarian tumors that are susceptible to therapy that targets this pathway. In addition, understanding the methods of BRCA1-dependent and independent repair of transcription-associated damage may be important in other diseases as well. Transcription occurs constantly in all cells, even after terminal differentiation, such as in neuronal cells and cardiac myocytes (Zhang et al., 2008). Transcription-associated DNA damage may play a role in the pathogenesis of certain diseases in these tissues.

Chapter 5-Analysis of sporadic basal-like breast cancer cell lines for BRCA1 pathway functional defects

-Chapters 5 and 6 were adapted from the following manuscript:

Title: BRCA1 pathway function in basal-like breast cancer cells

Authors: Sarah J. Hill[1,2], Allison P. Clark[2], Daniel P. Silver[2,3, †], and David M. Livingston[1,2, †,#]

Affiliations:
[1]Department of Genetics, Harvard Medical School, Boston, MA 02215, USA.
[2]Department of Cancer Biology, Dana-Farber Cancer Institute, 450 Brookline Avenue, Boston, MA 02215, USA.
[3]Department of Medical Oncology, Dana-Farber Cancer Institute, 450 Brookline Avenue, Boston, MA 02215, USA.

[†]These authors share equal seniority.

[#] To whom correspondence should be addressed: David M. Livingston
Professor of Genetics and Medicine
Harvard Medical School and
Dana-Farber Cancer Institute
450 Brookline Avenue,
Boston, MA 02215, USA
david_livingston@dfci.harvard.edu

-All writing for this chapter was done by SJH. All experiments in this chapter were performed by SJH. Allison P. Clark and Daniel P. Silver aided in the Southern blots shown in Figure 25. All figures in this chapter were generated by SJH.

Rationale

The overall goals for the work in this chapter were to determine which known or new functions of BRCA1 are altered in sporadic basal-like breast cancer cells, since these cells are alleged to be phenocopies of BRCA1 mutant cells.

Given the finding that BRCA1 plays a role in the response to transcription-associated DNA damage, and the discrepancy between the belief that sporadic basal-like cancers (BLC) harbor a defect in HR and the reality of current clinical trials with HR targeting drugs, we sought to determine what BRCA1 functional pathway(s) is/are defective in sporadic basal-like tumors. A major goal of this study was to determine whether sporadic BLC cells, like BRCA1 mutant tumor cells, are also defective in HR repair of DSBs and/or exhibit defects in other BRCA1-dependent DNA damage repair pathways. The answers to these questions might influence the application of mechanism-based approaches to sporadic BLC therapy.

Results

BRCA1 expression in sporadic BLC cell lines

A collection of sporadic, *BRCA1*+/+ human breast cancer cell lines shown by expression profiling to represent the BLC subtype (Bamford et al., 2004; Elstrodt et al., 2006; Neve et al., 2006) was analyzed, along with controls. The controls consisted of two independently derived, telomerase-immortalized, normal breast epithelial cell strains, BPE and HME (Ince et al., 2007). Before performing assays of DNA repair proficiency in these cells, we asked whether these

sporadic BLC lines and the control lines express full length BRCA1 using non-quantitative, standardized BRCA1 IP-western analysis performed on asynchronous, undamaged cells (Figure 18). All sporadic BLC lines and controls expressed readily detectable full length p220 and Δ11b (Figure 18). Thus, any HR defect observed in them cannot be attributed to a loss of BRCA1 p220 or Δ11b expression.

In addition, four BRCA1 mutant lines served as positive controls in all experiments. Two of them (SUM149 and L56BRC1) have sustained nonsense mutations in BRCA1 exon 11 which prevent them from expressing p220 but allow them to express Δ11b (Figure 18). HCC1937 carries a classical, disease-producing BRCA1 mutation, 5382insC, in the sequence that encodes one of its BRCT motifs, and SUM1315 contains another classical disease-producing mutation, 185delAG, which results in severe truncation of p220. Thus, no readily detected BRCA1 protein was observed in these two lines (Figure 18).

Evidence of post-damage DNA repair responses in nuclear foci

The repair of DSB by HR and the repair of stalled or collapsed replication forks are dependent upon BRCA1-containing complexes concentrating at sites of DNA damage in a defined temporal order (Greenberg, 2008; Huen et al., 2010). Thus, assessing the post-damage concentration of specific members of these protein complexes in IRIF by immunofluorescent (IF) staining can be used as an indirect, surrogate reporter of HR or stalled fork repair proficiency, at least up to the point of the arrival of the assayed proteins.

HR Repair of DSBs: To study HR, we assayed the formation or absence of post-IR BRCA1, Rad51, and 53BP1 nuclear foci (Figure 19A, B, C and Table 7), and all of the sporadic

Figure 18. Sporadic BLC cell lines express p220 and Δ11b: Full length BRCA1 and the Δ11b BRCA1 isoform were immunoprecipitated from lysates of the sporadic BLC lines, normal controls, and BRCA1 mutant lines, using a C-terminal epitope BRCA1 antibody (sc6954). Blots were performed with an N-terminal epitope BRCA1 antibody (MS110). p220 migrates between the 148 and 250kDa markers and is marked by a red arrow in the molecular weight marker lane. Δ11b migrates just above the 98 kDa marker and is marked by a green arrow in the molecular weight marker lane. Different colored circles mark the type of line that was tested in each blot, and the key for the circles is shown. Several BLC lines were blotted more than once to confirm the result.

Figure 18 (Continued)

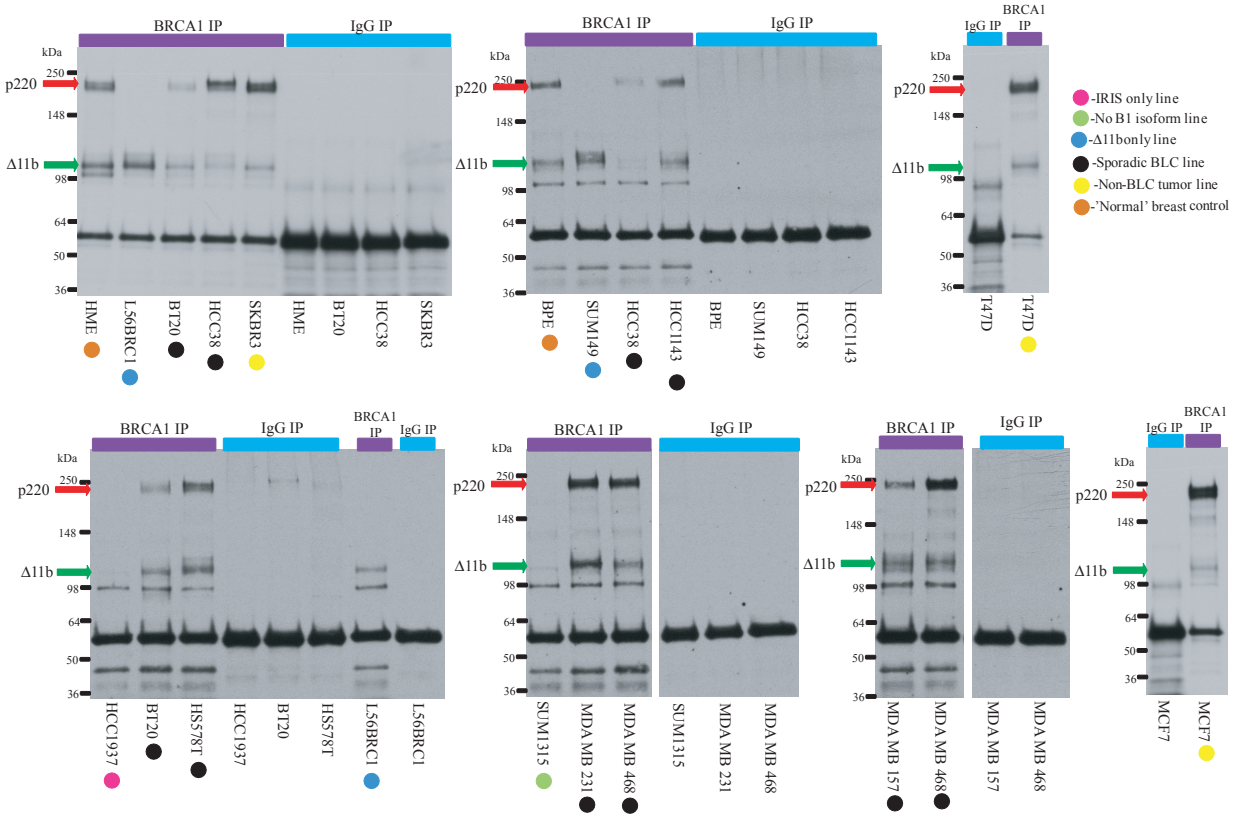

Figure 19. Representative immunofluorescence results associated with different DNA damaging agents: A) MDA MB 231 +/-5Gy irradiation stained with γH2AX and BRCA1 antibodies 8 hours after treatment. **B)** MDA MB 231 +/-5Gy irradiation stained with γH2AX and Rad51 antibodies 8 hours after treatment. **C)** MDA MB 231 +/-5Gy irradiation stained with γH2AX and 53BP1 antibodies 8 hours after treatment. **D)** MDA MB 231 four hours post 30J through micropores stained with BRCA1 and cyclobutane pyrimidine dimer (CPD) antibodies. CPDs are known to mark sites of UV damage. Yellow arrows are placed next to a few representative cells in which there is co-localization. The brightness has been increased by 20% and the contrast decreased by 20% using PowerPoint in every single panel to alleviate difficulties with the conversion of the images to PDF.

Figure 19 (Continued) MDA MB 231

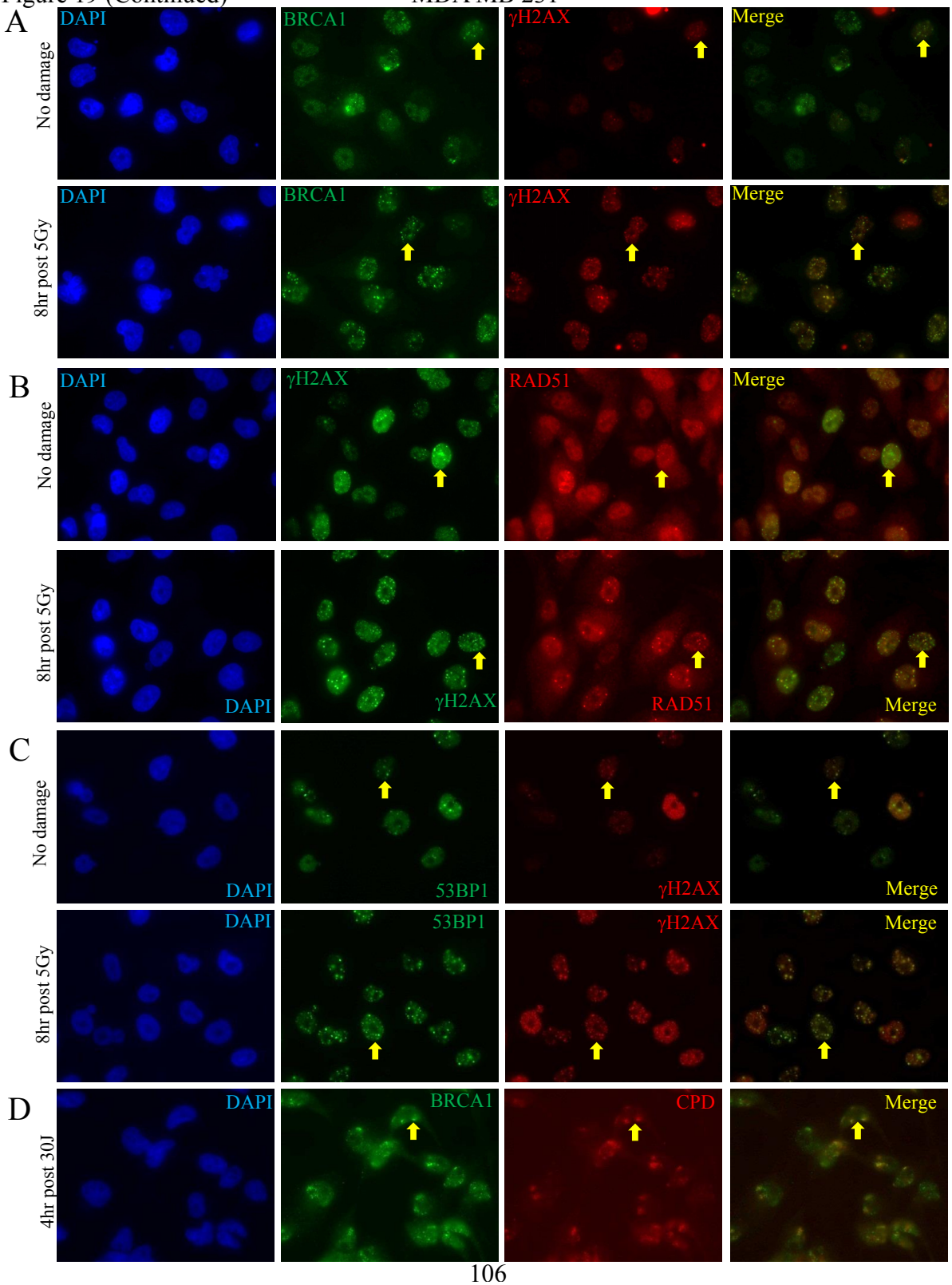

Table 7. Post-damage immunofluorescence results in all BLC lines and controls: Cell lines were exposed to various forms of DNA damaging agents on coverslips and then stained for different DNA damage markers. For gamma irradiation, one set was treated with 5Gy irradiation (IR) while a second, control set was not. The cells were allowed to recover at 37°C for 8-9 hours. For UV treatment, cells were treated with 30J through a UV micropore filter and then allowed to recover for 4hr at 37°C. A +++ in the BPE row indicates significantly more foci than in any other cell line. The colored circle next to the cell line name indicates the type of cell line (control vs. BLC) according to the key below the table.

Table 7 (Continued). **Post-damage immunofluorescence results in all BLC lines and controls**

Cell Line	Post-IR BRCA1 Foci	Post-IR Rad51 Foci	Post-IR 53BP1 Foci	Post-UV BRCA1-CPD Co-localization
BPE●	+	+++	+	+
HME●	+	+	+	+
HCC38●	+	+	+	+
HCC1143●	+	+	+	+
MDA MB 157 ●	+	+	+	+
MDA MB 231 ●	+	+	+	+
MDA MB 468 ●	+	+	+	+
BT20●	+	+	+	+
BT549●	+	+	+	+
HS578T●	+	+	+	+
HCC1937●	-	+	+	-
SUM1315 ●	-	-	+	-
SUM149 ●	+	+	+	+
L56BRC1●	+	+	+	+
MCF7 ●	+	+	+	+
T47D ●	+	+	+	+
SKBR3●	+	+	+	+

●=Normal Breast cell Line ●=BRCA1 mutant cell line ●=BLC cell Line ●=ER Positive tumor cell line ●=HER2 amplified tumor cell line

BLC lines and controls revealed post-IR BRCA1 and 53BP1-containing foci. While variable in prevalence, Rad51 foci were also regularly observed in all of these tumor cell lines.

We chose to analyze 53BP1 foci in the sporadic BLC lines, because loss of 53BP1 expression in BRCA1 mutant cells lead to restoration of HR in these cells (Bouwman et al., 2010). In cells deficient for both 53BP1 and BRCA1, DSB end excision can occur in an ATM-dependent manner in such a way that it results in HR mediated DSB repair, despite the loss of BRCA1 (Bunting et al., 2010). However, against the possibility that some or all of the sporadic BLC lines manifest a BRCA1-related defect in HR that is rescued by 53BP1 deficiency (Bunting et al., 2010), 53BP1 foci were readily detected in all sporadic BLC lines (Table 7). This implies that BRCA1-driven HR function and its regulation by 53BP1 are intact in these sporadic BLC lines, at least, up to the point of Rad51 loading.

IRIF formation was also analyzed in the BRCA1 mutant lines. 53BP1 foci were observed in all four BRCA1 mutant lines implying that any HR phenotypes observed in them are not due to 53BP1 loss. In addition, BRCA1 foci were observed in both SUM149 and L56BRC1, the two lines that still express Δ11b. These foci were absent when these lines were analyzed by IF using a BRCA1 antibody that recognizes an epitope in exon 11 (Figures 20, 21, and 22), and disappeared upon exposure to Δ11b-specific but not p220-specific siRNAs (Figure 23). Therefore, it is likely that the BRCA1 foci observed in these two lines contain Δ11b and lack p220. Finally, Rad51 foci were observed in three of the BRCA1 mutant lines, SUM149, L56BRC1, and HCC1937. Conceivably, SUM149 and L56BRC1 recruit Rad51 through Δ11b, or potentially all three lines recruit it by a BRCA1-independent route (Park et al., 2013).

Figures 20, 21, 22. Post-damage BRCA1 foci in Δ11b expressing mutant lines are not recognized by exon 11 specific BRCA1 antibodies: The two BRCA1 mutant control lines expressing Δ11b but not p220 (L56BRC1- **Figure 21** and SUM149-**Figure 22**), and a sporadic BLC line (MDA MB 231- **Figure 20**) were exposed to 5Gy gamma irradiation (IR) or no IR and allowed to recover for 8hr. All cells were then stained with a C-terminal specific BRCA1 antibody that recognizes both p220 and Δ11b **(Supplementary Figures 20A, 21A, 22A)** or an exon 11 BRCA1 antibody that cannot recognize Δ11b **(Supplementary Figures 20B, 21B, and 22B)**, both along with γH2AX to mark DNA damage. Yellow arrows are placed next to a few representative cells in which there is co-localization. The brightness has been increased by 20% and the contrast decreased by 20% using PowerPoint in every single panel to alleviate difficulties with the conversion of the images to PDF.

Figure 20 (Continued)

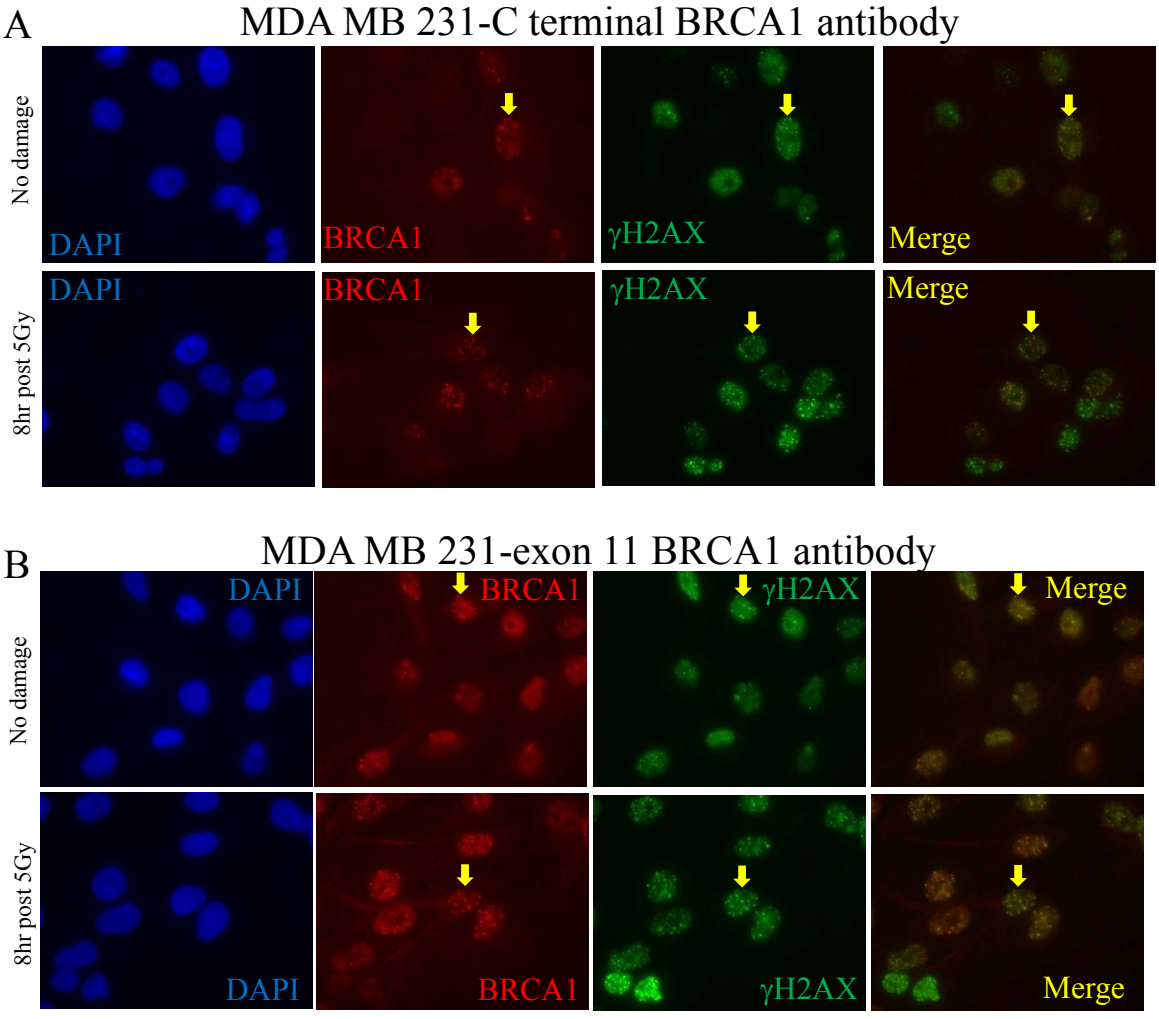

Figures 20, 21, 22 (Continued). Post-damage BRCA1 foci in Δ11b expressing mutant lines are not recognized by exon 11 specific BRCA1 antibodies: The two BRCA1 mutant control lines expressing Δ11b but not p220 (L56BRC1- **Figure 21** and SUM149-**Figure 22**), and a sporadic BLC line (MDA MB 231- **Figure 20**) were exposed to 5Gy gamma irradiation (IR) or no IR and allowed to recover for 8hr. All cells were then stained with a C-terminal specific BRCA1 antibody that recognizes both p220 and Δ11b **(Supplementary Figures 20A, 21A, 22A)** or an exon 11 BRCA1 antibody that cannot recognize Δ11b **(Supplementary Figures 20B, 21B, and 22B)**, both along with γH2AX to mark DNA damage. Yellow arrows are placed next to a few representative cells in which there is co-localization. The brightness has been increased by 20% and the contrast decreased by 20% using PowerPoint in every single panel to alleviate difficulties with the conversion of the images to PDF.

Figure 21 (Continued)

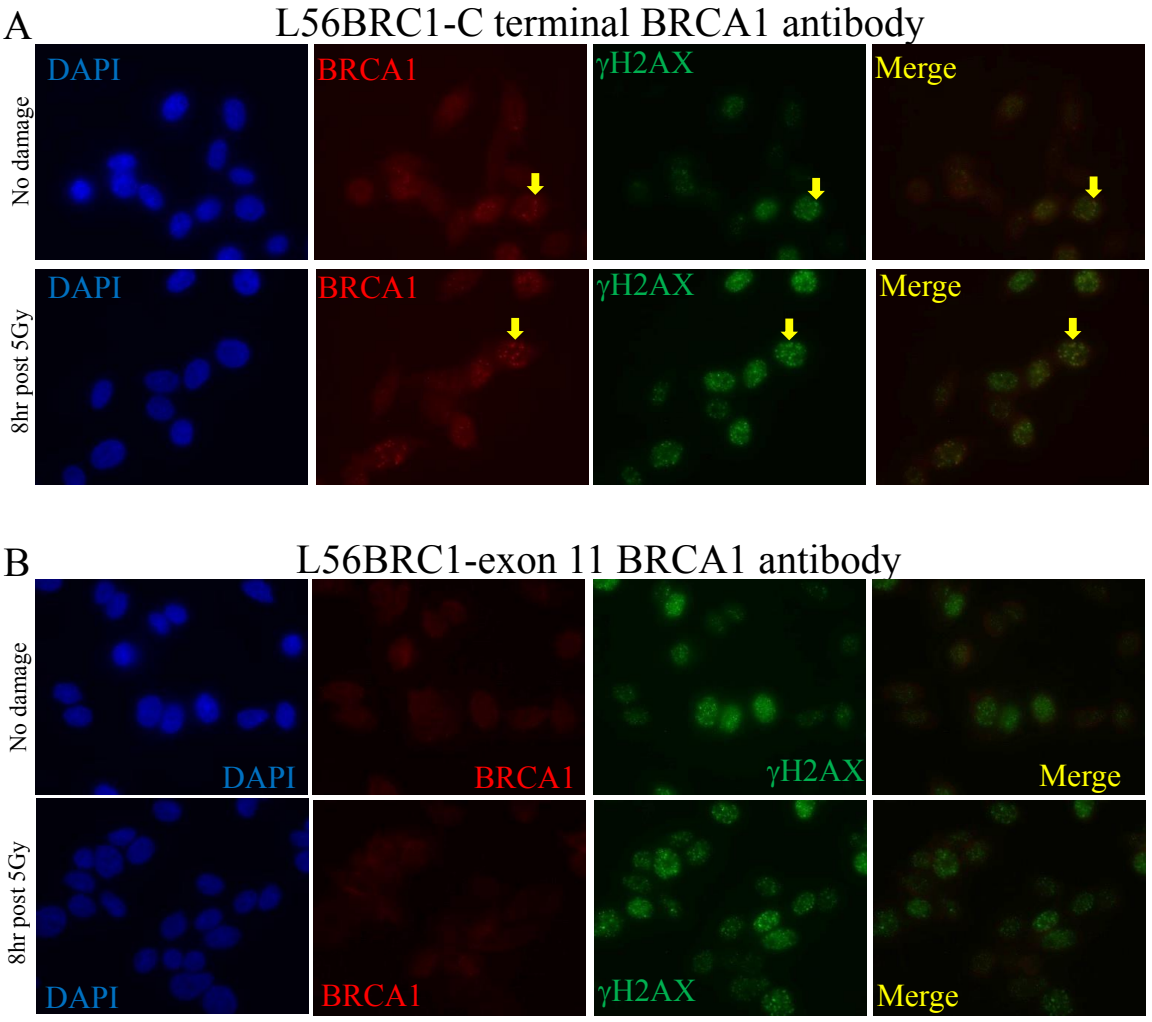

Figures 20, 21, 22 (Continued). Post-damage BRCA1 foci in Δ11b expressing mutant lines are not recognized by exon 11 specific BRCA1 antibodies: The two BRCA1 mutant control lines expressing Δ11b but not p220 (L56BRC1- **Figure 21** and SUM149-**Figure 22**), and a sporadic BLC line (MDA MB 231- **Figure 20**) were exposed to 5Gy gamma irradiation (IR) or no IR and allowed to recover for 8hr. All cells were then stained with a C-terminal specific BRCA1 antibody that recognizes both p220 and Δ11b **(Supplementary Figures 20A, 21A, 22A)** or an exon 11 BRCA1 antibody that cannot recognize Δ11b **(Supplementary Figures 20B, 21B, and 22B)**, both along with γH2AX to mark DNA damage. Yellow arrows are placed next to a few representative cells in which there is co-localization. The brightness has been increased by 20% and the contrast decreased by 20% using PowerPoint in every single panel to alleviate difficulties with the conversion of the images to PDF.

Figure 22 (Continued)

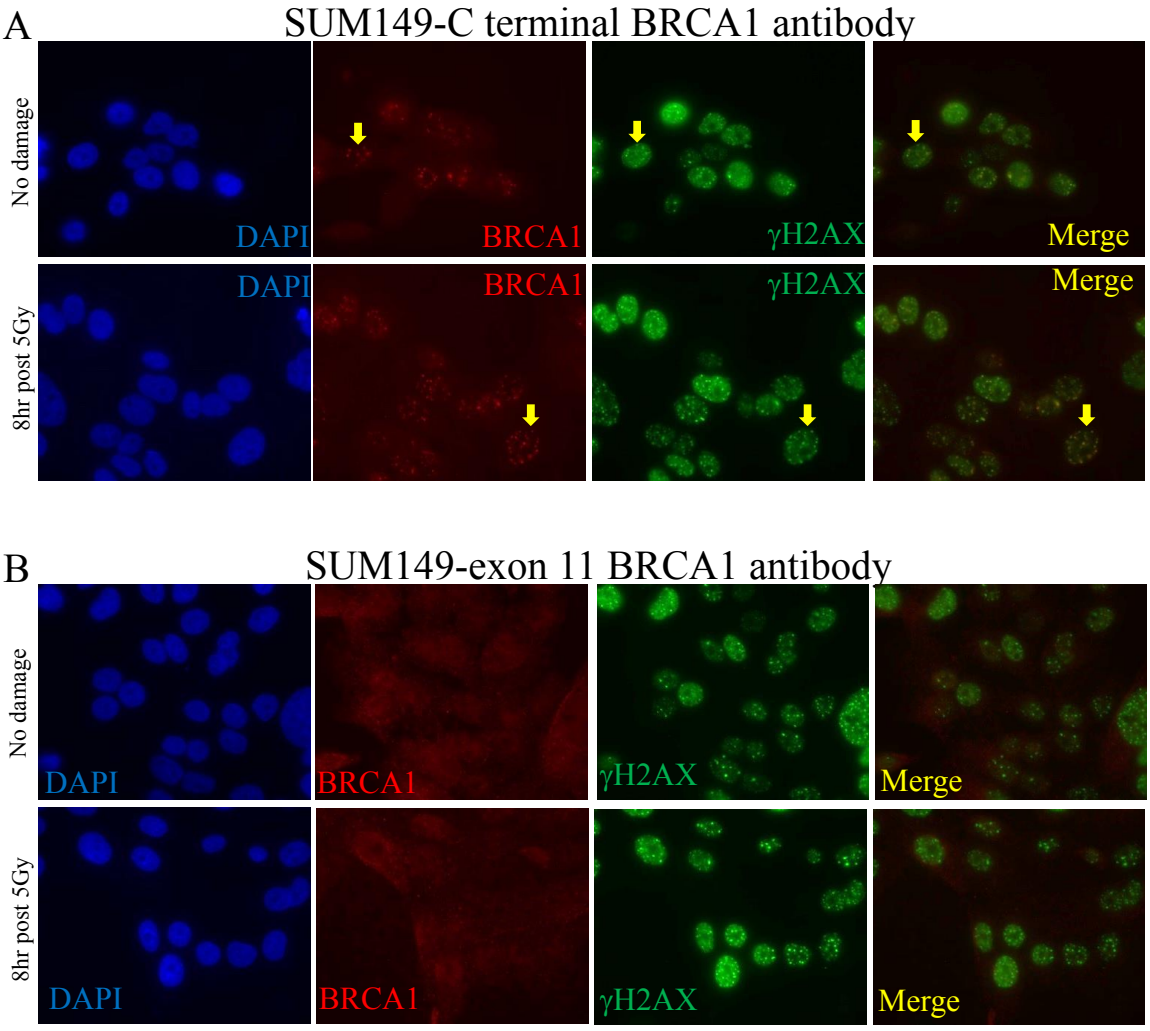

Figure 23. Post-Damage BRCA1 foci apparent in a BRCA1 mutant cell line able to express Δ11b disappeared when the line was transfected with a Δ11b-specific siRNA: The BRCA1 mutant cell line, SUM149, expresses Δ11b but not p220. It was transfected with either a control siRNA (siGL2) (**23A**), an exon 13-directed BRCA1 siRNA **(23B)**, an exon 11-directed BRCA1 siRNA **(23C)**, and a Δ11b junction-directed siRNA **(23D)**. These cells were exposed to either 5Gy gamma irradiation or mock treated, allowed to recover for 8hrs, and fixed. Immunofluorescence was then performed for BRCA1 with a C-terminal specific BRCA1 antibody and for γH2AX. Yellow arrows are placed next to a few representative cells in which there is co-localization. The brightness has been increased by 20% and the contrast decreased by 20% using PowerPoint in every single panel to alleviate difficulties with the conversion of the images to PDF.

Figure 23 (Continued)

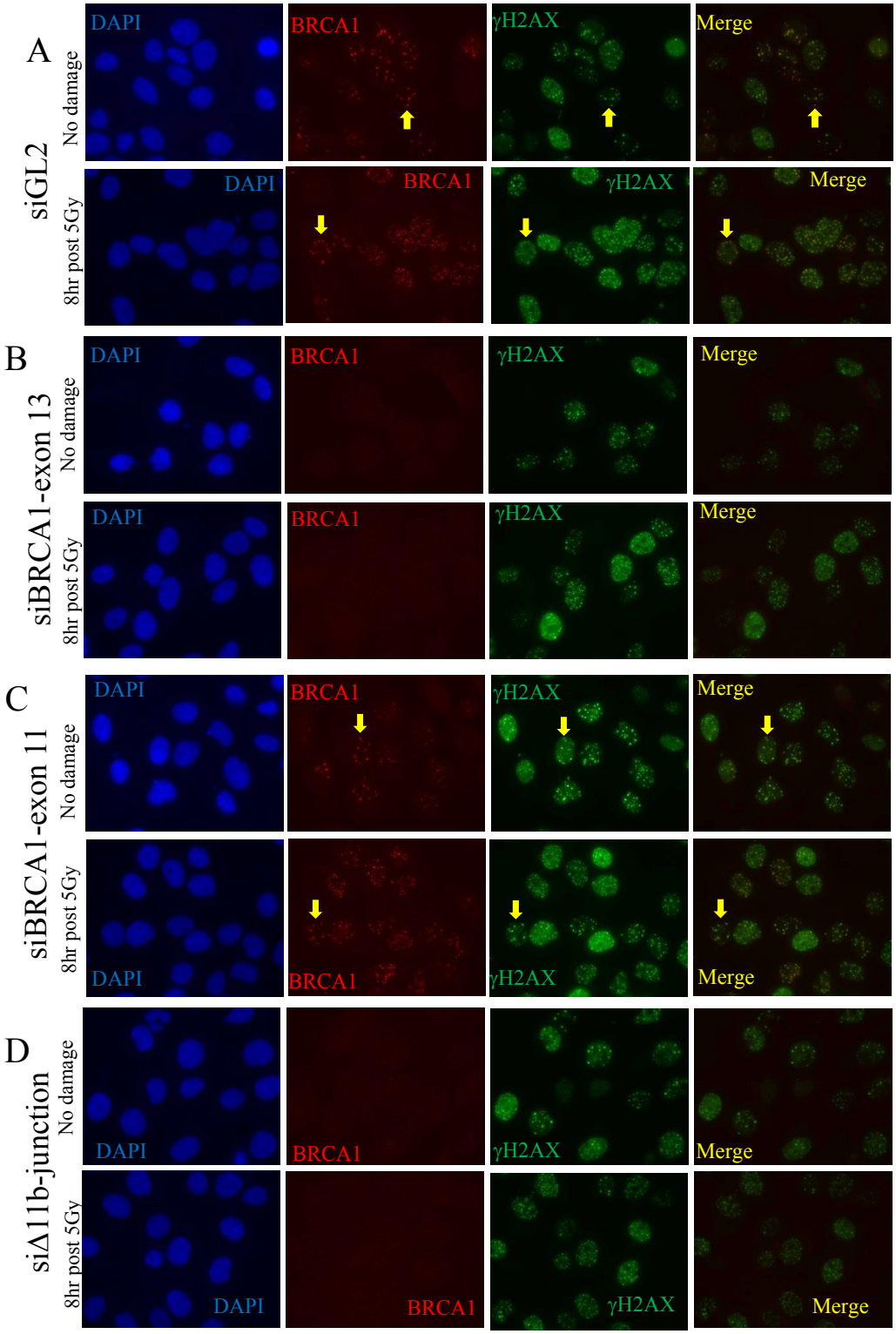

Stalled replication forks: We also assayed the cell lines for their ability to repair stalled or collapsed replication forks, another BRCA1 function (Pathania et al., 2011; Schlacher et al., 2012). This was undertaken by performing UV micropore analysis (Mone et al., 2001; Polo et al., 2006; Volker et al., 2001) (Figure 19D, Table 7). In these assays, BRCA1 concentrates in UV-irradiated micropore territories approximately 30 minutes after UV-C exposure in a replication dependent manner (Pathania et al., 2011). There it participates in the repair of stalled/collapsed replication forks (Pathania et al., 2011).

In all sporadic BLC lines and controls that were tested, BRCA1 was readily attracted to micropore territories (Figure 19D and Table 7), implying that the role of BRCA1 in stalled fork repair is intact in these cell lines up to the point of its recruitment to these structures. This does not mean that the function of some other BRCA1 partner in this pathway acting at the time of or after BRCA1 recruitment to these structures is not altered. In such a scenario, wild type (wt) BRCA1 would concentrate in sites at which stalled forks are co-located, but it would still result in defects in the repair of stalled or collapsed forks due to loss of function of a relevant BRCA1 binding partner.

In contrast, no BRCA1 was observed in micropores in the BRCA1 mutant lines, HCC1937 and SUM1315, and only faint BRCA1 micropore staining (suspected of reflecting the presence of Δ11b) was observed in SUM149 and L56BRC1, the two p220 negative, Δ11b-producing lines (Table 7).

DNA repair analysis:

Repair of mutagen-induced DNA damage

With these data in mind, we searched for defects in the repair of DNA damage elicited by various mutagens. We assayed all BLC cell lines for proficiency in the response to damage elicited by four, different mutagens by assessing colony formation after exposure to a range of doses (Figure 24).

To test DSB responses, we exposed the cell lines to gamma irradiation (IR) (Figure 24A). Half of the sporadic BLC lines were supersensitive to IR, like all BRCA1 mutant cell lines, suggesting the possibility of a functional defect, e.g. in a BRCA1 partner protein(s) that operates in DSB repair in these cells. However, half of the sporadic BLC lines were IR-resistant, like the controls. Since HR-incompetent cells are expected to be supersensitive to IR, these results suggested that not all of the sporadic BLC lines are defective in HR, in keeping with the above-noted IRIF analyses of these cells.

To test responses to interstrand cross link and stalled and collapsed replication forks, we exposed the cell lines to mitomycin C (MMC). All but one of the sporadic BLC lines and all but one of the BRCA1 mutant lines were supersensitive to MMC (Figure 24C). This suggests that these sporadic BLC lines are phenocopies of the BRCA1 mutant lines in manifesting defects in interstrand cross link repair and/or the subsequent replication fork stalling they are responsible for. BRCA1 contributes to such repair through multiple mechanisms (Bunting et al., 2012; Garcia-Higuera et al., 2001; Pathania et al., 2011; Schlacher et al., 2012; Vandenberg et al., 2003).

The responses to stalled and collapsed replication forks were independently tested by exposing the cells to UV irradiation. Here all sporadic BLC lines were supersensitive to UV irradiation when compared to controls (Figure 24B). The BRCA1 mutant lines had been

Figure 24. Sensitivity of cell lines to various DNA damaging agents: Enough cells for each line were plated in triplicate at a suitable density for colony formation, allowed to settle, treated with varying doses of different DNA damaging agents and then allowed to recover at 37°C until colonies became visible. After appropriately sized colonies had grown, the colonies were stained with crystal violet staining solution and counted with a Microbiology International ProtoCOL colony counter. IC50s for each cell line for each treatment were calculated based on the dose curves generated from these counts. The average IC50s for each cell line from 2-3 experiments are plotted for **A)** gamma irradiation, **B)** UV irradiation, **C)** Mitomycin C (MMC) treatment, and **D)** Methyl Methane Sulfonate (MMS) treatment. The color of the circle for each cell line represents the type of cell line as depicted in the key at the bottom of the figure.

Figure 24 (Continued)

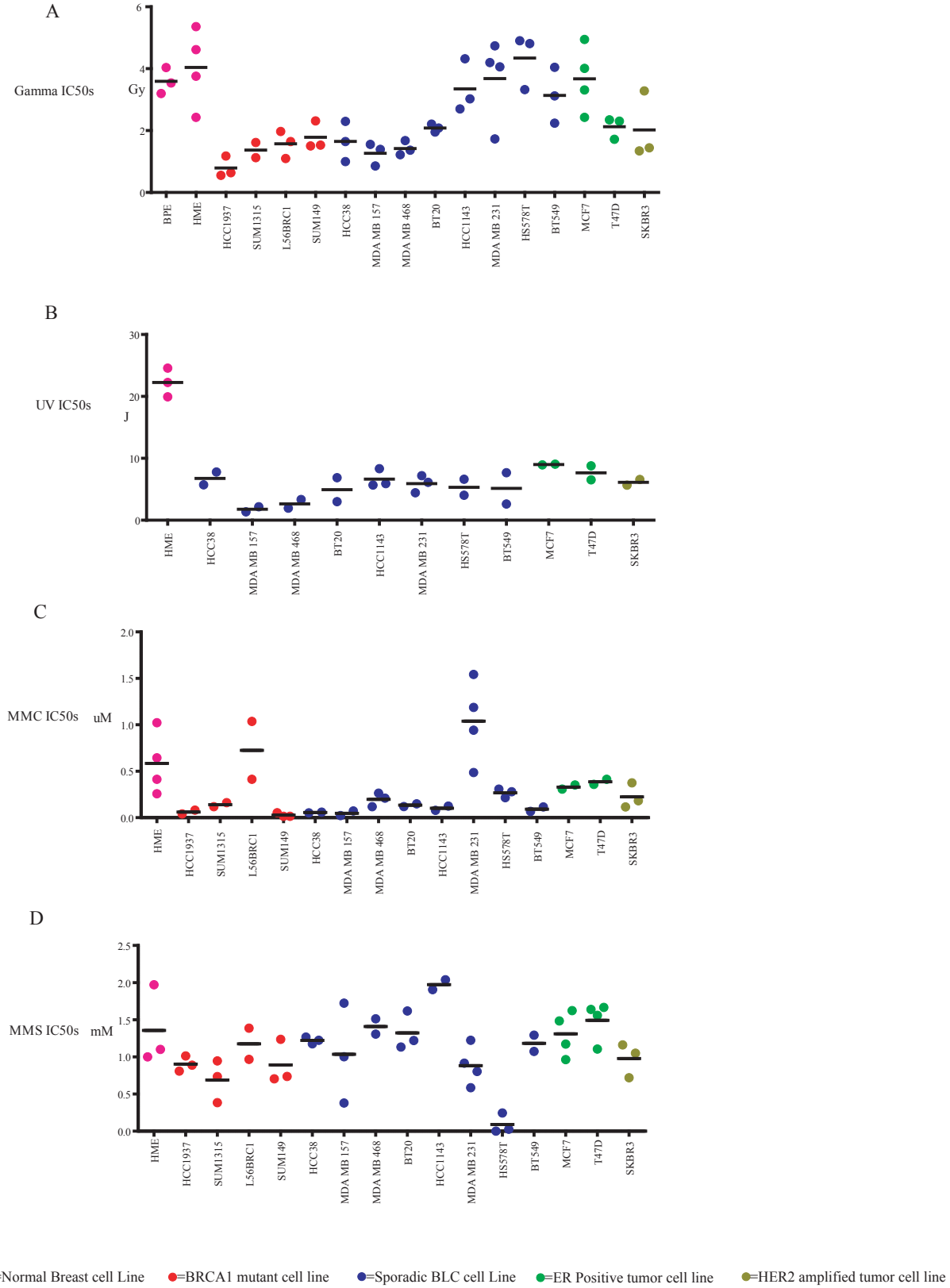

previously tested for sensitivity to UV (Pathania et al., 2011), and all were found to be supersensitive, with IC50s similar to or less than those of all the sporadic BLC lines shown here (Pathania et al., 2011).

When taken together, these and the MMC sensitivity results suggest that the sporadic BLC lines are phenocopies of BRCA1 mutant lines in their deficient responses to stalled replication fork development. When normally executed, stalled fork repair and the suppression of replication stress are known BRCA1 functions (Bunting et al., 2012; Garcia-Higuera et al., 2001; Pathania et al., 2011; Schlacher et al., 2012; Vandenberg et al., 2003). Since the sporadic BLC lines that were tested lack BRCA1 mutations, failed suppression of replication stalling and failed repair of collapsed forks in these cells may be a product of the defective function of a protein(s) that is/are active in these types of repair or of a non-genetically derived alteration in BRCA1 function, itself. These MMC and UV data suggest that stalled replication fork repair may be a commonly encountered problem in sporadic BLC lines.

Finally, in testing the cell lines for methyl-methane sulfonate [MMS] responsiveness, and thus an ability to perform base excision repair [BER], (Figure 24D), BRCA1 mutants and nearly all sporadic BLC lines revealed drug sensitivity similar to that of the controls. In fact, only one sporadic BLC line exhibited supersensitivity. This suggests that most of these lines are competent for base excision repair of MMS damage.

In contrast, most of these sporadic BLC lines and BRCA1 mutant controls are known to be supersensitive to hydrogen peroxide-induced oxidative damage, which can also be repaired by BER among other pathways (Alli et al., 2009). In addition, using an oxidative damage repair reporter, a decrease in oxidative damage repair efficiency has been observed in three of the

sporadic BLC lines, one of the BRCA1 mutant lines, and in a BRCA1-depleted line (Alli et al., 2009). Thus, loss of BRCA1 expression may result in a defect in oxidative damage-induced as opposed to base alkylation-induced BER (Alli et al., 2009). Moreover, there may be a defect in this form of BER in certain sporadic BLC.

Sporadic BLC lines are proficient in HR

Given the IR sensitivity results (Figure 24A), experiments were performed to test whether or not the above-noted sporadic BLC lines could perform HR, using a well-established HR reporter that allows an assessment of the ability of a cell line in which it is integrated to perform HR using FACS analysis (Pierce et al., 1999).

Stably transfected derivatives of three of the cell lines analyzed in the above-noted experiments were generated, each bearing a single, integrated copy of the above-noted HR reporter. One was a BRCA1 mutant line (SUM149), one an IR-resistant sporadic BLC line (MDA MB 231), and one an IR-sensitive sporadic BLC line (HCC38). Multiple clones of each were tested by southern blotting in search of any that contained a single, integrated copy of the HR reporter. One clone of each was identified (Figure 25A). Each was then studied for its ability to perform HR.

To test these cell lines for HR proficiency, we performed the above-noted HR reporter assay in cell lines transfected with either a firefly luciferase control siRNA (siGL2) or one of four, different BRCA1-specific siRNAs (Figure 25C, Table 8). To target Δ11b, we generated an siRNA targeting the unique junction sequence between the early part of exon 11, which is present in the Δ11b mRNA, and the 5' region of exon 12 (Figure 25B). An siRNA that targets exon 13 of BRCA1 was also employed. It should deplete both full length p220 and Δ11b (Figure

Figure 25. BLC lines are HR proficient regardless of gamma irradiation sensitivity status: **A)** Southern blots were performed on multiple clones of the three cell lines used in the above experiments to identify a clone from each line that carries a single, integrated copy of the I-SceI/GFP homologous recombination (HR) reporter. Blots for the three clones used in the HR reporter experiments are shown here. Based on the sequence of the reporter, we digested clonal genomic DNA separately with two different enzymes to assess reporter copy number. We digested with HindIII which should give rise to a band of 812 base pairs and another single band of varying size in clones bearing a single copy of the reporter. We also digested with StuI which should give a band of 2017 base pairs and another single band of varying size in clones bearing a single copy of the reporter. **B)** Map of the target sites of the four BRCA1 siRNAs used in the HR experiments on p220 and Δ11b. **C)** In the left panel, the average percentage of GFP-positive cells in the HR reporter assay for each cell line with each siRNA is represented in the bar graph. The error bars represent the standard deviation among four experiments. In the right panel, the HR reporter results have been normalized to the siGL2 control for each respective day in each respective cell line, and the bars in the graph represent the average percent GFP-positive cells relative to the siGL2 control for that cell line with the error bars representing the standard deviation among the four experiments. **D)** IP-western blotting was performed on extracts of each cell line transfected with each siRNA to demonstrate the efficacy of the specific isoform depletion of each siRNA. IPs were performed with a C-terminal BRCA1 antibody, and the blots were developed with an N-terminal BRCA1 antibody so that both the p220 and Δ11b isoform could be detected. A green arrow marks Δ11b and a red arrow p220. **E)** Western blots were performed on half of the cells from one round of the HR reporter assay to demonstrate the I-SceI

Figure 25. (Continued). BLC lines are HR proficient regardless of gamma irradiation sensitivity status: protein levels were the same in each cell line after each siRNA treatment. The I-SceI that was transfected was tagged with HA. After loading equivalent amounts of protein on the gel from each cell line transfected with each siRNA, the blots were stained with HA antibody to detect I-SceI. Tubulin blotting was performed to show that equivalent amounts of protein were loaded in each lane. (B1=BRCA1, ex=exon)

Figure 25 (Continued)

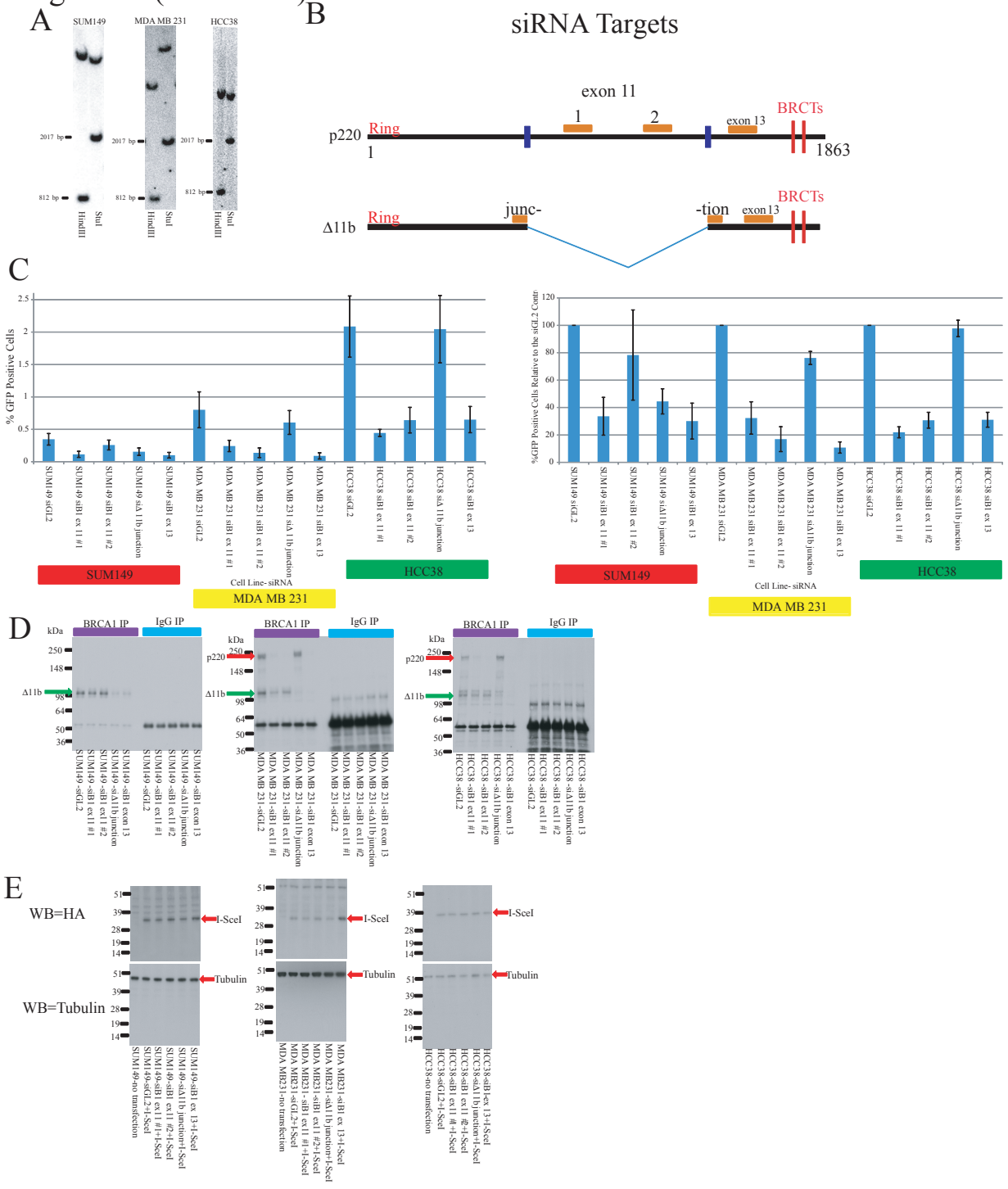

Table 8. HR reporter data corresponding to Figure 25C: Results from homologous recombination (HR) reporter assays on each cell line with each siRNA for four separate experiments. On the top panel, the percentage of GFP positive cells is reported. On the bottom panel the percentage of GFP positive cells relative to the siGL2 control is reported. (B1=BRCA1, ex=exon)

Table 8 (Continued). HR reporter data corresponding to Figure 25C

Percent GFP-positive cells for each cell line with each siRNA for each of four separate experiments

SUM149		Day 1	Day 2	Day 3	Day 4	Average of 4 days	Standard Deviation
	SUM149 siGL2	0.336	0.33991	0.465	0.24689	0.346949321	0.089660661
	SUM149 siB1 ex 11 #1	0.051	0.154	0.145	0.106	0.114	0.046882833
	SUM149 siB1 ex 11 #2	0.165	0.23	0.33	0.31	0.25875	0.075979712
	SUM149 si Δ11b junction	0.104	0.174	0.227	0.116	0.15525	0.056764866
	SUM149 siB1 ex 13	0.062	0.162	0.102	0.07994	0.101486052	0.043533134
MDA MB 231		Day 1	Day 2	Day 3	Day 4	Average of 4 days	Standard Deviation
	MDA MB 231 siGL2	0.482	0.841	0.733	1.15	0.8015	0.276758017
	MDA MB 231 siB1 ex 11 #1	0.188	0.37276	0.209	0.203	0.243191168	0.086832643
	MDA MB 231 siB1 ex 11 #2	0.034	0.18309	0.198	0.137	0.138022069	0.074049422
	MDA MB 231 si Δ11b junction	0.364	0.671	0.585	0.802	0.6055	0.184069733
	MDA MB 231 siB1 ex 13	0.033	0.139	0.07	0.119	0.09025	0.047926158
HCC38		Day 1	Day 2	Day 3	Day 4	Average of 4 days	Standard Deviation
	HCC38 siGL2	2.0464	1.43826	2.353	2.50525	2.085726817	0.471941768
	HCC38 siB1 ex 11 #1	0.458	0.385	0.512	0.42393	0.444731678	0.053857205
	HCC38 siB1 ex 11 #2	0.622	0.425	0.905	0.61485	0.641712031	0.197817165
	HCC38 si Δ11b junction	1.98	1.395	2.152	2.65274	2.044935959	0.518821277
	HCC38 siB1 ex 13	0.484	0.47	0.862	0.78409	0.650023291	0.202386573

Percent GFP-positive relative to the siGL2 transfection for each cell line with each siRNA for each of four separate experiments

SUM149		Day 1	Day 2	Day 3	Day 4	Average of 4 days	Standard Deviation
	SUM149 siGL2	100	100	100	100	100	0
	SUM149 siB1 ex 11 #1	15.1786	45.3066	31.1828	42.9339	33.65047371	13.77616905
	SUM149 siB1 ex 11 #2	49.1071	67.6657	70.9677	125.561	78.32551109	32.92776246
	SUM149 si Δ11b junction	30.9524	51.1906	48.8172	46.9843	44.48611456	9.185335681
	SUM149 siB1 ex 13	18.4524	47.6602	21.9355	32.3804	30.10710683	13.11344285
MDA MB 231		Day 1	Day 2	Day 3	Day 4	Average of 4 days	Standard Deviation
	MDA MB 231 siGL2	100	100	100	100	100	0
	MDA MB 231 siB1 ex 11 #1	39.0041	44.324	28.513	17.6522	32.37331592	11.80961034
	MDA MB 231 siB1 ex 11 #2	7.05394	21.7703	27.0123	11.913	16.93739252	9.088216902
	MDA MB 231 si Δ11b junction	75.5187	79.786	79.809	69.7391	76.21319395	4.764116973
	MDA MB 231 siB1 ex 13	6.84647	16.5279	9.5498	10.3478	10.81800935	4.090879335
HCC38		Day 1	Day 2	Day 3	Day 4	Average of 4 days	Standard Deviation
	HCC38 siGL2	100	100	100	100	100	0
	HCC38 siB1 ex 11 #1	22.3808	26.7684	21.7595	16.9215	21.95754929	4.030041933
	HCC38 siB1 ex 11 #2	30.3949	29.5495	38.4615	24.5424	30.73709044	5.761036661
	HCC38 si Δ11b junction	96.7555	96.9919	91.4577	105.887	97.77315153	5.982563043
	HCC38 siB1 ex 13	23.6513	32.6783	36.6341	31.298	31.06543338	5.435497527

25B). Finally, we employed two exon 11-specific siRNAs that depleted p220 but not Δ11b (Figure 25B).

IP-western blot analyses obtained with extracts of each of these single copy HR reporter-containing clones showed that these siRNAs deplete the predicted BRCA1 isoforms (Figure 25D). The slight depletion of Δ11b in the MDA MB 231 clone observed with the exon 11 siRNA #1 is likely due to slowing of the cell cycle caused by depletion of p220 and not an off target effect of the siRNA. Thus, with this possible exception, the siRNAs deplete the appropriate BRCA1 isoforms.

BRCA1 siRNAs were employed in these experiments for multiple reasons. First, BRCA1 is a physiological contributor to normal HR function (Li and Greenberg, 2012; Silver and Livingston, 2012; Walsh and King, 2007). Hence its depletion should result in a loss of HR capacity, if a given cell line can perform this function (Moynahan et al., 1999; Scully et al., 1999). Hence, in these experiments, BRCA1 depletion served as a positive control, employed to determine whether any GFP signals that were observed were a product of HR function. Second, using BRCA1 siRNAs made it possible to determine whether or not any HR activity that was measured in a reporter cell line was BRCA1-dependent. Finally, four, different BRCA1 siRNAs, each targeting a different region of the BRCA1 mRNA were employed (Figure 25B) to determine which isoform- p220, Δ11b, or both- was responsible for any HR activity that was observed in a given cell line. This question was particularly relevant for SUM149, which expresses the Δ11b but not the full length p220 isoform. IRIS does not concentrate in post IR-foci or bind BARD1, both HR-associated properties (ElShamy and Livingston, 2004). Therefore, it is not believed to be involved in HR and was not tested here.

In the HR analyses that were performed, it was not possible to compare, even semi-quantitatively, the HR functionality of the three lines that were tested. This is because the I-SceI driven HR reporter was integrated at different genomic sites in each cell line and because the cell lines are not isogenic. However, these considerations should not nullify the validity of an internal comparison within each cell line of I-SceI driven GFP production measured before and after BRCA1 depletion.

The results of the HR assay were presented as both the percent GFP-positive cells for each cell line as well as the percent GFP-positive cells relative to the siGL2 control for that line to facilitate their interpretation (Figure 25C, Table 8).

To control for variability in transfection efficiency of I-SceI, standardized western blotting for I-SceI was performed in conjunction with the HR assay (Figure 25E). I-SceI levels were relatively uniform in each cell line and were unaffected by the various BRCA1-directed siRNA treatments (Figure 25E). Thus, any differences in percent GFP- positive cells within a single cell line among the different siRNA transfections were not a product of varying transfection efficiency and/or I-SceI expression level. In initial experiments, we also co-transfected mCherry with the I-SceI and only scored mCherry positive cells in the FACS, also to control for transfection variability. There, too, the results were similar regardless of mCherry co-transfection (data not shown).

As shown in Figure 25C (for other related results, see Table 8), the SUM149 HR reporter-containing clone, which synthesizes Δ11b and not p220, exhibited measurable BRCA1-dependent HR function. When the line was transfected with the exon 13 siRNA, which depletes both p220 and the Δ11b BRCA1 isoform, or with the Δ11b-specific junction siRNA, the

percentage of GFP positive cells decreased, reflecting the presence of BRCA1 gene product-dependent HR in this line. As expected, one of the exon 11 siRNAs [#2] had no effect on HR activity in this line while the other [#1] caused a decrease. In light of the junction siRNA effect and the lack of effect of exon 11 siRNA #2, one can argue that SUM149 HR activity is Δ11b dependent. Given the HR-suppressing effect of the other exon 11 siRNA [#1], it is conceivable that a yet undetected, alternatively spliced BRCA1 mRNA is expressed in these cells and its product contributes to the observed HR function. Alternatively, HR suppression by this siRNA species represents an off-target effect.

Among sporadic BLC HR reporter-containing lines, MDA MB 231, which was relatively IR-resistant (Figure 24A), appeared to be HR-proficient. When this line was transfected with each of the exon 11 specific siRNAs or the exon 13 siRNA that depletes both isoforms, HR proficiency decreased significantly (Figure 25C, Table 8). In contrast, the Δ11b specific junction siRNA had no effect (Figure 25C, Table 8). Thus, this line appears to perform HR in a p220-dependent manner.

HCC38 cells were supersensitive to IR (Figure 24A), but they yielded a significant percentage of GFP positive cells after siGL2 transfection and a decreased percentage of GFP positive cells after exposure to either of the exon 11 siRNAs or the exon 13 siRNA (Figure 25C, Table 8). Like MDA MB 231 cells, its HR signal was unaffected by the Δ11b junction-specific siRNA (Figure 25C, Table 8). Thus, although it is supersensitive to IR, HCC38 is HR-proficient, and it too performs HR in a p220-dependent manner.

Taken together, these results strongly suggest that, in cells lacking a BRCA1 mutation (Bamford et al., 2004; Elstrodt et al., 2006), p220 is responsible for HR, but in cells only able to

express Δ11b, the Δ11b isoform is, itself, capable of performing HR. In addition, these results and those described earlier collectively suggest that the multiple sporadic BLC lines tested, regardless of their IR sensitivity, are each HR-proficient and, where tested, this DNA repair function is BRCA1 gene product-dependent.

Chapter 6-Discussion of BLC results

-All writing in this chapter was performed by SJH.

The work in chapter 5 was performed on a subset of human breast cancer cell lines that collectively represent the BLC subtype (Neve et al., 2006). The results fail to support the hypothesis that, as a general matter, sporadic BLCs exhibit an HR defect and, therefore, are valid phenocopies of BRCA1 mutant tumors in this regard. Rather, they suggest that other BRCA1-related DNA repair defect(s) exist in significant numbers of sporadic, BRCA1 wt, BLCs. Specifically, these defects affect the responses of cells to stalled and collapsed replication forks (Bunting et al., 2012; Garcia-Higuera et al., 2001; Pathania et al., 2011; Schlacher et al., 2012; Vandenberg et al., 2003). These data are supported by the results of recent clinical trials and retrospective studies of this tumor subtype (Chew et al., 2009; Hurley et al., 2013; Silver et al., 2010; Sirohi et al., 2008; Staudacher et al., 2011), and it suggests that therapeutic strategies aimed at inducing replication stress in tumor cells may be useful in this tumor type.

In keeping with this notion, PARP inhibitors, the toxicity of which relies on tumor cells exhibiting an HR defect (Farmer et al., 2005; Helleday, 2011; Murai et al., 2012), have been of particular interest. These agents have been tested in a wide variety of tumors, but they have been most promising in the clinic in the therapy of both BRCA1 and BRCA2 mutant breast and ovarian tumors (Fong et al., 2009; Gelmon et al., 2011; Liu et al., 2013), as well as in certain sporadic ovarian cancers (Gelmon et al., 2011; Liu et al., 2013). The notion that sporadic BLCs manifest a defect in HR and the success of these agents in BRCA1 mutant tumors has spurred clinical trials with PARP inhibitors in sporadic BLC. However, clinical trials of PARP inhibitors in sporadic BLC have failed both as single agents (Fong et al., 2009; Gelmon et al., 2011) and

when PARP inhibitors were combined with other drugs (Liu et al., 2013). We did not test our cell line panel for PARP inhibitor sensitivity, because most of the cell lines along with others representing different subtypes had already been tested for sensitivity to two different PARP inhibitors (Pierce et al., 2013). The results showed that sensitivity did not depend upon subtype or BRCA1 status (Pierce et al., 2013). These results, taken together with the lack of an HR defect in sporadic BLC cell lines observed in our results, may help to explain why PARP inhibitors have failed in the therapy of sporadic BLCs. In contrast, we did not test any ovarian cancer cell lines for HR proficiency, but, based on the PARP inhibitor trial results, this may be informative.

In contrast, clinical trials and retrospective studies examining the efficacy of the interstrand cross link-inducing and subsequent replication fork-stalling drug, cisplatin, have been successful in BLC (Chew et al., 2009; Hurley et al., 2013; Silver et al., 2010; Sirohi et al., 2008; Staudacher et al., 2011), and results presented here suggest a mechanism that underlies this success. These data reveal that all of the sporadic BLC lines tested were supersensitive to an interstrand cross link-inducing agent and UV irradiation (Figure 24), both of which ultimately give rise to stalled and collapsed replication forks. Moreover, BRCA1 participates in the repair of stalled and collapsed replication forks (Bunting et al., 2012; Garcia-Higuera et al., 2001; Pathania et al., 2011; Schlacher et al., 2012; Vandenberg et al., 2003). In addition, BRCA1 mutant cell lines proved to be supersensitive to agents that cause stalled replication forks such as MMC, cisplatin, and UV (Bhattacharyya et al., 2000; Pathania et al., 2011).

Given these findings, we propose that sporadic BLCs are phenocopies of BRCA1 tumors in manifesting a defect in various forms of stalled and collapsed replication fork repair (Bunting

et al., 2012; Garcia-Higuera et al., 2001; Pathania et al., 2011; Schlacher et al., 2012; Vandenberg et al., 2003). However, they do not appear to be uniformly defective in HR. These considerations suggest that pursuing agents which elicit replication fork stalling through a mechanism that threatens BLC survival because of their inability to repair it represent rational therapeutic strategies in sporadic BLC.

In addition, there may be a role for Δ11b in HR. We have confirmed that Δ11b is recruited to post-gamma irradiation damage foci (Table 7, Figures 20-23) (Huber et al., 2001), which suggests that Δ11b concentrates in a suitable nuclear location to participate in HR function. In addition, a BRCA1 mutant cell line that expresses Δ11b and not p220 exhibited a measurable level of Δ11b-driven HR in an HR reporter assay.

These data are supported by work in model organisms. Δ11b is the only BRCA1 isoform expressed in C. elegans, and it and the C. elegans BARD1 ortholog appeared to trigger DNA damage repair in that organism (Boulton et al., 2004). In addition, in HR reporter-bearing mouse ES cells in which p220 but not Δ11b is deleted, HR levels were still detectable, suggesting that Δ11b is an HR contributor in this setting an observation that has also been made by others (DelloRusso et al., 2007; Moynahan et al., 1999; Moynahan et al., 2001; Westermark et al., 2003).

The importance of this finding is highlighted by observations in patients and model organisms. Mice that only express Δ11b in a p53 heterozygous setting developed normally but exhibited early onset breast tumors (Xu et al., 2001b). Similarly, a patient with a bi-allelic mutation at the BRCA1 locus still expressing intact Δ11b but not p220 exhibited multiple developmental abnormalities and was diagnosed with early onset ovarian cancer (Domchek et

al., 2013). Taken together, these results suggest a scenario in which Δ11b expression, in the absence of p220, generates enough BRCA1 DNA repair function, manifest at least in part through HR, to prevent embryonic lethality. However, it does not generate enough other BRCA1 function to prevent embryonic development defects and BRCA1-related tumorigenesis. If validated, this would further imply that, even if it is required to suppress breast and ovarian cancer development, its HR function is insufficient to do so alone.

In summary, the results of this study demonstrate that tumor cell lines derived from a number of sporadic BLC (Neve et al., 2006) are BRCA1 mutant breast cancer cell phenocopies with respect to a subset of BRCA1 functions that direct the repair of stalled and collapsed replication forks (Bunting et al., 2012; Garcia-Higuera et al., 2001; Pathania et al., 2011; Schlacher et al., 2012; Vandenberg et al., 2003). These findings are consistent with successes observed in clinical trials (Chew et al., 2009; Silver et al., 2010) and retrospective studies (Hurley et al., 2013; Sirohi et al., 2008; Staudacher et al., 2011) of cisplatin in sporadic BLC and support efforts to adapt a state of increased, BLC-specific replication stress to its therapy.

Chapter 7-Conclusion

-All writing in this chapter was performed by SJH.

The work in this thesis focused on identifying new functions for BRCA1, on better understanding known functions, and on attempting to identify the functional pathways to which BRCA1 contributes that are defective and thus possibly therapeutic targets in BRCA1 mutant and sporadic BRCA1-like cancers.

Through a dual Y2H/TAP-MS screening effort we expanded the BRCA1 interactome. This was a particularly useful exercise, because there is still not a definitive list of known BRCA1 interactors available, despite multiple attempts at defining new interactors (Pujana et al., 2007; Wang et al., 2000; Woods et al., 2012). In assessing the quality of our dataset, we tried to ask how many known BRCA1 interactors we detected, and we found that 25 of the 147 hits from the dual screening effort had been detected as physical interactors in previous screens for BRCA1 protein binding partners (Pujana et al., 2007; Wang et al., 2000; Woods et al., 2012). This suggested that many of our hits may prove to be physiological interactors of BRCA1. In addition, the hits from our screen can now be taken together with the hits of other similar screens as a list of known BRCA1 interacting proteins.

In addition, the work also highlighted new groups of BRCA1 interacting partners that aid in some of the known and also in a new BRCA1 function. Among such associations, the screen revealed that BRCA1 interacts with multiple proteins involved in transcription and transcription-associated DNA damage. This led us to investigate whether BRCA1, perhaps along with some of those interactors, plays a role in that process.

We demonstrated that cells depleted of BRCA1 become more sensitive to transcription-arresting agents that cause DNA damage and that the DNA damage caused by those agents is exacerbated upon BRCA1 depletion. These findings indicate a role for BRCA1 in the prevention or repair of transcription-associated DNA damage. We validated the physiological interaction between BRCA1 and multiple transcription-associated hits from our screen by demonstrating genetic interactions between BRCA1 and TCEA2, TCEANC, SETX, and TONSL. These interactions supported the hypothesis that BRCA1 participates in transcription-associated DNA damage repair and also suggest multiple mechanisms through which it might do so. The identities of these proposed mechanisms are based on already known functions of the interactors.

Upon in depth analysis of the BRCA1-TONSL complex, we also found that BRCA1 interacts genetically with the TONSL-interacting FACT complex, which consists of SSRP1 and SUPT16H. This was interesting because FACT participates in chromatin remodeling during transcription to allow a transcription complex to move through DNA without interrupting its epigenetic signature (Reinberg and Sims, 2006). Based on additional results, we hypothesized that a FACT-TONSL-BRCA1 complex participates in repairing transcription-associated DNA damage after UV treatment. This was supported by the fact that, after UV irradiation, BRCA1 concentrates at sites of transcription-associated DNA damage.

Finally, we demonstrated that proteins engaged in this new functional pathway and some of the BRCA1 interactors from the screen are potentially important in tumorigenesis. We found that multiple hits from the screen exhibited altered expression levels in breast and ovarian tumors that are associated with bad clinical outcomes. In addition, we found that multiple hits from the screen, including a number of the transcription-associated proteins map to amplification or

deletion regions in breast, ovarian, and across 11 different tumor types. This suggests that some of the hits are also cancer genes.

The new role for BRCA1 in transcription-associated DNA damage identified by the screen may be clinically relevant. As previously stated, some of the hits may be the products of cancer genes, since our analysis mapped many of them, including some of the transcription-associated hits, to both amplification and deletion regions across multiple different cancer types. Also, the cross-linking agent cisplatin is effective in the therapy of some patients with sporadic, BRCA1-like basal-like breast cancer; and this success may be due to a defect in the ability of these cancer cells to repair transcription-associated DNA damage, one form of damage generated by cisplatin (Todd and Lippard, 2009). Further analysis must be performed to determine whether it is transcription-associated DNA damage repair, stalled fork repair, or both that are defective in these tumors.

In addition to the above-noted findings, the bipartite, complementary screening method and the approaches used to validate key results of it proved to be especially valuable. Hence, they may prove to be relevant to other such interaction screens.

While the overlap in hits detected in the two screening processes was small, it was meaningful, given results of previous screens of this nature (Rozenblatt-Rosen et al., 2012). It is not surprising that there were only three overlapping proteins between the two screening modalities since the two methods ask different questions and each has different limitations. The Y2H screen can only detect direct interactions that do not require post-translational modifications to either interactor, and it is limited to the library with which one is screening (in our case, a library of approximately 15,000 human open reading frames). The Y2H could miss

certain interactions detected in a TAP-MS screen, because those interactions may require post-translational modifications, may be indirect, or may involve complexes containing BRCA1/BARD1 and a protein or isoform of a protein not represented in the ORFeome library we screened. In contrast to the Y2H method, the TAP-MS method detects interactions between large complexes of proteins that may be indirect and may rely on either post-translational modifications or perhaps linking structures like chromatin to facilitate the interaction. These possibilities cannot be detected by Y2H. However, the TAP-MS method does not reveal whether or not an interaction is direct, as the Y2H does. These limitations explain the lack of overlap between the screens but also point out the value of performing a dual screen.

Despite the small overlap, the low number of overlapping hits detected amidst a relatively large number of total hits from the two screening approaches highlighted multiple benefits of performing a combined Y2H and TAP-MS screen. First, it demonstrated that large numbers of non-overlapping new interactors involved in similar functions could be identified at the same time by both methods, highlighting the fact that utilizing two screening methods at once can be helpful in identifying a greater number of unique interactions. In addition, the fact that there were sizable numbers of hits, including some of the overlapping interactors, that were engaged in a common set of transcription-associated functions led us to hypothesize and investigate a new functional role for BRCA1 in DNA damage responsiveness and repair. The genetic and cell biological evidence reported here strongly supports this hypothesis, namely that BRCA1 operates in response to defective transcription and transcription-associated events that give rise to DNA damage.

We employed a genetic assay to validate some of the hits from the screen. We chose this approach because a) many of our interactors were difficult to co-immunoprecipitate as endogenous polypeptides, and b) for some there was a lack of commercially available antibodies. Genetic approaches based upon synthetic lethality obtained in cells rendered heterozygous for one or more putative interacting proteins may be a useful way to validate protein-protein interactions in the future which is often a difficult goal to achieve using traditional methodology, and, even when successful, may not allow one to know that a given interaction is physiologically relevant. Genetic approaches can provide physiological insights, if suitably designed.

The results from the genetic interaction assays and also the DRB and alpha-Amanitin sensitivity testing in this thesis suggest that BRCA1 depletion is synthetically lethal in combination with halting of transcription or loss of function of one of the six genetic interactors. We have suggested that this is because BRCA1 operates in the repair of transcription-associated DNA damage by functioning in mechanistically similar ways as its genetic interactors or at least by recruiting those interactors to sites of transcription-associated DNA damage. However, one must be careful when making such an assessment of genetic results, since it is entirely possible that it is the BRCA1 function in HR and/or another DNA repair process that is synthetically lethal in combination with halting of transcription or loss of function of certain transcription-associated proteins.

An important aspect of the future work resulting from this screen will be in studying the mechanism(s) by which BRCA1 participates at sites of transcription-associated DNA damage. To ascertain whether or not the role of BRCA1 in HR is important at these sites, it will be necessary to test whether or not co-depletion of both BRCA1 and 53BP1 can rescue the

sensitivity of BRCA1 depleted cells to DRB or alpha-Amanitin. Depleting 53BP1 in BRCA1 depleted cells rescues the HR defect observed in these cells (Bouwman et al., 2010). Thus, if 53BP1 depletion rescues the DRB or alpha-Amanitin sensitivity in BRCA1 depleted cells, this would suggest that it is the role of BRCA1 in HR that helps repair transcription-associated DNA damage and not a role in repair that is unique to transcription-associated DNA damage sites.

It is likely that there will be some role for HR in the repair of transcription-associated DNA damage. However, it is also possible that BRCA1 plays a role in multiple aspects of the repair. Since BRCA1 is known to interact with RNA Polymerase II, it is possible that BRCA1 is recruited to active transcription complexes that have stalled at difficult to transcribe templates or sites of damage, that have collapsed, or that have been paused long enough for stabilization of an R-loop. Once recruited to these sites, BRCA1 may recruit different protein binding partners, such as SETX, TCEA2, TONSL, or FACT to help deal with various aspects of overcoming the obstacle or break or simply repairing the break. It will be important to establish an order of arrival at transcription-associated DNA damage sites for these proteins in the future, as well as any others identified in the dual screening effort. It will also be important to determine which, if any, BRCA1 HR repair machinery is recruited to these sites.

Generating a transcription reporter plasmid in which a single break or obstacle to transcription can be generated and easily detected by ChIP would be useful in this regard. One could follow the temporal and proximal binding dynamics of BRCA1, DNA damage response proteins, and transcription-related proteins at these sites in a quantitative and temporal manner by ChIP.

In addition to studying BRCA1 function at transcription-associated sites of DNA damage, it will also be important to study what other proteins are important in the repair or prevention of this type of damage. One approach to defining such proteins would be to perform an siRNA screen in cells exposed to a sub-lethal dose of DRB or alpha-Amanitin and determine which depletions lead to cell death in this setting. This may suggest new protein partners important in this type of repair and also may define new pathways associated with this type of DNA damage. It may also help to define therapeutic targets relevant in specifically treating tumors with defects in this type of repair.

In the second part of my work, multiple breast cancer cell lines were employed to search for the presence of any BRCA1 DNA damage response pathway defects present in sporadic BLC cells. The prevailing hypothesis was that, given the similarity to BRCA1-/- breast cancer, an HR defect would exist in some if not most BLC cancers. However, based on the results of our sensitivity screening and HR reporter assays, it appears that sporadic BLC lines are often competent for HR but defective in the repair of DNA damage generated by crosslinking agents and UV.

Crosslinking agents like MMC and cisplatin can arrest both transcription and DNA replication generating DNA damage by both methods (Todd and Lippard, 2009) as can UV damage. BRCA1 was known to be involved in the repair of stalled replication forks prior to this work (Pathania et al., 2011; Schlacher et al., 2012). Therefore, it is possible that sporadic BLC exhibit a defect in stalled fork repair. However, crosslinking agents and UV also cause transcription arrest and may give rise to transcription-associated DNA damage. We have identified a role for BRCA1 in this process, and thus at least some sporadic BLC may exhibit a

defect in this process. If so, some of those tumors should, in principle, be sensitive to DNA crosslinking agents, which clinical trials reveal is the case. The pathways responsible for the sensitivity must be studied further to test this hypothesis and determine whether it is clinically relevant.

Thus far, the BLC data is consistent with the results of current clinical trials. The fact that sporadic BLC do not harbor an HR defect fits with the finding that PARP inhibitors, drugs that rely on an HR defect for efficacy, have failed in trials of sporadic BLC (Fong et al., 2009; Gelmon et al., 2011; Liu et al., 2013). Our finding that sporadic BLC likely harbor a defect in stalled replication fork repair or transcription-associated DNA damage repair fits with the finding that some cases of sporadic BLC respond well to treatment with cisplatin (Chew et al., 2009; Hurley et al., 2013; Silver et al., 2010; Sirohi et al., 2008; Staudacher et al., 2011), which causes these types of damage (Todd and Lippard, 2009).

An important aspect of future work on this project will be to determine whether sporadic BLC harbor a defect in stalled replication fork repair, transcription-associated DNA damage repair, or both. Determining whether or not the panel of sporadic BLC lines is super-sensitive to alpha-Amanitin would suggest that the lines harbor a defect in repairing the type of DNA damage caused by this agent. If a subset of sporadic BLC cell lines are sensitive to alpha-Amanitin, it would be important to test the ability of those lines to restart transcription after various forms of DNA damage. This would allow one to be certain that the sensitivity to alpha-Amanitin was not due to a defect in repairing replication forks stalled by halted transcription. This could be achieved by staining for EdU nucleotide incorporation, which is specific to transcription, at various timepoints after UV damage or other forms of damage, which is an

effective method of studying transcription restart (Dinant et al., 2013). If some of the lines exhibit defects in repairing transcription-associated damage, it will be important to determine what the mechanistic defect is and whether or not this is a therapeutic target.

Determining the mechanism of the defect in sporadic BLC will be important regardless of whether it is in transcription- or replication-associated repair. In addition to the above experiments, it may be interesting to perform siRNA screens on a subset of the sporadic BLC lines and controls in the setting of cisplatin or alpha-Amanitin treatment in an attempt to determine which proteins or pathways make these lines exquisitely sensitive to these agents. This may be important in generating relevant targeted therapies that are directed against specific functional pathways or even specific proteins in these types of tumors.

Overall, the work reported in this thesis has identified a new BRCA1 functional pathway and potentially new cancer genes associated with it. These insights are based, in part, upon the genetic interactions detected between BRCA1 and relevant interactors in the screen. In addition, the work has shown that the prevailing hypothesis regarding a common/universal HR defect in sporadic BRCA1-like breast cancers is not correct. Rather, at least some of these cancers are defective in repairing DNA damage caused by interstrand crosslinks and/or in the repair of stalled replication forks and transcription complexes.

Gaining a better understanding of how stalled forks and halted transcription-associated damage are repaired by BRCA1 could lead to specific targeted therapies for this type of breast cancer. It could also lead to relevant biomarkers and somatic genetic mutation associations with this type of breast cancer. Finally, gaining a better understanding of transcription-associated DNA damage and its repair in general may be important in non-neoplastic diseases, as well.

This type of damage also occurs in G0 cells, such as axon-bearing cells in the CNS, cells of the myocardium, etc. Hence it might prove to be associated with the pathogenesis of certain diseases that affect these cell types.

Appendix

Materials and Methods for chapters 2-4

-All writing in this section was performed by SJH. Thomas Rolland assisted in the statistics sections, and Guillaume Adelmant assisted in the mass spectrometry section.

Statistics: All statistics were computed using the R software unless otherwise stated (R Core Team. *R: A language and environment for statistical computing.* R Foundation for Statistical Computing, Vienna, Austria, 2013). Calculations specific to each assay will be described with the assay below.

Yeast two-hybrid (Y2H) screen:

Generation of BRCA1 open reading frame clones: The full-length and ten selected fragments of the BRCA1 (p220) open reading frame (ORF) were generated by PCR from a sequenced p220 cDNA and cloned using Gateway recombinational cloning (Rual et al., 2004).

Preparation of Y2H bait and prey libraries: All BRCA1 ORFs were transferred into Y2H destination vectors pDEST-AD-CYH2 by Gateway recombinational cloning (Life Technologies) to generate Gal4 activation domain hybrid proteins (AD-ORFs). BRCA1 could only be screened as prey, because the BRCT domains render BRCA1 an autoactivator. The collection of ~15,000 ORFs of the human ORFeome v5.1 was previously transferred into the Y2H destination vector, pDEST-DB, to generate Gal4 DNA binding domain hybrid proteins (DB-ORFs) (Dreze et al., 2010). The opposite orientation was not tested since BRCA1 ORFs were found to be autoactivating when fused to the DB domain.

Y2H screen: All BRCA1 full length and fragment AD-ORFs were pooled and screened against each DB ORF, as described previously (Dreze et al., 2010). Two, independent screens were performed, and a mix of colonies was picked from each growth spot to account for multiple interactions involving different AD-ORFs, a result of the pooling strategy. We performed PCR amplification of each primary positive colony, and PCR amplicons were Sanger sequenced individually. Sequencing reads were matched to the hORFeome v5.1 database and to BRCA1 ORFs, using BLASTN with default parameters. The e-value cutoff was set to 1×10^{-15}, and the ORFs were assembled into Interacting Sequence Tags (ISTs). For each IST found, all combinations of each BRCA1 AD-ORF and the identified hORFeome v5.1 DB-ORF were considered and subjected to verification.

Y2H verification: Each candidate primary hit was verified multiple times by individual pair-wise retesting to obtain the highest possible quality (Dreze et al., 2010). Each primary hit was retested either in single pairwise retest screens or in high-throughput screens as quadruplicates. The individual pairwise retests were performed multiple times, and interactors had to appear in a retest in order to be considered positive. For the quadruplicates, only those found positive in at least three out of the four independent replicates were considered positive. To confirm identity of the verified interactors, positive colonies were picked and processed for Sanger sequencing and aligned to the corresponding ORFs as described above.

Filtering the Y2H results: Three proteins were not found to interact with the full-length BRCA1 protein but with products of non-overlapping fragments of the BRCA1 ORF. They were, therefore, removed from the list of positive BRCA1 interactors.

Cell Culture: U2OS, HeLa S3, and 293FT cells were cultured in DMEM containing 10%FBS and 1%PenStrep. Selective antibiotics were added as described in the various assays below. HCC38 cells were cultured in ATCC RPMI 1640 (ATCC Cat. #30-2001) with 10%FBS and 1%PenStrep. The BRCA1 stably transduced HCC38 cell line was cultivated in Blasticidin (2.5ug/mL)-containing medium.

Packaging and Infection of FLAG-StrepTactin-BARD1 and other retroviral cDNAs: TONSL and MAP3K14 were cloned into a retroviral expression vector, MSCV HA-FLAG-puro (a gift from Wade Harper), via Gateway cloning (Life Technologies). Full length BARD1 cDNA was cloned into the pSTR-N-IL2Rα vector. Plasmids were packaged into retroviruses using standard packaging plasmids (HDM.G and pMD.MLV) by co-transfection into 293FT cells using Polyfect (Qiagen Cat. # 301105). Cells were infected with virus and selected for infection 48 hours later. For the pSTR-N infections, the cells were sorted three times after infection using IL2Rα antibody (Millipore 05-170)-coated magnetic beads (Life Technologies Cat. # 11033). For the MSCV-HA-FLAG infections, cells were selected by adding 1ug/mL puromycin to the media.

Tandem Affinity Purification and MS: Nuclei were harvested from 30x15cm plates of pSTR-N-vector or pSTR-N-BARD1 containing HeLa S3 cells by dounce homogenization.

All buffers described in the remainder of the protocol contained Roche EDTA Free Protease Inhibitor (Roche Diagnostics 11 836 170 001) and a phosphatase inhibitor (Sigma P0044). The nuclei were lysed at 4°C in buffer containing 150mM NaCl, 50mM Tris-HCl pH

7.5, 1mM EDTA, 0.5% NP40, and 10% glycerol. The lysate from this step was saved and used as the soluble nuclear fraction. The pellet was digested with micrococcal nuclease (Roche Diagnostic 10107921001). For this digest, the pellet was first resuspended, by pipetting up and down multiple times, in micrococcal nuclease buffer (MNase buffer) containing 20mM Tris-HCl pH 7.5, 100mM KCl, 2mM MgCl2, and 1mM CaCl2. It was then pelleted in a microcentrifuge at maximum speed at 4°C. The pellet was then resuspended in MNase buffer containing micrococcal nuclease at 3 units/uL. Digestion was carried out with constant vortexing at room temperature for 30 minutes. The solubilized chromatin was diluted 1:2 in 2X StrepTactin IP buffer (300mM NaCl, 100mM Tris-HCl pH 8.0, 2mM EDTA, 0.1% NP-40, and 20% glycerol) and shaken at 4°C for 30 minutes. This extract was pelleted by spinning at 4°C in a microcentrifuge for 10 minutes at maximum speed. The lysate from this digest was used as the chromatin fraction.

TAP was carried out on both the soluble nuclear and chromatin fractions as follows. The various lysates were incubated with M2 FLAG beads (Sigma A2220) for 4 hours at 4°C. The lysate was removed from the beads and the beads were washed twice in the lysis buffer described above and a third time in StrepTactin IP buffer (150mM NaCl, 50mM Tris-HCl pH 8.0, 1mM EDTA, 0.05% NP40, and 10% glycerol). Proteins were then eluted from the beads by two sequential 30 minute incubations with FLAG peptide (Sigma F3290) dissolved in StrepTactin IP buffer. The elutions were performed while shaking the sample at 4°C. The eluates were combined and passed through a centrifuge filter tube (Millipore Cat. #UFC30HV00) prior to the next IP. The second precipitation was carried out on these elutions using StrepTactin sepharose (GE Healthcare 28-9355-99). The eluates were incubated with StrepTactin beads for 3 hours at

4°C with constant shaking. Proteins were eluted from the beads in two sequential 30 minute elutions with d-Desthiobiotin (Sigma D1411) diluted in StrepTactin IP buffer while shaking the samples at 4°C. d-Desthiobiotin was prepared at a concentration of 7.5mM in buffer containing 150mM NaCl and 50mM Tris-HCl pH 8.0. The elution buffer itself contained the d-Desthiobiotin stock diluted 5-fold in StrepTactin IP buffer. The final eluates were combined and passed through a centrifuge filter tube. 5% of the final elutions were electrophoresed through a 1.0mM 4-12% Bis-Tris gel (Life Technologies Cat. # NP0323BOX) together with Life Technologies' Benchmark Protein ladder (Cat. # 10747-012) which was loaded at a dilution of 1:100. The gel was subsequently silver stained using Life Technologies' kit (Cat. #LC6070). The final elutions were digested, analyzed by liquid chromatography-tandem mass spectrometry, and the results processed all as described below.

Protein digestion: Proteins from the TAP samples were directly processed in solution: Cysteine residues were reduced with 10 mM DTT for 30 minutes at 56°C and alkylated with 22.5 mM iodoacetamide for 20 minutes at room temperature in the dark. Proteins were digested overnight at 37ºC using 5 micrograms of trypsin after adjusting the pH to 8.0 with Tris. The resulting tryptic peptide solutions were acidified by adding TFA to a final concentration of 1% and desalted by C18 solid phase extraction followed by Strong Cation Exchange (SCX), both performed in batch-mode format. Eluted peptides were concentrated in a vacuum concentrator, and reconstituted with 20 µl of 0.1% TFA.

LC-MS/MS analysis: Purified tryptic peptides were analyzed by LC-MS/MS on an LTQ-Orbitrap-XL mass spectrometer (Thermo, Waltham, MA) equipped with a Digital PicoView electrospray source platform (New Objective, Woburn, MA) (Ficarro et al., 2009). The

instrument was operated in data dependent mode where the 8 most abundant ions in each MS scan were selected (isolation width = 2.8 Da, threshold = 20,000) for MS/MS by CAD (35% normalized collision energy). Dynamic exclusion was enabled with a repeat count of 1 and exclusion duration of 30 seconds. ESI voltage was set to 2.2 kV.

Data processing: MS/MS spectra were converted into peak lists (Mascot generic file format, .mgf) using multiplierz scripts (Askenazi et al., 2009; Parikh et al., 2009) and searched by with Mascot (version 2.3) against three appended databases consisting of: i) human protein sequences (downloaded from RefSeq on 08/11/2010); ii) common lab contaminants, and iii) a decoy database generated by reversing the sequences from these two databases. For Mascot searches, precursor mass tolerance was set to 20 ppm and product ion mass tolerance was set to 0.6 Da. Search parameters included trypsin specificity, up to 2 missed cleavages, fixed carbamidomethylation of cysteine (C, +57 Da), variable oxidation of methionine (M, +16 Da), and variable phosphorylation of serine and threonine (S, T, +80 Da). Spectra matching to peptides from the reverse database were used to calculate a global false discovery rate, and were discarded. Data were further processed to remove peptide spectral matches (PSMs) to the forward database with an FDR greater than 1.0%.

Data analysis: Entrez Gene IDs and corresponding HGNC (HUGO Gene Nomenclature Committee) symbols were retrieved for each protein group identified by Mascot. Entrez Gene IDs and HGNC symbols were used as unique protein identifiers for subsequent analyses. Proteins identified in more than 1% of 108 negative TAP controls (Rozenblatt-Rosen et al., 2012) were removed from the sets of BARD1 interactors. Proteins identified in any of three negative control TAP experiments (prepared independently from chromatin and nuclear

fractions) were also removed. Only proteins identified in at least 2 of 3 biological replicates (starting from 3 independent cell culture pellets, each separately processed for TAP/MS) were considered for further analyses.

Generation of TALEN induced heterozygotes: TALENs were generated for target sites in BRCA1 and TONSL using the Fast Ligation-based Automatable Solid-phase High-throughput (FLASH) assembly method as previously described (Reyon et al., 2012). The BRCA1 binding (green) and target cut (red) sites were composed of the following sequences: TTATCTGCTCTTCGCGTTGAAGAAGTACAAAATGTCATTAATGCTATGCAGA. The TONSL binding (green) and target cut (red) sites are as follows: TGGGCTGTGCCGTGGCCCACCGCAAGATCGGAGAGCGCCTGGCCGAGATGGA. The TALEN plasmids were introduced into U2OS cells using Amaxa's Nucleofector IIb and Cell Line Nucleofector Kit V (Lonza Cat. # VCA-1003). Two days after nucleofection, the cells were plated as single cells and clones were harvested into 96 well plates after approximately two weeks, using cloning discs. Once enough material was generated, whole genomic DNA was harvested from each clone, and the region around the cut site was amplified using PCR (Can use regular Taq or Phusion Polymerase (New England Biolabs Cat. # M0530L)). The PCR product was purified using Qiagen's PCR Purification kit (Qiagen Cat. #28106), and the purified PCR product was sequenced to search for mutations. Clones in which appropriate mutations were generated were sequenced multiple times, each using a different primer pair. The primers used included the following: B1-TAL-F2-tacccggtcagtcactcctc, B1-TAL-F4-aaggctaccaccacctaccc, B1-TAL-R3-tggaagaaaagccaaaatgc, TONSL-TAL-F2-tcttcctcccacagAGCTGA, TONSL-

TALnew-F3-ctcccacagAGCTGAGCAA, TONSL-TAL-R2-Tggtgccaggaaacctactc, and TONSL-TAL-R3-atgcacccctcacacaaga.

Transfection: Lipofectamine RNAiMax (Life Technologies Cat. # 13778150) was used for the transfection of all siRNAs. For siRNA transfection, cells were plated on day 1, transfected with 10pmol of each siRNA on day two, transfected with 10pmol of each siRNA again on day three, and used for various experimental procedures on day 4. Lipofectamine 2000 (Life Technologies Cat. # 11668019) was used for all transfections needed in overexpression co-IP experiments.

siRNAs: All siRNAs were purchased from Dharmacon. siGL2 (Dharmacon Cat. # D-001100-01-20). siBRCA1 exon 13 sequence: GGGAUACCAUGCAACAUAA (Dharmacon Cat. # D-003461-06-0020). siBRCA1 exon 11 sequence: CCAAAUCAGUAGAGAGUAAUU. siBRCA1 3'UTR sequence: CCAUACAGCUUCAUAAAUAUU. siTONSL #1 sequence: GAGCUGGACUUAAGCAUGA (Dharmacon Cat. # D-013665-01. siTONSL #2 sequence: CUACGGGCAUCUAGAAAUU, (Dharmacon Cat. # D-013665-02. siTCEANC #1 sequence: GGAAAGCUGUUUAUAAGCA, (Dharmacon Cat. #D-024910-01). siTCEANC #3 sequence: GCAUAGAGCUUCUUUACGC (Dharmacon Cat. #D-024910-03). siTCEA2 #2 sequence: GUAAGGCCAUGACCAAGGA (Dharmacon Cat. #D-016235-02). siTCEA2 #3 sequence: AGUCGUAUCUCCAACCUGA (Dharmacon Cat. #D-016235-03). siSETX #1 sequence: GCACGUCAGUCAUGCGUAA (Dharmacon Cat. #D-021420-01). siSETX #2 sequence: UAGCACAGGUUGUUAAUCA (Dharmacon Cat. #D-021420-02). siSUPT16H #1 sequence: GAAGAUAUGUGACGUGUAU (Dharmacon Cat. #D-009517-01). siSUPT16H #2 sequence:

GAACAAAGUCGAAGUAUGA (Dharmacon Cat. #D-009517-02). siSSRP1 #1 sequence: GAUGAGAUCUCCUUUGUCA (Dharmacon Cat. #D-011783-01). siSSRP1 #3 sequence: GACUUAAACUGCUUACAAA (Dharmacon Cat. #D-011783-03). siTCEA1 #1 sequence: GAAAGAACCUGCAAUUACA (Dharmacon Cat. #D-010496-01). siTCEA1 #3 sequence: CAAAGUCUCUCAUCAAAUC (Dharmacon Cat. #D-010496-03).

Packaging of pLX304 BRCA1:

Full length HA-myc tagged BRCA1 was cloned in the pLX304 vector. pLX304-HA-Myc-BRCA1 was packaged into lentiviruses in 293FT cells using the transfection reagent, TransIT-LT1 (Mirus Cat. # MIR 2306) and standard lentiviral packaging plasmids (pHDM.Hgpm2, pRev, pTat, pHDM.G). After infection, cells were selected by incubation in medium containing 2.5ug/mL Blasticidin.

Oligos for qPCR: TCEANC Set 1: TCEANC F1-TGAGGATCTTGGCAACCACC and TCEANC R1-CCACAGAGGGGCAGTTTTTG. TCEANC Set 2: TCEANC F3-GGATCTTGGCAACCACCTTA and TCEANC R3-TTCCTCGCTTTGGAGTGAGT. TCEA2 Set 1: TCEA2 F1-CACGCAGACAGACCTGTTCA and TCEA2 R1-AACTTCCAGCGGTTTCCACA. TCEA2 Set 2: TCEA2 F2-CAGAGGAGATGGCCAGTGAT and TCEA2 R2-GCAGACAACAAAGGTGGTCA. Housekeeping Gene Control Set (Target is RPLP0 aka human 36B4): h36b 4F-ATCAACGGGTACAAACGAGTCCTG and h36b 4R-AAGGCAGATGGATCAGCCAAGAAG.

cDNA generation and qPCR: Whole cell RNA was harvested from cells transfected with various siRNAs using Qiagen's RNEASY kit (Cat. #74104), and the concentration of this RNA was measured. cDNA was generated from equal amounts of the RNA derived from each cell line using the Superscript III 1st Strand Synthesis System from Life Technologies (Cat. #18080051). This cDNA was used in qPCR reactions run in quintuplicate replicates for each cDNA with each pair of oligos listed above using iTAQ Universal SYBR Green Supermix from Bio-Rad (Cat. #172-5124). The qPCR results are represented in Figures 6F and 6G as $2^{-\Delta\Delta CT}$, the calculation method of which was described previously (Livak and Schmittgen, 2001). The deviation between replicates, which is represented by the error bars in these figures was calculated as follows. The positive deviation=High Range-$2^{-\Delta\Delta CT}$, where the High Range=$2^{-(\Delta\Delta CT-\delta)}$ and δ=SQRT((SD of CT replicates for 36B4)^2+ (SD of CT replicates for GOI)^2). The negative deviation= $2^{-\Delta\Delta CT}$-Low Range, where the Low Range= $2^{-(\Delta\Delta CT+\delta)}$ and δ=SQRT((SD of CT replicates for 36B4)^2+ (SD of CT replicates for GOI)^2). In the above equations, SQRT=square root, SD=standard deviation, and GOI=gene of interest

The above-noted cDNA was also used to clone various interactors from the Y2H and TAP-MS screens into expression vectors. Gateway cloning using BP and LR recombinases (Life Technologies) was used to move the cloned cDNAs between various plasmids (pDNR223 was the only donor vector; pDEST-CMV-Myc and pDEST-MSCV-HA-FLAG puro were the final DEST vectors).

Antibodies for Immunoprecipitation and Western Blotting: Two polyclonal TONSL antibodies were generated in rabbits using GST-tagged fragments of TONSL. Affinity purified

versions of these antibodies were used for all experiments. The fragments used were residues 450-850 (antibody-Q5) and 850-1378 (antibody-Q6). Two polyclonal SETX antibodies were generated in rabbits using GST tagged fragments of SETX, and affinity purified versions of these antibodies were used for all experiments. The fragments used were residues 1-398 (antibody-R1) and 2271-2677 (antibody-R2). For the overexpression co-IPs, FLAG M2 beads (Sigma A2220) were used for the IP and FLAG peptide (Sigma F3290) was used for the elution. Antibodies for these blots included FLAG M5 (Sigma F4042) and Myc (Santa Cruz sc-40). BRCA1 antibodies included the monoclonal BRCA1 C-terminal epitope antibody sc6954 (Santa Cruz), and the N-terminal BRCA1 antibody MS110 (Abcam Cat. #AB-16780). Mouse anti-SSRP1 (BioLegend Cat. Number 609702) was used for blots. Mouse anti-SUPT16H (BioLegend Cat. Number 607001) was used for immunoprecipitation, and rabbit anti-SUPT16H (Santa Cruz Cat. Number sc-28734) was used for blots. Mouse anti-Tubulin was also used for blots (Sigma Cat. #T-5168).

Immunoprecipitation and Western Blotting: Cell lines were grown to near 80% confluence, trypsinized, and lysed in lysis buffer containing 300mM NaCl, 50mM Tris-HCl pH 7.5, 1mM EDTA, 0.5% NP40, and 10% Glycerol. Lysates containing equivalent amounts of protein were incubated overnight at 4°C with the appropriate antibodies accompanied by end over end rocking. The next day the lysates were incubated, again rocking end over end at 4°C, with 10uL protein A beads for 1 hour. The beads were washed three times with the above-noted lysis buffer, and equal amounts of Laemmli Buffer containing BME were added to each sample. LDS sample buffer (Life Technologies NP0007) was used for SETX immunoprecipitations.

Equivalent amounts of each sample were electrophoresed through 4-12% Bis-Tris gels (3-8% Tris-Acetate gels for SETX) which were transferred to 0.45uM nitrocellulose membranes. For the overexpression co-IPs, the lysates were incubated with FLAG M2 beads for 4 hours and then eluted with FLAG peptide diluted in lysis buffer for 30 minutes. Laemelli buffer was added to the eluate, and blots were electrophoresed as described above. All blots were incubated with the appropriate primary antibodies overnight, washed, incubated with HRP-conjugated secondary antibodies, washed, and detected using standard chemiluminescence reagents and film.

Immunofluorescence: If the cells were treated with siRNA, the experiment was as follows: U2OS cells were plated on cover-slips in a 6cm plate on day 1, transfected with 10pmol siRNA on day 2, transfected with 10pmol siRNA on day 3, and treated with DNA damage and stained on day 4. Otherwise, U2OS were plated on coverslips in 12-well plates and allowed to settle overnight.

For DRB treatment (Sigma D1916 dissolved in ethanol), the media was changed to medium containing either 40uM DRB or medium containing an equivalent amount of ethanol, and the cells were allowed to incubate in this medium for 24hr. The cells were then fixed in 4% paraformaldehyde, permeabilized with 0.5% Triton, and stained with the appropriate antibodies. For alpha-Amanitin treatment (Sigma A2263 dissolved in ddH2O), the medium was changed to medium containing either 0.35uM alpha amanitin or medium containing an equivalent amount of ddH2O; and the cells were allowed to incubate in this media for 24hr. The cells were then fixed in 4% paraformaldehyde, permeabilized with 0.5% Triton, and stained with the appropriate antibodies. For mimosine arrest, cells were plated on day 1, the media was changed to either

media containing 0.5mM mimosine on day 2 (Sigma Cat. #M0253 dissolved at a concentration of 252.3mM in 1M NaOH) or media containing an equivalent volume of 1M NaOH, and 24 hours later on day three were treated with DNA damage and eventually stained. UV irradiation was carried out using a 254 nm UV-C lamp (UVP Inc., Upland, CA). Doses were measured using a UVX radiometer (UVP Inc., Upland, CA). Cell-loaded coverslips were washed once with PBS and then irradiated with $30J/m^2$ through a 3 mm isopore/micropore polycarbonate filter (Millipore TSTP02500) as described previously (Pathania et al., 2011; Polo et al., 2006). The cells were then allowed to recover for varying amounts of time at 37°C and then fixed in 4% paraformaldehyde, permeabilized with 0.5% Triton, and stained with either the appropriate antibodies or for cyclobutane pyrimidine dimers (CPDs) as described previously (Pathania et al., 2011; Polo et al., 2006). For SSRP1 staining, the cells were permeabilized with 0.5% Triton first and then fixed in 4% paraformaldehyde due to the ubiquitous staining pattern of this protein. For the above staining, cells were incubated at 37°C for 30 minutes with primary antibody, washed, incubated for 30 minutes at 37°C with secondary, washed, and mounted with DAPI containing mounting medium. Primary antibodies included the monoclonal BRCA1 C-terminal epitope sc6954 (Santa Cruz), the polyclonal BRCA1 C-terminal antibody (Upstate 07-434), the polyclonal TONSL antibodies Q5 and Q6 described above, a mouse SSRP1 antibody (BioLegend Cat. Number 609702), and a monoclonal anti-CPD antibody clone TDM-2 (Cosmo Bio #CAC-NM-DND-001). Secondary antibodies were from Jackson labs.

For the RNA Polymerase II pS5 staining, the cells were treated with either 0J (equivalent time air exposure) or $25J/m^2$ (carried out as described above). Fixation and staining were performed as described previously (Espinosa et al., 2003). Briefly, the cells were fixed four

hours after UV treatment in a 3:1 mixture of chilled methanol:acetic acid at 4°C. After washing in PBS, the cells were blocked for 30 minutes at 37°C in 1mg/mL BSA, 5% normal goat serum, 1% Triton X-100, and PBS. After washing in PBS, the cells were stained with primary and secondary antibodies diluted in 1mg/mL BSA, 5% normal goat serum, 1% Triton X-100, and PBS. The coverslips were then mounted using DAPI containing mounting medium. Primary antibodies included rabbit polyclonal RNA Polymerase II pS5 (Abcam Cat. #AB5131), mouse monoclonal anti-human BRCA1 SD123 (targets residues 758-1313 of human BRCA1) (Chen et al., 1998), mouse anti-γH2AX (Millipore 05-636-KC), rabbit anti-γH2AX (Upstate 07-164), rabbit anti-phospho-RPA (Bethyl Cat. #A300-245A), and mouse anti-TFIIS (BD Cat. #611204). Secondaries included Jackson lab antibodies and Alexa Fluor 488 anti-rabbit and 594 anti-mouse antibodies from Abcam (Cat. #Ab150077 and Ab150116).

For the RNA Polymerase II peptide competition experiments, 2ug of either un-phosphorylated RNA-PolII C terminal domain (CTD) peptide (Abcam Cat. #AB12795) or RNA-PolII CTD peptide phosphorylated on Serine 5 (Abcam Cat. #AB18488) were incubated with the antibody mixture to be used for staining the cells (containing RNA PolII pS5 antibody, 1mg/mL BSA, 5% normal goat serum, 1% Triton-X-100, and PBS) for 2 hours at 4°C rocking end over end. This mixture was then used to stain the methanol:acetic acid fixed cells as described above.

Colony Formation Assays: U2OS and HCC38 cells were tested for colony forming efficiency after piloting various siRNA transfection conditions. Enough cells for each line were plated in triplicate (six replicates for the genetic interaction experiments) to form between 100-300 colonies. Cells were transfected with 10pmol of the appropriate siRNAs on days one and two

and plated for the following experiments on the third day. For genetic interaction experiments, cells were plated on day three and cultivated until colonies formed. For DNA damage treatment experiments, the cells were plated on day three and then allowed to settle for at least 4 hours. Plates were then treated with varying doses of DRB, alpha-Amanitin, or UV and then allowed to recover at 37°C until colonies became visible. For DRB treatment, after the initial plating, the medium was removed and replaced with medium containing 0uM (an equivalent volume of ethanol as was used in the highest DRB dose was added to the 0uM medium), 5uM, 10uM, 15uM, 20uM, or 25uM, 30uM, 35uM, 40uM, or 50uM DRB for 24 hours. There were three replicates for each dose in every experiment. The cells were then washed once with PBS, and medium containing no drug was added to allow the cells to recover. For alpha-Amanitin treatment, after the initial plating, the medium was removed and for the U2OS cells it was replaced with medium containing 0uM (an equivalent volume of ddH2O to that used in adding the highest alpha-Amanitin dose was added to the culture medium), 0.025uM, 0.05uM, 0.075uM, 0.1uM, or 0.125uM, 0.15uM, 0.175uM, 0.2uM, 0.225uM, 0.25uM, or 0.35uM alpha-Amanitin for 24 hours. There were three replicates for each dose in every experiment. For HCC38 cells, the dose curve was 0uM (an equivalent volume of ddH2O to that used in the highest alpha-Amanitin dose was added to media), 0.1uM, 0.2uM, 0.25uM, 0.3uM, or 0.35uM, 0.4uM, 0.5uM, 0.75uM, or 1uM. There were three replicates for each dose in every experiment. After 24 hours, the cells were washed once with PBS, and medium containing no drug was added to allow the cells to recover. For UV treatment, the cells were plated at the appropriate density and then treated with UV (dosage and treatment method described in above immunofluorescence section). The dose curve was as follows 0J (exposed to air for the equivalent amount of time as the highest

UV dose), 1J, 3J, 5J, 7J, 10J, 20J, and 50J. After appropriately sized colonies had grown, the cells were stained with crystal violet, and the colonies were counted using Microbiology International's ProtoCOL colony counter. For the genetic interaction experiments, the average number of colonies was calculated from these results. For the drug treatments, dose curves from each experiment were generated from these counts.

Statistics for genetic interaction colony formation experiments: For each replicate of each experiment, we estimated the significance of the difference in number of colonies between wild-type cell lines and heterozygous cell lines. For each replicate, six independent measurements of the numbers of colonies were compared between the two cell lines and the p-value was estimated using a two-sided Student's t-test of equality of the means. The p-values were also estimated for the union of all replicates.

Statistical analysis of the DRB, alpha-Amanitin, and UV colony formation assays: For each replicate of each experiment, dose curves were obtained as described above, and the average and standard deviation of the data were calculated based on the three or more independent replicates of the fraction of untreated cells at each individual dose. The average percentage of viable cells for each siRNA at each dose from a minimum of three separate experiments for each damaging agent was entered into the GraphPad Prism statistical software program, and a non-linear regression curve was fit to these data. From this curve, an IC50 was estimated for each siRNA and each treatment, and the error in these calculations was estimated by generating a 95% confidence interval for the IC50 estimate in GraphPad Prism.

BrdU FACS analysis: Cells were treated with 10uM BrdU for 30 minutes at 37°C. Cells were trypsinized, washed once in PBS, and then fixed in 70% ethanol for a minimum of 30 minutes. The cells were washed with PBS once and incubated in fresh 2N HCL at room temperature for 15 minutes. The cells were then washed once in PBS and incubated in 0.1M Na2B4O7, pH8.5 for 30 minutes at room temperature. This solution was aspirated, and the cells were resuspended in blocking solution (Pierce #37545) containing either FITC conjugated anti-BrdU or FITC conjugated anti-mouse IgG antibodies (BD Biosciences 556028) for 30 minutes at room temperature in the dark. The cells were washed in 10mL PBS, resuspended in 0.5mL PI/RNASE solution (BD Biosciences Cat. # 550825), and analyzed on the flow cytometer.

Comet Assays: Cells were transfected with 10pmol of the appropriate siRNAs two days in a row. Media containing 0.35uM alpha-Amanitin or an equivalent volume of water was added on the third day for 24hr. 24hr after addition of the drug, alkaline comet assays were carried out on these cells using Trevigen's comet assay kit (Cat. # 4250-05-0-K) according to their protocol. Comet tail length was analyzed using TriTek's CometScore Software.

Statistical analysis of comet assays:

For each replicate of each experiment, we measured the fraction of damaged cells with tail lengths from 0 to 230 pixels for the cell line treated with different siRNAs and with or without alpha-Amanitin. For each tail length threshold and each treatment / siRNA, we measured the standard error of the proportion of the measured fraction of damaged cells, and drew a normal distribution of 100 values based on the fraction of damaged cells and the standard error of the proportion. The p-value for the significance of the difference in the fraction of damaged

cells between compound and siRNA treatments was estimated using a one-sided Student's t-test comparing the normal distributions.

Oncomine Analysis: The list of 147 interactors was used as a primary concept in Oncomine Concepts Map (Life Technologies) and compared to all the datasets in the Concepts Map program. We focused specifically on clinical outcome, stage, and grade for both breast and ovarian cancer and only accepted datasets with odds ratios of 2.0 or better or p-values less than 0.01 in the initial analysis. From the datasets found to overlap with the genes in our dataset, we plotted only datasets with a $p<0.05$ and $q<0.25$ for the overlap using Cytoscape. Analysis results were last checked on the Oncomine site on 11-23-13.

Overlap between Y2H and TAP-MS screens and between screen hits and known cancer genes: The significance of the overlap between the hits of the two screens was measured by comparing the observed overlap with the overlap when randomizing the Y2H and/or TAP-MS hits 1,000 times. The Y2H hits were randomized so that as many hits were selected at random in the space tested in the experiment (hORFeome v5.1, see above). To control for any expression bias of the TAP-MS experiment, the TAP-MS hits where randomized by controlling for their expression in HeLa S3 cells. The expression data was extracted from the GEO Platform Accession GPL5175-78, corresponding to three biological replicates of an RNAseq experiment in HeLa S3 cells, to match the cell lines used in the TAP-MS experiment. The expression level of each gene in all three replicates was averaged, and we divided all genes into bins corresponding to the four quartiles of the expression level distribution. In any randomization of

the TAP-MS hits, we selected one gene from the expression bin in which the TAP-MS gene was found for every TAP-MS gene. Y2H and TAP-MS hits were randomized both separately and collectively to measure the significance of the overlap as an empirical p-value, being the number of randomizations giving rise to at least as many overlapping hits as was observed in the original experiment. The same randomization strategy was adopted to measure the significance of the overlap between the two screens and known cancer genes.

Cancer-related data sets: The following data sets were extracted and compared to the BRCA1 screen hits. All lists were matched to the most up-to-date Entrez Gene IDs:

- Sleeping Beauty: We extracted 1,359 candidate cancer genes from four "Sleeping Beauty" transposon-based murine insertional mutagenesis screens (Mann et al., 2012; March et al., 2011; Starr et al., 2009; Starr et al., 2011), originally unified in a previous publication (Rozenblatt-Rosen et al., 2012).
- Somatic Mutations: 928 somatically mutated genes were extracted from a previous publication (Rozenblatt-Rosen et al., 2012), based on catalogues of somatic mutations from nine genome-wide cancer sequencing studies (2011; Agrawal et al., 2011; Chapman et al., 2011; Lee et al., 2010; Parsons et al., 2008; Parsons et al., 2011; Pleasance et al., 2010; Puente et al., 2011; Stransky et al., 2011).
- Virhost: We extracted 947 proteins through TAP-MS association, Y2H interaction or differentially expressed transcription factors from expression array analysis, from a previous study (Rozenblatt-Rosen et al., 2012).
- GWAS: 278 gene products described in another report were used (Tasan et al., 2014).

- SCNA: We extracted 225 genes from loci significantly amplified or deleted in cancer (Beroukhim et al., 2010).
- Sanger Cancer Gene Census: A list of 485 cancer-associated genes (Futreal et al., 2004) downloaded on March 15, 2013 was used.
- Vogelstein et al.: We extracted 125 genes found to be cancer drivers (Vogelstein et al., 2013).
- Woods et al.: The 717 proteins from the BRCT-based screen were used (Woods et al., 2012).
- Pujana et al.: The 69 proteins of the BRCA-centered network (BCN) were used (Pujana et al., 2007).
- Wang et al.: The 8 proteins found to be part of the BASC complex were used (Wang et al., 2000).

Interactome maps

The connectivity between the Y2H and TAP-MS screen hits and with BRCA1 and BARD1 was derived from the following up-to-date protein-protein interaction/association maps:

- The union of all CCSB human protein-protein interaction maps (Rual et al., 2005; Tasan et al., 2014; Venkatesan et al., 2009; Yu et al., 2011), and binary literature with multiple evidences (Tasan et al., 2014) formed the “binary literature” data set.
- The union of a co-fractionation experiment (Havugimana et al., 2012) and a prediction-based map (Zhang et al., 2012) of precision comparable to high-throughput experiments (PrePPI LR cutoff of 15000) formed the “non-binary” data set.

Functional enrichment of BRCA1 interactors: The list of all Gene Ontology (GO) terms annotated as children of the DNA damage (GO:0006974), DNA replication (GO:0006220) and Transcription DNA Dependent (GO:0006351) terms were extracted from the Gene Ontology server (Ashburner et al., 2000). The list of BRCA1 interactors found in the Y2H and TAP-MS screens were unified to form a list of query proteins for a GO term enrichment analysis using the FuncAssociate program (Berriz et al., 2009). All significantly enriched GO terms were extracted (adjusted p-value < 0.05) with their corresponding query proteins. For each query protein in each enriched GO term, we assigned the corresponding parental GO term(s) using the DNA damage, DNA replication and Transcription children lists.

TCGA Data Analysis: The significance of amplifications and deletions involving genes from the BRCA1-interacting network was determined using GISTIC 2.0 applied to 4934 cancer samples across 11 cancer types, including 872 breast cancers and 563 ovarian cancers, as previously described (Zack et al., 2013). The genes with q-values less than 0.25 and p-values less than 0.05 were plotted in amplification and deletion region networks using Cytoscape.

Materials and Methods for chapters 5 and 6

-All writing in this section was performed by SJH

Cell Culture: All cell lines were cultured according to Neve and Gray, 2006 (Neve et al., 2006). For cell lines into which a single copy of the DR-GFP reporter (Pierce et al., 1999) had been integrated, puromycin (1ug/mL) was added to the culture media to select for the constant presence of the integrated sequence.

Immunoprecipitation (IP) and Western Blotting: Cell lines were grown to approximately 80% confluence, pelleted, and lysed in buffer containing 300mM NaCl, 50mM Tris pH 7.5, 1mM EDTA, 0.5% NP40, 10% Glycerol, and a protease inhibitor (Roche Diagnostics Cat. # 11836170001). Lysates containing equivalent amounts of protein were incubated overnight with either the C-terminal BRCA1 antibody sc6954 (Santa Cruz) or a mouse IgG control (Santa Cruz sc-2025). The next day these lysates were incubated with protein A beads for 1 hour at 4°C. The beads were washed three times in the above-noted lysis buffer, and equal amounts of Laemmli Buffer (Boston BioProducts Cat. # BP-110NR) containing 2.5% beta-mercaptoethanol (BME) (Sigma Cat. # M6250) were added to each sample. Equivalent amounts of protein from each cell extract were IPd and equivalent amounts of protein from each IP were electrophoresed in 4-12% Tris-Glycine gels (Life Technologies Cat. # EC60385BOX) which were then transferred to 0.45uM nitrocellulose membranes. These were incubated in the N-terminal BRCA1 monoclonal antibody MS110 (Abcam ab16780) overnight, and incubated with HRP-conjugated anti-mouse light chain secondary antibody (BD Biosciences Cat. # 559751) for 1 hour the next day. Bands in each blot were developed using standard ECL solution (Perkin

Elmer Cat. # NEL105001EA) and visualized by exposing film to the blot for various amounts of time. For the HA-tagged I-SceI blots, the lysates were harvested from the cells in the lysis buffer described above and appropriate amounts of Laemmli sample buffer containing 2.5% BME were added to each sample to normalize the concentrations. Equivalent amounts of cell extract were electrophoresed in 4-12% Bis-Tris gels (Life Technologies Cat. # NP0336BOX) which were then transferred to 0.45uM nitrocellulose membranes. The blots were carried out as described above except the primary antibodies were a monoclonal HA antibody (Covance Cat. # MMS-101P) and a tubulin antibody (Sigma Cat. #T-5168).

Immunofluorescence: Cells were plated on coverslips in 6- or 12-well plates and allowed to settle overnight. For gamma irradiation, the next day one set was treated with 5Gy, while a second control set was not. Cells were allowed to recover at 37°C for 8 hours, fixed in 4% paraformaldehyde, permeabilized with 0.5% Triton, and then stained with primary and secondary antibodies.

For UV treatment, cells on coverslips were irradiated at $30J/m^2$ (dose measured using a UVX radiometer (UVP Inc., Upland, CA) using a 254 nm UV-C lamp (UVP Inc., Upland, CA) through 3 mm isopore/micropore polycarbonate filters (Millipore TSTP02500), as described in Polo et al., 2006 (Polo et al., 2006). They were then allowed to recover for 4 hours at 37°C and were then fixed in 4% paraformaldehyde, permeabilized with 0.5% Triton, and stained for cyclobutane pyrimidine dimers (CPDs) as described in Polo, et al., 2006 (Polo et al., 2006).

If the cells were to be transfected with siRNAs, the cells were plated on coverslips in a 6cm plate on day 1, transfected with 10pmol of the appropriate siRNAs on day 2, transfected

again with 10pmol of the appropriate siRNAs on day 3, and treated with DNA damaging agents, fixed, permeabilized, and stained on day 4.

Primary antibodies in these assays included the monoclonal BRCA1 C-terminal antibody sc6954 (Santa Cruz), a polyclonal BRCA1 C-terminal antibody (Upstate 07-434), a purified monoclonal antibody targeting exon 11 of BRCA1 called SD118 (Chen et al., 1998), a monoclonal anti-cyclobutane pyrimidine dimer (CPD) antibody, clone TDM-2 (Cosmo Bio #CAC-NM-DND-001), a polyclonal γH2AX antibody (Upstate 07-164), a monoclonal γH2AX antibody (Millipore 05-636-KC), a monoclonal 53BP1 antibody (BD 612523), and a polyclonal Rad51 (H-92) antibody (Santa Cruz sc-8349). Secondary antibodies were from Jackson labs.

Colony Formation Assays: All BLC lines and controls were tested for colony forming efficiency. Enough cells of each line were plated in triplicate to form between 80 and 300 colonies. The cells were allowed to settle overnight. Plates were then treated with varying doses of each of a series of DNA damaging agents and allowed to recover at 37°C until colonies became visible (7-14 days depending on the cell line).

For gamma irradiation, cells were treated with 0Gy, 1Gy, 2Gy, 3Gy, 4Gy, or 5Gy using a cesium source.

For UV irradiation, cells were treated with 0J/m^2 (air exposure time equal to longest UV exposure time), 1J/m^2, 2J/m^2, 4J/m^2, 5J/m^2, 10J/m^2, 20J/m^2, or 50J/m^2 using a 254 nm UV-C lamp (UVP Inc., Upland, CA). UV doses were measured with a UVX radiometer (UVP Inc., Upland, CA).

For mitomycin C (MMC) treatment, the medium was removed and replaced with medium containing 0uM (added volume of ethanol to this medium equivalent to that added with the highest MMC dose), 0.1uM, 0.2uM, 0.3uM, 0.4uM, or 0.5uM MMC (Sigma Cat. #M4287 dissolved in ethanol) for 4 hours. The cells were then washed with PBS, and medium containing no drug was added to allow the cells to recover.

For methyl methane sulfonate (MMS), the medium was removed after the initial cell plating and replaced with medium containing 0mM, 1mM, 2mM, 3mM, 4mM, or 5mM MMS (Sigma Cat. #129925) for 4 hours. The cells were then washed once with PBS and drug-free medium was added to allow the cells to recover.

After appropriate sized colonies had grown, the cells were stained with crystal violet and counted with a Microbiology International ProtoCOL colony counter. The average number of colonies for each cell line at each treatment level was calculated, and, from these values, the percentage of cells that survived at each level of treatment was compared to untreated controls. These values were plotted as cell killing curves using GraphPad Prism Software, and IC50s were obtained for each cell line in each experiment. Cells lines were tested with each damaging agent 2-3 times, and the IC50s were calculated in this way each time.

Southern Blots: Genomic DNA was prepared from each clone after phenol/chloroform extraction. 50ug of DNA was digested with either HindIII or StuI overnight. The digested DNA was electrophoresed through a 0.8% agarose gel and transferred to a nylon membrane (Whatman Cat# 10416282) by neutral transfer. Membranes were then probed with an 812 base pair GFP sequence-containing fragment derived from hprt pDR-GFP puro by HindIII digestion (Pierce et

al., 1999). The probe was labeled using the Ladderman Labeling Kit by Takara (Cat #6046), and blotting was performed, using a modification of the Church-Gilbert method (Church and Gilbert, 1984).

siRNAs: siGL2 was purchased from Dharmacon (Cat. # D-001100-01-20). The sequence of siBRCA1 exon 13 was GGGAUACCAUGCAACAUAA (Dharmacon Cat. # D-003461-06-0020). The sequence of siBRCA1 exon 11 #1 was CCAAAUCAGUAGAGAGUAAUU. The sequence of siBRCA1 exon 11 #2 was GUUAGAUGAUGGUGAAAUA. The siΔ11b junction sequence was GUAUCAGGGUGAAGCAGCAUU.

Transfection: Lipofectamine RNAiMax (Life Technologies Cat. # 13778150) was used for the transfection of all siRNAs. Lipofectamine 2000 (Life Technologies Cat. # 11668019) was used for the transfection of I-SceI.

HR Reporter Assay: Plating efficiencies were determined for each cell line such that the cells could reach the end of the assay without becoming completely confluent. Cells were plated in a 6cm plate at an appropriate density on day one. On day two cells were transfected with 10pmol of each siRNA. On day three cells were transfected with 2ug of the I-SceI plasmid (pCBAS). Cells were then allowed to recover for 72 hours. At that point, one half of the cells were harvested for an I-SceI-HA western blot; and the other half were fixed with 4% paraformaldehyde and assayed for GFP positive cells by FACS.

For the IP/western blots performed to test the effects of the various siRNAs introduced into each cell line, the transfection sequence and siRNA amounts were different than those used in the HR assays. The cells were plated on day one, transfected with 75pmol of each siRNA on day 2, transfected with 75pmol of each siRNA on day 3, transfected with 2ug I-SceI on day 4, and harvested and extracted for IP 72 hours after I-SceI transfection.

References:

(1997). Pathology of familial breast cancer: differences between breast cancers in carriers of BRCA1 or BRCA2 mutations and sporadic cases. Breast Cancer Linkage Consortium. Lancet *349*, 1505-1510.

(2011). Integrated genomic analyses of ovarian carcinoma. Nature *474*, 609-615.

Adelman, C.A., and Boulton, S.J. (2010). Metabolism of postsynaptic recombination intermediates. FEBS Lett *584*, 3709-3716.

Agrawal, N., Frederick, M.J., Pickering, C.R., Bettegowda, C., Chang, K., Li, R.J., Fakhry, C., Xie, T.X., Zhang, J., Wang, J., *et al.* (2011). Exome sequencing of head and neck squamous cell carcinoma reveals inactivating mutations in NOTCH1. Science *333*, 1154-1157.

Aguilera, A., and Garcia-Muse, T. (2012). R loops: from transcription byproducts to threats to genome stability. Mol Cell *46*, 115-124.

Al-Minawi, A.Z., Lee, Y.F., Hakansson, D., Johansson, F., Lundin, C., Saleh-Gohari, N., Schultz, N., Jenssen, D., Bryant, H.E., Meuth, M., *et al.* (2009). The ERCC1/XPF endonuclease is required for completion of homologous recombination at DNA replication forks stalled by inter-strand cross-links. Nucleic Acids Res *37*, 6400-6413.

Alli, E., Sharma, V.B., Sunderesakumar, P., and Ford, J.M. (2009). Defective repair of oxidative dna damage in triple-negative breast cancer confers sensitivity to inhibition of poly(ADP-ribose) polymerase. Cancer Research *69*, 3589-3596.

Alpi, A.F., Pace, P.E., Babu, M.M., and Patel, K.J. (2008). Mechanistic insight into site-restricted monoubiquitination of FANCD2 by Ube2t, FANCL, and FANCI. Mol Cell *32*, 767-777.

Anand, R.P., Lovett, S.T., and Haber, J.E. (2013). Break-induced DNA replication. Cold Spring Harb Perspect Biol *5*, a010397.

Antoniou, A., Pharoah, P.D., Narod, S., Risch, H.A., Eyfjord, J.E., Hopper, J.L., Loman, N., Olsson, H., Johannsson, O., Borg, A., *et al.* (2003). Average risks of breast and ovarian cancer associated with BRCA1 or BRCA2 mutations detected in case Series unselected for family history: a combined analysis of 22 studies. Am J Hum Genet *72*, 1117-1130.

Ashburner, M., Ball, C.A., Blake, J.A., Botstein, D., Butler, H., Cherry, J.M., Davis, A.P., Dolinski, K., Dwight, S.S., Eppig, J.T., *et al.* (2000). Gene ontology: tool for the unification of biology. The Gene Ontology Consortium. Nature Genetics *25*, 25-29.

Askenazi, M., Parikh, J.R., and Marto, J.A. (2009). mzAPI: a new strategy for efficiently sharing mass spectrometry data. Nature Methods *6*, 240-241.

Bamford, S., Dawson, E., Forbes, S., Clements, J., Pettett, R., Dogan, A., Flanagan, A., Teague, J., Futreal, P.A., Stratton, M.R., *et al.* (2004). The COSMIC (Catalogue of Somatic Mutations in Cancer) database and website. Br J Cancer *91*, 355-358.

Becherel, O.J., Yeo, A.J., Stellati, A., Heng, E.Y., Luff, J., Suraweera, A.M., Woods, R., Fleming, J., Carrie, D., McKinney, K., *et al.* (2013). Senataxin plays an essential role with DNA damage response proteins in meiotic recombination and gene silencing. PLoS Genet *9*, e1003435.

Beroukhim, R., Mermel, C.H., Porter, D., Wei, G., Raychaudhuri, S., Donovan, J., Barretina, J., Boehm, J.S., Dobson, J., Urashima, M., *et al.* (2010). The landscape of somatic copy-number alteration across human cancers. Nature *463*, 899-905.

Berriz, G.F., Beaver, J.E., Cenik, C., Tasan, M., and Roth, F.P. (2009). Next generation software for functional trend analysis. Bioinformatics *25*, 3043-3044.

Bhattacharyya, A., Ear, U.S., Koller, B.H., Weichselbaum, R.R., and Bishop, D.K. (2000). The breast cancer susceptibility gene BRCA1 is required for subnuclear assembly of Rad51 and survival following treatment with the DNA cross-linking agent cisplatin. J Biol Chem *275*, 23899-23903.

Boulton, S.J., Martin, J.S., Polanowska, J., Hill, D.E., Gartner, A., and Vidal, M. (2004). BRCA1/BARD1 orthologs required for DNA repair in Caenorhabditis elegans. Curr Biol *14*, 33-39.

Bouwman, P., Aly, A., Escandell, J.M., Pieterse, M., Bartkova, J., van der Gulden, H., Hiddingh, S., Thanasoula, M., Kulkarni, A., Yang, Q., *et al.* (2010). 53BP1 loss rescues BRCA1 deficiency and is associated with triple-negative and BRCA-mutated breast cancers. Nat Struct Mol Biol *17*, 688-695.

Branzei, D., and Foiani, M. (2010). Maintaining genome stability at the replication fork. Nat Rev Mol Cell Biol *11*, 208-219.

Bryant, H.E., Schultz, N., Thomas, H.D., Parker, K.M., Flower, D., Lopez, E., Kyle, S., Meuth, M., Curtin, N.J., and Helleday, T. (2005). Specific killing of BRCA2-deficient tumours with inhibitors of poly(ADP-ribose) polymerase. Nature *434*, 913-917.

Bunting, S.F., Callen, E., Kozak, M.L., Kim, J.M., Wong, N., Lopez-Contreras, A.J., Ludwig, T., Baer, R., Faryabi, R.B., Malhowski, A., *et al.* (2012). BRCA1 functions independently of homologous recombination in DNA interstrand crosslink repair. Mol Cell *46*, 125-135.

Bunting, S.F., Callen, E., Wong, N., Chen, H.T., Polato, F., Gunn, A., Bothmer, A., Feldhahn, N., Fernandez-Capetillo, O., Cao, L., *et al.* (2010). 53BP1 inhibits homologous recombination in Brca1-deficient cells by blocking resection of DNA breaks. Cell *141*, 243-254.

Cantor, S.B., Bell, D.W., Ganesan, S., Kass, E.M., Drapkin, R., Grossman, S., Wahrer, D.C., Sgroi, D.C., Lane, W.S., Haber, D.A., *et al.* (2001). BACH1, a novel helicase-like protein, interacts directly with BRCA1 and contributes to its DNA repair function. Cell *105*, 149-160.

Cary, R.B., Peterson, S.R., Wang, J., Bear, D.G., Bradbury, E.M., and Chen, D.J. (1997). DNA looping by Ku and the DNA-dependent protein kinase. Proc Natl Acad Sci U S A *94*, 4267-4272.

Chapman, J.R., Taylor, M.R., and Boulton, S.J. (2012). Playing the end game: DNA double-strand break repair pathway choice. Mol Cell *47*, 497-510.

Chapman, M.A., Lawrence, M.S., Keats, J.J., Cibulskis, K., Sougnez, C., Schinzel, A.C., Harview, C.L., Brunet, J.P., Ahmann, G.J., Adli, M., *et al.* (2011). Initial genome sequencing and analysis of multiple myeloma. Nature *471*, 467-472.

Chen, J., Silver, D.P., Walpita, D., Cantor, S.B., Gazdar, A.F., Tomlinson, G., Couch, F.J., Weber, B.L., Ashley, T., Livingston, D.M., *et al.* (1998). Stable interaction between the products of the BRCA1 and BRCA2 tumor suppressor genes in mitotic and meiotic cells. Mol Cell *2*, 317-328.

Chen, L., Nievera, C.J., Lee, A.Y., and Wu, X. (2008). Cell cycle-dependent complex formation of BRCA1.CtIP.MRN is important for DNA double-strand break repair. J Biol Chem *283*, 7713-7720.

Chen, S., Iversen, E.S., Friebel, T., Finkelstein, D., Weber, B.L., Eisen, A., Peterson, L.E., Schildkraut, J.M., Isaacs, C., Peshkin, B.N., *et al.* (2006). Characterization of BRCA1 and BRCA2 mutations in a large United States sample. J Clin Oncol *24*, 863-871.

Chew, H.K., Doroshow, J.H., Frankel, P., Margolin, K.A., Somlo, G., Lenz, H.J., Gordon, M., Zhang, W., Yang, D., Russell, C., *et al.* (2009). Phase II studies of gemcitabine and cisplatin in heavily and minimally pretreated metastatic breast cancer. J Clin Oncol *27*, 2163-2169.

Chodosh, L.A., Fire, A., Samuels, M., and Sharp, P.A. (1989). 5,6-Dichloro-1-beta-D-ribofuranosylbenzimidazole inhibits transcription elongation by RNA polymerase II in vitro. J Biol Chem *264*, 2250-2257.

Church, G.M., and Gilbert, W. (1984). Genomic sequencing. Proc Natl Acad Sci U S A *81*, 1991-1995.

Ciccia, A., Ling, C., Coulthard, R., Yan, Z., Xue, Y., Meetei, A.R., Laghmani el, H., Joenje, H., McDonald, N., de Winter, J.P., *et al.* (2007). Identification of FAAP24, a Fanconi anemia core complex protein that interacts with FANCM. Mol Cell *25*, 331-343.

Collis, S.J., Ciccia, A., Deans, A.J., Horejsi, Z., Martin, J.S., Maslen, S.L., Skehel, J.M., Elledge, S.J., West, S.C., and Boulton, S.J. (2008). FANCM and FAAP24 function in ATR-mediated checkpoint signaling independently of the Fanconi anemia core complex. Mol Cell *32*, 313-324.

Costantino, L., Sotiriou, S.K., Rantala, J.K., Magin, S., Mladenov, E., Helleday, T., Haber, J.E., Iliakis, G., Kallioniemi, O.P., and Halazonetis, T.D. (2014). Break-induced replication repair of damaged forks induces genomic duplications in human cells. Science *343*, 88-91.

Crook, T., Brooks, L.A., Crossland, S., Osin, P., Barker, K.T., Waller, J., Philp, E., Smith, P.D., Yulug, I., Peto, J., *et al.* (1998). p53 mutation with frequent novel condons but not a mutator phenotype in BRCA1- and BRCA2-associated breast tumours. Oncogene *17*, 1681-1689.

Deans, A.J., and West, S.C. (2011). DNA interstrand crosslink repair and cancer. Nature Reviews *11*, 467-480.

Delacote, F., and Lopez, B.S. (2008). Importance of the cell cycle phase for the choice of the appropriate DSB repair pathway, for genome stability maintenance: the trans-S double-strand break repair model. Cell Cycle *7*, 33-38.

DelloRusso, C., Welcsh, P.L., Wang, W., Garcia, R.L., King, M.C., and Swisher, E.M. (2007). Functional characterization of a novel BRCA1-null ovarian cancer cell line in response to ionizing radiation. Mol Cancer Res *5*, 35-45.

Dinant, C., Ampatziadis-Michailidis, G., Lans, H., Tresini, M., Lagarou, A., Grosbart, M., Theil, A.F., van Cappellen, W.A., Kimura, H., Bartek, J.*, et al.* (2013). Enhanced chromatin dynamics by FACT promotes transcriptional restart after UV-induced DNA damage. Mol Cell *51*, 469-479.

Domchek, S.M., Tang, J., Stopfer, J., Lilli, D.R., Hamel, N., Tischkowitz, M., Monteiro, A.N., Messick, T.E., Powers, J., Yonker, A.*, et al.* (2013). Biallelic deleterious BRCA1 mutations in a woman with early-onset ovarian cancer. Cancer Discov *3*, 399-405.

Dreze, M., Monachello, D., Lurin, C., Cusick, M.E., Hill, D.E., Vidal, M., and Braun, P. (2010). High-quality binary interactome mapping. Methods Enzymol *470*, 281-315.

Duro, E., Lundin, C., Ask, K., Sanchez-Pulido, L., MacArtney, T.J., Toth, R., Ponting, C.P., Groth, A., Helleday, T., and Rouse, J. (2010). Identification of the MMS22L-TONSL complex that promotes homologous recombination. Mol Cell *40*, 632-644.

Dworkin, A.M., Huang, T.H., and Toland, A.E. (2009). Epigenetic alterations in the breast: Implications for breast cancer detection, prognosis and treatment. Semin Cancer Biol *19*, 165-171.

ElShamy, W.M., and Livingston, D.M. (2004). Identification of BRCA1-IRIS, a BRCA1 locus product. Nat Cell Biol *6*, 954-967.

Elstrodt, F., Hollestelle, A., Nagel, J.H., Gorin, M., Wasielewski, M., van den Ouweland, A., Merajver, S.D., Ethier, S.P., and Schutte, M. (2006). BRCA1 mutation analysis of 41 human breast cancer cell lines reveals three new deleterious mutants. Cancer Research *66*, 41-45.

Espinosa, J.M., Verdun, R.E., and Emerson, B.M. (2003). p53 functions through stress- and promoter-specific recruitment of transcription initiation components before and after DNA damage. Mol Cell *12*, 1015-1027.

Evans, D.G., Shenton, A., Woodward, E., Lalloo, F., Howell, A., and Maher, E.R. (2008). Penetrance estimates for BRCA1 and BRCA2 based on genetic testing in a Clinical Cancer Genetics service setting: risks of breast/ovarian cancer quoted should reflect the cancer burden in the family. BMC Cancer *8*, 155.

Farmer, H., McCabe, N., Lord, C.J., Tutt, A.N., Johnson, D.A., Richardson, T.B., Santarosa, M., Dillon, K.J., Hickson, I., Knights, C.*, et al.* (2005). Targeting the DNA repair defect in BRCA mutant cells as a therapeutic strategy. Nature *434*, 917-921.

Ficarro, S.B., Zhang, Y., Lu, Y., Moghimi, A.R., Askenazi, M., Hyatt, E., Smith, E.D., Boyer, L., Schlaeger, T.M., Luckey, C.J.*, et al.* (2009). Improved electrospray ionization efficiency compensates for diminished chromatographic resolution and enables proteomics analysis of tyrosine signaling in embryonic stem cells. Analytical Chemistry *81*, 3440-3447.

Fong, P.C., Boss, D.S., Yap, T.A., Tutt, A., Wu, P., Mergui-Roelvink, M., Mortimer, P., Swaisland, H., Lau, A., O'Connor, M.J.*, et al.* (2009). Inhibition of poly(ADP-ribose) polymerase in tumors from BRCA mutation carriers. N Engl J Med *361*, 123-134.

Ford, D., Easton, D.F., Stratton, M., Narod, S., Goldgar, D., Devilee, P., Bishop, D.T., Weber, B., Lenoir, G., Chang-Claude, J.*, et al.* (1998). Genetic heterogeneity and penetrance analysis of the BRCA1 and BRCA2 genes in breast cancer families. The Breast Cancer Linkage Consortium. Am J Hum Genet *62*, 676-689.

Futreal, P.A., Coin, L., Marshall, M., Down, T., Hubbard, T., Wooster, R., Rahman, N., and Stratton, M.R. (2004). A census of human cancer genes. Nature Reviews *4*, 177-183.

Garcia-Higuera, I., Taniguchi, T., Ganesan, S., Meyn, M.S., Timmers, C., Hejna, J., Grompe, M., and D'Andrea, A.D. (2001). Interaction of the Fanconi anemia proteins and BRCA1 in a common pathway. Mol Cell *7*, 249-262.

Gelmon, K.A., Tischkowitz, M., Mackay, H., Swenerton, K., Robidoux, A., Tonkin, K., Hirte, H., Huntsman, D., Clemons, M., Gilks, B.*, et al.* (2011). Olaparib in patients with recurrent high-grade serous or poorly differentiated ovarian carcinoma or triple-negative breast cancer: a phase 2, multicentre, open-label, non-randomised study. Lancet Oncol *12*, 852-861.

Gottlieb, T.M., and Jackson, S.P. (1993). The DNA-dependent protein kinase: requirement for DNA ends and association with Ku antigen. Cell *72*, 131-142.

Grawunder, U., Wilm, M., Wu, X., Kulesza, P., Wilson, T.E., Mann, M., and Lieber, M.R. (1997). Activity of DNA ligase IV stimulated by complex formation with XRCC4 protein in mammalian cells. Nature *388*, 492-495.

Greenberg, R.A. (2008). Recognition of DNA double strand breaks by the BRCA1 tumor suppressor network. Chromosoma *117*, 305-317.

Greenberg, R.A., Sobhian, B., Pathania, S., Cantor, S.B., Nakatani, Y., and Livingston, D.M. (2006). Multifactorial contributions to an acute DNA damage response by BRCA1/BARD1-containing complexes. Genes Dev *20*, 34-46.

Gu, J., Lu, H., Tsai, A.G., Schwarz, K., and Lieber, M.R. (2007). Single-stranded DNA ligation and XLF-stimulated incompatible DNA end ligation by the XRCC4-DNA ligase IV complex: influence of terminal DNA sequence. Nucleic Acids Res *35*, 5755-5762.

Hashimoto, Y., Ray Chaudhuri, A., Lopes, M., and Costanzo, V. (2010). Rad51 protects nascent DNA from Mre11-dependent degradation and promotes continuous DNA synthesis. Nat Struct Mol Biol *17*, 1305-1311.

Hashizume, R., Fukuda, M., Maeda, I., Nishikawa, H., Oyake, D., Yabuki, Y., Ogata, H., and Ohta, T. (2001). The RING heterodimer BRCA1-BARD1 is a ubiquitin ligase inactivated by a breast cancer-derived mutation. J Biol Chem *276*, 14537-14540.

Havugimana, P.C., Hart, G.T., Nepusz, T., Yang, H., Turinsky, A.L., Li, Z., Wang, P.I., Boutz, D.R., Fong, V., Phanse, S., *et al.* (2012). A census of human soluble protein complexes. Cell *150*, 1068-1081.

Helleday, T. (2011). The underlying mechanism for the PARP and BRCA synthetic lethality: clearing up the misunderstandings. Mol Oncol *5*, 387-393.

Helmrich, A., Ballarino, M., Nudler, E., and Tora, L. (2013). Transcription-replication encounters, consequences and genomic instability. Nat Struct Mol Biol *20*, 412-418.

Herrera-Moyano, E., Mergui, X., Garcia-Rubio, M.L., Barroso, S., and Aguilera, A. (2014). The yeast and human FACT chromatin-reorganizing complexes solve R-loop-mediated transcription-replication conflicts. Genes Dev *28*, 735-748.

Hopfner, K.P., Craig, L., Moncalian, G., Zinkel, R.A., Usui, T., Owen, B.A., Karcher, A., Henderson, B., Bodmer, J.L., McMurray, C.T., *et al.* (2002). The Rad50 zinc-hook is a structure joining Mre11 complexes in DNA recombination and repair. Nature *418*, 562-566.

Hsu, L.C., Doan, T.P., and White, R.L. (2001). Identification of a gamma-tubulin-binding domain in BRCA1. Cancer Research *61*, 7713-7718.

http://research.nhgri.nih.gov/bic/ (Breast Cancer Information Core (BIC) Database).

Hu, Y., Scully, R., Sobhian, B., Xie, A., Shestakova, E., and Livingston, D.M. (2011). RAP80-directed tuning of BRCA1 homologous recombination function at ionizing radiation-induced nuclear foci. Genes Dev *25*, 685-700.

Huber, L.J., Yang, T.W., Sarkisian, C.J., Master, S.R., Deng, C.X., and Chodosh, L.A. (2001). Impaired DNA damage response in cells expressing an exon 11-deleted murine Brca1 variant that localizes to nuclear foci. Mol Cell Biol *21*, 4005-4015.

Huen, M.S., Sy, S.M., and Chen, J. (2010). BRCA1 and its toolbox for the maintenance of genome integrity. Nat Rev Mol Cell Biol *11*, 138-148.

Hurley, J., Reis, I.M., Rodgers, S.E., Gomez-Fernandez, C., Wright, J., Leone, J.P., Larrieu, R., and Pegram, M.D. (2013). The use of neoadjuvant platinum-based chemotherapy in locally advanced breast cancer that is triple negative: retrospective analysis of 144 patients. Breast Cancer Res Treat *138*, 783-794.

Ince, T.A., Richardson, A.L., Bell, G.W., Saitoh, M., Godar, S., Karnoub, A.E., Iglehart, J.D., and Weinberg, R.A. (2007). Transformation of different human breast epithelial cell types leads to distinct tumor phenotypes. Cancer Cell *12*, 160-170.

Johannsson, O.T., Staff, S., Vallon-Christersson, J., Kytola, S., Gudjonsson, T., Rennstam, K., Hedenfalk, I.A., Adeyinka, A., Kjellen, E., Wennerberg, J., *et al.* (2003). Characterization of a novel breast carcinoma xenograft and cell line derived from a BRCA1 germ-line mutation carrier. Lab Invest *83*, 387-396.

Jones, R.M., and Petermann, E. (2012). Replication fork dynamics and the DNA damage response. Biochem J *443*, 13-26.

Joukov, V., Chen, J., Fox, E.A., Green, J.B., and Livingston, D.M. (2001). Functional communication between endogenous BRCA1 and its partner, BARD1, during Xenopus laevis development. Proc Natl Acad Sci *98*, 12078-12083.

Joukov, V., Groen, A.C., Prokhorova, T., Gerson, R., White, E., Rodriguez, A., Walter, J.C., and Livingston, D.M. (2006). The BRCA1/BARD1 heterodimer modulates ran-dependent mitotic spindle assembly. Cell *127*, 539-552.

Joung, J.K., and Sander, J.D. (2013). TALENs: a widely applicable technology for targeted genome editing. Nat Rev Mol Cell Biol *14*, 49-55.

Kim, H., Chen, J., and Yu, X. (2007a). Ubiquitin-binding protein RAP80 mediates BRCA1-dependent DNA damage response. Science *316*, 1202-1205.

Kim, H., Huang, J., and Chen, J. (2007b). CCDC98 is a BRCA1-BRCT domain-binding protein involved in the DNA damage response. Nat Struct Mol Biol *14*, 710-715.

Kim, J.E., McAvoy, S.A., Smith, D.I., and Chen, J. (2005). Human TopBP1 ensures genome integrity during normal S phase. Mol Cell Biol *25*, 10907-10915.

Kim, S.S., Cao, L., Lim, S.C., Li, C., Wang, R.H., Xu, X., Bachelier, R., and Deng, C.X. (2006). Hyperplasia and spontaneous tumor development in the gynecologic system in mice lacking the BRCA1-Delta11 isoform. Mol Cell Biol *26*, 6983-6992.

Kleiman, F.E., and Manley, J.L. (1999). Functional interaction of BRCA1-associated BARD1 with polyadenylation factor CstF-50. Science *285*, 1576-1579.

Kleiman, F.E., and Manley, J.L. (2001). The BARD1-CstF-50 interaction links mRNA 3' end formation to DNA damage and tumor suppression. Cell *104*, 743-753.

Kleiman, F.E., Wu-Baer, F., Fonseca, D., Kaneko, S., Baer, R., and Manley, J.L. (2005). BRCA1/BARD1 inhibition of mRNA 3' processing involves targeted degradation of RNA polymerase II. Genes Dev *19*, 1227-1237.

Kumaraswamy, E., and Shiekhattar, R. (2007). Activation of BRCA1/BRCA2-associated helicase BACH1 is required for timely progression through S phase. Mol Cell Biol *27*, 6733-6741.

Lakhani, S.R., Reis-Filho, J.S., Fulford, L., Penault-Llorca, F., van der Vijver, M., Parry, S., Bishop, T., Benitez, J., Rivas, C., Bignon, Y.J., *et al.* (2005). Prediction of BRCA1 status in patients with breast cancer using estrogen receptor and basal phenotype. Clin Cancer Res *11*, 5175-5180.

Lakhani, S.R., Van De Vijver, M.J., Jacquemier, J., Anderson, T.J., Osin, P.P., McGuffog, L., and Easton, D.F. (2002). The pathology of familial breast cancer: predictive value of immunohistochemical markers estrogen receptor, progesterone receptor, HER-2, and p53 in patients with mutations in BRCA1 and BRCA2. J Clin Oncol *20*, 2310-2318.

Le Page, F., Randrianarison, V., Marot, D., Cabannes, J., Perricaudet, M., Feunteun, J., and Sarasin, A. (2000). BRCA1 and BRCA2 are necessary for the transcription-coupled repair of the oxidative 8-oxoguanine lesion in human cells. Cancer Research *60*, 5548-5552.

Lee, J.H., and Paull, T.T. (2004). Direct activation of the ATM protein kinase by the Mre11/Rad50/Nbs1 complex. Science *304*, 93-96.

Lee, W., Jiang, Z., Liu, J., Haverty, P.M., Guan, Y., Stinson, J., Yue, P., Zhang, Y., Pant, K.P., Bhatt, D., *et al.* (2010). The mutation spectrum revealed by paired genome sequences from a lung cancer patient. Nature *465*, 473-477.

Li, M.L., and Greenberg, R.A. (2012). Links between genome integrity and BRCA1 tumor suppression. Trends Biochem Sci *37*, 418-424.

Li, X., and Manley, J.L. (2005a). Inactivation of the SR protein splicing factor ASF/SF2 results in genomic instability. Cell *122*, 365-378.

Li, X., and Manley, J.L. (2005b). New talents for an old acquaintance: the SR protein splicing factor ASF/SF2 functions in the maintenance of genome stability. Cell Cycle *4*, 1706-1708.

Li, X., and Manley, J.L. (2006). Cotranscriptional processes and their influence on genome stability. Genes Dev *20*, 1838-1847.

Lindell, T.J., Weinberg, F., Morris, P.W., Roeder, R.G., and Rutter, W.J. (1970). Specific inhibition of nuclear RNA polymerase II by alpha-amanitin. Science *170*, 447-449.

Liu, J.F., Tolaney, S.M., Birrer, M., Fleming, G.F., Buss, M.K., Dahlberg, S.E., Lee, H., Whalen, C., Tyburski, K., Winer, E.*, et al.* (2013). A Phase 1 trial of the poly(ADP-ribose) polymerase inhibitor olaparib (AZD2281) in combination with the anti-angiogenic cediranib (AZD2171) in recurrent epithelial ovarian or triple-negative breast cancer. Eur J Cancer.

Liu, Z., Wu, J., and Yu, X. (2007). CCDC98 targets BRCA1 to DNA damage sites. Nat Struct Mol Biol *14*, 716-720.

Livak, K.J., and Schmittgen, T.D. (2001). Analysis of relative gene expression data using real-time quantitative PCR and the 2(-Delta Delta C(T)) Method. Methods *25*, 402-408.

Lorick, K.L., Jensen, J.P., Fang, S., Ong, A.M., Hatakeyama, S., and Weissman, A.M. (1999). RING fingers mediate ubiquitin-conjugating enzyme (E2)-dependent ubiquitination. Proc Natl Acad Sci *96*, 11364-11369.

Ma, Y., Pannicke, U., Schwarz, K., and Lieber, M.R. (2002). Hairpin opening and overhang processing by an Artemis/DNA-dependent protein kinase complex in nonhomologous end joining and V(D)J recombination. Cell *108*, 781-794.

Makiniemi, M., Hillukkala, T., Tuusa, J., Reini, K., Vaara, M., Huang, D., Pospiech, H., Majuri, I., Westerling, T., Makela, T.P.*, et al.* (2001). BRCT domain-containing protein TopBP1 functions in DNA replication and damage response. J Biol Chem *276*, 30399-30406.

Malkova, A., and Ira, G. (2013). Break-induced replication: functions and molecular mechanism. Curr Opin Genet Dev *23*, 271-279.

Manie, E., Vincent-Salomon, A., Lehmann-Che, J., Pierron, G., Turpin, E., Warcoin, M., Gruel, N., Lebigot, I., Sastre-Garau, X., Lidereau, R.*, et al.* (2009). High frequency of TP53 mutation in BRCA1 and sporadic basal-like carcinomas but not in BRCA1 luminal breast tumors. Cancer Research *69*, 663-671.

Manke, I.A., Lowery, D.M., Nguyen, A., and Yaffe, M.B. (2003). BRCT repeats as phosphopeptide-binding modules involved in protein targeting. Science *302*, 636-639.

Mann, K.M., Ward, J.M., Yew, C.C., Kovochich, A., Dawson, D.W., Black, M.A., Brett, B.T., Sheetz, T.E., Dupuy, A.J., Chang, D.K., *et al.* (2012). Sleeping Beauty mutagenesis reveals cooperating mutations and pathways in pancreatic adenocarcinoma. Proc Natl Acad Sci *109*, 5934-5941.

March, H.N., Rust, A.G., Wright, N.A., ten Hoeve, J., de Ridder, J., Eldridge, M., van der Weyden, L., Berns, A., Gadiot, J., Uren, A., *et al.* (2011). Insertional mutagenesis identifies multiple networks of cooperating genes driving intestinal tumorigenesis. Nature Genetics *43*, 1202-1209.

Matsuzawa, A., Kanno, S., Nakayama, M., Mochiduki, H., Wei, L., Shimaoka, T., Furukawa, Y., Kato, K., Shibata, S., Yasui, A., *et al.* (2014). The BRCA1/BARD1-interacting protein OLA1 functions in centrosome regulation. Mol Cell *53*, 101-114.

Mechali, M., and Lutzmann, M. (2008). The cell cycle: now live and in color. Cell *132*, 341-343.

Meetei, A.R., Medhurst, A.L., Ling, C., Xue, Y., Singh, T.R., Bier, P., Steltenpool, J., Stone, S., Dokal, I., Mathew, C.G., *et al.* (2005). A human ortholog of archaeal DNA repair protein Hef is defective in Fanconi anemia complementation group M. Nature Genetics *37*, 958-963.

Melchor, L., and Benitez, J. (2013). The complex genetic landscape of familial breast cancer. Hum Genet *132*, 845-863.

Miki, Y., Swensen, J., Shattuck-Eidens, D., Futreal, P.A., Harshman, K., Tavtigian, S., Liu, Q., Cochran, C., Bennett, L.M., Ding, W., *et al.* (1994). A strong candidate for the breast and ovarian cancer susceptibility gene BRCA1. Science *266*, 66-71.

Mischo, H.E., Gomez-Gonzalez, B., Grzechnik, P., Rondon, A.G., Wei, W., Steinmetz, L., Aguilera, A., and Proudfoot, N.J. (2011). Yeast Sen1 helicase protects the genome from transcription-associated instability. Mol Cell *41*, 21-32.

Mone, M.J., Volker, M., Nikaido, O., Mullenders, L.H., van Zeeland, A.A., Verschure, P.J., Manders, E.M., and van Driel, R. (2001). Local UV-induced DNA damage in cell nuclei results in local transcription inhibition. EMBO Rep *2*, 1013-1017.

Moshous, D., Callebaut, I., de Chasseval, R., Corneo, B., Cavazzana-Calvo, M., Le Deist, F., Tezcan, I., Sanal, O., Bertrand, Y., Philippe, N., *et al.* (2001). Artemis, a novel DNA double-strand break repair/V(D)J recombination protein, is mutated in human severe combined immune deficiency. Cell *105*, 177-186.

Moynahan, M.E., Chiu, J.W., Koller, B.H., and Jasin, M. (1999). Brca1 controls homology-directed DNA repair. Mol Cell *4*, 511-518.

Moynahan, M.E., Cui, T.Y., and Jasin, M. (2001). Homology-directed dna repair, mitomycin-c resistance, and chromosome stability is restored with correction of a Brca1 mutation. Cancer Research *61*, 4842-4850.

Murai, J., Huang, S.Y., Das, B.B., Renaud, A., Zhang, Y., Doroshow, J.H., Ji, J., Takeda, S., and Pommier, Y. (2012). Trapping of PARP1 and PARP2 by Clinical PARP Inhibitors. Cancer Research *72*, 5588-5599.

Nakuci, E., Mahner, S., Direnzo, J., and ElShamy, W.M. (2006). BRCA1-IRIS regulates cyclin D1 expression in breast cancer cells. Exp Cell Res *312*, 3120-3131.

Neve, R.M., Chin, K., Fridlyand, J., Yeh, J., Baehner, F.L., Fevr, T., Clark, L., Bayani, N., Coppe, J.P., Tong, F., *et al.* (2006). A collection of breast cancer cell lines for the study of functionally distinct cancer subtypes. Cancer Cell *10*, 515-527.

Nikkila, J., Christin Parplys, A., Pylkas, K., Bose, M., Huo, Y., Borgmann, K., Rapakko, K., Nieminen, P., Xia, B., Pospiech, H., *et al.* (2013). Heterozygous mutations in PALB2 cause DNA replication and damage response defects. Nat Commun *4*, 2578.

O'Connell, B.C., Adamson, B., Lydeard, J.R., Sowa, M.E., Ciccia, A., Bredemeyer, A.L., Schlabach, M., Gygi, S.P., Elledge, S.J., and Harper, J.W. (2010). A genome-wide camptothecin sensitivity screen identifies a mammalian MMS22L-NFKBIL2 complex required for genomic stability. Mol Cell *40*, 645-657.

O'Donnell, L., Panier, S., Wildenhain, J., Tkach, J.M., Al-Hakim, A., Landry, M.C., Escribano-Diaz, C., Szilard, R.K., Young, J.T., Munro, M., *et al.* (2010). The MMS22L-TONSL complex mediates recovery from replication stress and homologous recombination. Mol Cell *40*, 619-631.

O'Donovan, P.J., and Livingston, D.M. (2010). BRCA1 and BRCA2: breast/ovarian cancer susceptibility gene products and participants in DNA double-strand break repair. Carcinogenesis *31*, 961-967.

Panier, S., and Boulton, S.J. (2014). Double-strand break repair: 53BP1 comes into focus. Nat Rev Mol Cell Biol *15*, 7-18.

Parikh, J.R., Askenazi, M., Ficarro, S.B., Cashorali, T., Webber, J.T., Blank, N.C., Zhang, Y., and Marto, J.A. (2009). multiplierz: an extensible API based desktop environment for proteomics data analysis. BMC Bioinformatics *10*, 364.

Park, J., Long, D.T., Lee, K.Y., Abbas, T., Shibata, E., Negishi, M., Luo, Y., Schimenti, J.C., Gambus, A., Walter, J.C.*, et al.* (2013). The MCM8-MCM9 complex promotes RAD51 recruitment at DNA damage sites to facilitate homologous recombination. Mol Cell Biol *33*, 1632-1644.

Parrilla-Castellar, E.R., Arlander, S.J., and Karnitz, L. (2004). Dial 9-1-1 for DNA damage: the Rad9-Hus1-Rad1 (9-1-1) clamp complex. DNA Repair (Amst) *3*, 1009-1014.

Parsons, D.W., Jones, S., Zhang, X., Lin, J.C., Leary, R.J., Angenendt, P., Mankoo, P., Carter, H., Siu, I.M., Gallia, G.L.*, et al.* (2008). An integrated genomic analysis of human glioblastoma multiforme. Science *321*, 1807-1812.

Parsons, D.W., Li, M., Zhang, X., Jones, S., Leary, R.J., Lin, J.C., Boca, S.M., Carter, H., Samayoa, J., Bettegowda, C.*, et al.* (2011). The genetic landscape of the childhood cancer medulloblastoma. Science *331*, 435-439.

Pathania, S., Nguyen, J., Hill, S.J., Scully, R., Adelmant, G.O., Marto, J.A., Feunteun, J., and Livingston, D.M. (2011). BRCA1 is required for postreplication repair after UV-induced DNA damage. Mol Cell *44*, 235-251.

Paull, T.T., and Gellert, M. (1998). The 3' to 5' exonuclease activity of Mre 11 facilitates repair of DNA double-strand breaks. Mol Cell *1*, 969-979.

Paulsen, R.D., Soni, D.V., Wollman, R., Hahn, A.T., Yee, M.C., Guan, A., Hesley, J.A., Miller, S.C., Cromwell, E.F., Solow-Cordero, D.E.*, et al.* (2009). A genome-wide siRNA screen reveals diverse cellular processes and pathways that mediate genome stability. Mol Cell *35*, 228-239.

Perou, C.M., Sorlie, T., Eisen, M.B., van de Rijn, M., Jeffrey, S.S., Rees, C.A., Pollack, J.R., Ross, D.T., Johnsen, H., Akslen, L.A., *et al.* (2000). Molecular portraits of human breast tumours. Nature *406*, 747-752.

Pierce, A., McGowan, P.M., Cotter, M., Mullooly, M., O'Donovan, N., Rani, S., O'Driscoll, L., Crown, J., and Duffy, M.J. (2013). Comparative antiproliferative effects of iniparib and olaparib on a panel of triple-negative and non-triple-negative breast cancer cell lines. Cancer Biol Ther *14*, 537-545.

Pierce, A.J., Johnson, R.D., Thompson, L.H., and Jasin, M. (1999). XRCC3 promotes homology-directed repair of DNA damage in mammalian cells. Genes Dev *13*, 2633-2638.

Piwko, W., Olma, M.H., Held, M., Bianco, J.N., Pedrioli, P.G., Hofmann, K., Pasero, P., Gerlich, D.W., and Peter, M. (2010). RNAi-based screening identifies the Mms22L-Nfkbil2 complex as a novel regulator of DNA replication in human cells. EMBO J *29*, 4210-4222.

Pleasance, E.D., Cheetham, R.K., Stephens, P.J., McBride, D.J., Humphray, S.J., Greenman, C.D., Varela, I., Lin, M.L., Ordonez, G.R., Bignell, G.R., *et al.* (2010). A comprehensive catalogue of somatic mutations from a human cancer genome. Nature *463*, 191-196.

Polo, S.E., Roche, D., and Almouzni, G. (2006). New histone incorporation marks sites of UV repair in human cells. Cell *127*, 481-493.

Press, J.Z., De Luca, A., Boyd, N., Young, S., Troussard, A., Ridge, Y., Kaurah, P., Kalloger, S.E., Blood, K.A., Smith, M., *et al.* (2008). Ovarian carcinomas with genetic and epigenetic BRCA1 loss have distinct molecular abnormalities. BMC Cancer *8*, 17.

Puente, X.S., Pinyol, M., Quesada, V., Conde, L., Ordonez, G.R., Villamor, N., Escaramis, G., Jares, P., Bea, S., Gonzalez-Diaz, M., *et al.* (2011). Whole-genome sequencing identifies recurrent mutations in chronic lymphocytic leukaemia. Nature *475*, 101-105.

Pujana, M.A., Han, J.D., Starita, L.M., Stevens, K.N., Tewari, M., Ahn, J.S., Rennert, G., Moreno, V., Kirchhoff, T., Gold, B., *et al.* (2007). Network modeling links breast cancer susceptibility and centrosome dysfunction. Nature Genetics *39*, 1338-1349.

Reinberg, D., and Sims, R.J., 3rd (2006). de FACTo nucleosome dynamics. J Biol Chem *281*, 23297-23301.

Reyon, D., Tsai, S.Q., Khayter, C., Foden, J.A., Sander, J.D., and Joung, J.K. (2012). FLASH assembly of TALENs for high-throughput genome editing. Nat Biotechnol *30*, 460-465.

Rhodes, D.R., Kalyana-Sundaram, S., Tomlins, S.A., Mahavisno, V., Kasper, N., Varambally, R., Barrette, T.R., Ghosh, D., Varambally, S., and Chinnaiyan, A.M. (2007). Molecular concepts analysis links tumors, pathways, mechanisms, and drugs. Neoplasia *9*, 443-454.

Rozenblatt-Rosen, O., Deo, R.C., Padi, M., Adelmant, G., Calderwood, M.A., Rolland, T., Grace, M., Dricot, A., Askenazi, M., Tavares, M., *et al.* (2012). Interpreting cancer genomes using systematic host network perturbations by tumour virus proteins. Nature *487*, 491-495.

Rual, J.F., Hirozane-Kishikawa, T., Hao, T., Bertin, N., Li, S., Dricot, A., Li, N., Rosenberg, J., Lamesch, P., Vidalain, P.O., *et al.* (2004). Human ORFeome version 1.1: a platform for reverse proteomics. Genome Res *14*, 2128-2135.

Rual, J.F., Venkatesan, K., Hao, T., Hirozane-Kishikawa, T., Dricot, A., Li, N., Berriz, G.F., Gibbons, F.D., Dreze, M., Ayivi-Guedehoussou, N., *et al.* (2005). Towards a proteome-scale map of the human protein-protein interaction network. Nature *437*, 1173-1178.

Ruffner, H., Joazeiro, C.A., Hemmati, D., Hunter, T., and Verma, I.M. (2001). Cancer-predisposing mutations within the RING domain of BRCA1: loss of ubiquitin protein ligase activity and protection from radiation hypersensitivity. Proc Natl Acad Sci *98*, 5134-5139.

Sakaue-Sawano, A., Kurokawa, H., Morimura, T., Hanyu, A., Hama, H., Osawa, H., Kashiwagi, S., Fukami, K., Miyata, T., Miyoshi, H., *et al.* (2008). Visualizing spatiotemporal dynamics of multicellular cell-cycle progression. Cell *132*, 487-498.

Savage, K.I., Matchett, K.B., Barros, E.M., Cooper, K.M., Irwin, G., Gorski, J.J., Orr, K.S., Vohhodina, J., Kavanagh, J.N., Madden, A.F., *et al.* (2014). Brca1 Deficiency Exacerbates Estrogen Induced DNA Damage and Genomic Instability. Cancer Research.

Schlacher, K., Christ, N., Siaud, N., Egashira, A., Wu, H., and Jasin, M. (2011). Double-strand break repair-independent role for BRCA2 in blocking stalled replication fork degradation by MRE11. Cell *145*, 529-542.

Schlacher, K., Wu, H., and Jasin, M. (2012). A distinct replication fork protection pathway connects Fanconi anemia tumor suppressors to RAD51-BRCA1/2. Cancer Cell *22*, 106-116.

Scully, R., Anderson, S.F., Chao, D.M., Wei, W., Ye, L., Young, R.A., Livingston, D.M., and Parvin, J.D. (1997a). BRCA1 is a component of the RNA polymerase II holoenzyme. Proc Natl Acad Sci *94*, 5605-5610.

Scully, R., Chen, J., Ochs, R.L., Keegan, K., Hoekstra, M., Feunteun, J., and Livingston, D.M. (1997b). Dynamic changes of BRCA1 subnuclear location and phosphorylation state are initiated by DNA damage. Cell *90*, 425-435.

Scully, R., Ganesan, S., Vlasakova, K., Chen, J., Socolovsky, M., and Livingston, D.M. (1999). Genetic analysis of BRCA1 function in a defined tumor cell line. Mol Cell *4*, 1093-1099.

Silver, D.P., and Livingston, D.M. (2012). Mechanisms of BRCA1 tumor suppression. Cancer Discov *2*, 679-684.

Silver, D.P., Richardson, A.L., Eklund, A.C., Wang, Z.C., Szallasi, Z., Li, Q., Juul, N., Leong, C.O., Calogrias, D., Buraimoh, A., *et al.* (2010). Efficacy of neoadjuvant Cisplatin in triple-negative breast cancer. J Clin Oncol *28*, 1145-1153.

Sirohi, B., Arnedos, M., Popat, S., Ashley, S., Nerurkar, A., Walsh, G., Johnston, S., and Smith, I.E. (2008). Platinum-based chemotherapy in triple-negative breast cancer. Ann Oncol *19*, 1847-1852.

Skourti-Stathaki, K., Proudfoot, N.J., and Gromak, N. (2011). Human senataxin resolves RNA/DNA hybrids formed at transcriptional pause sites to promote Xrn2-dependent termination. Mol Cell *42*, 794-805.

Smogorzewska, A., Matsuoka, S., Vinciguerra, P., McDonald, E.R., 3rd, Hurov, K.E., Luo, J., Ballif, B.A., Gygi, S.P., Hofmann, K., D'Andrea, A.D., *et al.* (2007). Identification of the FANCI protein, a monoubiquitinated FANCD2 paralog required for DNA repair. Cell *129*, 289-301.

Sobhian, B., Shao, G., Lilli, D.R., Culhane, A.C., Moreau, L.A., Xia, B., Livingston, D.M., and Greenberg, R.A. (2007). RAP80 targets BRCA1 to specific ubiquitin structures at DNA damage sites. Science *316*, 1198-1202.

Sorlie, T., Perou, C.M., Tibshirani, R., Aas, T., Geisler, S., Johnsen, H., Hastie, T., Eisen, M.B., van de Rijn, M., Jeffrey, S.S., *et al.* (2001). Gene expression patterns of breast carcinomas distinguish tumor subclasses with clinical implications. Proc Natl Acad Sci *98*, 10869-10874.

Sorlie, T., Tibshirani, R., Parker, J., Hastie, T., Marron, J.S., Nobel, A., Deng, S., Johnsen, H., Pesich, R., Geisler, S., *et al.* (2003). Repeated observation of breast tumor subtypes in independent gene expression data sets. Proc Natl Acad Sci *100*, 8418-8423.

Starr, T.K., Allaei, R., Silverstein, K.A., Staggs, R.A., Sarver, A.L., Bergemann, T.L., Gupta, M., O'Sullivan, M.G., Matise, I., Dupuy, A.J., *et al.* (2009). A transposon-based genetic screen in mice identifies genes altered in colorectal cancer. Science *323*, 1747-1750.

Starr, T.K., Scott, P.M., Marsh, B.M., Zhao, L., Than, B.L., O'Sullivan, M.G., Sarver, A.L., Dupuy, A.J., Largaespada, D.A., and Cormier, R.T. (2011). A Sleeping Beauty transposon-mediated screen identifies murine susceptibility genes for adenomatous polyposis coli (Apc)-dependent intestinal tumorigenesis. Proc Natl Acad Sci *108*, 5765-5770.

Staudacher, L., Cottu, P.H., Dieras, V., Vincent-Salomon, A., Guilhaume, M.N., Escalup, L., Dorval, T., Beuzeboc, P., Mignot, L., and Pierga, J.Y. (2011). Platinum-based chemotherapy in metastatic triple-negative breast cancer: the Institut Curie experience. Ann Oncol *22*, 848-856.

Stelzl, U., Worm, U., Lalowski, M., Haenig, C., Brembeck, F.H., Goehler, H., Stroedicke, M., Zenkner, M., Schoenherr, A., Koeppen, S., *et al.* (2005). A human protein-protein interaction network: a resource for annotating the proteome. Cell *122*, 957-968.

Stransky, N., Egloff, A.M., Tward, A.D., Kostic, A.D., Cibulskis, K., Sivachenko, A., Kryukov, G.V., Lawrence, M.S., Sougnez, C., McKenna, A., *et al.* (2011). The mutational landscape of head and neck squamous cell carcinoma. Science *333*, 1157-1160.

Svendsen, J.M., and Harper, J.W. (2010). GEN1/Yen1 and the SLX4 complex: Solutions to the problem of Holliday junction resolution. Genes Dev *24*, 521-536.

Sy, S.M., Huen, M.S., and Chen, J. (2009). PALB2 is an integral component of the BRCA complex required for homologous recombination repair. Proc Natl Acad Sci *106*, 7155-7160.

Szabo, C., Masiello, A., Ryan, J.F., and Brody, L.C. (2000). The breast cancer information core: database design, structure, and scope. Hum Mutat *16*, 123-131.

Takata, M., Sasaki, M.S., Sonoda, E., Morrison, C., Hashimoto, M., Utsumi, H., Yamaguchi-Iwai, Y., Shinohara, A., and Takeda, S. (1998). Homologous recombination and non-homologous end-joining pathways of DNA double-strand break repair have overlapping roles in the maintenance of chromosomal integrity in vertebrate cells. EMBO J *17*, 5497-5508.

Tammaro, C., Raponi, M., Wilson, D.I., and Baralle, D. (2012). BRCA1 exon 11 alternative splicing, multiple functions and the association with cancer. Biochem Soc Trans *40*, 768-772.

Taniguchi, T., Garcia-Higuera, I., Andreassen, P.R., Gregory, R.C., Grompe, M., and D'Andrea, A.D. (2002). S-phase-specific interaction of the Fanconi anemia protein, FANCD2, with BRCA1 and RAD51. Blood *100*, 2414-2420.

Tasan, M., Rolland, T., Pevzner, S.P., Charloteaux, B., Lemmens, I., Fontanillo, C., Mosca, R., Sahni, N., Yi, S., Kamburov, A., *et al.* (2014). Expanding views of the human interactome network (Boston, MA, Dana Farber Cancer Institute).

Telli, M.L., and Ford, J.M. (2010). PARP inhibitors in breast cancer. Clin Adv Hematol Oncol *8*, 629-635.

Todd, R.C., and Lippard, S.J. (2009). Inhibition of transcription by platinum antitumor compounds. Metallomics *1*, 280-291.

Tung, N., Miron, A., Schnitt, S.J., Gautam, S., Fetten, K., Kaplan, J., Yassin, Y., Buraimoh, A., Kim, J.Y., Szasz, A.M., *et al.* (2010). Prevalence and predictors of loss of wild type BRCA1 in estrogen receptor positive and negative BRCA1-associated breast cancers. Breast Cancer Res *12*, R95.

Valentin, M.D., da Silva, S.D., Privat, M., Alaoui-Jamali, M., and Bignon, Y.J. (2012). Molecular insights on basal-like breast cancer. Breast Cancer Res Treat *134*, 21-30.

van 't Veer, L.J., Dai, H., van de Vijver, M.J., He, Y.D., Hart, A.A., Mao, M., Peterse, H.L., van der Kooy, K., Marton, M.J., Witteveen, A.T., *et al.* (2002). Gene expression profiling predicts clinical outcome of breast cancer. Nature *415*, 530-536.

Vandenberg, C.J., Gergely, F., Ong, C.Y., Pace, P., Mallery, D.L., Hiom, K., and Patel, K.J. (2003). BRCA1-independent ubiquitination of FANCD2. Mol Cell *12*, 247-254.

Venkatesan, K., Rual, J.F., Vazquez, A., Stelzl, U., Lemmens, I., Hirozane-Kishikawa, T., Hao, T., Zenkner, M., Xin, X., Goh, K.I., *et al.* (2009). An empirical framework for binary interactome mapping. Nat Methods *6*, 83-90.

Venkitaraman, A.R. (2002). Cancer susceptibility and the functions of BRCA1 and BRCA2. Cell *108*, 171-182.

Vogelstein, B., Papadopoulos, N., Velculescu, V.E., Zhou, S., Diaz, L.A., Jr., and Kinzler, K.W. (2013). Cancer genome landscapes. Science *339*, 1546-1558.

Volker, M., Mone, M.J., Karmakar, P., van Hoffen, A., Schul, W., Vermeulen, W., Hoeijmakers, J.H., van Driel, R., van Zeeland, A.A., and Mullenders, L.H. (2001). Sequential assembly of the nucleotide excision repair factors in vivo. Mol Cell *8*, 213-224.

Walker, J.R., Corpina, R.A., and Goldberg, J. (2001). Structure of the Ku heterodimer bound to DNA and its implications for double-strand break repair. Nature *412*, 607-614.

Walsh, T., and King, M.C. (2007). Ten genes for inherited breast cancer. Cancer Cell *11*, 103-105.

Walter, J., and Newport, J. (2000). Initiation of eukaryotic DNA replication: origin unwinding and sequential chromatin association of Cdc45, RPA, and DNA polymerase alpha. Mol Cell *5*, 617-627.

Wang, B., Matsuoka, S., Ballif, B.A., Zhang, D., Smogorzewska, A., Gygi, S.P., and Elledge, S.J. (2007). Abraxas and RAP80 form a BRCA1 protein complex required for the DNA damage response. Science *316*, 1194-1198.

Wang, X., Andreassen, P.R., and D'Andrea, A.D. (2004). Functional interaction of monoubiquitinated FANCD2 and BRCA2/FANCD1 in chromatin. Mol Cell Biol *24*, 5850-5862.

Wang, Y., Cortez, D., Yazdi, P., Neff, N., Elledge, S.J., and Qin, J. (2000). BASC, a super complex of BRCA1-associated proteins involved in the recognition and repair of aberrant DNA structures. Genes Dev *14*, 927-939.

Wechsler, T., Newman, S., and West, S.C. (2011). Aberrant chromosome morphology in human cells defective for Holliday junction resolution. Nature *471*, 642-646.

Westermark, U.K., Reyngold, M., Olshen, A.B., Baer, R., Jasin, M., and Moynahan, M.E. (2003). BARD1 participates with BRCA1 in homology-directed repair of chromosome breaks. Mol Cell Biol *23*, 7926-7936.

Wind, M., and Reines, D. (2000). Transcription elongation factor SII. Bioessays *22*, 327-336.

Woods, N.T., Mesquita, R.D., Sweet, M., Carvalho, M.A., Li, X., Liu, Y., Nguyen, H., Thomas, C.E., Iversen, E.S., Jr., Marsillac, S.*, et al.* (2012). Charting the landscape of tandem BRCT domain-mediated protein interactions. Sci Signal *5*, rs6.

Wooster, R., Neuhausen, S.L., Mangion, J., Quirk, Y., Ford, D., Collins, N., Nguyen, K., Seal, S., Tran, T., Averill, D.*, et al.* (1994). Localization of a breast cancer susceptibility gene, BRCA2, to chromosome 13q12-13. Science *265*, 2088-2090.

Wu, L.C., Wang, Z.W., Tsan, J.T., Spillman, M.A., Phung, A., Xu, X.L., Yang, M.C., Hwang, L.Y., Bowcock, A.M., and Baer, R. (1996). Identification of a RING protein that can interact in vivo with the BRCA1 gene product. Nature Genetics *14*, 430-440.

Xia, B., Sheng, Q., Nakanishi, K., Ohashi, A., Wu, J., Christ, N., Liu, X., Jasin, M., Couch, F.J., and Livingston, D.M. (2006). Control of BRCA2 cellular and clinical functions by a nuclear partner, PALB2. Mol Cell *22*, 719-729.

Xu, B., Kim, S., and Kastan, M.B. (2001a). Involvement of Brca1 in S-phase and G(2)-phase checkpoints after ionizing irradiation. Mol Cell Biol *21*, 3445-3450.

Xu, B., O'Donnell, A.H., Kim, S.T., and Kastan, M.B. (2002). Phosphorylation of serine 1387 in Brca1 is specifically required for the Atm-mediated S-phase checkpoint after ionizing irradiation. Cancer Research *62*, 4588-4591.

Xu, J., Huo, D., Chen, Y., Nwachukwu, C., Collins, C., Rowell, J., Slamon, D.J., and Olopade, O.I. (2010). CpG island methylation affects accessibility of the proximal BRCA1 promoter to transcription factors. Breast Cancer Res Treat *120*, 593-601.

Xu, X., Aprelikova, O., Moens, P., Deng, C.X., and Furth, P.A. (2003). Impaired meiotic DNA-damage repair and lack of crossing-over during spermatogenesis in BRCA1 full-length isoform deficient mice. Development *130*, 2001-2012.

Xu, X., Qiao, W., Linke, S.P., Cao, L., Li, W.M., Furth, P.A., Harris, C.C., and Deng, C.X. (2001b). Genetic interactions between tumor suppressors Brca1 and p53 in apoptosis, cell cycle and tumorigenesis. Nature Genetics *28*, 266-271.

Xu, X., Wagner, K.U., Larson, D., Weaver, Z., Li, C., Ried, T., Hennighausen, L., Wynshaw-Boris, A., and Deng, C.X. (1999a). Conditional mutation of Brca1 in mammary epithelial cells results in blunted ductal morphogenesis and tumour formation. Nature Genetics *22*, 37-43.

Xu, X., Weaver, Z., Linke, S.P., Li, C., Gotay, J., Wang, X.W., Harris, C.C., Ried, T., and Deng, C.X. (1999b). Centrosome amplification and a defective G2-M cell cycle checkpoint induce genetic instability in BRCA1 exon 11 isoform-deficient cells. Mol Cell *3*, 389-395.

Yan, J., Kim, Y.S., Yang, X.P., Li, L.P., Liao, G., Xia, F., and Jetten, A.M. (2007). The ubiquitin-interacting motif containing protein RAP80 interacts with BRCA1 and functions in DNA damage repair response. Cancer Research *67*, 6647-6656.

Yaneva, M., Kowalewski, T., and Lieber, M.R. (1997). Interaction of DNA-dependent protein kinase with DNA and with Ku: biochemical and atomic-force microscopy studies. EMBO J *16*, 5098-5112.

Yoo, S., and Dynan, W.S. (1999). Geometry of a complex formed by double strand break repair proteins at a single DNA end: recruitment of DNA-PKcs induces inward translocation of Ku protein. Nucleic Acids Res *27*, 4679-4686.

Yu, H., Tardivo, L., Tam, S., Weiner, E., Gebreab, F., Fan, C., Svrzikapa, N., Hirozane-Kishikawa, T., Rietman, E., Yang, X., *et al.* (2011). Next-generation sequencing to generate interactome datasets. Nat Methods *8*, 478-480.

Yu, X., and Baer, R. (2000). Nuclear localization and cell cycle-specific expression of CtIP, a protein that associates with the BRCA1 tumor suppressor. J Biol Chem *275*, 18541-18549.

Yu, X., Chini, C.C., He, M., Mer, G., and Chen, J. (2003). The BRCT domain is a phospho-protein binding domain. Science *302*, 639-642.

Yu, X., Jacobs, S.A., West, S.C., Ogawa, T., and Egelman, E.H. (2001). Domain structure and dynamics in the helical filaments formed by RecA and Rad51 on DNA. Proc Natl Acad Sci *98*, 8419-8424.

Yu, X., Wu, L.C., Bowcock, A.M., Aronheim, A., and Baer, R. (1998). The C-terminal (BRCT) domains of BRCA1 interact in vivo with CtIP, a protein implicated in the CtBP pathway of transcriptional repression. J Biol Chem *273*, 25388-25392.

Yuce, O., and West, S.C. (2013). Senataxin, defective in the neurodegenerative disorder ataxia with oculomotor apraxia 2, lies at the interface of transcription and the DNA damage response. Mol Cell Biol *33*, 406-417.

Yun, M.H., and Hiom, K. (2009). CtIP-BRCA1 modulates the choice of DNA double-strand-break repair pathway throughout the cell cycle. Nature *459*, 460-463.

Zack, T.I., Schumacher, S.E., Carter, S.L., Cherniack, A.D., Saksena, G., Tabak, B., Lawrence, M.S., Zhang, C.Z., Wala, J., Mermel, C.H., *et al.* (2013). Pan-cancer patterns of somatic copy number alteration. Nature Genetics *45*, 1134-1140.

Zeman, M.K., and Cimprich, K.A. (2014). Causes and consequences of replication stress. Nat Cell Biol *16*, 2-9.

Zhang, F., Ma, J., Wu, J., Ye, L., Cai, H., Xia, B., and Yu, X. (2009). PALB2 links BRCA1 and BRCA2 in the DNA-damage response. Curr Biol *19*, 524-529.

Zhang, J., and Powell, S.N. (2005). The role of the BRCA1 tumor suppressor in DNA double-strand break repair. Mol Cancer Res *3*, 531-539.

Zhang, Q.C., Petrey, D., Deng, L., Qiang, L., Shi, Y., Thu, C.A., Bisikirska, B., Lefebvre, C., Accili, D., Hunter, T., *et al.* (2012). Structure-based prediction of protein-protein interactions on a genome-wide scale. Nature *490*, 556-560.

Zhang, Z., Lotti, F., Dittmar, K., Younis, I., Wan, L., Kasim, M., and Dreyfuss, G. (2008). SMN deficiency causes tissue-specific perturbations in the repertoire of snRNAs and widespread defects in splicing. Cell *133*, 585-600.

Zhu, Q., Pao, G.M., Huynh, A.M., Suh, H., Tonnu, N., Nederlof, P.M., Gage, F.H., and Verma, I.M. (2011). BRCA1 tumour suppression occurs via heterochromatin-mediated silencing. Nature *477*, 179-184.

Zou, L., and Elledge, S.J. (2003). Sensing DNA damage through ATRIP recognition of RPA-ssDNA complexes. Science *300*, 1542-1548.